1993

Determination of losses in the Beaver Valley and Hatfield Ferry low pressure steam turbine exhaust hoods and their modifications

Mark J. Pechulis
Lehigh University

AUTHOR:

Pechulis, Mark J.

TITLE:

Determination of Losses in the Beaver Valley and Hatfield Ferry Low Pressure Steam Turbine Exhaust Hoods and Their Modifications

DATE: January 16, 1994

Determination of Losses in the Beaver Valley and Hatfield Ferry Low Pressure Steam Turbine Exhaust Hoods and Their Modifications

by

Mark J. Pechulis

A Thesis

Presented to the Graduate and Research Committee

of Lehigh University

in Candidacy for the Degree of

Master of Science

in

Mechanical Engineering

Lehigh University

December 1993

This thesis is accepted and approved in partial fulfillment of the requirements for the degree of Master of Science.

10 December 1993

Date

Thesis Advisor

Chairperson of Department

TABLE OF CONTENTS

NOTATION

a = speed of sound

A = cross-sectional area

A_A = annulus advance

AR = area ratio

b = 2-D diffuser depth

B = measurement of blocked to total cross-sectional area

B_L = hood length

C = discharge coefficient

C_P = pressure recovery coefficient

C_{Pi} = ideal pressure recovery coefficient

C_P1 = pressure recovery coefficient - first definition

C_P2 = pressure recovery coefficient - second definition

$C_P1_{,LOCAL}$ = local pressure recovery coefficient - first definition

D = hood width

e = internal energy per unit mass

E = ratio of effective to total cross-sectional area

°F = degrees Farenheit

$f_n(M_{AN})$ = function of Mach number in the annulus, n = 1,2,3

Fa = thermal expansion factor

f(r) = Simpson's rule function

h = enthalpy

H = hood height

HL = hood loss

HL/LL = hood loss coefficient

(H+C)L = hood and condenser neck loss

(H+C)L/LL = hood and condenser neck loss coefficient

L = length of 2-dimensional diffuser wall

L_B = last blade height

(L-0) = last rotating blade

LL = leaving loss

LP = low pressure

M = Mach number

N = length of diffuser centerline measured from the throat to the exit

P = static pressure

q = dynamic pressure

r = radius

R = radius of curvature

R = gas constant, radius of axisymmetric diffuser

°R = degrees Rankine

R_H = last blade root radius, annular diffuser hub radius

R_T = annular diffuser radius

s = entropy

S = specific humidity

T = temperature (absolute)

V = velocity

U = maximum velocity

W = width, mass flow rate

$(W\sqrt{RT_{T,AN}})/A_{AN}P_{T,AN}$ = non -dimensional mass flow rate

x = horizontal component of distance

y = vertical component of distance

Y = compressibility expansion factor

GREEK SYMBOLS

α = kinetic energy flux velocity profile parameter

β = curved diffuser turning angle

γ = gas constant (= 1.4 for air)

Δ = change

$2\delta_1^*/W_1$ = inlet boundary-layer thickness (2-D diffuser)

η = diffuser effectiveness

θ = divergence angle of one wall of a 2-D diffuser

$2\theta_{eff}$ = angle measuring the divergence of a curved diffuser

ρ = fluid density

ρ^{FL}_{AN} = average fluid density between the annulus and the flange of the exhaust hood

ρ_d = density of dry air

υ = specific volume

Φ = relative humidity

ϕ_i = inner divergence angle (annular diffuser)

ϕ_o = outer divergence angle (annular diffuser)

SUBSCRIPTS

1 = condition at diffuser or exhaust hood inlet

2 = condition at diffuser or exhaust hood outlet

AN = static condition in the annulus

ATM = atmospheric condition

B = blocked portion of area

CF = centerline flange

DB = dry bulb

E = effective

FL,EFF = effective flange open area

g = vapor condition

i = condition at a point (except for C_pi), or inner

o = outer

T = total condition

T,AN = total condition in the annulus

T1 = total condition at inlet

T2 = total condition at outlet

V = venturi

VI = venturi inlet

LIST OF FIGURES

APPENDIX G:

APPENDIX H:

LIST OF TABLES

1 ABSTRACT

The losses in a low pressure steam turbine exhaust end are a measure of the fluid frictional losses within the exhaust hood. These losses represent energy which is not available to the turbine and result in a decrease of power produced by the unit. The objectives for this experimental model study were to determine the losses of the present Beaver Valley and Hatfield Ferry low pressure steam turbine exhaust hoods tested with and without the condenser necks attached, and to internally modify these hoods in an attempt to reduce the losses. The objectives were carried out using air model testing at Lehigh University. It was found that the size of the exhaust hood, the fixed guide vane design, the shape of the bearing cone, and the slanted back wall were all factors which affected the hood losses.

A procedure for calculating the hood losses using pressure and mass flow rate measurements on model exhaust hoods is discussed, and results are presented for both the Beaver Valley and Hatfield Ferry hood models. A diffuser review, with an emphasis on curved diffusers, is also given.

2 INTRODUCTION

A low pressure (LP) steam turbine exhaust hood consists of an annulus through which flow enters from the last stage, a flow guide, a bearing cone, turbine outer shell, internal support struts, and a condenser-connecting flange to the condenser. Figure 1 shows a typical LP steam turbine exhaust hood.

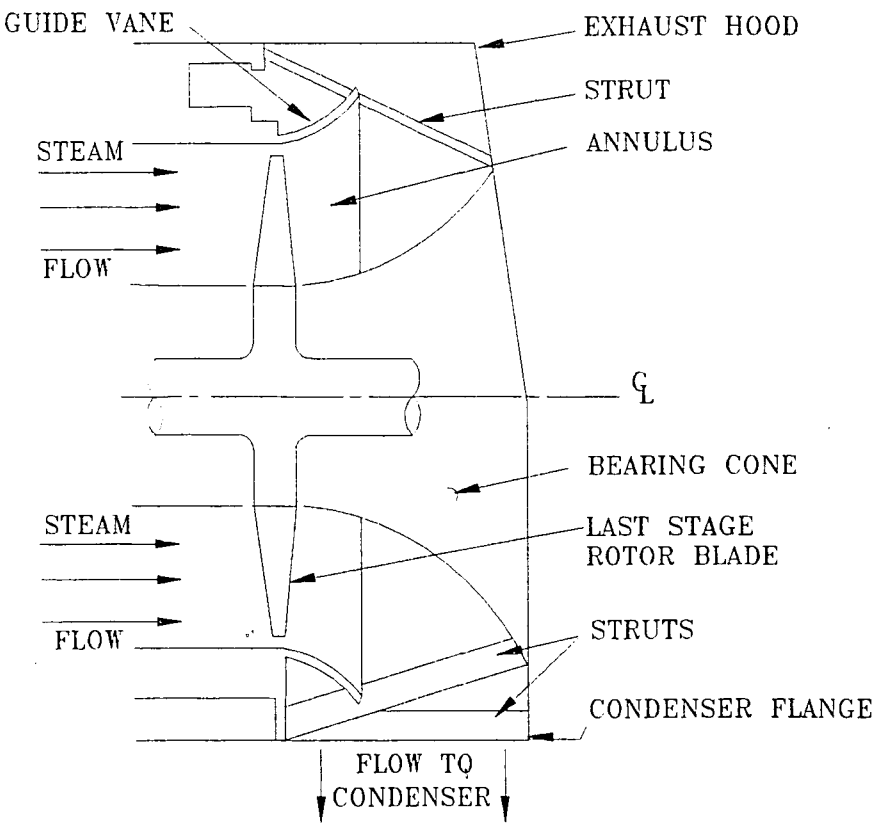

Figure 1: Diagram of a low pressure steam turbine exhaust hood

The purpose of an exhaust hood is to receive low pressure exhaust steam from a turbine

and direct it into a condenser. This seemingly simple may task account for a considerable portion of the fluid dynamic losses of a steam turbine. Seglem and Brown [22] reported that this loss can be as high as 10 percent of all the fluid dynamic losses associated with a turbine. In a relatively short distance, the steam traveling axially from the last rotating turbine blade at a high Mach number flows through a diffuser to recover some kinetic energy, and then makes a 90 degree turn into the condenser. In the exhaust hood the steam flows over supporting struts and beams which act as obstacles to the flow.

The losses in an exhaust hood are fluid frictional losses which cause an increase in the static pressure at the exit of the last rotating blade. They depend on the exhaust hood geometry, the Mach number, the Reynolds number, and the kinetic energy of the steam exiting the last rotating blade. Modification of exhaust hood geometry to lower these kinetic energy losses represents a potential area of improvement in steam turbine performance.

Figure 2 shows an enthalpy-entropy (h-s) diagram displaying the thermodynamic states of the working fluid when it leaves the last rotating blade of a turbine. This h-s diagram is for an expanding exhaust hood, one in which the average annulus static pressure, P_{AN}, is greater than the average flange static pressure, P_{FL}. The hood loss (HL), or hood/condenser neck loss ((H+C)L), is defined as the isentropic enthalpy difference between P_{AN} and P_{FL}. This hood loss can be nondimensionalized using the leaving loss , LL, which is the average kinetic energy of the flow leaving the last stage blade. This dimensionless parameter is called the hood loss or hood/condenser neck

loss coefficient and is denoted as HL/LL or (H+C)L/LL, respectively . A reduction in the value of this loss coefficient results in a power gain for the turbine.

There were two objectives for this experimental model study. The first was to determine the losses of the present Beaver Valley and Hatfield Ferry exhaust hoods with and without condenser necks attached, and the second was to internally modify these hoods in an attempt to reduce the losses and thus produce a power gain. This study was carried out at Lehigh University using models and a specially designed air test loop.

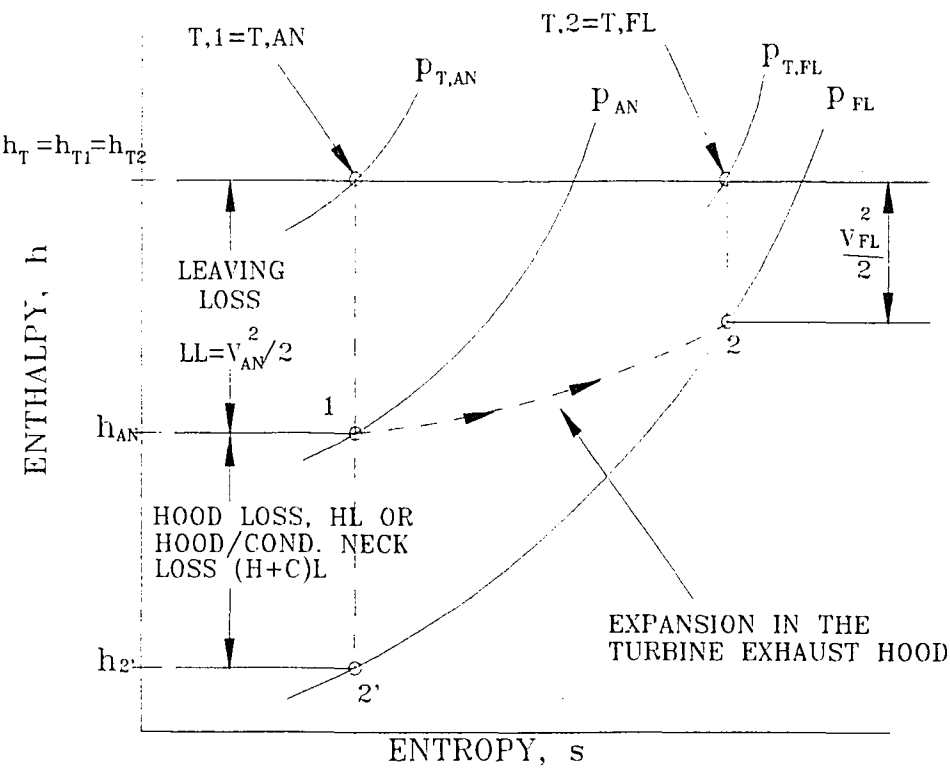

Figure 2: h-s diagram for an expanding exhaust hood ($P_{AN} > P_{FL}$)

3 CURVED DIFFUSERS

In industrial practice, it is often desirable to decelerate a fluid moving through a system to recover the kinetic energy of the flow and thus increase the static pressure. The main objective of diffuser design is optimum performance. Several factors must be considered when optimizing a diffuser. These factors include geometrical parameters, flow regime, and inlet conditions.

The performance of diffusers is commonly judged by the following characteristics:

1) Pressure recovery coefficient, C_P

$$C_P = \frac{P_2 - P_1}{\frac{\rho V_1^2}{2}} \tag{1}$$

2) Ideal pressure recovery coefficient, C_{Pi}

$$C_{Pi} = 1 - \frac{1}{(AR)^2} \tag{2}$$

3) Diffuser effectiveness, η

$$\eta = \frac{P_2 - P_1}{\frac{\rho V_1^2}{2}\left[1 - \left(\frac{A_1}{A_2}\right)^2\right]} = \frac{C_P}{C_{Pi}} \tag{3}$$

Most of the information about diffusers has been collected through experimental work. Recently, researchers have been concentrating their effort on trying to analytically predict the performance of a diffuser but the results have had only limited success when inlet distortion velocity profile, swirl, and turbulence effects are taken into account. Reports by a few authors have shown that the effects of changes in the Reynolds number on conical and straight two-dimensional diffusers has almost no effect on both the flow regime and performance as long as the Reynolds number of the flow is above about 10^3. Researchers have concluded that the flow regime is primarily dependent on diffuser geometry, but the performance also depends on other factors such as inlet turbulence, boundary layer thickness, swirl, and Mach number.

3.1 GEOMETRIC PARAMETERS

3.1.1 TWO-DIMENSIONAL STRAIGHT-WALLED DIFFUSERS

Two-dimensional straight-walled diffuser geometry is discussed first since extensive studies have been performed on them and curved diffusers use the results as a comparison. A two-dimensional, symmetric, straight-walled diffuser can be described by the geometric parameters shown in figure 3. These are the area ratio ($AR=W_2/W_1$), the total divergence angle (2θ), the ratio of diffuser wall length to entry width (L/W_1), and the aspect ratio (b/W_1).

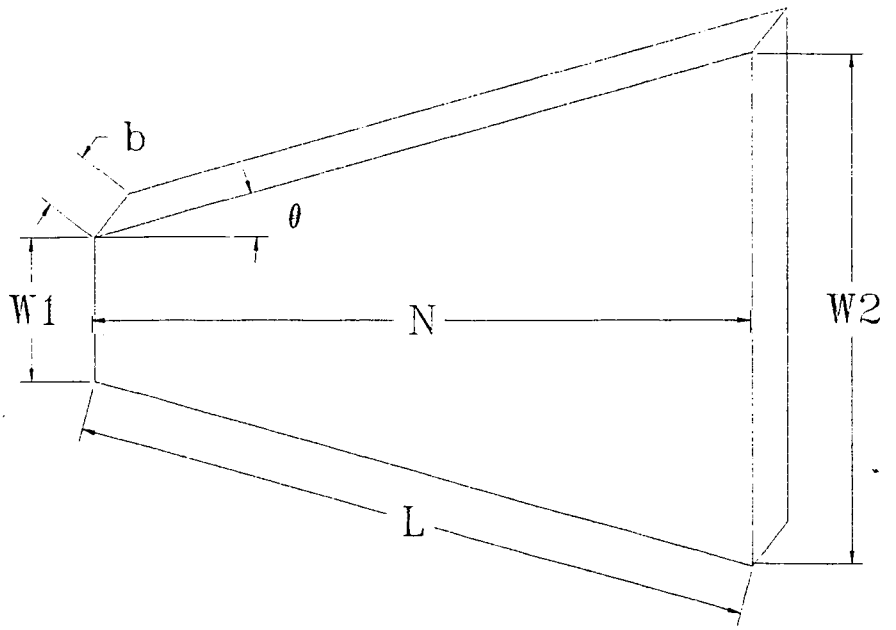

Figure 3: Geometric parameters of a two-dimensional straight-walled diffuser

3.1.2 TWO-DIMENSIONAL CURVED DIFFUSERS

Because of geometrical constraints, it is often necessary to use curved diffusers. Definition of curved diffuser geometric parameters is not as straight-forward as it is for two-dimensional straight-walled diffusers

One of the first detailed studies was by Fox and Kline in 1962 [3]. They considered two-dimensional curved diffusers which have a circular arc centerline as shown in figure 4.

In the experiments performed, the length of the diffuser centerline measured from the throat to the exit, N, was kept constant for a range of N/W_1 values. The radius of curvature of the circular arc centerline was determined as a function of the turning angle, β, from the expression

$$R = \frac{360}{\beta}\frac{N}{2\pi} \tag{4}$$

This geometry was used since it was desired to have a plane-walled two-dimensional diffuser as the limiting geometry (as $\beta \rightarrow 0$) so that a direct comparison could be made.

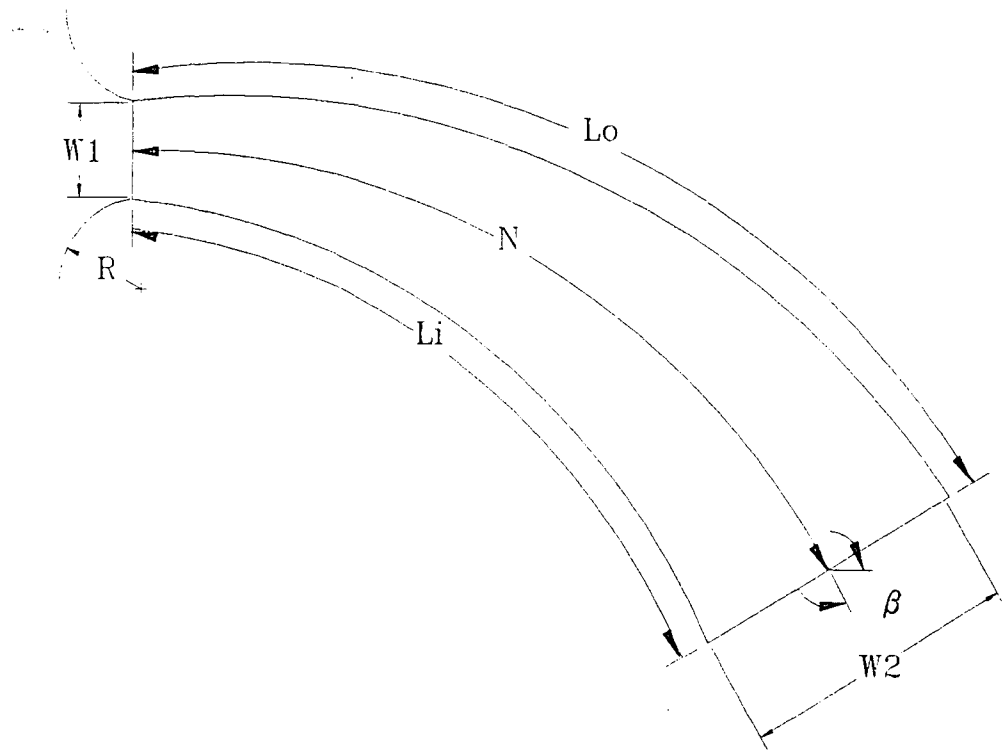

Figure 4: Two-dimensional curved diffuser geometry of reference [3]

Another study of curved two-dimensional diffusers was made in 1967 by Sagi and Johnson [12]. As shown in figure 5, five dimensionless parameters were required to describe these curved diffusers. They are: $(x_2-x_1)/W_1$, $(y_2-y_1)/W_1$, $AR=W_2/W_1$, $AS=b/W_1$ (where b denotes the diffuser depth) ,and $\Delta\beta$.

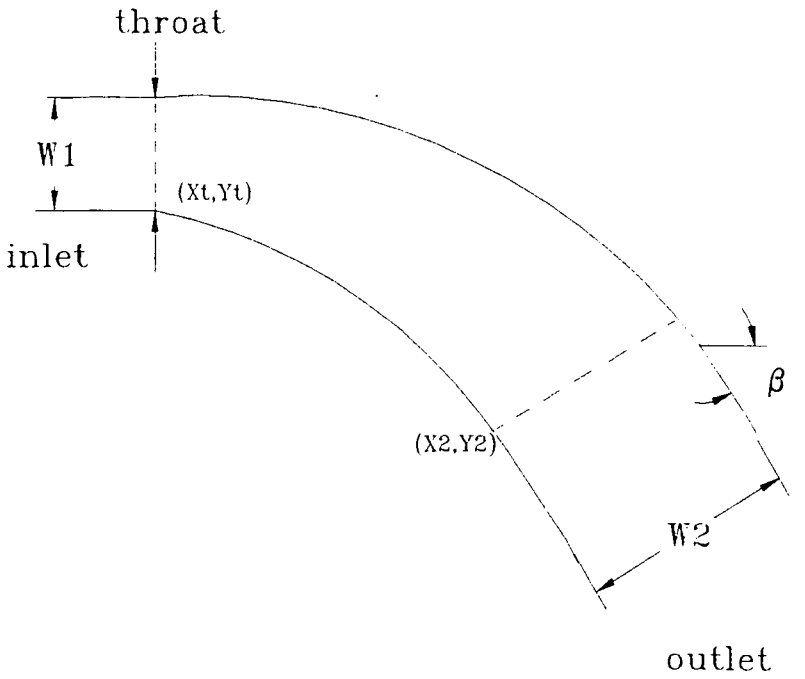

Figure 5: Two-dimensional curved diffuser geometry of reference [12]

3.1.3 ANNULAR DIFFUSERS

Very little information is available on annular curved diffusers, so only the straight-walled type will be considered. According to Sovran and Klomp [5], four parameters are required to specify the geometry of straight-walled annular diffusers. These are the outer and inner wall angles, ϕ_0 and ϕ_i, the inlet radius ratio, R_H/R_T, and the non-dimensional length, $L/\Delta R$ ($L = (Li+Lo)/2$). As shown in figure 6, the geometry of a straight-walled annular diffuser can be completely described using these parameters.

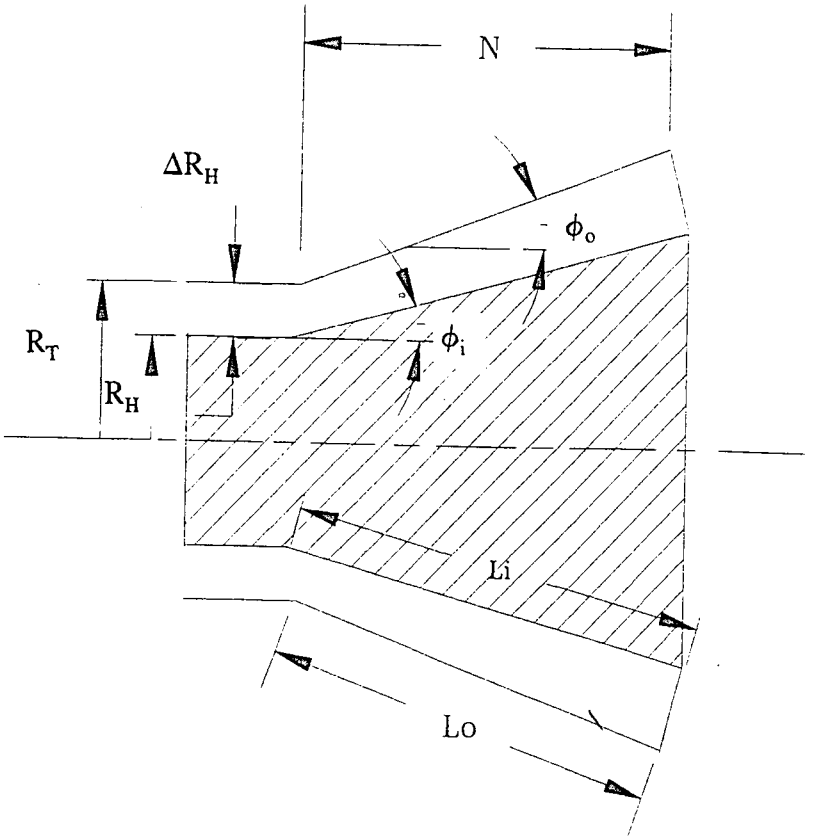

Figure 6: Annular straight-walled diffuser geometry

3.2 FLOW REGIMES

A diffuser flow regime has an important effect on the optimum operating conditions. Subsonic diffuser flow regimes have been classified according to the type of stall present [1,4]. Flow regime charts for two-dimensional straight-walled diffusers have been created using experimental results obtained by continuously increasing the diffuser divergence angle from zero degrees while holding the inlet flow conditions, the wall length, and throat width constant. Four major flow regimes were determined using flow visualization techniques. These are (refer to figures 7 and 8):

1) ***No appreciable stall regime*** (figure 7a) - This flow region is located below line a-a in figure 8. The diffuser geometry is characterized by small divergence angles and area ratios. The pressure and velocity profiles are symmetrical about the center plane and are relatively constant.

2) ***Large transitory stall regime*** (figure 7b) - Located in a region between line a-a and b-b in figure 8, this flow is erratic and is subject to large fluctuations. Also, large pressure fluctuations exist throughout the diffuser.

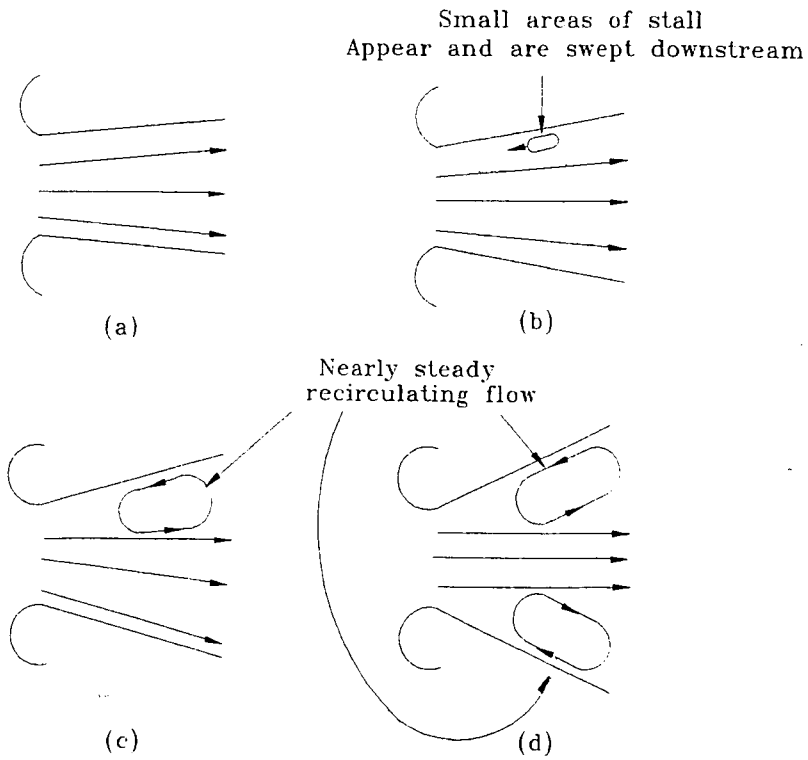

Figure 7: Four categories of flow regime: (a) no appreciable stall, (b) large transitory stall, (c) fully developed stall, (d) jet flow

3) ***Fully developed stall regime*** (figure 7c)- This steady two-dimensional stall region lies above line b-b in figure 8 and exists up to line c-c. The flow is separated near the

diffuser throat and follows one wall. Stall blocks a large fraction of available flow and thereby decreases the diffuser performance.

4) ***Jet flow regime*** (fig 7d) - This flow regime is located above line c-c and may exist down to line d-d shown in figure 8. The flow separates from both diverging walls near the diffuser throat and creates large stall areas. The velocity and pressure profiles are relatively steady.

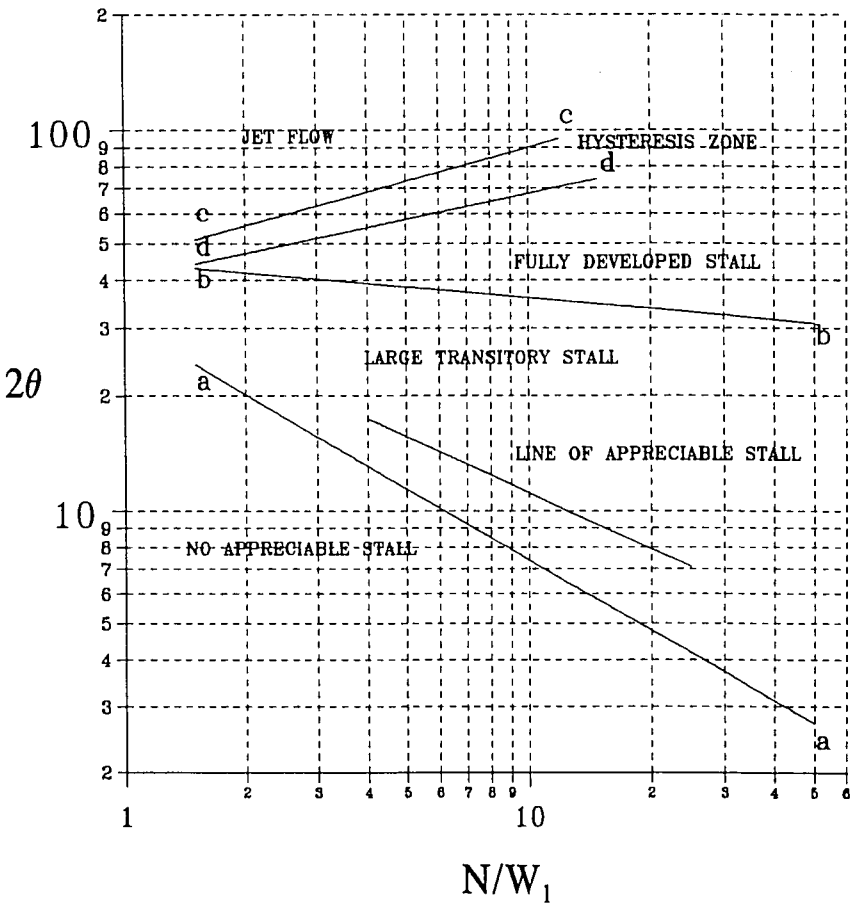

Figure 8: Two-dimensional straight-walled diffuser flow regime chart; 2θ-N/W_1 plane

The above discussion of flow regimes in two-dimensional straight-walled diffusers forms the basis for a study of flow regimes in curved diffusers. Curved

diffusers have been subjected to less systematic study than straight-walled diffusers. Important studies are reviewed below.

In 1962 Fox and Kline [3] performed an experimental study of curved diffusers using the circular arc centerline geometry shown in figure 4. The range of parameter N/W_1 covered was $3 \leq N/W_1 \leq 24$ and β, the turning angle, was varied between 0 and 90 degrees with ten degree increments. The investigation was performed to locate two lines of stall, the line of first appreciable stall (a-a) and the line indicating fully developed stall (b-b). These lines were compared to the location of those of the two dimensional straight-walled diffuser. The comparison is shown in figures 9(a) and 9(b).

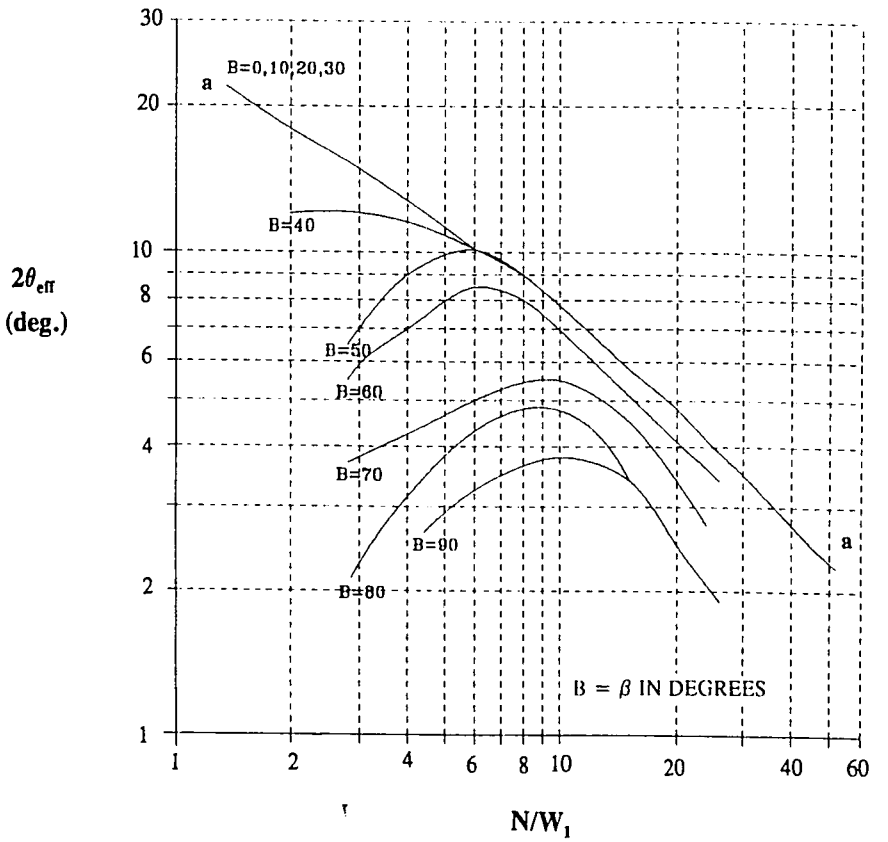

Figure 9: Two-dimensional curved diffuser flow regimes based on [3] (a) location of first appreciable stall line, a-a

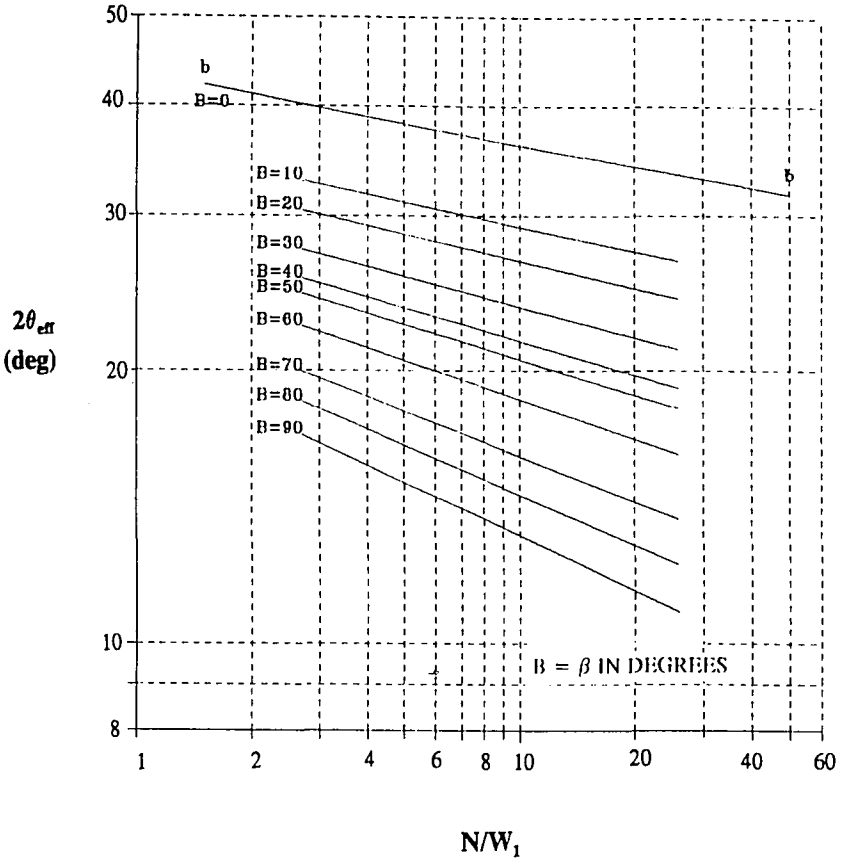

Figure 9: (b) location of transition to fully-developed stall, b-b

These plots were created by introducing the divergence angle of the diffuser, $2\theta_{eff}$,, using the relation

$$AR=1+2\frac{N}{W_1}\tan\theta_{eff} \qquad (6)$$

For straight two-dimensional diffusers, $\theta = \theta_{eff}$ since $\beta=0$.

Figure 9(a) shows the location of first appreciable stall (line a-a). On this figure, lines of constant angle β are drawn. The case where $\beta=0$ degrees is taken from the two-dimensional straight- walled diffuser performance plot. It is shown that for curved diffusers, the turning angle has no significant effect on line a-a for $\beta=30$ degrees or

less. For turning angles of $50 \leq \beta \leq 90$ degrees, all lines of first appreciable stall show a peak. To the right of this peak (higher values of N/W_1), the curves are approximately parallel but lie below line a-a for the two-dimensional plane-wall case.

Figure 9(b) indicates the location of the fully developed stall line (b-b). The stall occurs at decreasing divergence angle 2θeff as the turning angle β increases.

Studies by both Fox and Kline [3] and Sagi and Johnson [12] indicate the existence of a secondary flow above a certain angle within the curved diffusers presented in figures 4 and 5 (above 30 degrees for the curved diffuser shown in figure 4 and above 40 degrees for the diffuser of figure 5). This secondary flow is in the form of a long helical coil and is believed to contribute to a drop in performance and first stall limits of large turning angle curved diffusers [12]. These secondary motions also exist for curved ducts as indicated in reference [20] which is concerned with a flow which turns by 90 degrees in a curved duct with square cross-sections. Secondary motions observed were described as "rotational fluid phenomena" which were directly affected by inlet boundary layer thickness, turbulence intensity, and whether the flow is laminar or turbulent.

No flow regime charts exist for annular diffusers. Sovran and Klomp [5] indicated that the same general type of behavior that exists for straight-walled two-dimensional diffusers is to be expected for straight-walled annular diffusers.

3.3 INLET CONDITIONS

The inlet conditions of a diffuser can significantly affect its operation.

Turbulence, swirl, and boundary layer thickness can influence the flow regime, performance, and even the outlet velocity profile of the diffuser.

Sovran and Klomp [5] discussed a kinetic energy flux velocity profile parameter, α. If the static pressure is considered constant across a cross-section of an incompressible flow system, then the stagnation (or total) pressure can be expressed as

$$\overline{P_T} = P + \alpha \overline{q} \tag{7}$$

where $\overline{q}$ = dynamic pressure = $1/2\rho\overline{V}^2$ (the bar above the symbols refer to average values, $\overline{V}$ refers to the mass flow averaged velocity of a cross-section). The parameter α represents the ratio of the actual kinetic energy flux at a given cross-section to the minimum kinetic energy flux at the particular flow rate, that is, for uniform flow speed. Any velocity non-uniformity will make α greater than one, and it increases as the velocity nonuniformity increases. Using the expression

$$P_2 - P_1 = (\alpha_1 \overline{q_1} - \alpha_2 \overline{q_2}) - (\overline{P_{T1}} - \overline{P_{T2}}) \tag{8}$$

the diffuser effectiveness, η, can be represented as

$$\eta = \frac{\alpha_1 \left[1 - \frac{\frac{\alpha_2}{\alpha_1}}{AR^2}\right]}{\left[1 - \frac{1}{AR^2}\right]} - \frac{\frac{\overline{P_{T1}} - \overline{P_{T2}}}{\overline{q_1}}}{\left[1 - \frac{1}{AR^2}\right]} \tag{9}$$

This equation shows that if α increases through the diffuser due to velocity profile distortion ($\alpha_2/\alpha_1 > 1$) and/or if losses exist ($(\overline{P}_{T1} - \overline{P}_{T2})/ \overline{q}$) > 0), the resulting effectiveness, η, will have a value of less than one. Any increase in α through a

diffuser represents a reduction in the amount of diffusion.

3.3.1 THE EFFECT OF TURBULENCE

Several authors have discussed how an increase in turbulence at the entrance to a diffuser increases the performance. Hoffman and Gonzalez [6] tested two-dimensional straight-walled diffusers at angles of $2\theta = 9$ and 20 degrees. Turbulence was created at the diffuser inlet by rods placed in front of the entrance. Improvements in the pressure recovery were found. It was noted that, with turbulence, the separation of flow from diffuser walls was delayed and the centerplane velocity profiles were very symmetrical. On the other hand, without turbulence, separation was found on the walls of the diffuser and the velocity profiles were distorted.

Studies performed on conical and annular diffusers have also reported an increase in performance with increasing turbulence at the diffuser entrance. Stevens and Williams [21] researched annular diffusers and reported that increased turbulent mixing lowered the outlet blockage, and kinetic energy coefficient, α_2, which resulted in an increase in pressure recovery. Also, a marked improvement in the stability of the outlet flow was discovered with a turbulent inlet flow. The authors indicated that the presence of turbulence at the diffuser inlet resulted in up to 20% gain in pressure recovery with only small increases in total pressure loss.

Some curved channel and diffuser studies have shown that curvature has a large effect on turbulent mixing. In a curved section, turbulent mixing increases on the outer wall and helps to energize the outer wall boundary layer. However, the inner wall

experiences less turbulent mixing and therefore has a thicker boundary layer. It is reasonable to assume that any increase in turbulence intensity at the entrance of a curved diffuser will lead to an increase in performance as it does for two-dimensional straight-walled, conical, and annular diffusers.

Studies of curved ducts have also indicated that turbulence has a positive effect on pressure recovery. Taylor, Whitelaw, and Yianneskis [20] observed that more pronounced secondary flows were produced in laminar flows as opposed to turbulent flows. These secondary flows have a negative effect on pressure recovery.

3.3.2 THE EFFECT OF BOUNDARY LAYER THICKNESS

The maximum velocities at the diffuser inlet and outlet can be related by the concept of effective and blocked area [5]. The effective area, A_E, is the area which could pass the particular volume flow rate of the system if the velocity were uniform and equal to the maximum velocity in the cross-section. The blocked area, A_B, is the total cross-sectional area minus the effective area ($A_B = A - A_E$). Two new variables can be introduced:

$$E = \frac{A_E}{A} = 1 - B \leq 1 \tag{10}$$

where,

$$B = \frac{A_B}{A} \geq 0 \tag{11}$$

Through some manipulation, Sovran and Klomp [5] arrived at an expression for E as $E=U/\overline{V}$, where $\overline{V}$ is the mass flow averaged velocity of a cross-section and U is the maximum velocity of the cross-section. The effectiveness could then be expressed as:

$$\eta = \frac{1}{E_1^2} \frac{[1-\frac{(\frac{E_1}{E_2})^2}{AR^2}]}{[1-\frac{1}{AR^2}]} - \frac{\frac{(\overline{P_{T1}}-\overline{P_{T2}})}{\overline{q_1}}}{[1-\frac{1}{AR^2}]} \qquad (12)$$

Often the term $((\overline{P}_{T1}-\overline{P}_{T2})/\overline{q}1$ is small compared to the term representing the profile distortion (the first part on the right side of equation 9), so Sovran and Klomp concluded that the problem of many diffusers is insufficient diffusion rather than inefficient diffusion. Therefore, blockage due to the boundary layer thickness is mainly responsible for lowering the performance of a diffuser.

Many investigators have found that inlet boundary layer profile has only a slight effect on flow regime but a large effect on recovery and losses. The effect of boundary layer thickness on pressure recovery and losses has been reported for two-dimensional straight and curved wall diffusers and annular diffusers in references [1], [12], and [21].

A series of performance charts for two-dimensional straight-walled diffusers were created by Reneau, Johnson, and Kline [1] which showed the effect of an increasing boundary layer thickness on both pressure recovery and effectiveness. A wide range of geometries were investigated; $1.5 < N/W_1 < 25$, and $5 < 2\theta < 30$

degrees. These geometries were used to create performance charts with four nondimensional inlet boundary layer thicknesses, $2\delta_1^*/W_1$. These charts show that the recovery at a given geometry decreases when the inlet boundary layer is increased from thin to thick. Effectiveness charts are also included in reference [1] for the same set of inlet boundary layer thicknesses. The maximum value of effectiveness appears to decrease with an increase in the inlet boundary layer thickness.

The effect of curvature influences diffuser performance due to an undesirable inner wall boundary layer growth. This inner wall boundary layer is increased often by secondary flows off the end walls of the diffuser [12]. Reference [20] indicated that for curved ducts, the thickness of the boundary layer at the inlet to the duct has a direct effect on these secondary flows. A thinner entry boundary layer thickness will result in less pronounced secondary flows.

3.3.3 THE EFFECT OF SWIRL

In general, a swirling flow always exists at the exit of turbomachines. When diffusers are used in this location, the effect of swirl should be considered since it may have an effect on performance.

The effect of swirl on the performance of annular straight-walled diffusers was studied by Kumar and Kumar [17]. The conclusion reached was that a swirl generally increases the overall pressure recovery. This pressure recovery is more significant for stalled diffusers rather than unstalled diffusers. Swirl angles between 0 and 25 degrees were investigated.

McDonald, Fox, and Van Dewoestine [18] also indicated an increase in performance (measured as an increase in pressure recovery) of conical diffusers with a swirl at the diffuser entrance. However, they found that swirls at angles higher than optimum resulted in poorer performance. The work of reference [17] mentioned in the previous paragraph also observed the existence of an optimum swirl angle.

Very little literature is available on the effect of swirl in curved diffusers. Thayer [19] investigated the effect of swirl on curved-wall annular diffuser performance. The effect of swirl angle on pressure recovery at different Mach numbers with and without struts positioned in the diffuser was studied. The data obtained without struts indicated that a slight increase in the pressure recovery occurred for swirl angles between 0 and 20 degrees. However, the pressure recovery decreased for swirl angles between 20 and 30 degrees.

3.4 THE EFFECT OF MACH NUMBER

The effect of subsonic Mach number on performance of diffusers depends on the flow regime. For lower Mach numbers there is very little effect on performance and flow regime as long as there is no stall within the diffuser. Kline, Abbott, and Fox [15] have found that a flow through a two-dimensional straight-walled diffuser corresponding to the region below line a-a in figure 9 shows little change in performance with Mach number up to about 0.5. However, as the flow speed increases close to a Mach number of unity there is a sudden decrease in performance.

Nineteen conical diffuser geometries were tested by Van Dewoestine and Fox

[16]. In all cases tested the flow tended toward separation with increasing Mach number. The conclusions were correlated with flow regime in the following way:

- Below the line of first appreciable stall the flow showed a slight increase in performance as the Mach number is increased until choking is reached
- Close to the line of first appreciable stall line, performance is approximately constant until choking is reached
- Above the line of first appreciable stall the performance decreases with increasing Mach number

Thayer (ref. [19]) has found that the pressure recovery in curved wall annular diffusers without struts remained constant in the range of Mach numbers from 0.25 to 0.45. After six struts were installed in the diffuser, the pressure recovery generally decreased. The author indicated that decreased pressure recovery with struts in the diffuser was due partially to a small increase in blockage and partially due to an increase in the size of strut wakes with increasing Mach number.

3.5 PREDICTION OF PERFORMANCE

There is a relationship between the flow regime and the performance of a two-dimensional straight-walled diffuser. It has been reported by Reneau, Johnson, and Kline [1] and others that the peak pressure recovery occurs when the diffuser is lightly

stalled. The location of peak performance is just above the line of first stall (a-a) shown before in figure 8. Figure 10 indicates how pressure recovery, C_P, is generally related to flow regime.

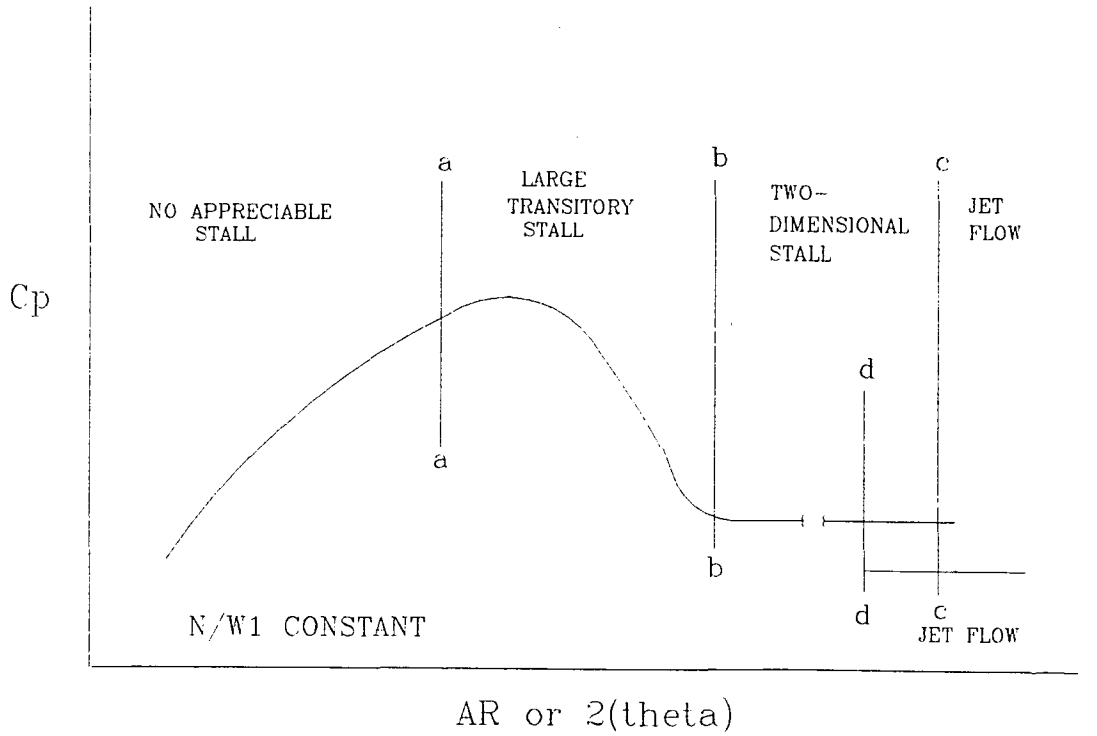

Figure 10: General relationship between flow regime and performance for two-dimensional straight-walled diffusers

Performance charts for two-dimensional straight-walled diffusers were produced by Reneau, Johnson, and Kline [1]. A typical performance chart with a low inlet boundary layer thickness is shown in figure 11. This chart indicates that the greatest pressure recovery occurs in two-dimensional straight-walled diffusers which are long and have large area ratios.

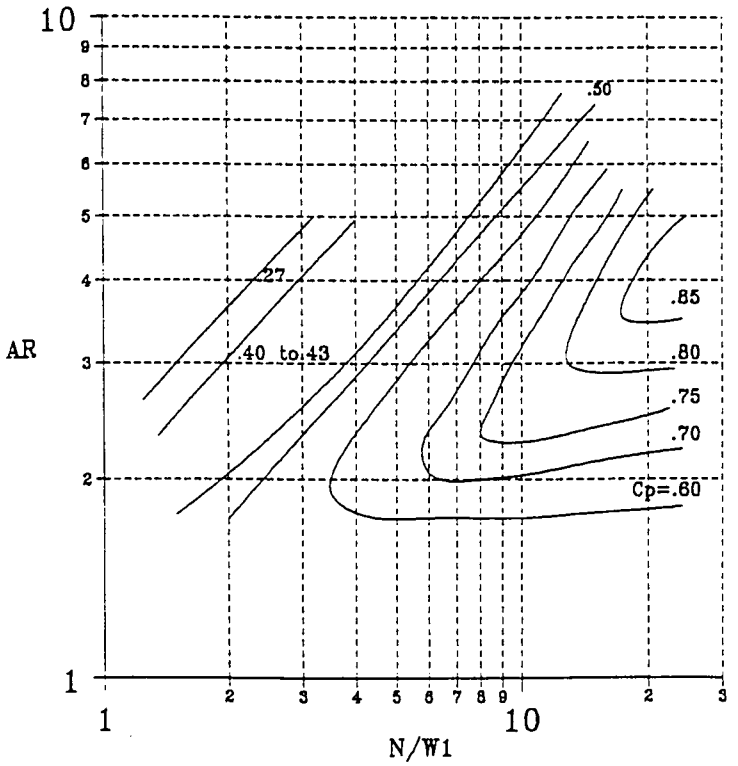

Figure 11: Performance chart for two-dimensional straight-walled diffusers according to reference [1]

It is not as easy to describe the performance of curved diffusers as it is for straight-walled diffusers. One of the major problems in predicting curved diffuser performance is that most of the published reports have used different curved diffuser designs. Information on curved diffusers can be found in references [12] and [24]. Reference [24] by Parsons and Hill, which is more recent than reference [12] by Sagi and Johnson, discusses a design method for curved diffusers which incorporates the prediction of the existing boundary layer within the diffuser.

In 1967 Sovran and Klomp [5] reported an investigation of annular straight-walled diffusers. Over 100 diffuser geometries were tested. An annular diffuser

performance chart based on their findings was created and is shown in figure 12. The authors also located two optimum diffuser performance lines, Cp* and Cp**, which are shown in the figure. Line Cp* represents the locus of points which define the diffuser area ratio producing maximum pressure recovery in a prescribed non-dimensional diffuser length. Line Cp** is the locus of points which define the diffuser non-dimensional length producing maximum pressure recovery at a prescribed area ratio. Sovran and Klomp have shown also that the area ratio and non-dimensional length are the factors which determine optimum diffuser geometry regardless of diffuser type.

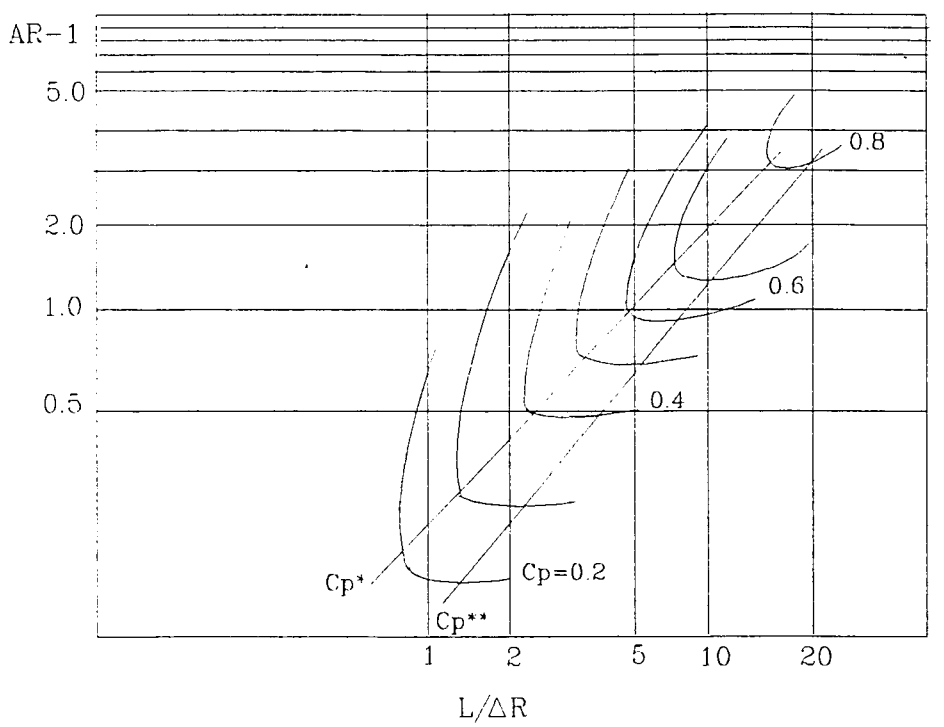

Figure12: Performance chart for annular straight-walled diffusers according to reference [5]

4 DEVELOPMENT OF EQUATIONS FOR EXHAUST HOOD LOSS

4.1 EXHAUST HOOD LOSS EQUATIONS

Figure 2 shows an enthalpy-entropy (h-s) diagram displaying the thermodynamic states of the working fluid as it leaves the last rotating blade of a turbine. This diagram is for an expanding exhaust hood, one in which the annulus average static pressure, P_{AN}, is higher than the average flange static pressure, P_{FL}. Indicated on this diagram are the defining components of the hood loss coefficient: the hood loss, HL (or the hood and condenser neck loss, (H+C)L), and the leaving loss, LL. Using these definitions and isentropic gas dynamic relations for an ideal compressible fluid (air), an analysis of exhaust hood performance can be made. This analysis allows the hood and hood and condenser neck loss coefficients to be determined from experimental measurements of annulus and flange static pressures, annulus total pressure and temperature, and annulus mass flow rate in a model exhaust hood. This methodology has been developed by Prof. J.A. Owczarek [7] and will be explained in this section of the report.

The hood and hood and condenser neck losses are the fluid frictional losses associated with the exhaust flow leaving the last rotating blade of the turbine. The hood loss, HL (or hood and condenser neck loss, (H+C)L) is defined as the isentropic enthalpy drop between the average annulus static pressure after the the last turbine blade and the average exit flange static pressure, see figure 2. This enthalpy difference can be expressed as

$$HL=h_1-h_2'=(h_T-h_2')-(h_T-h_1) \tag{13}$$

Since air is used as the working fluid and the difference between the total and static temperatures is low, the assumption of an ideal gas with constant specific heats can be made. Therefore

$$dh=C_p dT \tag{14}$$

where C_P = constant. Integrating equation (14) and combining with equation (13) results in the expression

$$HL=C_p T_T(1-\frac{T'^2}{T_T})-LL \tag{15}$$

because $h_T = h_{T,1} = h_{T,AN}$ and $h_1 = h_{AN}$.

The hood loss can be nondimensionalized using the leaving loss, LL. The leaving loss is defined as the kinetic energy of the fluid leaving the last stage blade, or

$$LL=\frac{1}{2}V_{AN}^2 \tag{16}$$

This loss represents fluid energy which cannot be converted into useful work by a turbine. As shown in figure 2, the leaving loss corresponds to the difference between the average total and static enthalpy in the annulus measured at constant entropy:

$$LL=\frac{1}{2}V_{AN}^2=h_{T,AN}-h_{AN}=h_T-h_1 \tag{17}$$

or,

$$LL=(h_{T,AN}-h_{AN})=c_P(T_{T,AN}-T_{AN}) \tag{18}$$

As a result,

$$LL=c_P T_{T,AN}(1-\frac{T_{AN}}{T_{T,AN}}) \tag{19}$$

Dividing equation (15) by equation (19) produces the non-dimensional hood loss coefficient:

$$\frac{HL}{LL}=\frac{c_P T_T(1-\frac{T_2'}{T_T})}{c_P T_T(1-\frac{T_{AN}}{T_{T,AN}})}-1 \tag{20}$$

Since, for an isentropic process,

$$\frac{T}{T_T}=(\frac{P}{P_T})^{\frac{\gamma-1}{\gamma}} \tag{21}$$

equation (20) can be written as

$$\frac{HL}{LL}=\frac{c_P T_T[1-(\frac{P_{FL}}{P_{T,AN}})^{\frac{\gamma-1}{\gamma}}]}{c_P T_T[1-(\frac{P_{AN}}{P_{T,AN}})^{\frac{\gamma-1}{\gamma}}]}-1 \tag{22}$$

Equation (22) can be rearranged to express the nondimensional hood loss coefficient as

$$\frac{HL}{LL}=\frac{(\frac{P_{AN}}{P_{T,AN}})^{\frac{\gamma-1}{\gamma}}-(\frac{P_{FL}}{P_{T,AN}})^{\frac{\gamma-1}{\gamma}}}{1-(\frac{P_{AN}}{P_{T,AN}})^{\frac{\gamma-1}{\gamma}}} \tag{23}$$

For an ideal gas with constant specific heats,

$$c_P T_T=c_P T+\frac{V^2}{2} \tag{24}$$

$$c_P=\frac{\gamma R}{\gamma-1} \tag{25}$$

Combining equations (24) and (25) results in

$$\frac{T_T}{T}=1+\frac{\gamma-1}{2}(\frac{u}{a})^2=1+\frac{\gamma-1}{2}M^2 \tag{26}$$

From equations (26) and (21), an expression for P/P_T can be formed:

$$\frac{P}{P_T}=(1+\frac{\gamma-1}{2}M^2)^{-\frac{\gamma}{\gamma-1}} \tag{27}$$

Equation (27) shows that one of the two terms which make up the definition of the non-dimensional hood loss coefficient (eq. 22),

$$(\frac{P_{AN}}{P_{T,AN}})^{\frac{\gamma-1}{\gamma}} \tag{28}$$

depends only on the Mach number. The second term in the non-dimensional hood loss coefficient,

$$(\frac{P_{FL}}{P_{T,AN}})^{\frac{\gamma-1}{\gamma}} \tag{29}$$

can be measured directly from air model tests, and depends on both the annulus Mach number and the Reynolds number of the working fluid. The air test Reynolds number in the exit annulus is so close to that of steam at the (L-0) blade in an actual turbine exhaust hood that $P_{FL}/P_{T,AN}$ is only considered to be a function of Mach number (at $M_{AN}=0.6$, $Re_{STEAM}=12.3x10^5$, and $Re_{AIR}=4.5x10^5$). Therefore, the hood loss coefficient, HL/LL, can be considered a function of Mach number only,

$$\frac{HL}{LL}=f_1(M_{AN}) \tag{30}$$

The dimensionless hood loss coefficient can be obtained graphically at various annulus Mach numbers, M_{AN}, by plotting the variation with Mach number the terms

$$(\frac{P_{AN}}{P_{T,AN}})^{\frac{\gamma-1}{\gamma}},(\frac{P_{FL}}{P_{T,AN}})^{\frac{\gamma-1}{\gamma}} \tag{31}$$

as shown in appendix A, or by calculations.

An alternative measurement of exhaust hood performance can be made using the dimensionless pressure coefficient, C_P1

$$C_P1=\frac{P_{AN}-P_{FL}}{[\frac{\rho V^2}{2}]_{AN}} \tag{32}$$

It represents the non-dimensional difference between the average annulus static pressure at the last rotating blade and the average flange static pressure.

In tests, twelve static pressures were measured on both the hub and shroud of the models to determine, by interpolation, the annulus static pressure at each point of total pressure measurement. This was also done to get an idea of the magnitude of the last stage blade excitation which occurs as a result of circumferential pressure variation in the last stage annulus. These pressures are put in the form of a non-dimensional local pressure coefficient, $C_P1,_{LOCAL}$:

$$C_P1,_{LOCAL}=\frac{P_{AN,LOCAL}-P_{FL}}{[\frac{\rho V^2}{2}]_{AN}} \tag{33}$$

The pressure coefficient C_P1 of equation (32) has a value which is close to that of the hood loss coefficient. This is so because of the following reason: From the First

Law of Thermodynamics,

$$Tds = de + Pdv \tag{34}$$

also, from the definition of enthalpy

$$h = e + Pv \tag{35}$$

Differentiating equation (35) and combining with equation (34) gives

$$Tds = dh - vdP = dh - \frac{1}{\rho}dP \tag{36}$$

At constant entropy,

$$\frac{P_{AN} - P_{FL}}{\rho^{FL}_{AN}} \cong h_{AN} - h_{FL} = h_1 - h_2' = HL \tag{37}$$

where ρ^{FL}_{AN} represents the average fluid density between the annulus and the flange of the exhaust hood.

The equation for C_P1 (eq. 32) can be transformed so that it can be calculated from experimentally measured values of P_{AN}, P_{FL}, $P_{T,AN}$, and M_{AN} [10]. As a result,

$$\frac{HL}{LL} = \frac{P_{AN} - P_{FL}}{\rho^{FL}_{AN}\frac{V^2}{2}} \cong C_P1 = \frac{P_{AN} - P_{FL}}{\left[\frac{\rho V^2}{2}\right]_{AN}} \tag{38}$$

Using the relation,

$$\frac{\rho V^2}{2P_T} = \frac{\gamma M^2}{2}\left(1 + \frac{\gamma - 1}{2} M^2\right)^{-\frac{\gamma}{\gamma - 1}} \tag{39}$$

the pressure coefficient C_p1 can be expressed as

$$C_p1 = \frac{\frac{P_{AN}}{P_{T,AN}} - \frac{P_{FL}}{P_{T,AN}}}{\frac{\gamma M_{AN}^2}{2}\left(1 + \frac{\gamma - 1}{2} M_{AN}^2\right)^{-\frac{\gamma}{\gamma - 1}}} \tag{40}$$

The hood loss can also be expressed as the dimensionless pressure coefficient

$$C_p2 = \frac{P_{AN} - P_{FL}}{P_{T,AN} - P_{AN}} \tag{41}$$

For an incompressible flow, $C_p1 = C_p2$. Upon analyzing the test data, in addition to the hood loss coefficient, both pressure coefficients, C_p1 and C_p2, were calculated for each test.

Another variable of interest is the non-dimensional mass flow rate. It can be expressed as:

$$\frac{W\sqrt{RT_{T,AN}}}{A_{AN} P_{T,AN}} = \sqrt{\gamma} M_{AN}\left(1 + \frac{\gamma - 1}{2} M_{AN}^2\right)^{\frac{\gamma + 1}{2(\gamma - 1)}} \tag{42}$$

This value of the dimensionless mass flow rate for various Mach numbers is listed in gas tables such as the one shown in appendix C for $\gamma = 1.4$.

A summary of the equations discussed up to this point is shown in table 1.

TABLE 1 : Dimensionless Hood Loss, Pressure Coefficient, and Mass Flow Equations

Equation	Description	Equation #
$$\frac{HL}{LL}=\frac{(\frac{P_{AN}}{P_{T,AN}})^{\frac{\gamma-1}{\gamma}}-(\frac{P_{FL}}{P_{T,AN}})^{\frac{\gamma-1}{\gamma}}}{1-(\frac{P_{AN}}{P_{T,AN}})^{\frac{\gamma-1}{\gamma}}}$$	Hood Loss Coefficient	**(23)**
$$C_P1=\frac{\frac{P_{AN}}{P_{T,AN}}-\frac{P_{FL}}{P_{T,AN}}}{\frac{\gamma M_{AN}^2}{2}(1+\frac{\gamma-1}{2}M_{AN}^2)^{-\frac{\gamma}{\gamma-1}}}$$	Pressure Coefficient (first definition)	**(40)**
$$C_P2=\frac{P_{AN}-P_{FL}}{P_{T,AN}-P_{AN}}$$	Pressure Coefficient (second definition)	**(41)**
$$C_P1_{,LOCAL}=\frac{P_{AN,LOCAL}-P_{FL}}{[\frac{\rho V^2}{2}]_{AN}}$$	Local Pressure Coefficient (using first definition)	**(33)**
$$\frac{W\sqrt{RT_{T,AN}}}{A_{AN}P_{T,AN}}=\sqrt{\gamma}M_{AN}(1+\frac{\gamma-1}{2}M_{AN}^2)^{\frac{\gamma+1}{2(\gamma-1)}}$$	Mass Flow Rate	**(42)**

4.2 MASS-AVERAGING TECHNIQUE

Mass flow-weighted averages were calculated to determine the average values of ($P_{T,AN}$), (P_{AN}), and ($P_{AN}/P_{T,AN}$) in the exhaust hood model annulus. This process was introduced in reference [10] and will be described below.

Seven traverses were used to collect 217 total pressure values (31 points for each traverse spaced .05 inch apart). The static pressure in the annulus was assumed to vary linearly between the values measured at the hub and shroud.

The mass flow averaged total pressure was found using the equation

$$P_{T,AN} = \frac{\int (P_{T,AN} \rho V)_i dA}{\int (\rho V)_i dA} \tag{43}$$

or

$$P_{T,AN} = \frac{\int (P_{T,AN} \frac{W}{A_{AN}})_i dA}{\int (\frac{W}{A_{AN}})_i dA} = \frac{\int (P_{T,AN}) f(r)_i dr}{\int f(r)_i dr} \tag{44}$$

where: r = annulus radius
W = mass flow rate
$(P_{T,AN})_i$ = total pressure at each traverse point
$f(r)_i dr = (W/A_{AN})_i dA$

The value in the denominator of equation (44) represents the total mass flow rate.

The integration was performed using Simpson's Rule by which an integration can be performed using the following equation: For n points, the integral between a and b can be found numerically from the equation

$$\int f(x)dx = \frac{h}{3}\{f(x_1) + 4f(x_2) + \cdots + 2f(x_{n-2}) + 4f(x_{n-1}) + f(x_n)\} \quad \textbf{(45)}$$

where h=(b-a)/(n). In this work, n (the number of sub-intervals) = 30 and (b-a) = 1.5 inches; therefore, h = .05.

The integral desired for finding total pressure is

$$\int (P_{T,AN}\frac{W}{A_{AN}})_i dA \quad \textbf{(46)}$$

The differential area dA=(2πr/12)dr because the annulus is divided into twelve equal sections, as shown in figure 13. Since no swirl is introduced into the flow, the values of P_{AN}, $P_{T,AN}$ and $(P_{AN}/P_{T,AN})$ for area segments 8,9,10,11, and 12 correspond to area segments 4,2,1,6, and 5 respectively.

Simpson's Rule can be used to find the integral

$$\int (\frac{W}{A_{AN}})_i \frac{2\pi r_i}{12} dr \quad \textbf{(47)}$$

By combining the equation for the non-dimensional mass flow rate, equation (42), and the equation

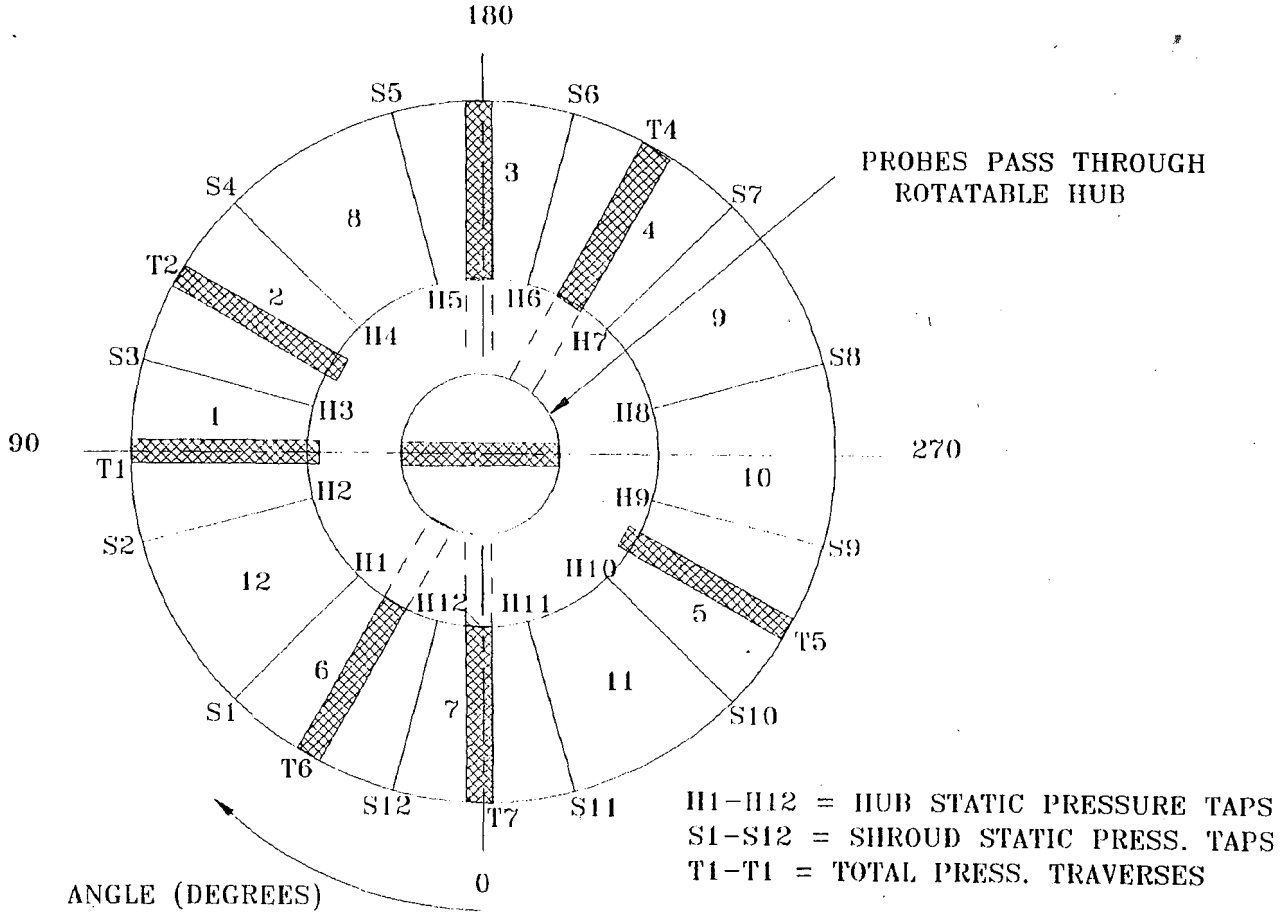

Figure 13: Location of total pressure traverses and static pressure taps

$$M_{AN}=[\frac{2}{\gamma-1}[(\frac{P_{T,AN}}{P_{AN}})^{\frac{\gamma-1}{\gamma}}-1]]^{\frac{1}{2}} \quad (48)$$

an expression for W/A_{AN} can be formed:

$$\frac{W}{A_{AN}}=\frac{P_{T,AN}}{\sqrt{RT_{T,AN}}}\sqrt{\frac{2\gamma}{\gamma-1}[(\frac{P_{AN}}{P_{T,AN}})^{\frac{2}{\gamma}}-(\frac{P_{AN}}{P_{T,AN}})^{\frac{\gamma+1}{\gamma}}]} \quad (49)$$

Substituting in the values of $\gamma=1.4$ and $R=53.35$ $lb_f ft/lb_m °R$ for air into equation (49) and simplifying results in the equation

$$(\frac{W}{A_{AN}})_i=111.8273\frac{(P_{T,AN})_i}{\sqrt{T_{T,AN}}}\sqrt{7[(\frac{P_{AN}}{P_{T,AN}})_i^{\frac{2}{1.4}}-(\frac{P_{AN}}{P_{T,AN}})_i^{\frac{2.4}{1.4}}]} \quad (50)$$

where W/A_{AN} is in units of lb_m/ft^2sec, $P_{T,AN}$ in psi_a and $T_{T,AN}$ in R. The expression for $f(r)_i$ becomes

$$f(r)_i=111.8273\frac{(P_{T,AN})_i}{\sqrt{T_{T,AN}}}\sqrt{7[(\frac{P_{AN_i}}{P_{T,AN_i}})^{\frac{2}{1.4}}-(\frac{P_{AN_i}}{P_{T,AN_i}})^{\frac{2.4}{1.4}}]}\ [\frac{2\pi r_i}{12}] \quad (51)$$

The average annulus static pressure is found similarly. In this case

$$P_{AN} = \frac{\int (P_{AN} \frac{W}{A_{AN}}_i) \, dA}{\int (\frac{W}{A_{AN}}_i) \, dA} \tag{52}$$

or,

$$P_{AN} = \frac{\int (P_{AN})_i f(r)_i dr}{\int f(r)_i dr} \tag{53}$$

The average annulus pressure ratio is also found in the same manner

$$\frac{P_{AN}}{P_{T,AN}} = \frac{\int (\frac{P_{AN}}{P_{T,AN}})_i f(r)_i dr}{\int f(r)_i dr} \tag{54}$$

Table 2 summarizes the equations used to calculate the average values of P_{AN},$P_{T,AN}$, and $P_{AN}/P_{T,AN}$ using Simpson's rule.

TABLE 2: Equations used to find the mass flow-weighted values of P_{AN}, $P_{T,AN}$, and $P_{AN}/P_{T,AN}$

Equation	Calculated Value	Equation #
$P_{T,AN}=\frac{\int (P_{T,AN})_i f(r)_i dr}{\int f(r)_i dr}$	Average annulus total pressure	**(44)**
$P_{AN}=\frac{\int (P_{AN})_i f(r)_i dr}{\int f(r)_i dr}$	Average annulus static pressure	**(53)**
$\frac{P_{AN}}{P_{T,AN}}=\frac{\int (\frac{P_{AN}}{P_{T,AN}})_i f(r)_i dr}{\int f(r)_i dr}$	Average annulus pressure ratio	**(54)**

$$f(r)_i=111.8273\frac{(P_{T,AN})_i}{\sqrt{T_{T,AN}}}\sqrt{7[(\frac{P_{AN_i}}{P_{T,AN_i}})^{\frac{2}{1.4}}-(\frac{P_{AN_i}}{P_{T,AN_i}})^{\frac{2.4}{1.4}}]}\ [\frac{2\pi r_i}{12}]$$

4.3 CALCULATION OF MASS FLOW RATE THROUGH THE VENTURI METER

The mass flow rate through the venturi meter was calculated using the following variables [25]:

- C = discharge coefficient
- F_a = thermal expansion factor
- ρ_1 = corrected density at meter inlet corrected for specific humidity (lb_m/ft^3)
- ρ_d = density of dry air (lb_m/ft^3)
- ΔP = pressure drop across the venturi
- P_{ATM} = atmospheric pressure (psia)
- P_g = saturated water vapor pressure (psia)
- P_V = water vapor pressure (psia)
- P_{VI} = venturi meter inlet pressure (psig)
- S = specific humidity
- T_{ATM} = atmospheric temperature (°F)
- T_{DB} = dry bulb temperature (°F)
- T_{VI} = venturi meter inlet temperature (°F)
- Y = compressibility expansion factor
- W = Calculated mass flow rate through venturi (lb_m/s)

- Φ = relative humidity
- β = venturi throat diameter to pipe diameter ratio (=0.5281)

The mass flow rate through the venturi was calculated from the equation

$$W(\frac{lb_m}{\text{sec}}) = 45.285 \cdot C \cdot Y \cdot Fa \cdot \sqrt{\rho_1(\frac{lb_m}{ft^3}) \cdot \Delta P(psi)} \quad (55)$$

The variables within this equation are calculated as follows:

Using average values of Φ (relative humidity), T_{DB}, and T_{ATM} recorded in the laboratory for each test, the atmospheric pressure in psia was first calculated. P_{ATM} was found by the expression

$$P_{ATM}(psia) = P_{ATM}(\text{in. Hg}) \text{ x Specific weight of Hg @ } T_{ATM}(psia)$$

Once P_{ATM} was found, the specific humidity, S, could be calculated using

$$S = .622 \frac{P_V}{P_{ATM} - P_V} \quad (56)$$

In the above equation, P_V is derived from the expression for the relative humidity

$$\Phi = \frac{P_V}{P_g} \quad (57)$$

where P_g is found from the steam tables at the dry bulb temperature, T_{DB}.

The average reading of P_{VI} (psig) was then taken from the raw data sheets and converted to psia by adding it to P_{ATM}. The venturi inlet temperature, T_{VI}, was also taken from the raw data sheet and converted to degrees Rankine (°R = °F + 459.67).

Next, the density at the inlet to the venturi meter was determined from

$$\rho_1 = (1+S)\frac{P_{ATM}-P_{VI}}{P_{ATM}}\rho_d \qquad (58)$$

where

$$\rho_d = \frac{P_{atm}}{R_{AIR}T_{ATM}} = \frac{P_{ATM}(psia)}{53.35[\frac{lb_f \cdot ft}{lb_m \cdot °R}]T_{VI}(°R)} \qquad (59)$$

Therefore, the expression for the density at the inlet to the venturi meter is

$$\rho_1 = 2.6991(1+S)\frac{(P_{ATM}-P_{VI})}{T_{VI}} \qquad (60)$$

The pressure drop across the venturi, ΔP, was converted to psia from inches of water using the chart shown in appendix C:

$$\Delta P(psia) = \Delta P_{VENT}(in.\ H_2O) \times \text{conversion factor}(lb_f/in^3 H_2O)$$

The value of C, the discharge coefficient for the venturi meter is given in appendix C as .9989. This value depends on the pipe Reynolds number but is constant for the Reynolds number range of the exhaust hood loss model tests.

Next, the value of the thermal expansion factor, Fa, was found from

$$Fa = 1 + .00001393(T_{VI} - 528) \qquad (61)$$

which is valid for the steel piping surrounding the venturi.

The compressibility expansion factor, Y, was taken from the graph which can

be found in reference [25] and is reproduced in appendix C.

5 PROCEDURE FOR TESTING AND ANALYSIS OF THE TEST DATA

5.1 EXPERIMENTAL PROCEDURE

Before testing, the exhaust hood model was secured in place and the necessary Tygon® tubing connections were made. The five total pressure probes for traverses 1 through 5 (see figure 13) were positioned at the annulus shroud and the passage hole in the hub was closed. (The passage hole allowed the 1/8" Kiel probes to pass through the hub so total pressure could be measured along traverses six and seven.)

For each exhaust hood model test, four data sheets were prepared. Sample test data sheets are shown in appendix D. Meanwhile, the compressor was started to allow its temperature to stabilize. The raw data was collected using the procedure which follows.

The first step in the experiment was to take the initial reading of the test room and venturi conditions. These include:

- Barometric pressure of the test room (inches of Hg)
- Barometric temperature of test room (°F)
- Dry and wet bulb temperatures (°F) - Relative Humidity (%)
- Temperature of the air at inlet to venturi (°F)
- Pressure of the air at inlet to venturi (psig)
- Change in pressure across venturi meter (inches of H_2O)
- Temperature of air at inlet to the model(°F)
- Compressor discharge temperature (°F)

The above values were recorded on the first raw data sheet and the readings were repeated several times throughout the test.

The next step was to record the static pressure at the exit flange (or condenser neck) on data sheet number two. The static pressure taps were connected by Tygon® tubing to a Scanivalve® signal conditioner having a range of 2.5 psid. A Fluke® 75 series II Analog/Digital multimeter was used to read the static pressure in volts from the signal conditioner. Twenty-eight static pressure values were recorded for the Hatfield Ferry exit flange and the Beaver Valley and Hatfield Ferry condenser necks. These flange static pressure readings were repeated at the end of each test.

The 12 static pressures at the hub and shroud and the four upstream pipe (US) static pressures were measured and recorded on data sheet #3. The signal conditioner having a range of 15 psid and the same type of multimeter previously mentioned was used to read pressure values in volts. The readings of these static pressures were again taken at the end of each test.

The total pressure was measured along seven traverses (see figure 13). Using Rotadata® traversing equipment (one main control unit and five actuators), the 1/8" Kiel probes recorded 31 total pressure values at .05 inch intervals. The probe was moved initially .025 inches inward radially to bring the probe holes to the shroud wall. Like the hub and shroud static pressures the signal conditioner having a range of 15 psid was used with the same multimeter. The main control unit was connected to traverse number one and the Kiel probe was positioned at the annulus shroud. The total pressure at 31 points were then measured in volts. This process was continued for traverses

2,3,4, and 5. After the fifth traverse measurements were read, a passage hole in the hub was opened to enable the probe for traverse number four to pass through the center of the annulus and record total pressure values along the path of traverse number six (see figure 13). This process was repeated for traverse number seven using the probe used for traverse number three.

A test was finished when all the static and total pressures and instrument readings were filled in on the data sheet. The compressor speed would then be changed to produce a different flow Mach number within the annulus and a new test started.

Both the Beaver Valley and Hatfield Ferry original model hoods were studied and their hood loss curves were produced. Four sets of tests were performed for each model; 1) hood alone, with screen, 2) hood alone, without screen, 3) hood with condenser neck, with screen, and 4) hood with condenser neck, without screen. These original hood loss curves were used to evaluate the relative performance of the same hoods with internal modifications.

5.2 ANALYTICAL PROCEDURE

The following raw data was collected for each hood test:

- 28 static pressures at the exit flange measured in volts
- 12 hub and shroud static pressure readings measured in volts
- 31 total pressure values measured in volts for each of seven traverses
- test room and venturi meter operating conditions

The computer package Quatro Pro® was used to create a spreadsheet which would process the desired results. Data could be transported from Quatro Pro® into the computer package Grapher® so total pressure traverse curves could be obtained without having to re-enter the many total pressure values.

Before any experimental testing was done, the equipment in the laboratory was calibrated. The multimeter reading voltage from the 2.5 psid signal conditioner was calibrated first. The gage pressures corresponding to a range of possible voltage values were recorded. One volt corresponds to approximately 0.5 psig as shown on the calibration curve #1 shown in appendix C. The 15 psid signal conditioner was calibrated in the same manner. In this case 1 volt corresponded to approximately 3 psig as shown on the calibration curve #2 (appendix C).These calibration curves were used to convert all voltage values assigned to the raw data into psig values. This process was programmed into the spreadsheet.

The raw data was entered onto the spreadsheet as follows:

(1) The average values of the test room and venturi meter conditions (raw data sheet #1) were entered. From these values, the mass flow rate through the venturi meter was calculated as explained earlier in this section.

(2) The flange static pressure values (in volts) were typed in. These numbers were converted to psig using the 2.5 psid calibration curve. A numeric average of the 28 static pressure values was calculated which was added to P_{ATM} to arrive at the flange static pressure in psia.

(3) The 12 hub and 12 shroud static pressures were entered. These pressures

were converted to psig using the 15 psid calibration curve. From these 24 pressures, a static pressure was determined for each of the corresponding 217 total pressures measured (7 traverses, each with 31 points). The static pressure was linearly interpolated between corresponding hub and shroud pressures. Since the static pressure taps were located at circumferential locations between the total pressure traverses, an average between the static pressure traverse values on either side of the total pressure values was taken. For example, for the total pressure traverse number 1 (denoted as T1 in figure 13) the 31 static pressures were found by averaging the linearly interpolated static pressures corresponding to taps 2 & 3).

(4) The 217 total pressure points were entered on the spreadsheet and were converted to psig using the 15 psia calibration curve.

Once the raw data was entered, the hood (or hood and condenser neck) loss coefficient, HL/LL, and the pressure coefficients, C_P1 and C_P2, were calculated. Two methods of evaluation were used. One was based on calculated average total and static pressure in the annulus and the other was based on the calculated mass flow rate through the venturi meter.

5.2.1 METHOD 1: RESULTS BASED ON AVERAGE $P_{T,AN}$ AND P_{AN}

A pressure ratio $(P_{AN}/P_{T,AN})_i$ was calculated at each of the 217 traverse points. At the hub and shroud of the annulus, $P_{T,AN}$ was taken as P_{AN} since the velocity was assumed to be zero there (so $(P_{AN}/P_{T,AN})_i = 1$ at these points). This pressure ratio at each point along with the measured values of total pressure and linearly interpolated

values of static pressure were used to find the mass flow-weighted averages of total pressure, static pressure, and pressure ratio using Simpson's rule and equations (44), (53) and (54), respectively. From these average values, the hood loss or hood and condenser neck loss, C_P1, C_P2, and the flow Mach number were calculated using equations (23), (40), (41), and (48), respectively.

Using equation (34) the local pressure coefficient was calculated for both the 12 hub and shroud static pressures. These values were used to determine the values of the C_P at each tap location and to produce the curves of appendix H.

5.2.2 METHOD 2: RESULTS BASED ON THE MASS FLOW RATE THROUGH THE VENTURI

The mass flow rate through the venturi was calculated using the method explained earlier in this section of the report. This mass flow rate value was used, along with the annulus total temperature, the annulus area, and the total pressure (calculated as explained in method #1) to find the value of the term

$$\frac{W\sqrt{RT_{T,AN}}}{A_{AN}P_{T,AN}}$$

This value is listed in air tables (appendix C) which gives the corresponding annulus Mach number based on equation (42).

The average annulus pressure ratio was then found using equation (48). Multiplying the average annulus pressure ratio by the average annulus total pressure, the average annulus static pressure was calculated.

Having the values of P_{AN}, $P_{T,AN}$ and $(P_{AN}/P_{T,AN})_i$, the hood loss or hood and condenser neck loss coefficient, HL/LL or (H+C)L/LL, and the pressure coefficients, C_P1, and C_P2, could be determined.

Sample test calculations are presented in Appendix D.

6 LABORATORY SETUP AND MODEL DESCRIPTIONS

6.1 TEST LOOP

Figure 14 shows a diagram of the air test loop used in the exhaust hood model testing. This test loop was designed and assembled at Lehigh University. A detailed description of its design can be found in reference [11].

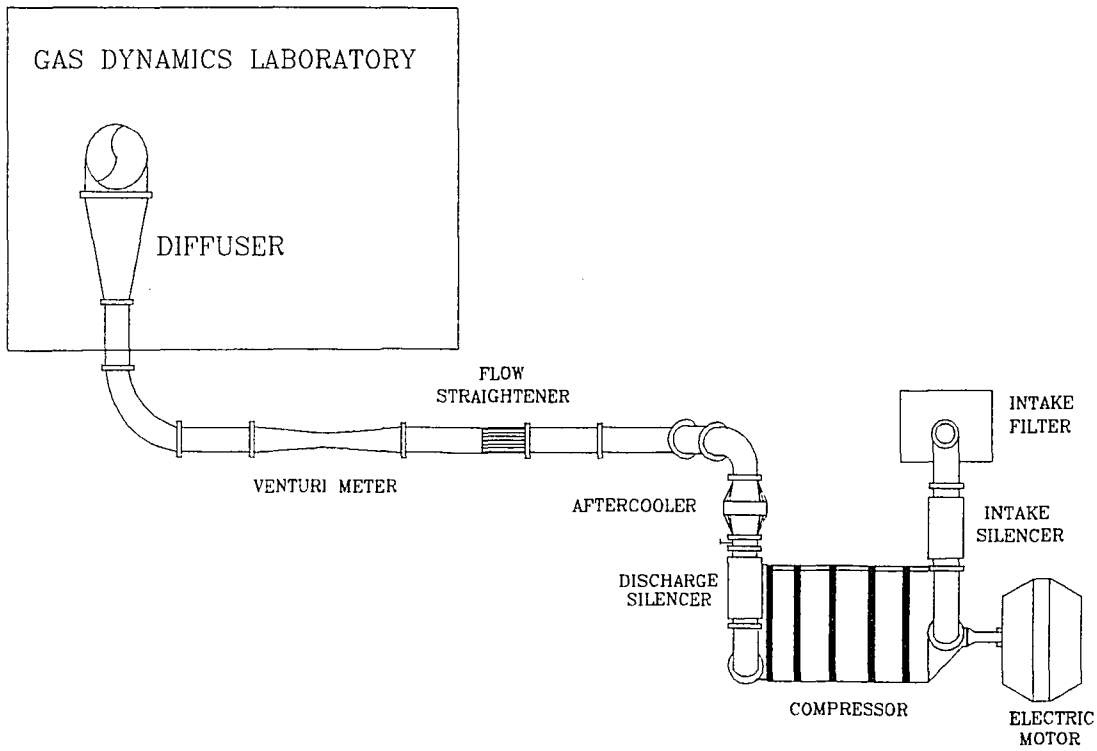

Figure 14: Air test loop used in exhaust hood model testing

A Hoffman model 67106A compressor provided up to 10,000 scfm of flow at 12.5 psig. The compressor was driven by a three-phase electric motor which had a capacity of 800 horsepower at 3600 RPM. Air was taken through an inlet filter,

traveled through an intake silencer, entered the compressor, then the air left the compressor through a discharge silencer.

Subsequently, the compressed air entered an aftercooler which decreased its the temperature to approximately 100 degrees F. The air then traveled through a 36" long flow straightener and entered an ASME standard Venturi meter. The Venturi had a diameter ratio of .5281 and was designed to produce a differential pressure of 20 inches of water at a maximum flow rate of 11,000 scfm, with a coefficient of discharge of 0.995. A water filled U-tube manometer was used to measure the static pressure difference between the inlet and throat of the meter.

The test loop was carefully designed to produce a uniform flow at the inlet to the model hood. The flow leaving the venturi meter made a 90 degree turn through a large radius elbow and entered a diffuser with an area ratio of 1.78 with the pipe diameter increasing from 1.5 feet to 2 feet. The air was then directed through an upward 90 degree elbow in which turning vanes created a uniform flow. The change in pressure across the elbow was calculated to be 0.034 psi at maximum flow rate [11]. Before reaching the model, the air entered a contraction duct with a contraction ratio of 16 along a length of 19.3 inches.

The exhaust hood model was situated above the contraction duct. The air flowed from the outlet of the duct and over the bullet nose of the model and into the model annulus. It was then turned by 90 degrees and flowed out of the model through the condenser flange.

6.2 EXHAUST HOOD MODELS

6.2.1 GOVERNING GEOMETRIC PARAMETERS

An analysis of the geometry of LP turbine exhaust hoods involves the use of the following dimensionless parameters which define the geometry and relative exhaust hood size[23]:

$$\frac{R_H}{L_B} = \frac{last\ blade\ root\ radius}{last\ blade\ height\ (annulus\ height)}$$

$$\frac{H}{L_B} = \frac{hood\ height}{last\ blade\ height}$$

$$\frac{B_L}{L_B} = \frac{hood\ length}{last\ blade\ height}$$

$$\frac{D}{L_B} = \frac{hood\ width}{last\ blade\ height}$$

$$\frac{A_A}{B_L} = \frac{annulus\ advance}{hood\ length}$$

$$\frac{A_{CF}}{\frac{1}{2}A_{AN}} = \frac{centerline\ flange\ open\ area}{\frac{1}{2}(annulus\ area)}$$

$$\frac{A_{FL}}{A_{AN}} = \frac{condenser\ flange\ open\ area}{annulus\ area}$$

$$\frac{A_{FL,EFF}}{A_{AN}} = \frac{effective\ flange\ open\ area}{annulus\ area}$$

An experimental study which would investigate the effect of all of the above parameters would be a long, difficult and expensive task. Fortunately, in large steam turbines, a few of the parameters change very little from one design to another. For example, R_H/L ranges only from 1.0 to 1.3, A_A/B_L ranges between 0.3 and 0.5, and B_L/L_B can be found to be 4.0 to 4.6.

The parameter $A_{CF}/(1/2\ A_{AN})$ indicates whether or not the flow from the upper half of the annulus can diffuse. Using figure 15 , the parameter $A_{CF}/(1/2\ A_{AN})$ can be expressed as:

$$\frac{A_{CF}}{\frac{1}{2}A_{AN}} \cong \frac{[D-2(L_B+R_H)]B_L}{\frac{1}{2}\pi(2RH+L_B)L_B} = \frac{2[\frac{D}{L_B}-2-2\frac{R_H}{L_B}]\frac{B_L}{L_B}}{\pi[2\frac{R_H}{L_B}+1]}$$

If this value is less than 1.0, the flow cannot diffuse.

According to figure 15 the parameter A_{FL}/A_{AN} can be expressed as

$$\frac{A_{FL}}{A_{AN}} = \frac{B_L D}{\pi(2R_H+L_B)L_B} = \frac{\frac{B_L}{L_B}\frac{D}{L_B}}{\pi(2\frac{R_H}{L_B}+1)}$$

Blockage of flow by the turbine cylinder, beams, and struts in the annulus of the exhaust hood causes actual flange flow area A_{FL} to be smaller than the flange open area, DB_L. A more realistic flange area ratio can be expressed using $A_{FL,EFF}/(A_{AN})$:

$$\frac{A_{FL,EFF}}{A_{AN}} = \frac{DB_L-2(R_H+L_B)(A+L_V)}{\pi(2R_H+L_B)L_B}$$

where L_V is the axial length of the guide vane.

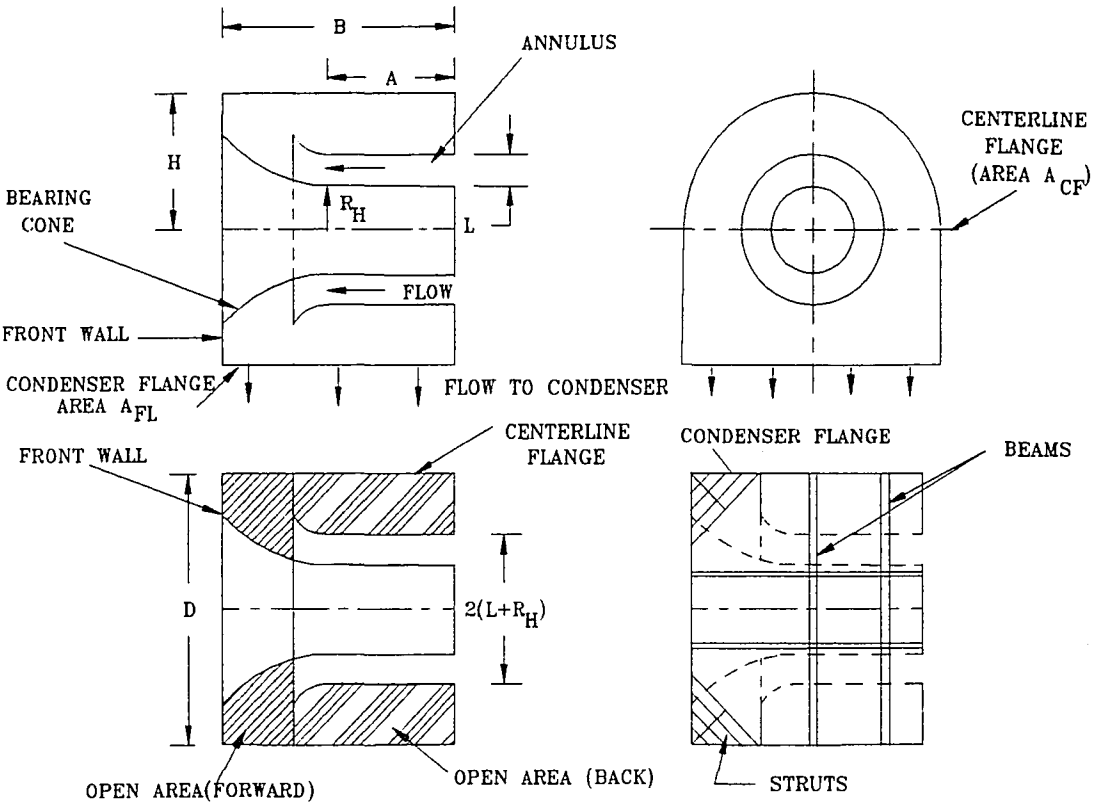

Figure 15: Parameters which define exhaust hood geometry

6.3 GENERIC EXHAUST HOOD MODEL

A series of experiments were carried out at Lehigh University to study the effect of the exhaust hood size relative to the last rotating blade height on the exhaust hood performance (see reference [10]). These experiments were performed on a "generic" exhaust hood model which was designed to allow testing at 3 different values of the ratios: hood width/last blade height), D/L_B, and hood height/last blade height, H/L_B. The generic model is shown in figure 16 and its dimensions are listed in table 3. More information about the generic model can be found in reference [11].

Parameter	Dimensionless Value		
R_H/L_3	1.0		
B_L/L_3	4.4		
A_A/B_L	0.5		
L_W/L_3	0.75		
H/L_3	3.0	3.4	3.8
D/L_3	7.0	7.5	8.15
$\frac{A_{CF}}{\frac{1}{2}A_{AN}} = \frac{(D-2(L_3+R_H))B_L}{\frac{1}{2}\pi(2R_H+L_B)L_3}$	2.8	3.27	3.87
$\frac{A_{FL}}{A_{AN}} = \frac{DB_L}{\pi(2R_H+L_B)L_3}$	3.27	3.5	3.81
$\frac{A_{FLEFF}}{A_{AN}} = \frac{DB_L-2(R_H+L_B)(A+L_W)}{\pi(2R_H+L_B)L_3}$	2.12	2.36	2.66

Table 3: Generic model dimensionless lengths

The height, H, and the width, D, were the only variable parameters of the generic model tests. A total of nine different configurations were tested and were designated as configuration 1 through 9 as shown in figure 17. Configuration #9 was the smallest hood in overall size while configuration #1 was the largest.

Curves showing the variation of the hood loss coefficient (HL/LL) with the annulus Mach number were produced for each configuration. These curves combined

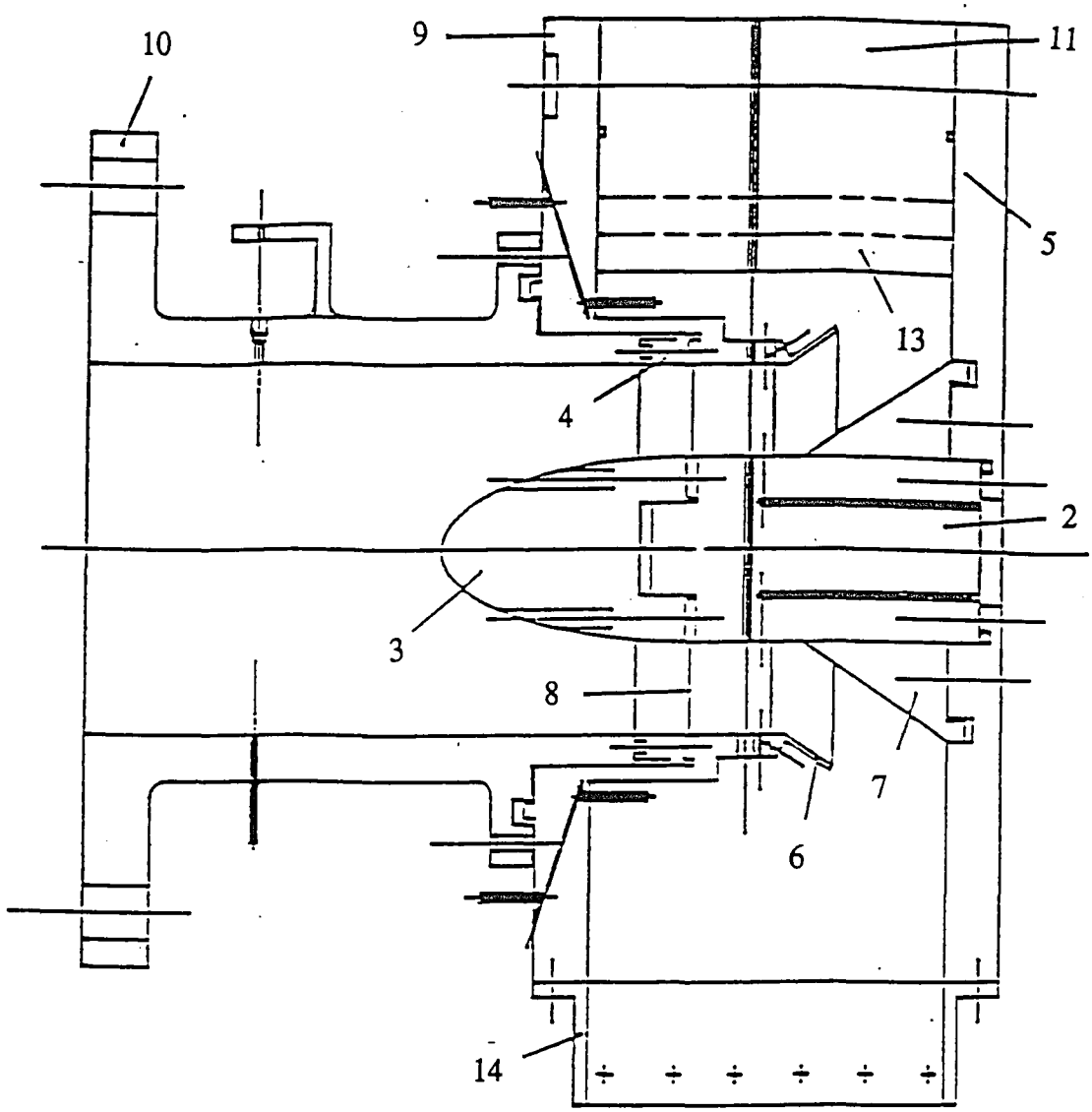

PART NO.	NAME	PART NO.	NAME
2	HUB	9	BODY
3	ELLIPTICAL NOSE	10	UPSTREAM PIPE
4	RING PIECE	11	SHELL
5	BACK PLATE	12	INSERT TO CHANGE WIDTH
6	GUIDE VANE	13	INSERT TO CHANGE HEIGHT
7	BEARING CONE	14	OUTLET DUCT
8	ANNULUS SCREEN		

Figure 16: Generic exhaust hood model

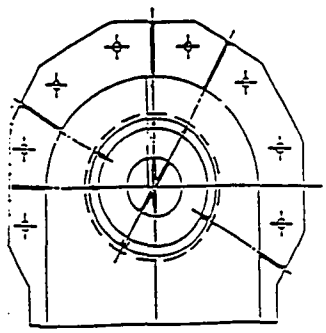

CONFIGURATION 1
D/L = 8.15
H/L = 3.8

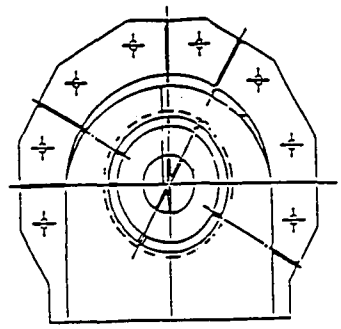

CONFIGURATION 2
D/L = 8.15
H/L = 3.4

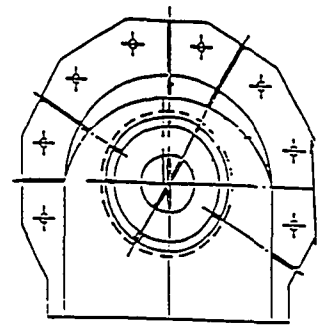

CONFIGURATION 3
D/L = 8.15
H/L = 3.0

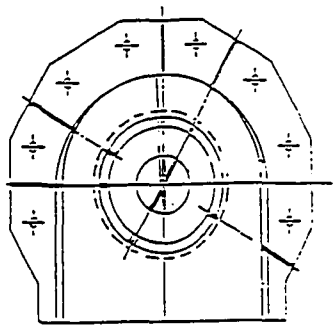

CONFIGURATION 4
D/L = 7.5
H/L = 3.8

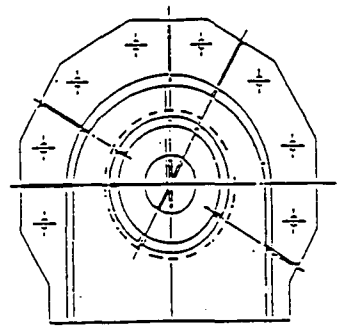

CONFIGURATION 5
D/L = 7.5
H/L = 3.4

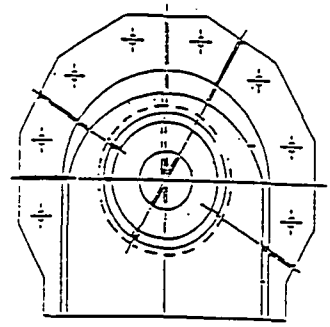

CONFIGURATION 6
D/L = 7.5
H/L = 3.0

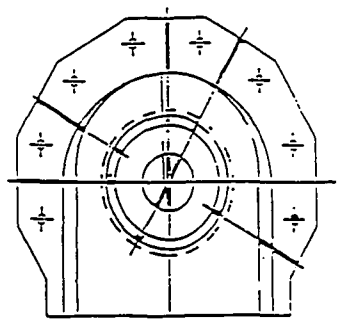

CONFIGURATION 7
D/L = 7.0
H/L = 3.8

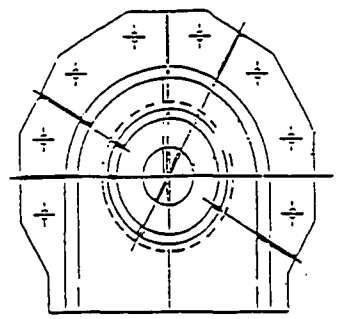

CONFIGURATION 8
D/L = 7.0
H/L = 3.4

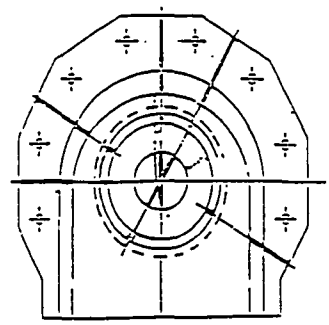

CONFIGURATION 9
D/L = 7.0
H/L = 3.0

Figure 17: Nine generic model configurations tested

the results of the generic model tested with and without screen in the annulus. The screen was used to produce a uniform inlet flow around the annulus. As a result, the corresponding test points represent more accurately the actual flow in a steam turbine exhaust hood than the test points obtained without a screen. At annulus Mach numbers of about 0.7 the flow through the screen becomes choked. Therefore, the test points for the exhaust hood model without the screen were used as a guide to determine the values of the hood loss coefficient beyond an annulus Mach number of about 0.7.

The resulting hood loss coefficient curves for configurations 1 through 9 show clearly how the hood loss decreases as the hood size increases when all other parameters are held constant. Figure 18 shows a comparison of the hood loss coefficients between the largest hood (configuration #1), the smallest hood (configuration #9), and an intermediate size hood (configuration #6). It can be seen that it is possible to very significantly affect the loss of an exhaust hood by changing its size. Figures B.1 to B.9 in Appendix B show the exhaust hood loss curves for configurations 1 through 9. These figures present for the generic model the combination curves of tests run with and without screen (solid curves) and also the test results obtained with and without the screen in the model (broken lines).

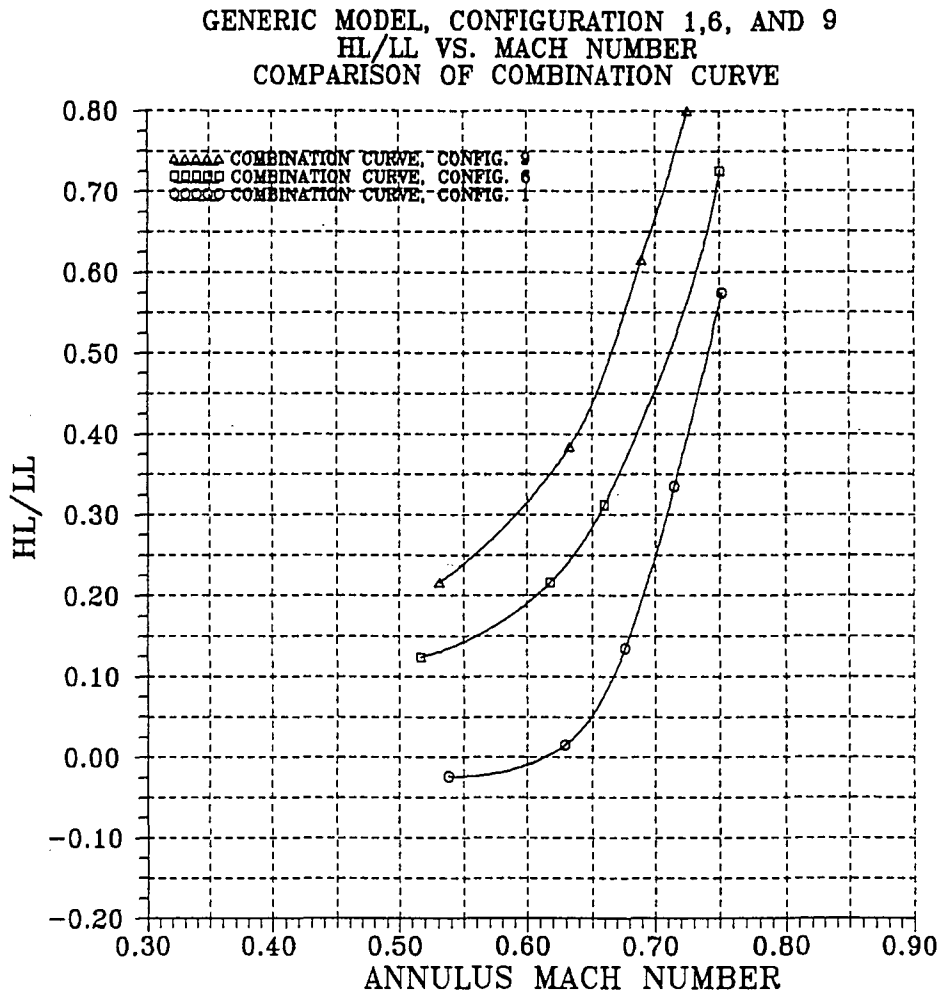

Figure 18: Generic model exhaust hood loss curves for configuration 1,6, and 9

6.4 BEAVER VALLEY AND HATFIELD FERRY MODELS

The Beaver Valley and Hatfield Ferry exhaust hood models were designed using information supplied by the Allegheny Power Company and the Duquesne Light Company. The generic model was designed so that only a few relatively minor changes in the hood would be needed to produce the Beaver Valley and Hatfield Ferry models. Only the guide vane, the bearing cone, the back plate, and the condenser flange needed

to be changed. The characteristic dimensionless parameters for both models are listed in table 4.

Parameter	Beaver Valley	Hatfield Ferry
R_H/L_B	1.0	1.0
B_L/L_B	4.64	4.0
A_A/B_L	0.51	0.45
L_V/L_B	0.77	0.56
H/L_B	3.8	3.1
D/L_B	8.13	7.5
$\frac{A_{CF}}{\frac{1}{2}A_{AN}} = \frac{(D-2(L_B+R_B))B_L}{\frac{1}{2}\pi(2R_B+L_B)L_B}$	4.07	3.16
$\frac{A_{FL}}{A_{AN}} = \frac{DB_L}{\pi(2R_B+L_B)L_B}$	4.00	3.3
$\frac{A_{FL\_EFF}}{A_{AN}} = \frac{DB_L-2(R_B+L_B)(A+L_V)}{\pi(2R_B+L_B)L_B}$	2.67	2.38

Table 4: Beaver Valley and Hatfield Ferry dimensionless lengths

6.5 EXHAUST HOOD MODIFICATIONS

One of the objectives of this exhaust hood model study was to internally modify the original Beaver Valley and Hatfield Ferry hoods in order to lower their overall losses. The modifications made to the exhaust hood models are discussed below.

6.5.1 BEAVER VALLEY MODIFICATIONS

6.5.1.1 BV MODIFICATION A:

The main objective of the first modification of the Beaver Valley model was to allow the flow from the top of the hood to flow out toward the exit separately from the flow from the bottom of the hood. The purpose of dividing the two flows was to allow for both flows to exit from the hood without interfering with each other. The flow was divided using fixed baffle walls as shown in figure 19 (a). Two rounded V-shaped inserts were also mounted in the upper part of the hood (see figure 19 (b)) to help guide the flow and eliminate the vortex which was known to exist in the upper part of the hood. To accomodate these wooden inserts, the fixed guide vane was cut back as shown in figure 19 (b).

To control the amount of flow behind the fixed baffle walls, two moveable guide vanes were placed on the back of the bearing cone, as shown in figures 19 (a) and 19 (c). The guide vanes could be moved to one of two positions, position A (flow passage area ratio = 1.45) or B (flow passage area ratio = 1.47), from outside of the hood as shown in figure 19 (c).

6.5.1.2 BV MODIFICATION A1:

This modification was the same as BV Modification A except the V-shaped wooden block in the upper part of the hood was enlarged as shown in figure 20 (a) and 20 (b). This was done since there appeared to be very little effect of the smaller wooden insert of BV Modification A.

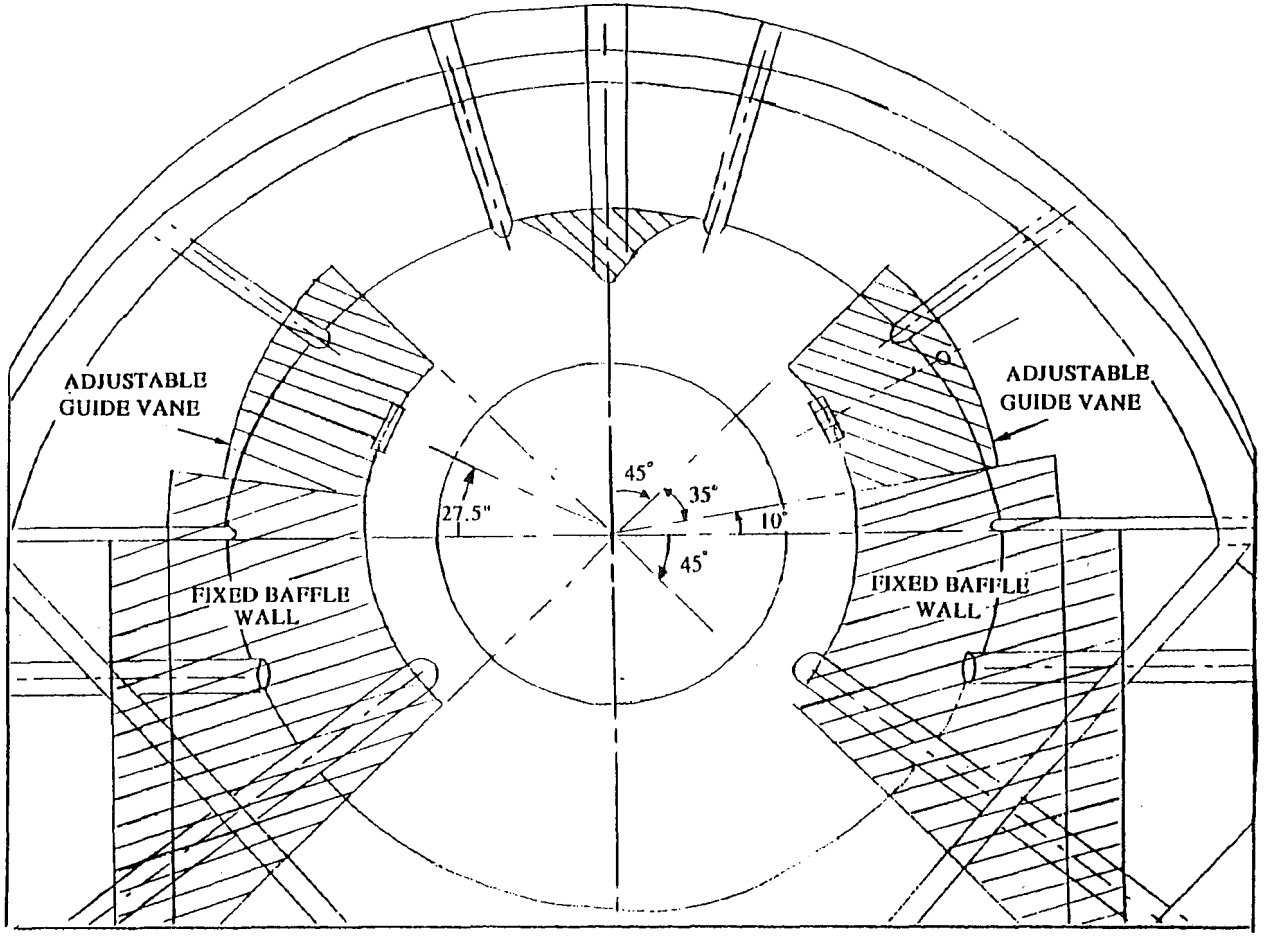

Figure 19: Beaver Valley model modification A; (a) view in direction of flow at the entrance of the model

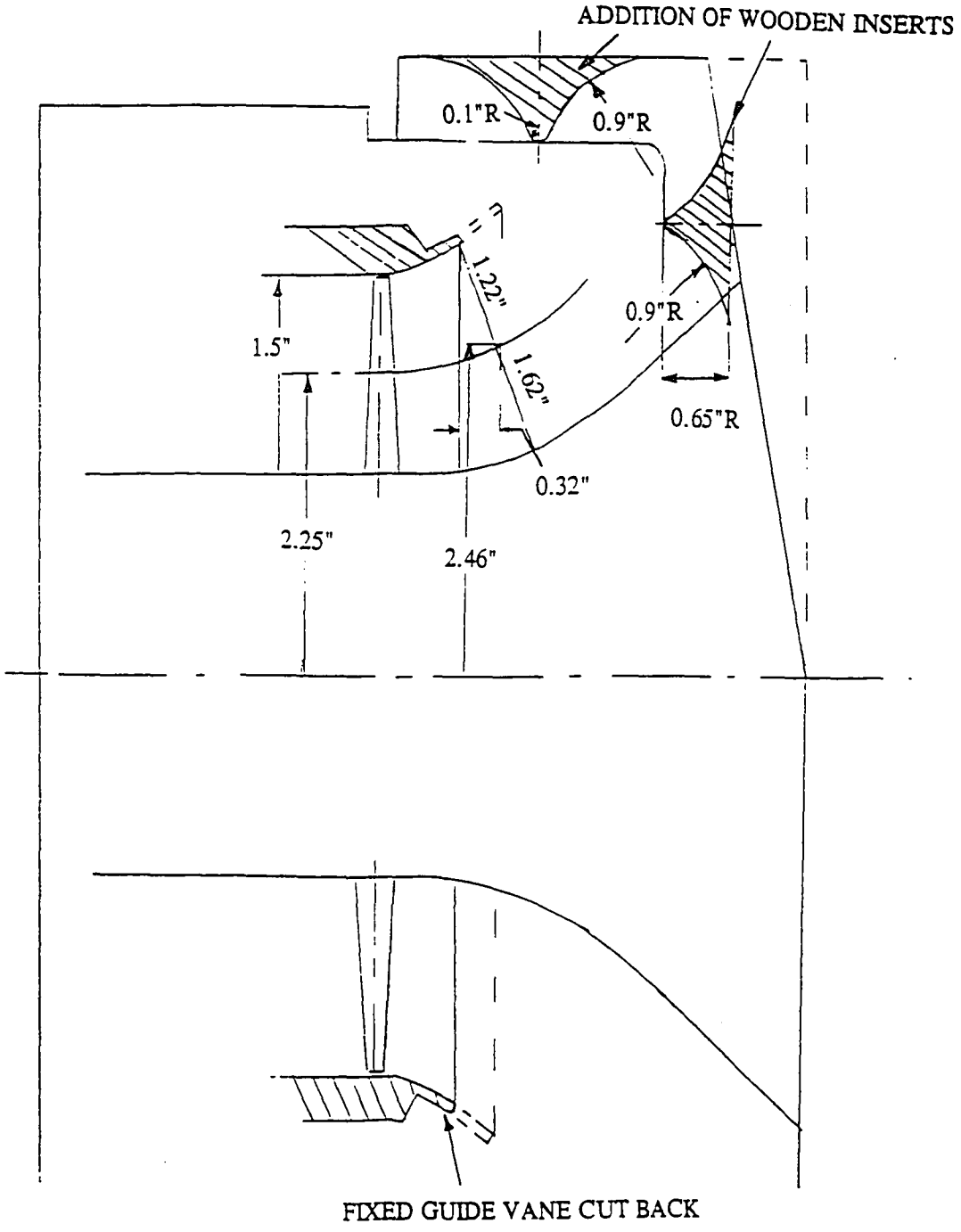

Figure 19: Beaver Valley model modification A;(b) elevation view

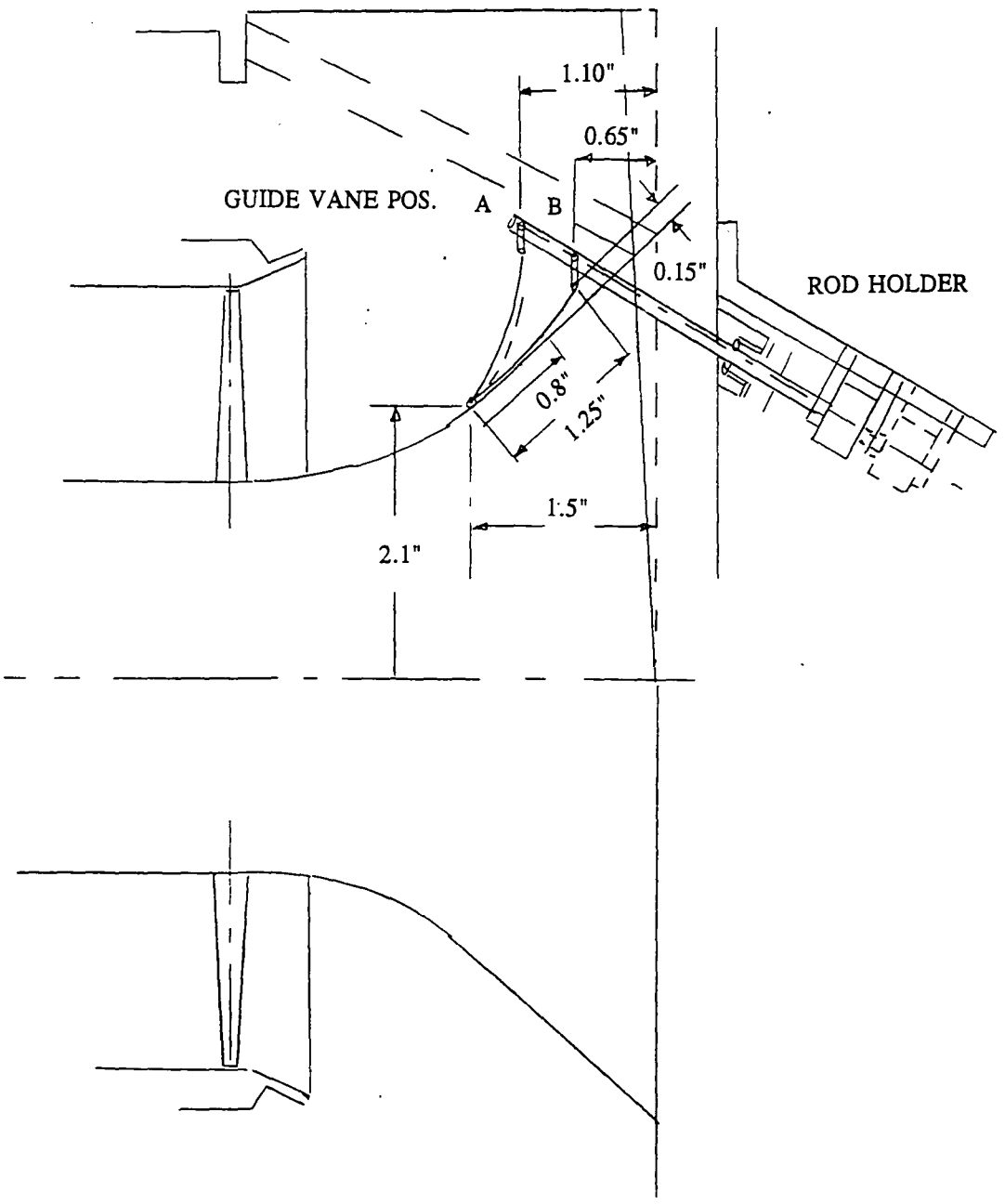

Figure 19: Beaver Valley model modification A;(c) view 27.5 deg. from the horizontal (through centerline of adjustable guide vane)

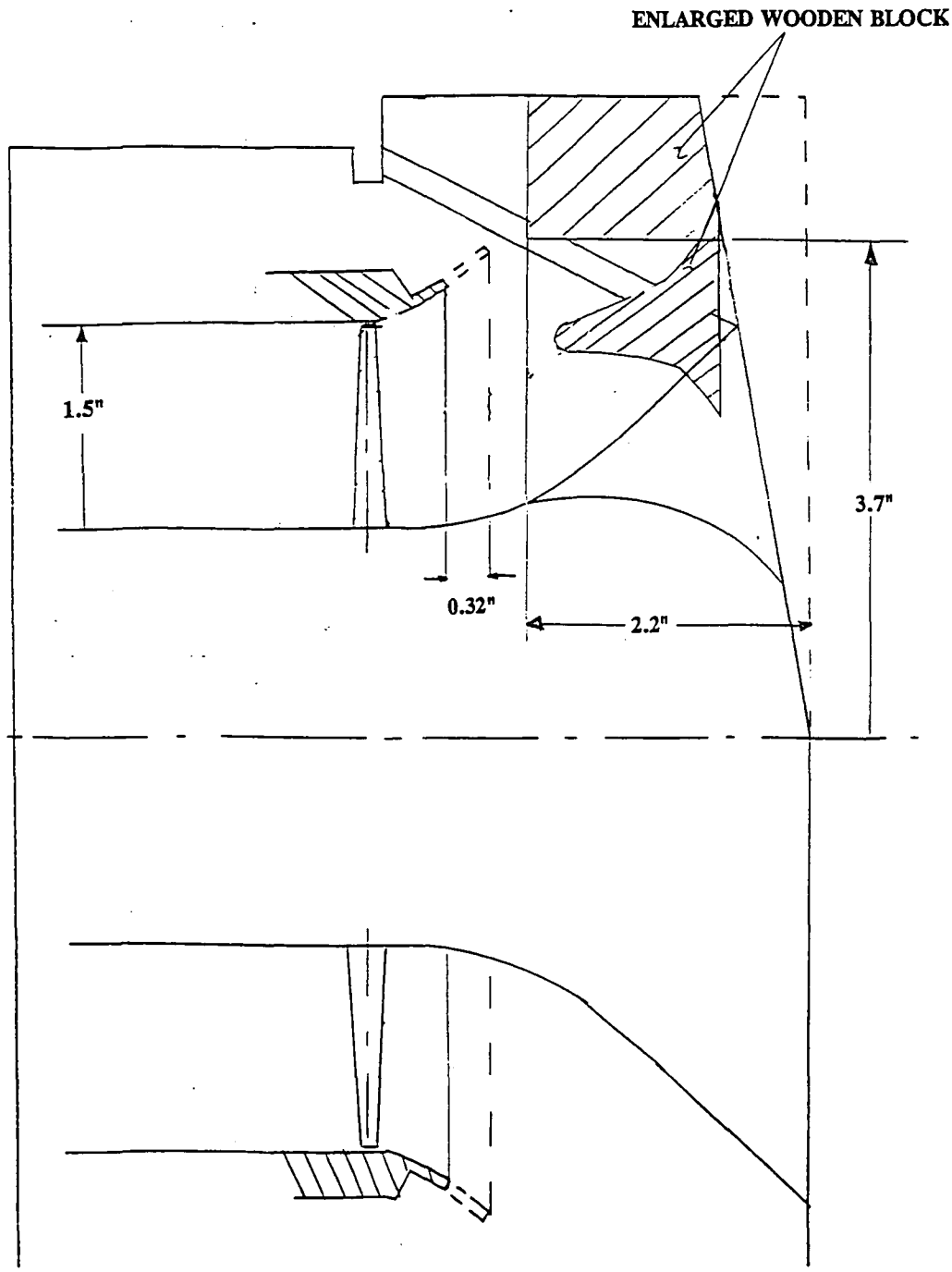

Figure 20: Beaver Valley model modification A1; (a) elevation view

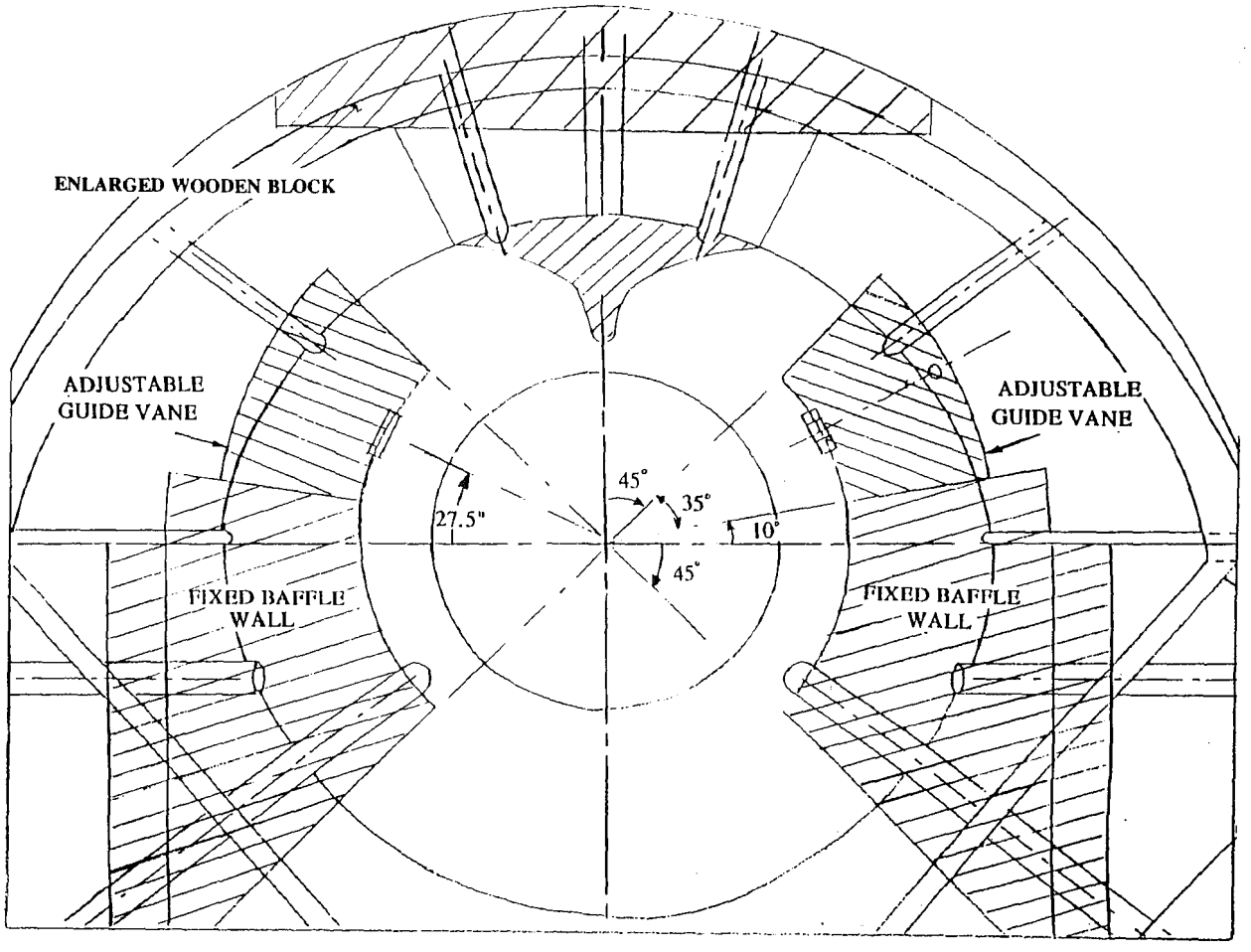

Figure 20: Beaver Valley model modification A1; (b) view in the direction of flow at entrance to the model

6.5.1.3 BV MODIFICATION B:

In this modification, six 1/32" partitions were attached to the upper base of the bearing cone below the flow guide as shown in figures 21 (a) and 21 (b). These partitions were placed symmetrically at angles of 10, 35, and 37.5 degrees from the horizontal plane. They were added to help guide the flow in the upper region of the hood.

6.5.1.4 BV MODIFICATION C:

The changes from BV Modification B to BV Modification C include the addition of an intermediate guide vane position between A and B (position C) and the removal of the fixed baffle walls. The new guide vane position was added to test the effect of an area ratio between that of A and B. Position C had an area ratio of 1.65. BV Modification C is shown in figures 22 (a) and 22 (b).

6.5.1.5 BV MODIFICATION D:

A new bearing cone was designed for this modification. The new bearing cone was much smaller than the original, as shown in figure 23 (a).

This modification also used a new fixed guide vane which produced a longer diffusing flow passage on top of the hood (see figure 23 (b)) and like BV Modification C, had 3 positions, 0, 2, and 4. Four adjustable guide vanes covered the entire upper portion of the hood as shown in figure 23 (c). The guide vane in position 4 rested flat against the new bearing cone (flow passage area ratio = 1.42), while the guide vane in position 2 was located in a position which represented the original bearing cone

(flow passage area ratio = 1.39). The guide vane in position 0 was located furthest from the new bearing cone with a flow passage area ratio of 1.34.

Other changes in BV Modification D included: a new wooden insert in the top half of the hood which could be removed to study the effect of increased height, the six partitions were taken out from the hub, and the slanted wooden back plate was removed from the top of the hood.

BV Modification D was tested with the enlarged height and also was tested with and without the slanted back plate from the upper half of the hood.

6.5.1.6 BV MODIFICATION E:

The original Beaver Valley bearing cone was used for this modification (no movable guide vanes). Also the fixed guide vane of BV Modification D was inserted into the model. The slanted back plate was removed to see if losses would be affected.

6.5.1.7 BV MODIFICATION F:

This modification was the same as BV Modification E except the slanted back plate was placed back inside the hood.

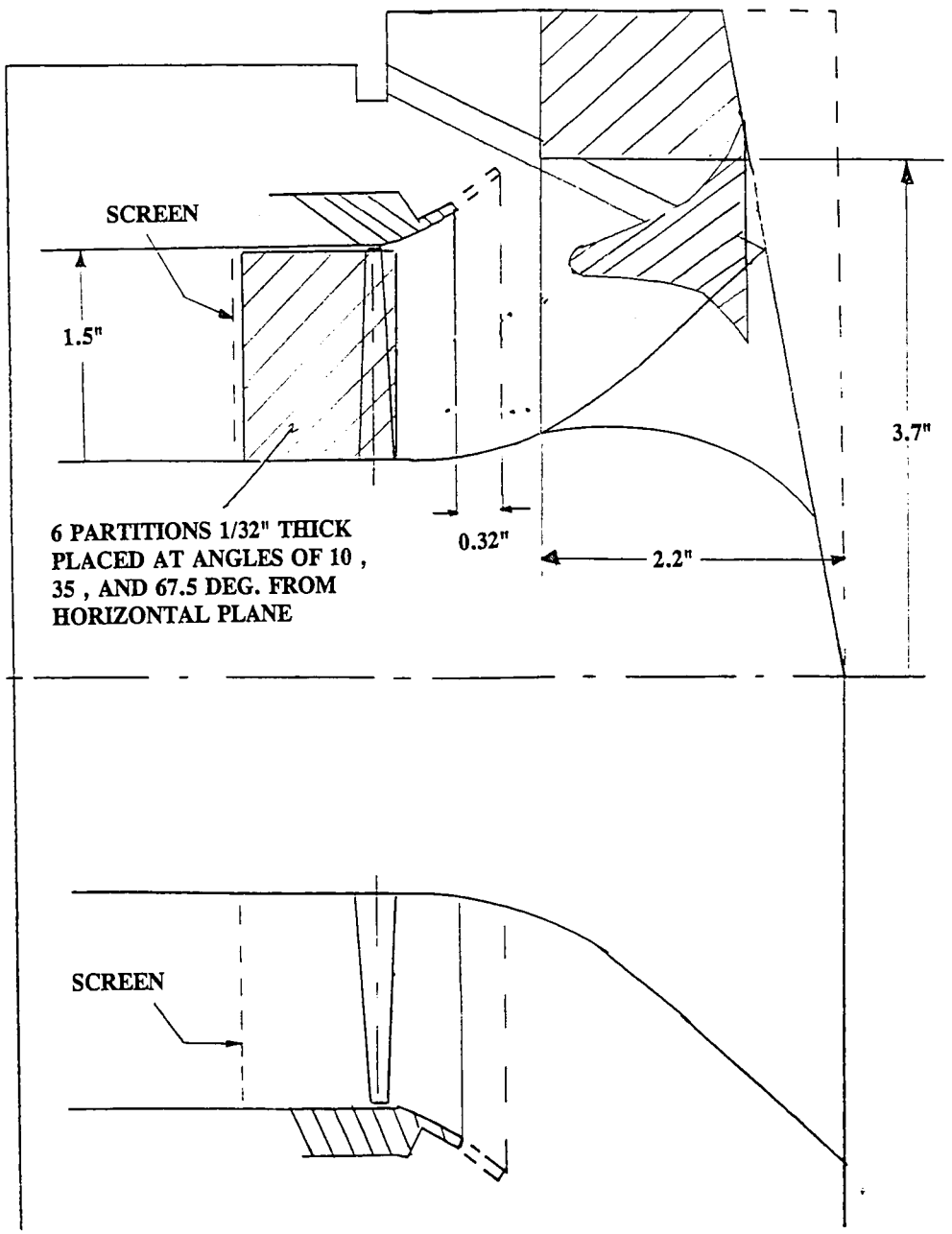

Figure 21: Beaver Valley model modification B; (a) elevation view

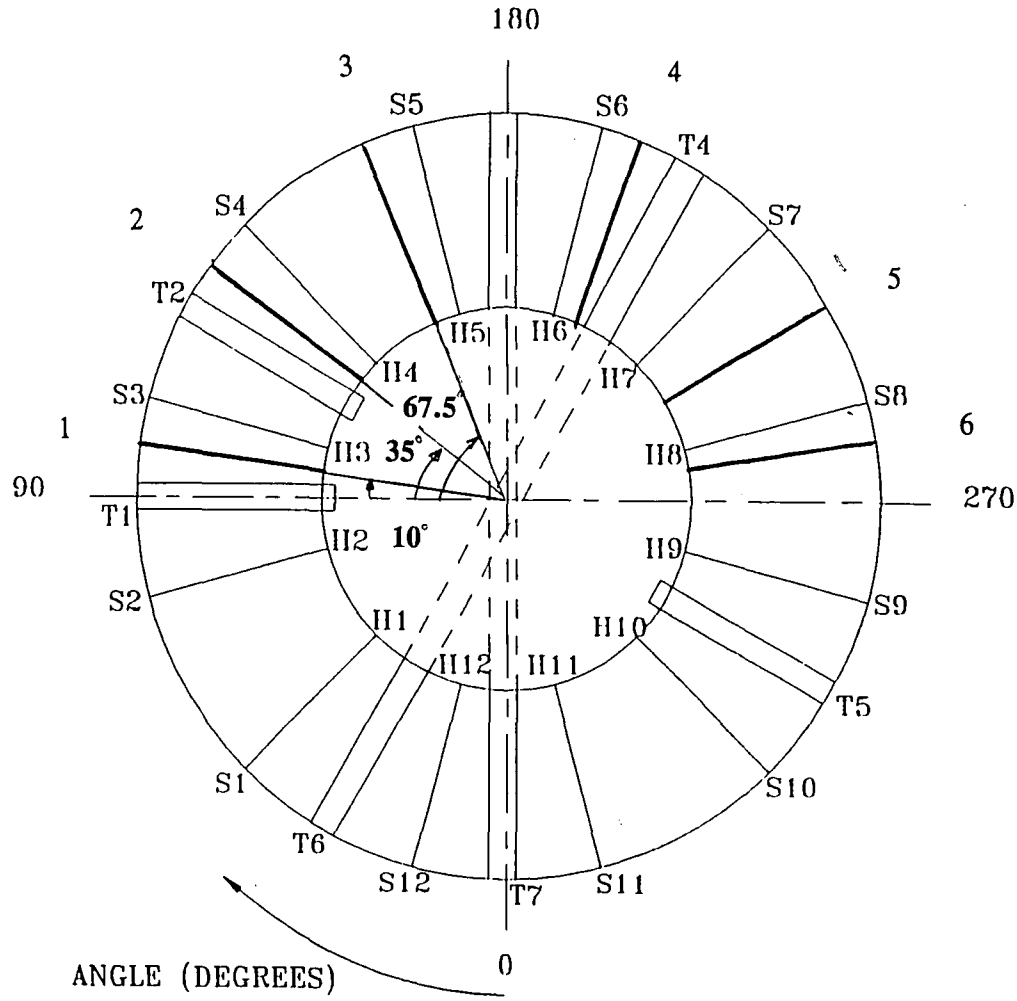

Figure 21: Beaver Valley model modification B; (b) cross-section of the annulus

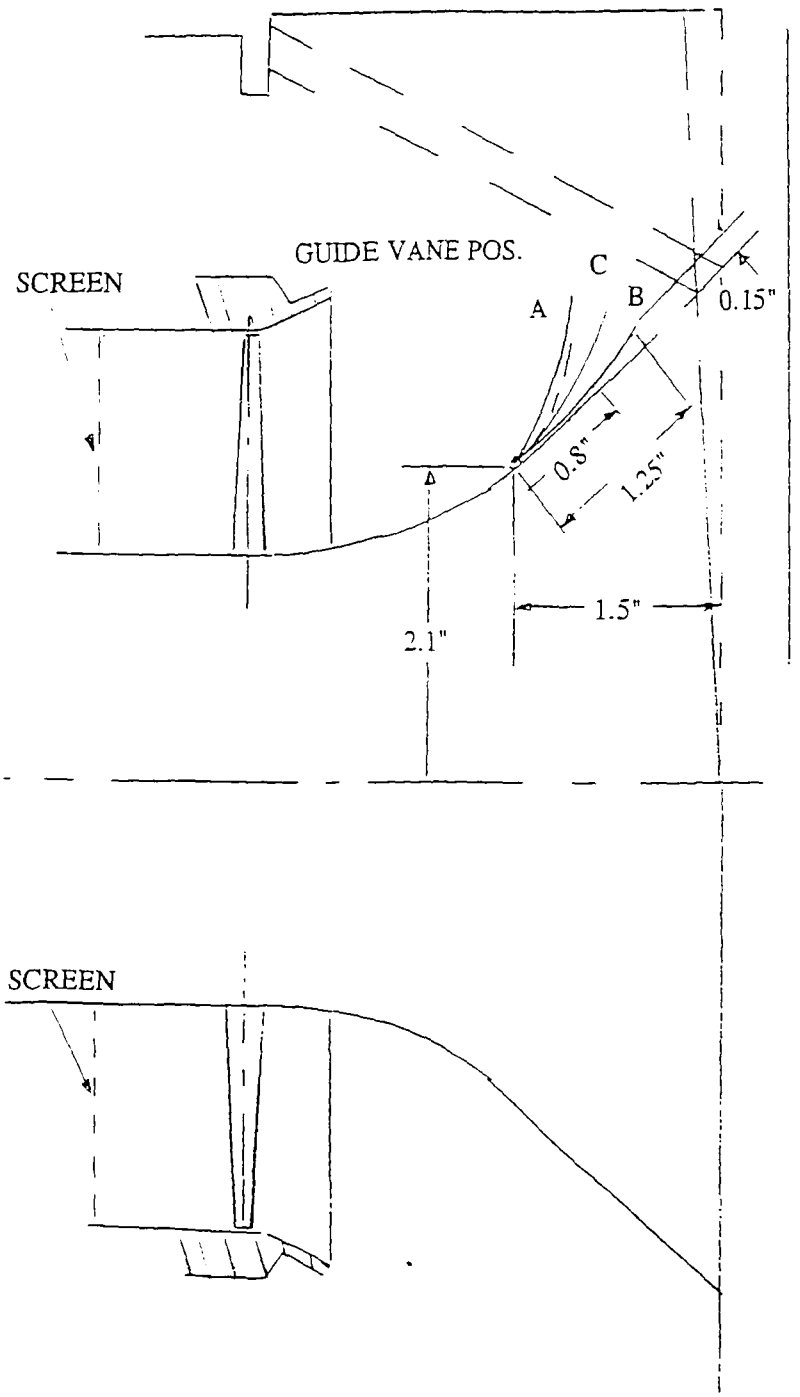

Figure 22: Beaver Valley model model modification C: (a) elevation view

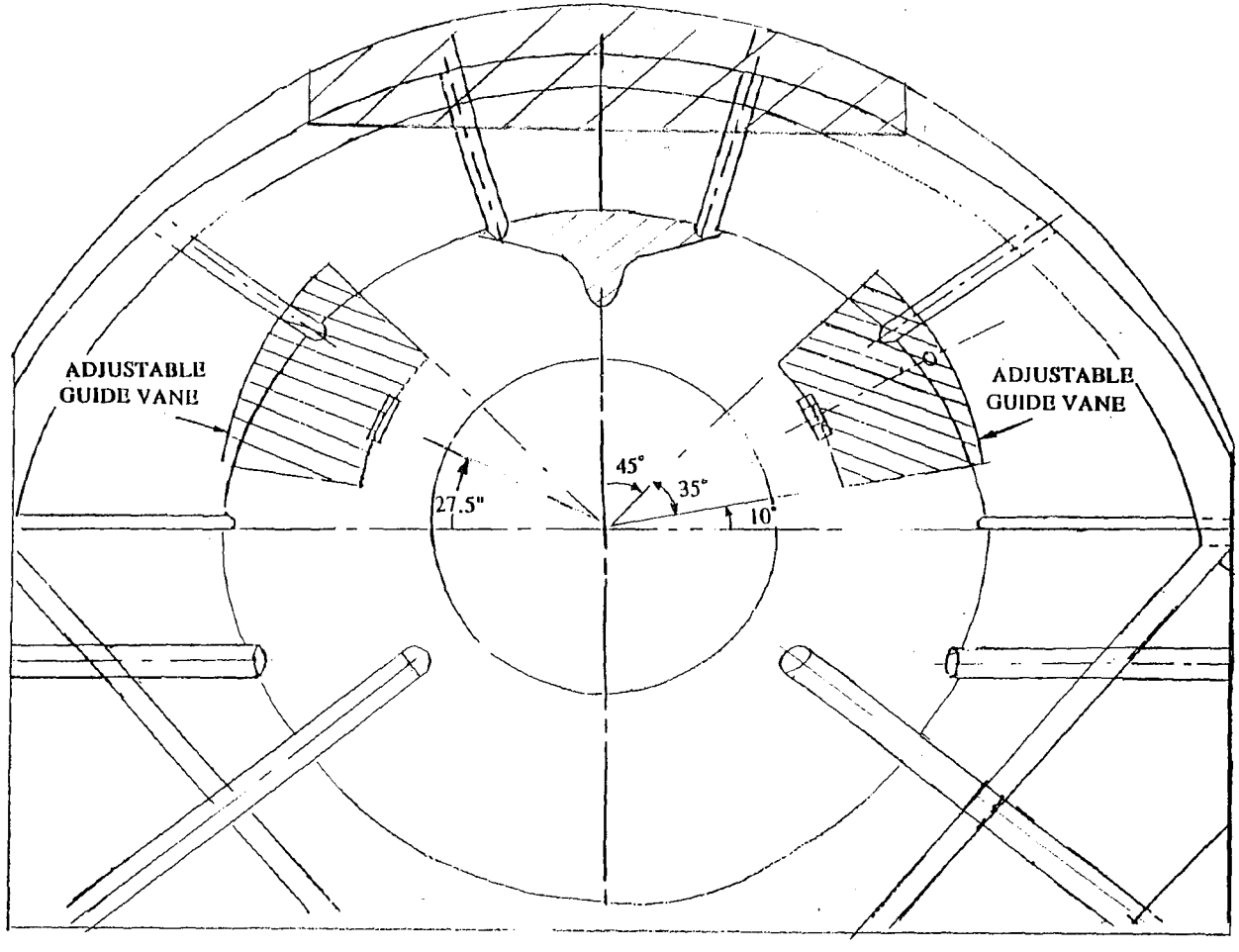

Figure 22: Beaver Valley model model modification C: (b) view in direction of flow at the entrance to the exhaust hood

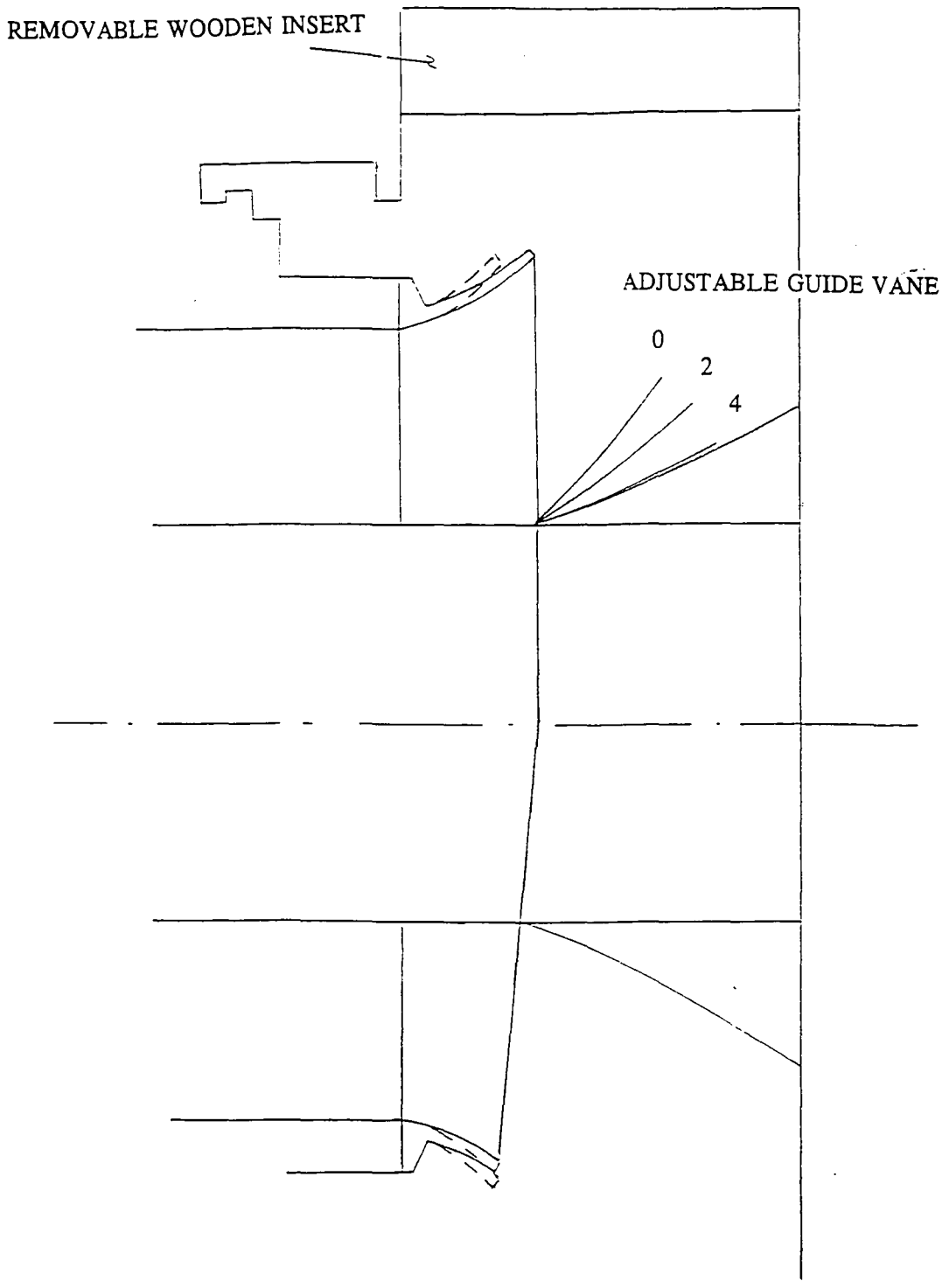

Figure 23: Beaver Valley model modification D; (a) view 27.5 degrees from the horizontal (through centerline of adjustable guide vane)

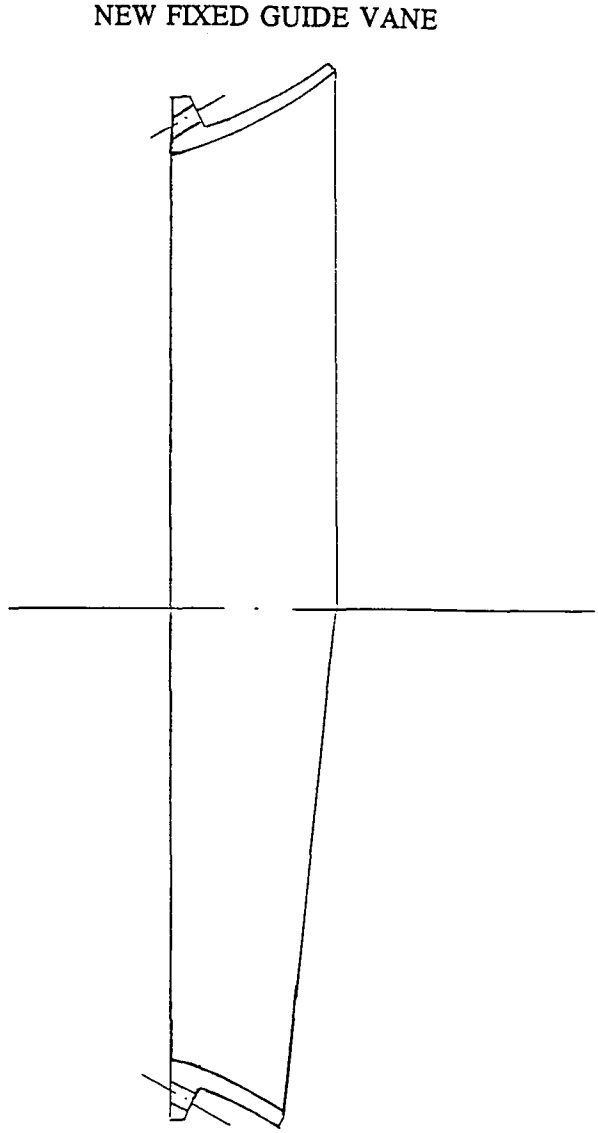

Figure 23: Beaver Valley model modification D; (b) new fixed guide vane

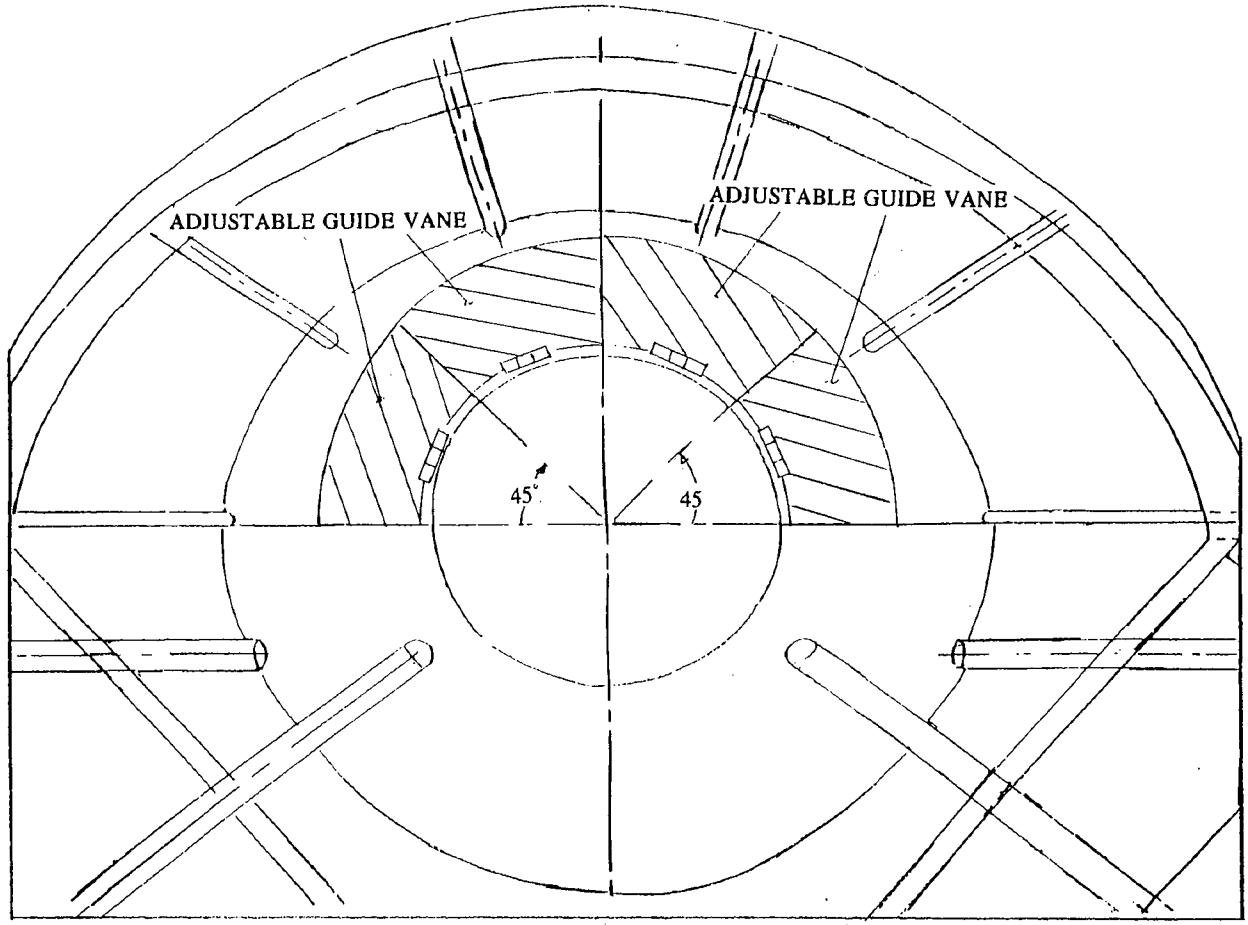

Figure 23: Beaver Valley model modification D; (c) view in the direction of flow at the entrance to the model

6.5.2 HATFIELD FERRY MODIFICATIONS

The results of the Beaver Valley exhaust hood study indicated that the design of the fixed guide vane had a significant effect on the hood loss curves. Because of this, several fixed guide vane designs were investigated with the Hatfield Ferry model to see if lowering of losses would result. The bearing cone was also cut back initially to see what changes in the losses would result.

6.5.2.1 HF MODIFICATION A:

The first modification to the Hatfield Ferry model concentrated mainly on reducing the size of the bearing cone to allow more area for air to flow through. The major drawback with this modification was that a restriction, placed by the power utilities, limiting the decrease in size of the bearing cone only to the upper 180 degree section of the hood. Therefore, HF Modification A consisted of a bearing cone that was smaller than the original at the top but remained the original size on the bottom half. This modified bearing cone is shown in figures 24 (a) and 24 (b).

A new fixed guide vane was also created for this modification. The top part of the vane decreased linearly in length from the upper section of the guide vane to the centerline of the hood. The bottom part of the vane which was of different shape than the top part, was constant in length. This new guide vane is shown in figure 24 (c).

6.5.2.2 HF MODIFICATION B:

Since no improvements in performance were found after testing HF Modification A, the original bearing cone was replaced in the Hatfield Ferry model. The new fixed guide vane of HF Modification A was also placed inside the hood. HF Modification B is shown in figure 25.

6.5.2.3 HF MODIFICATION C:

This modification tested the Hatfield Ferry hood with the original bearing cone like HF Modification B. The guide vane design was changed to one which corresponded to the bottom half of the guide vane of HF Modification A. This modification is shown in figure 26.

6.5.2.4 HF MODIFICATION D:

This modification was the same as HF Modification C except that a different fixed guide vane was used in the model. The guide vane was a shortened version of the original guide vane as shown in figure 27.

6.5.2.5 HF MODIFICATION E:

The final modification was the same as HF Modification C except the guide vane of BV Modification D was placed in the hood.

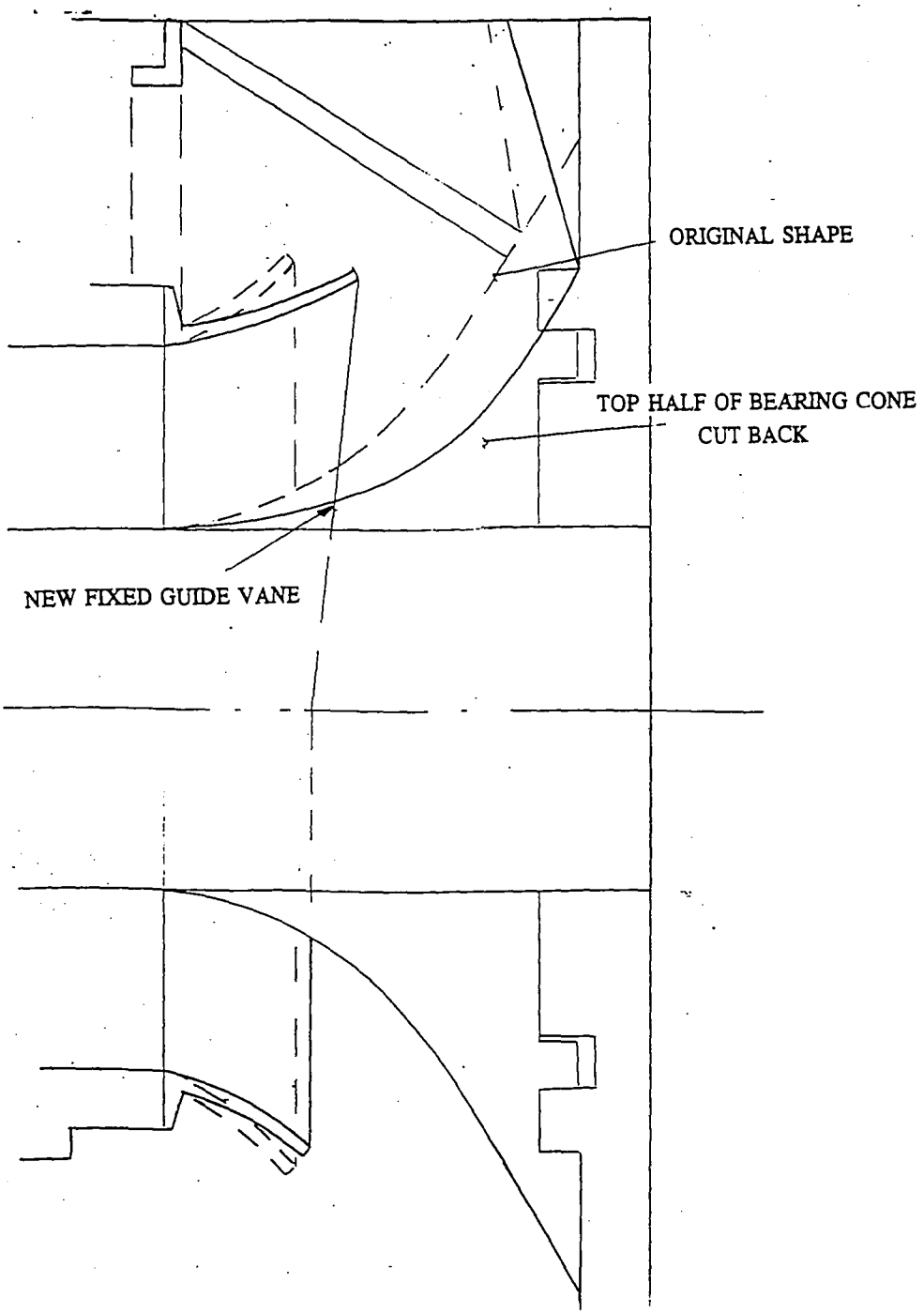

Figure 24: Hatfield Ferry model Modification A; (a) Elevation View

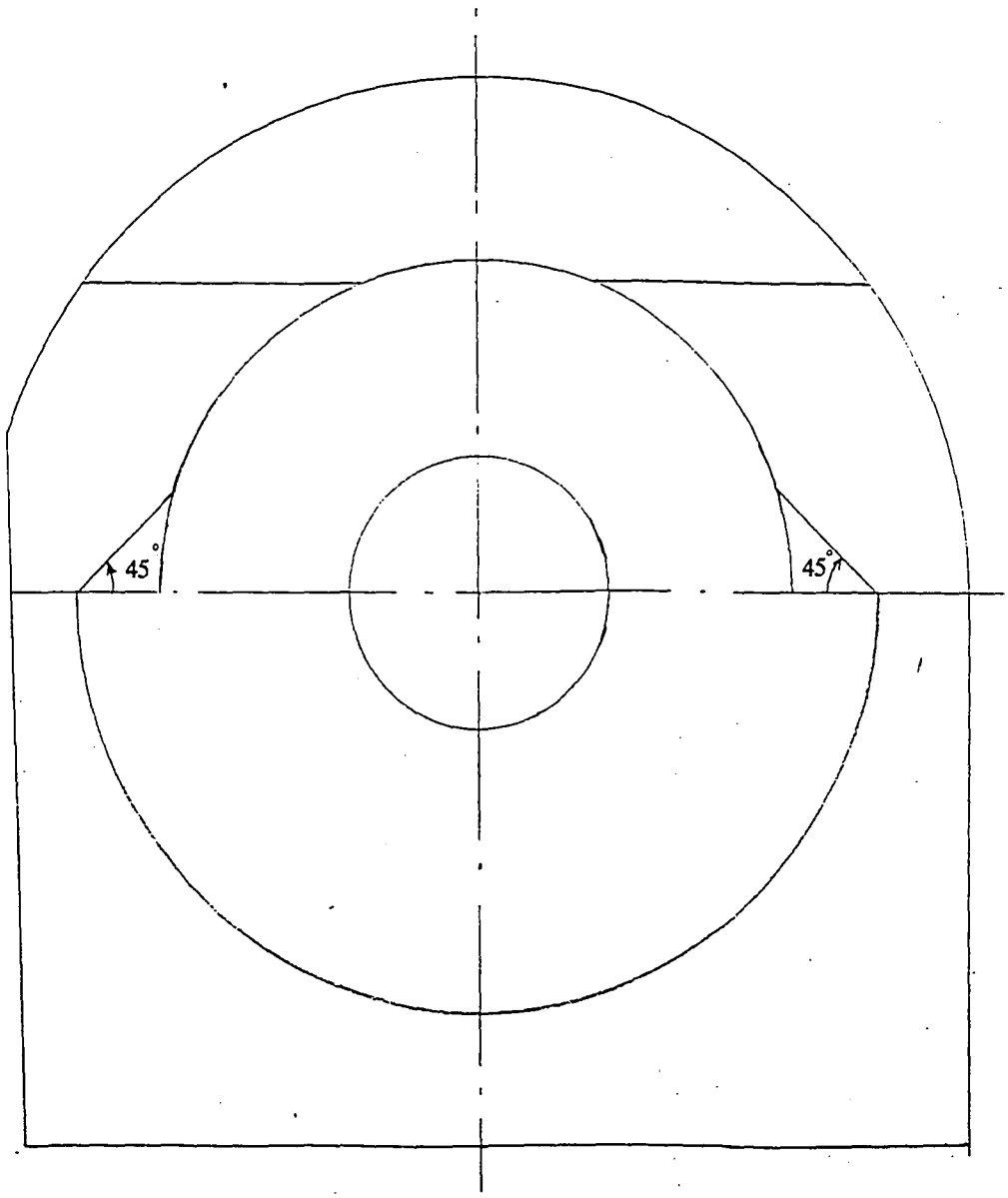

Figure 24: Hatfield Ferry model Modification A; (b) view of new bearing cone

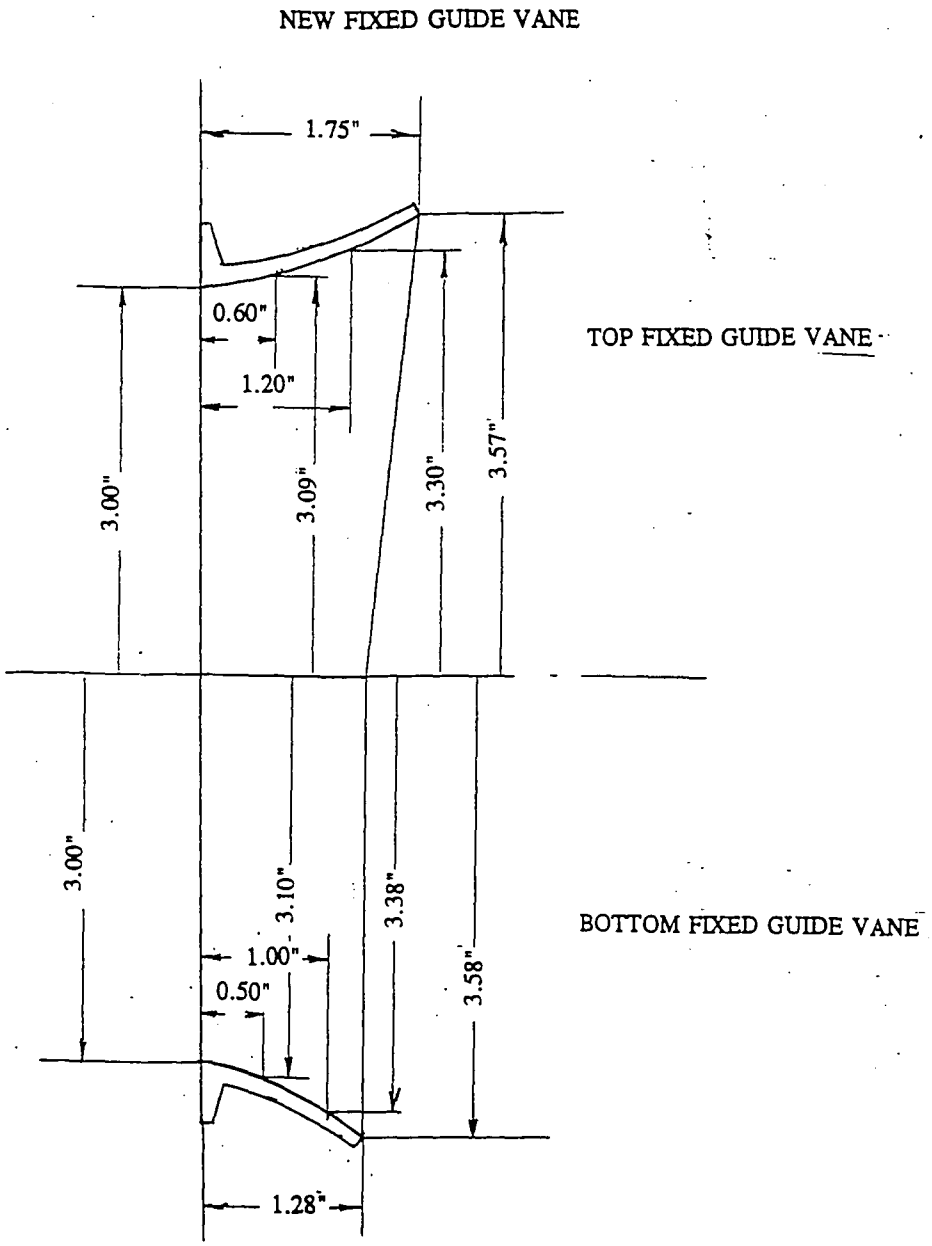

Figure 24: Hatfield Ferry model Modification A; (c) new fixed guide vane

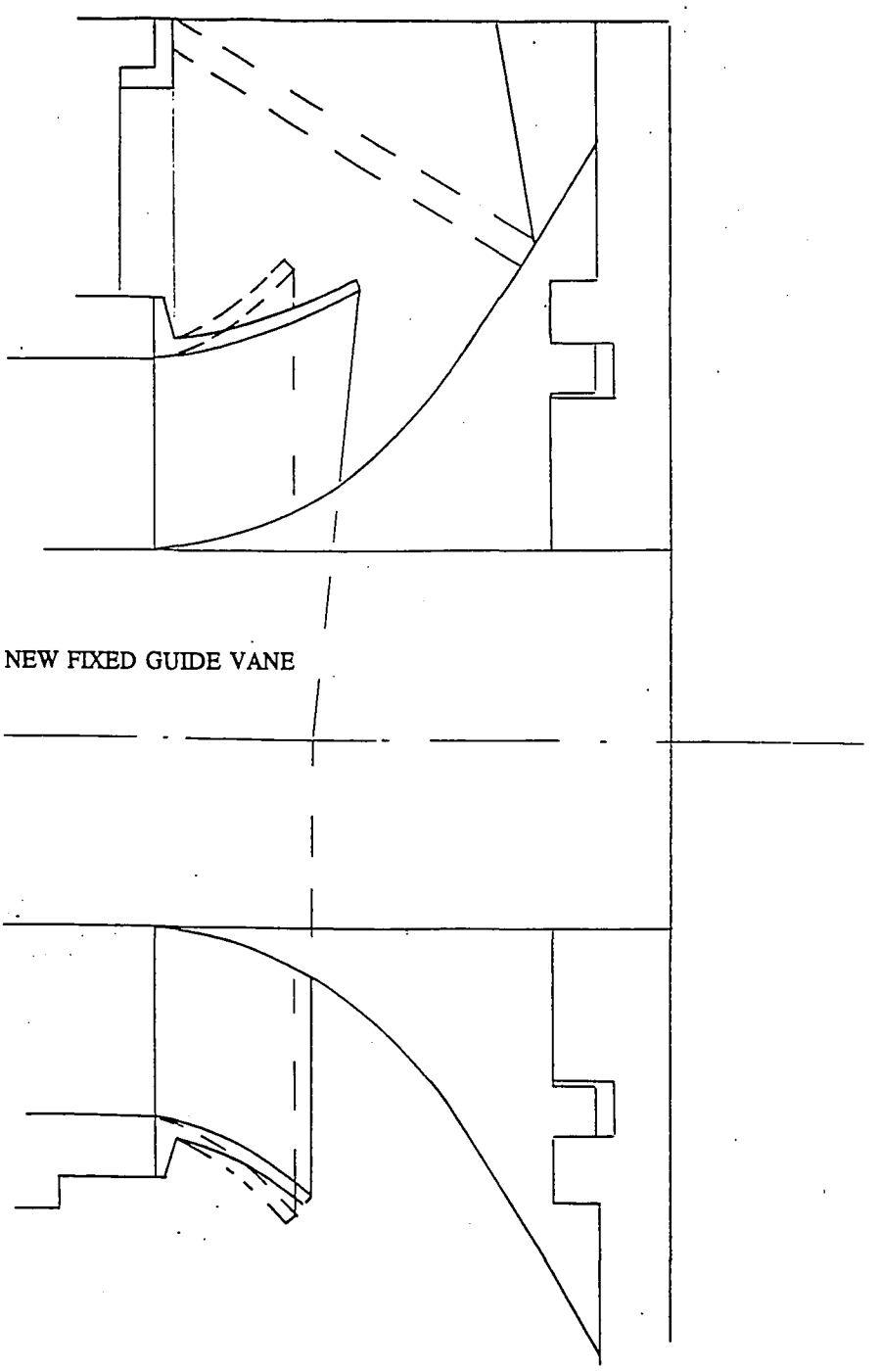

Figure 25: Hatfield Ferry model modification B; elevation view

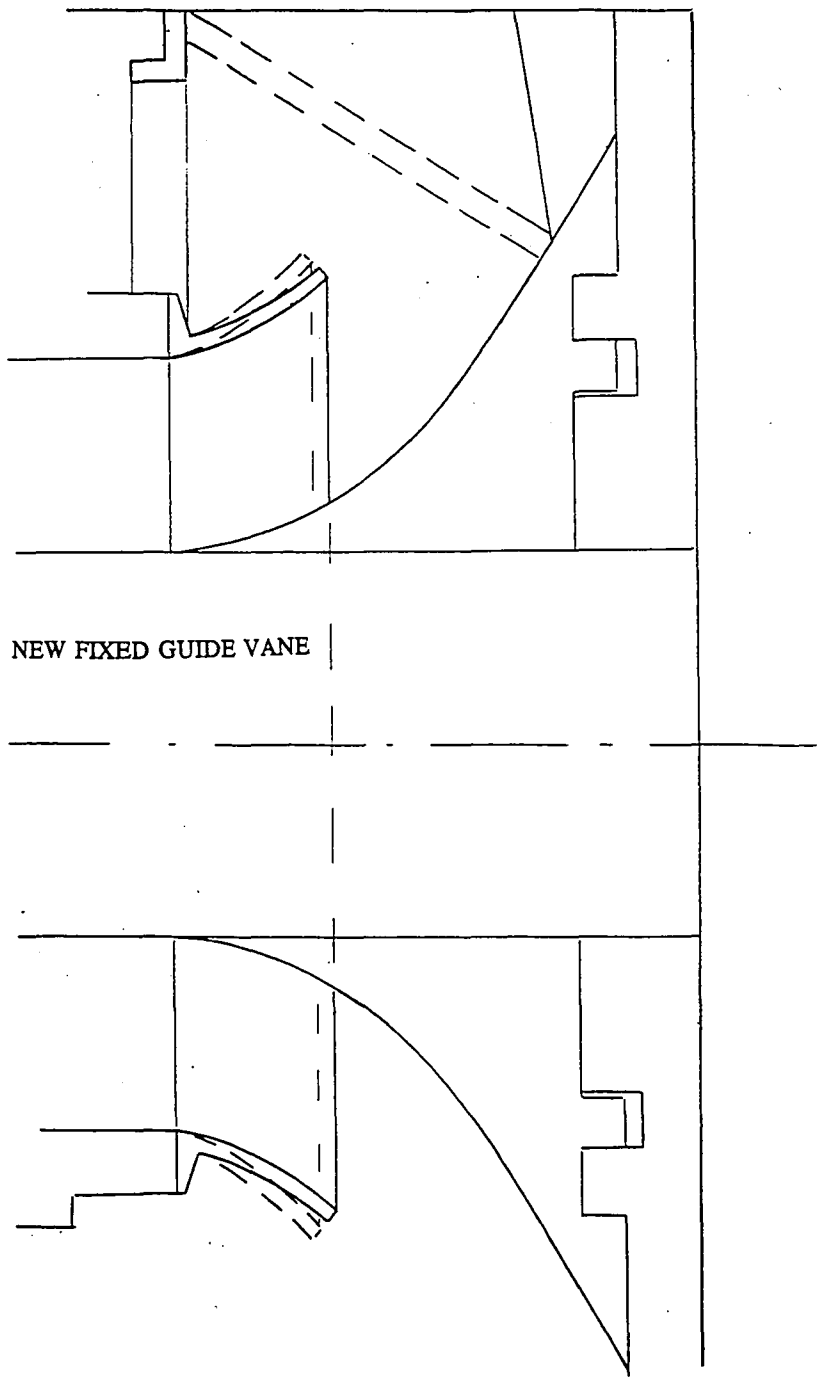

Figure 26: Hatfield Ferry model modification C; elevation view

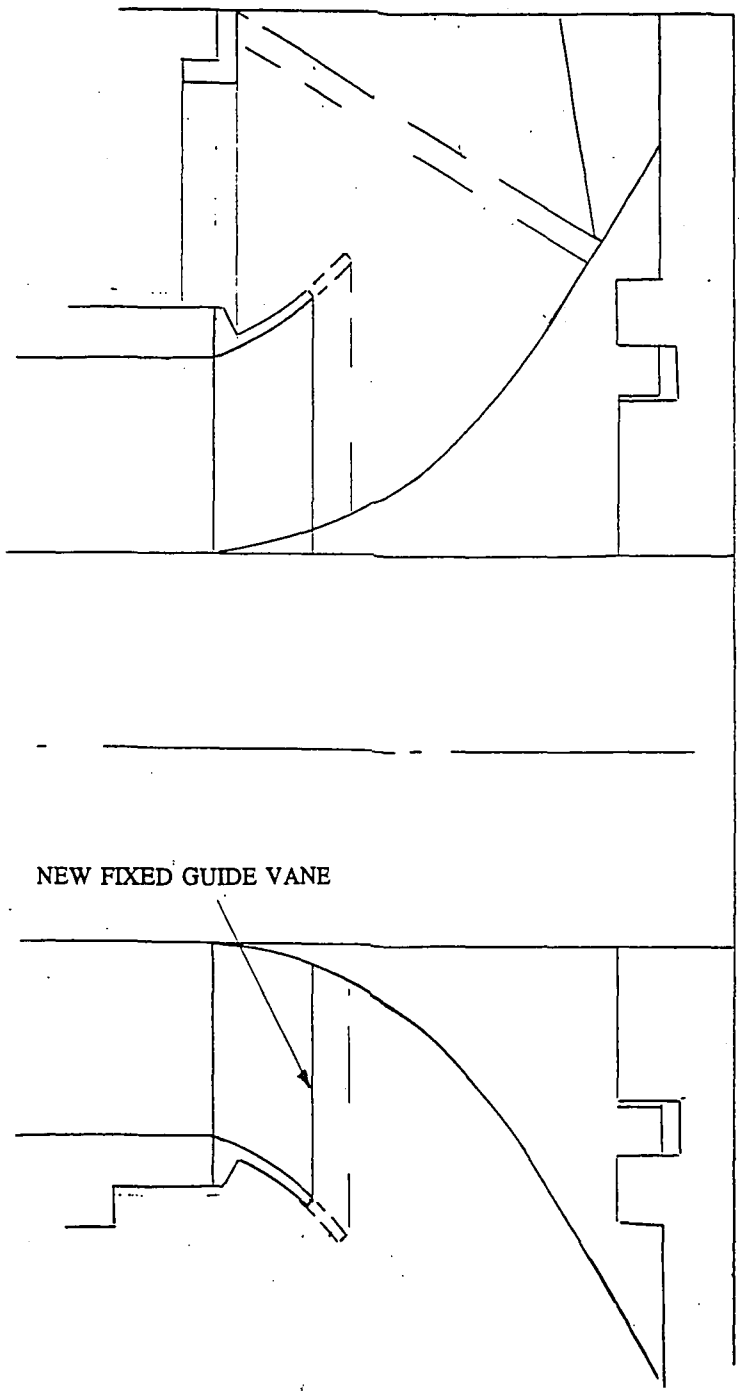

Figure 27: Hatfield Ferry model modification D; elevation view

7 RESULTS AND DISCUSSION

7.1 EXHAUST HOOD LOSS CURVES

The Beaver Valley and Hatfield Ferry model exhaust hood test data was used to calculate the nondimensional hood loss, HL/LL or (H+C)L/LL, and the nondimensional pressure coefficients, C_P1 and C_P2. As explained in section 5, two calculation methods were used to produce these values. The first method, Method 1, bases its calculations on the experimentally measured values of total and static pressure in the model hood annulus. The second method, Method 2, is based on the mass flow rate through the venturi meter and the measured values of total pressure. There should be little difference between the values produced using the two methods. However, Method 1 was less reliable since it required the interpolation of the hub and shroud static pressures to determine the static-to-total pressure ratios and the annulus Mach number. Because of this, it is felt that the hood loss curves produced using the values calculated using Method 2 represent better the losses in the exhaust hood model.

Curves showing values of HL/LL (and (H+C)L/LL), C_P1, and C_P2 versus annulus Mach number, M_{AN}, were produced. Also, exhaust hood loss curves were created which combined the results of the model tested with and without a screen. As was explained in section 6.3, at lower annulus Mach numbers (about $M_{AN} \leq 0.7$) the test points representing the hood with the screen are more reliable than those without the screen. This is true because the screen creates a uniform flow distribution more closely approximating the flow from the last stage turbine blading. (The flow

distribution at the inlet to the hood model was not subject to swirl which usually exists at the exit of a steam turbine). At higher annulus Mach numbers ($M_{AN} > 0.7$) the test points representing the hood model tested without a screen can be considered to be more reliable since the screen caused the flow to choke. Therefore, the resulting combination curve followed the "with screen" loss curve at lower and medium annulus Mach numbers and followed, or ran parallel to, the "no screen" loss curve at higher annulus Mach numbers.

The nondimensional hood loss, HL/LL, versus annulus Mach number, M_{AN}, curves exhibit certain similar characteristics:

- The hood loss coefficient generally increases as the Mach number increased.
- The hood loss curves with the screen in the model are lower than the loss curves without the screen at the same annulus Mach number. (This was true up to about $M_{AN}=0.7$ at which the flow across the screen was choked.)
- The nondimensional hood loss, HL/LL, and the nondimensional pressure coefficients, C_P1 and C_P2, for individual test points were quite close for both calculation methods (Method 1 and Method 2) except for annulus Mach numbers above about 0.65.
- The addition of the condenser neck at the model exit resulted in higher loss curves than with the hood alone.

7.1.1 BEAVER VALLEY ORGINAL HOOD LOSS CURVES

Twenty-five tests were performed on the original Beaver Valley exhaust hood model in order to create the curves of the hood loss coefficient variation with the annulus Mach number. The results are listed in tables E.1 and F.1 in Appendix E and Appendix F, respectively.

Figure 28 (a) shows the hood loss curves for the case of hood alone (no condenser neck) with the screen placed in the model. The full points represent the calculations based on the mass flow rate through the venturi (Method 2) while the empty points represent the calculations based on the average total and static pressure in the annulus (Method 1). The plot shows that the curve made using Method 2 rapidly increases as the annulus Mach number approaches the value of 0.8. The curve produced Method 1, on the other hand, drops off before $M_{AN} = 0.8$. This is most likely due to the choking of the flow in of the screen

Figure 28 (b) shows a pair of curves similar to those in figure 28 (a) for the tests without a screen.

Figures 28 (a) and 28 (b) show that in the tests with a screen the hood losses ranged between HL/LL = 0.043 to 0.077 at annulus Mach numbers, M_{AN}, of 0.454 and 0.750, respectively (all values were based on Method 2). The hood losses in tests without a screen were somewhat higher than those without a screen up until $M_{AN} = 0.75$. They ranged between HL/LL = 0.095 to 0.423 at $M_{AN} = 0.48$ and 0.842, respectively.

Figure 29 shows a single curve (solid curve) which combines the results shown

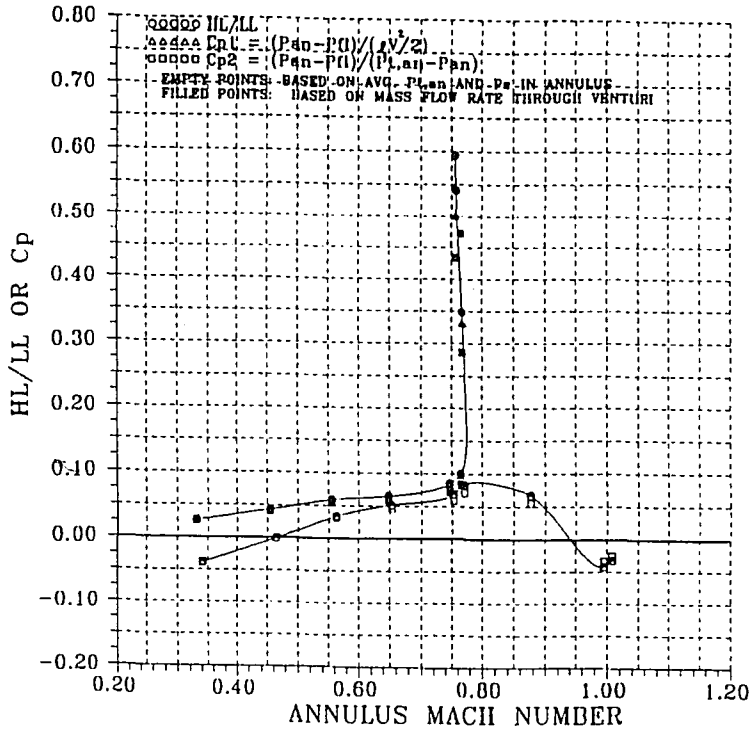

(a)

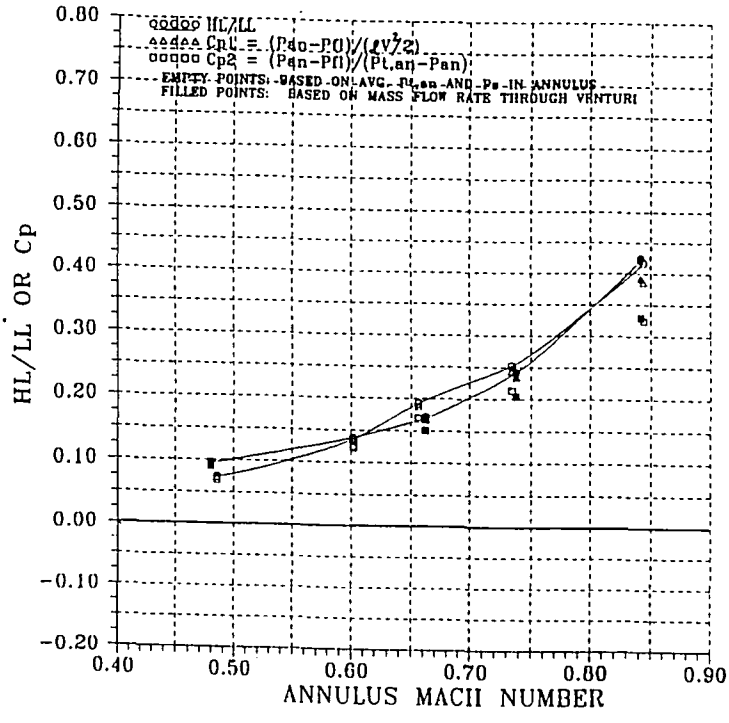

(b)

Figure 28: Beaver Valley original hood loss curve (a) hood alone with screen (b) hood alone without screen

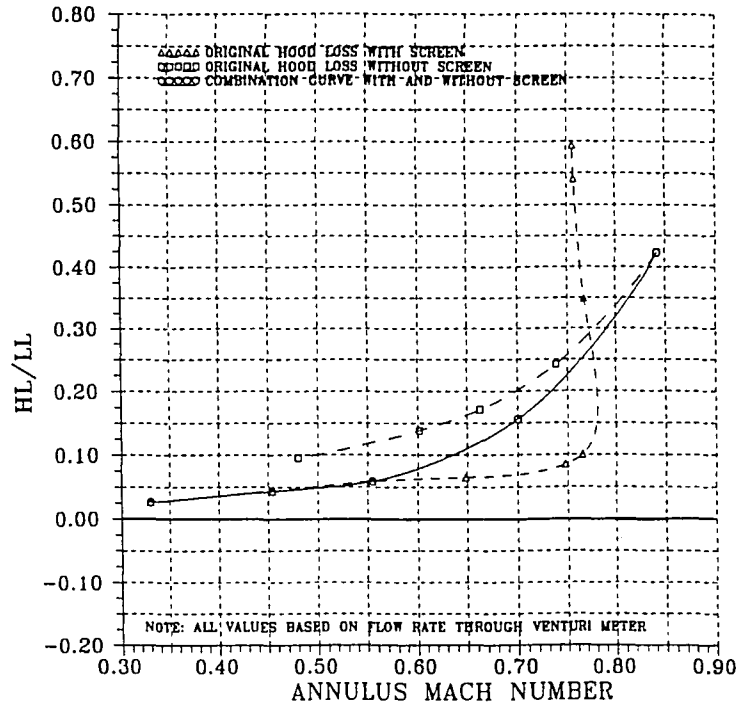

Figure 29: Beaver Valley original exhaust hood combination curve

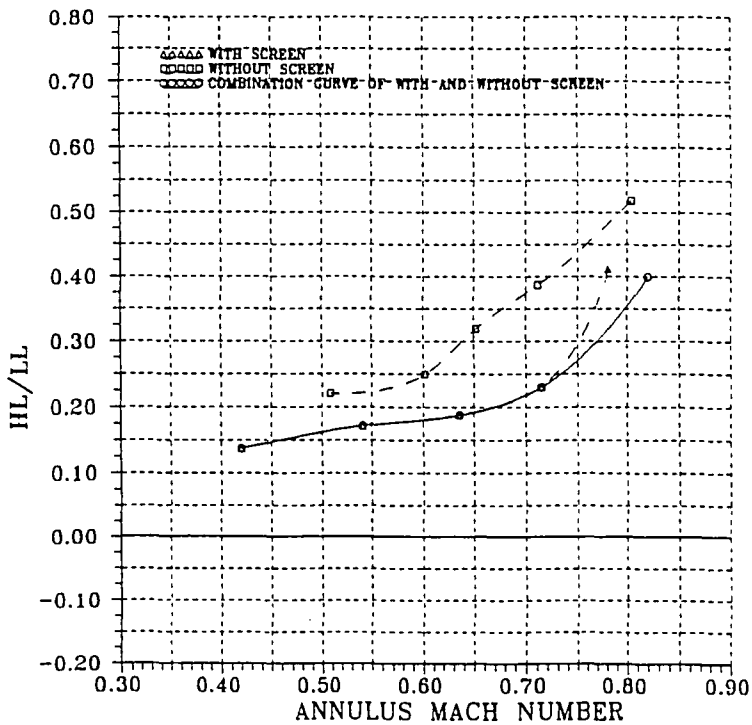

Figure 30: Beaver Valley original exhaust hood with condenser neck combination curve

in figures 28 (a) and 28 (b). The results of the tests with a screen and without a screen appear as broken lines in the figure.

Figure 30 shows exhaust hood loss curves for the Beaver Valley model with the condenser neck added. As expected, the losses with the condenser neck are greater than without.

7.1.2 MODIFIED BEAVER VALLEY EXHAUST HOOD LOSS CURVES

The results for the modified Beaver Valley exhaust hood tests are listed in tables E.2 to E.5 and tables F.2 to F.5 in Appendix E and Appendix F, respectively. The corresponding hood loss curves are discussed below.

7.1.2.1 BV MODIFICATION A

As stated earlier, the objective of this modification was to allow the flow from the top of the hood to flow out toward the exit separately from the flow from the bottom of the hood, and thus decrease the magnitude of the nondimensional hood loss, HL/LL. A moveable guide vane controlled the amount of flow behind fixed baffle walls. Two positions were tested, position A, which was located away from the bearing cone, and position B which followed the original bearing cone contour.

A plot comparing the original nondimensional hood loss versus annulus Mach number (the "with screen" case) to BV Modification A, for both movable guide vane positions A and B, is shown in figure G.1 in Appendix G. It is apparent from this plot that, for guide vane positions, the hood losses were much higher than the original model. The hood losses for guide vane position A were slightly higher than position

B.

7.1.2.2 BV MODIFICATION A1

The V-shaped wooden block, which was designed for BV Modification A to eliminate the large vortex which existed at the top of the hood, was enlarged in an effort to again eliminate this vortex. Two tests were performed at guide vane position A which showed that there was no decrease of the hood losses. Figure G.2 in Appendix G shows the two test points and their relation to the original Beaver Valley loss curve.

7.1.2.3 BV MODIFICATION B

This modification added six 1/32" partitions below the base of the bearing cone in order to better guide the flow in the upper region of the hood.

Figure G.3 in appendix G shows the results of this modification. It is shown in the figure that guide vane position A resulted in an even higher losses than position A for both modification A and modification A1. Position B appeared to have resulted in a slightly lower nondimensional hood loss than the original curve between annulus Mach numbers of 0.55 to 0.7, but it was higher at all other points. The shape of the curve for guide vane position B indicates that there may have been a test error at $M_{AN} \approx 0.64$.

7.1.2.4 BV MODIFICATION C

The fixed baffle walls were removed for this modification and an intermediate adjustable guide vane position (position C) was added. A few test points were investigated for each of the guide vane positions as shown in figure G.4 in appendix

G. The nondimensional hood loss was greater in the original exhaust hood model in all three cases. Guide vane position A corresponded again to the highest losses and position B to the lowest of the three.

7.1.2.5 BV MODIFICATION D

This modification had a smaller bearing cone than the original Beaver Valley model hood. It had a new fixed guide vane and four adjustable guide vanes with three positions: Position 0 was furthest away from the new bearing cone, position 2 corresponded to the shape of the original bearing cone contour, and position 4 corresponded to the new small bearing cone contour (it lay flat against the new bearing cone). A new wooden insert in the top half of the hood was removable to enable the investigation of the effect of height on the exhaust hood.

Modification D was first tested with the exhaust hood height enlarged and without a screen. A comparison of these results to the original Beaver Valley (the "no screen" case) is shown in figure G.5 in Appendix G. The hood loss curves for all three positions (0, 2, and 4) were lower than the original. The hood losses were lowest for guide vane position 4 and highest for guide vane position 0. From figure G.5 it can be concluded that the Beaver Valley exhaust hood with an increased height has lower exhaust losses with the new bearing cone (guide vane position 4) than with the original bearing cone (guide vane position 0).

Modification D was also tested with the original hood height at the three moveable guide vanes positions. The results are compared to the original hood curve (tests without the screen) in figure G.6. The guide vane position 4 produced higher

losses than the original exhaust hood. The lowest losses occurred for guide vane position 2 which represented the original bearing cone contour.

7.1.2.6 BV MODIFICATION E

This modification had no movable guide vanes and used the original Beaver Valley bearing cone. The fixed guide vane of BV Modification D was placed in the model and the slanted back plate was removed.

The results of BV Modification E produced a loss curve which was lower than the original Beaver Valley hood loss curve as shown in figure G.7 in Appendix G. These losses, however, were not lower than those of BV Modification D. These results indicate that the back plate is important and it should be in the hood.

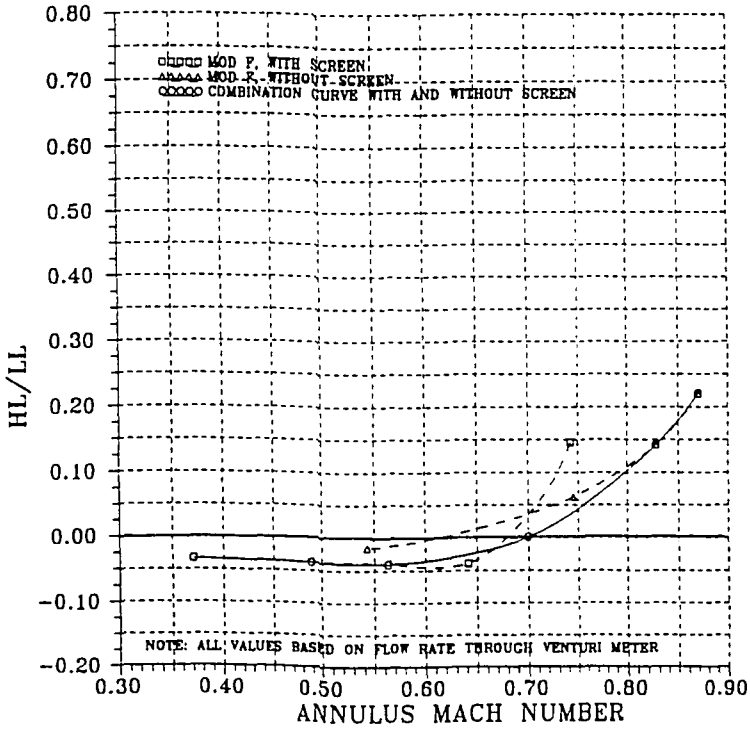

Figure 31: Beaver Valley model modification F combination curve

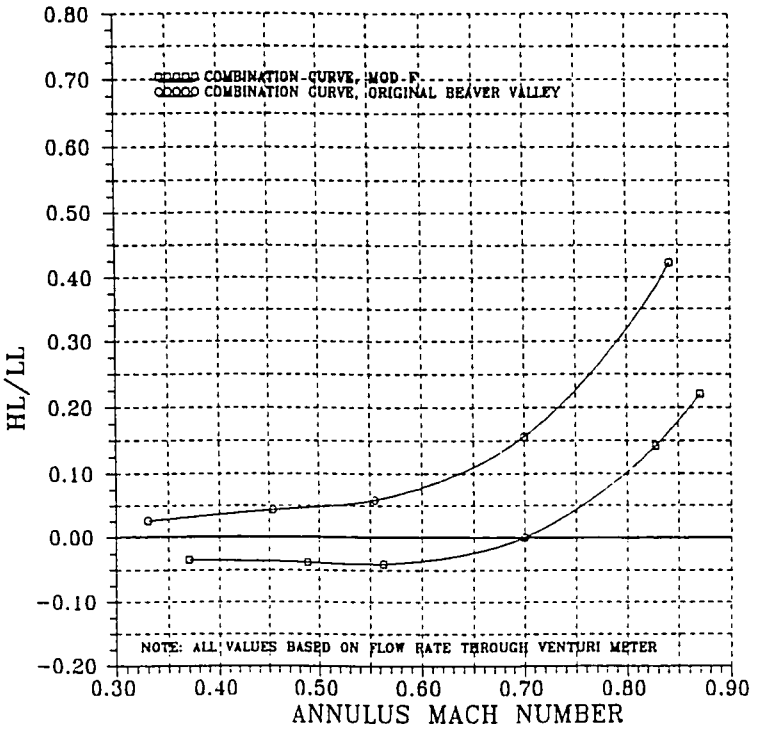

Figure 32: Comparison of original Beaver Valley hood loss curve to that of modification F

7.1.2.7 BV MODIFICATION F

This modification was the same as BV Modification E except that the back plate was replaced in the model.

The hood losses for this modification were lower than BV Modification E, but almost identical to the losses for BV Modification D. This modification corresponded to the original Beaver Valley exhaust hood with a different guide vane (see figure 23 (c)).

A curve for BV Modification F which combines the test results obtained with and without the screen is shown in figure 31 (solid curve). Figure 32 compares this

combination curve to the original Beaver Valley combination curve. The hood loss curve of BV Modification F is much lower than the original, especially at high Mach numbers. At an annulus Mach number of 0.84, the hood loss coefficient for modification F is smaller by approximately 0.25 than for the original hood, while at a Mach number of 0.40, the hood loss coefficient is lower by about 0.08.

7.1.3 HATFIELD FERRY ORIGINAL HOOD LOSS CURVES

The original Hatfield Ferry exhaust hood results are listed in tables E.5 and F.5 in Appendix E and Appendix F, respectively. Tests were performed, similarly to Beaver Valley, with and without a screen and with and without a condenser neck.

The hood loss, HL/LL, and pressure coefficients, C_p1 and C_p2, versus annulus Mach number curves for the case of "with screen" are shown in figure 33 (a). The hood loss curve for the "no screen" case is shown in figure 33 (b). The original Hatfield Ferry exhaust hood losses are much lower than those of the original Beaver Valley hood which were shown in figures 28 (a) and 28 (b). The reason why these losses were lower is that the Hatfield Ferry exhaust hood was more open (larger hood). Lower exhaust hood losses were expected since the results of the generic model (as shown in figure 18) indicated that, in general, a larger hood has lower losses than a smaller hood.

Figures 33 (a) and 33 (b) show that the hood losses for the tests with a screen case ranged between -0.146 to 0.462 at annulus Mach numbers of 0.462 and 0.781, respectively (based on calculation method 2). The exhaust hood losses for the tests without a ranged between -0.087 and 0.467 at annulus Mach numbers of 0.397 and

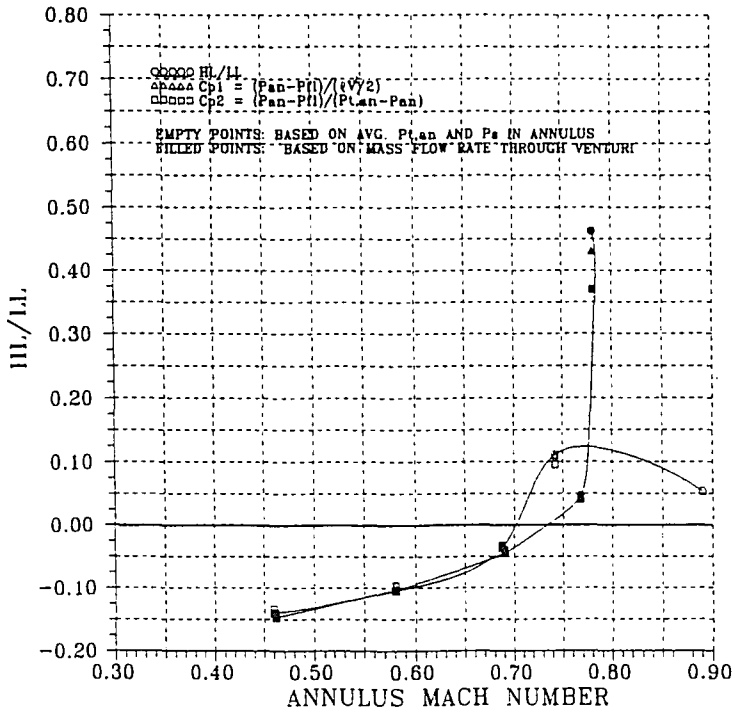

(a)

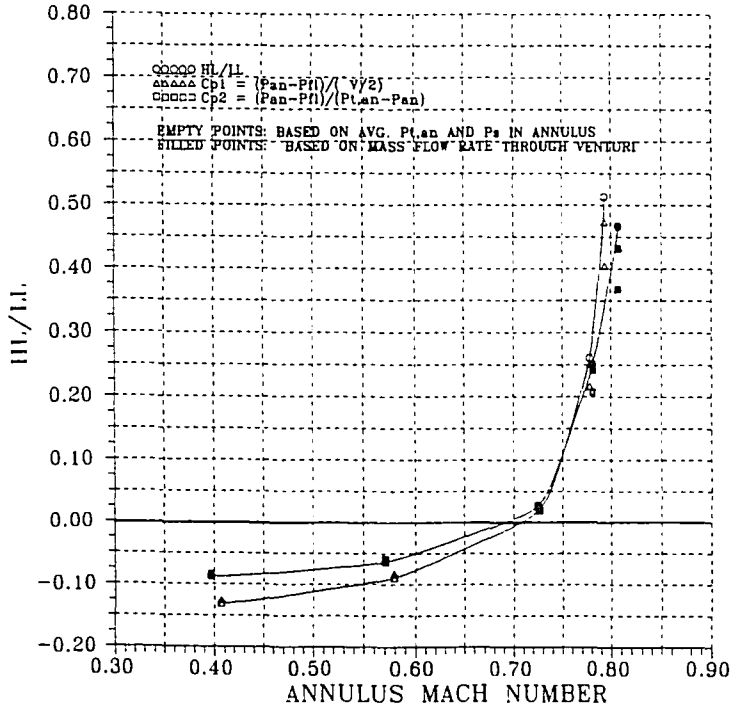

(b)

Figure 33: Hatfield Ferry original hood loss curve (a) hood alone with screen, (b) hood alone without screen

0.807, respectively. The losses for the "no screen" case are higher than the "with screen" case, but the difference between the two curves is not as high as for the Beaver Valley original hood loss curves.

Figure 34 shows a combination curve of with and without a screen for the original Hatfield Ferry model. The dotted lines are the Hatfield Ferry model "with screen" and "no screen" hood loss curves.

The original Hatfield Ferry model results with the condenser neck added to the model are shown in figure 35. Like the Beaver Valley curves, the losses are generally higher with the condenser neck than without.

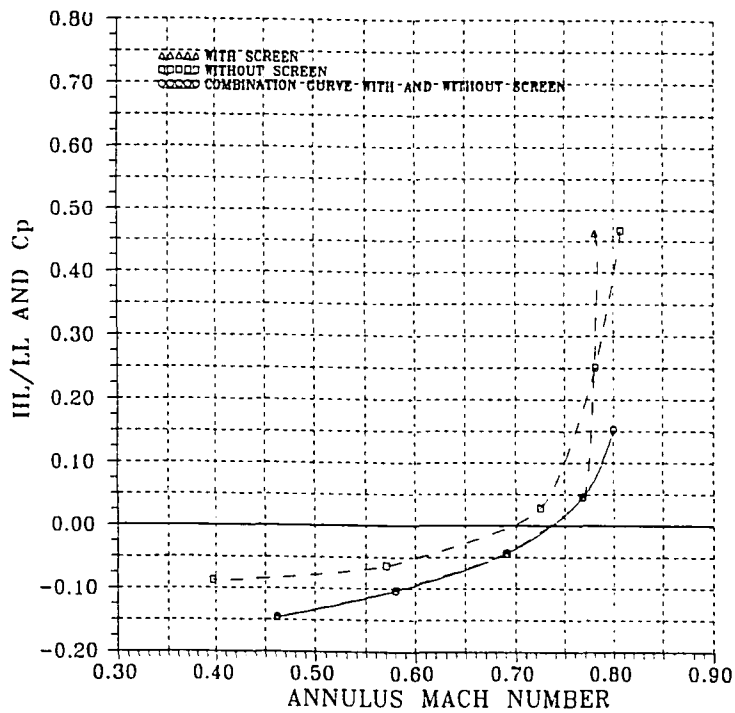

Figure 34: Hatfield Ferry original exhaust hood combination curve

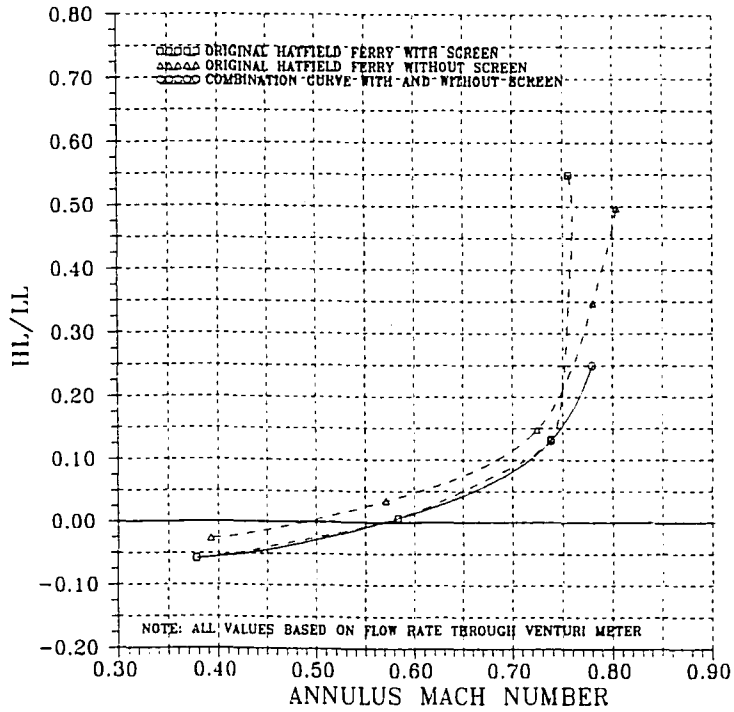

Figure 35: Hatfield Ferry original exhaust hood with condenser neck combination curve

7.1.4 MODIFIED HATFIELD FERRY EXHAUST HOOD LOSS RESULTS

The modified Hatfield Ferry exhaust hood results are listed in tables E.7 and F.7 in Appendix E and Appendix F, respectively. No improvement in performance was found for any of the modifications tested. The results of Modifications C,D, and E indicate that the fixed guide vane has a significant effect on the exhaust hood losses. The Hatfield Ferry modifications are discussed below.

7.1.4.1 HF MODIFICATION A

The size of the bearing cone was reduced on the upper 180 degree section to allow for more flow through the model. A new fixed guide vane was also created for this modification as shown in figure 24 (c).

A comparison of HF Modifications A,C,D, and E to the original Hatfield Ferry (with the screen) is shown in figure 36. The losses for HF Modification A, represented as the squares in figure 36, are the same as those of the original Hatfield Ferry.

7.1.4.2 HF MODIFICATION B

The original Hatfield Ferry bearing cone was put back in the model. The fixed guide vane of HF Modification A was also inserted into the hood.

This modification was not plotted in figure 36 because it was discovered by a measurement of the mass flow rate through the venturi meter during testing that there would be no improvement from the original.

7.1.4.3 HF MODIFICATION C

This modification was the same as HF Modification B except a different guide vane was placed in the hood. The guide vane corresponded to one which had the shape of the bottom half of the guide vane of HF Modification A.

The exhaust hood loss for one test point is shown in figure 36 (represented as a triangle in the figure). The hood loss was higher than the original Hatfield Ferry hood losses.

7.1.4.4 HF MODIFICATION D

This modification was the same as HF Modification C except it used a shorter

fixed guide vane.

The exhaust hood loss for one test point is shown in figure 36 (represented as a diamond in the figure). This hood loss was higher than any other modification.

7.1.4.5 HF MODIFICATION E

This modification was the same as modification D but used the guide vane of BV Modification D.

Figure 36 shows the hood loss for one test point for this modification (represented as an x). The hood loss was somewhat higher than the original.

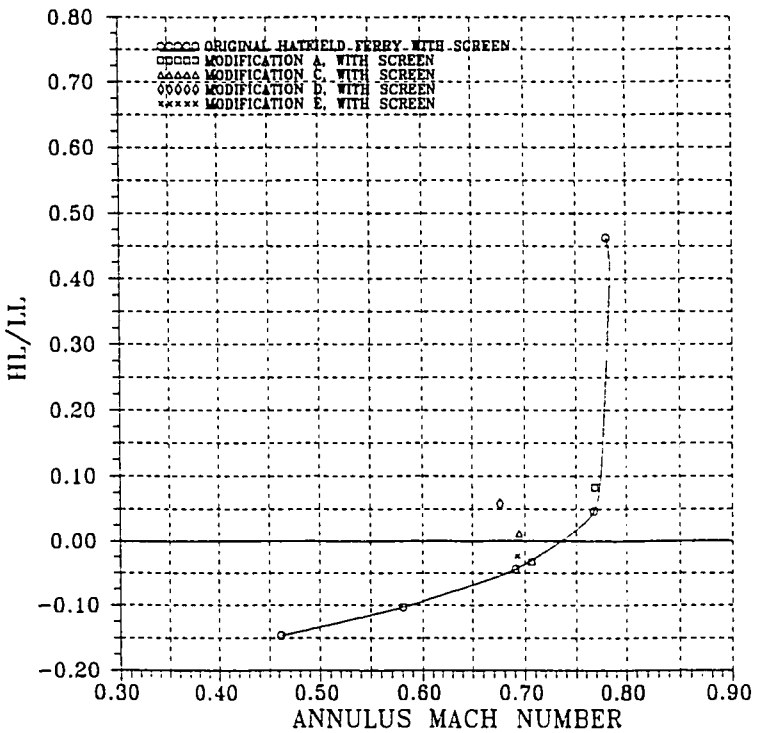

Figure 36: Comparison of Hatfield Ferry original hood loss curve to that of modification A,C,D, and E

7.2 CIRCUMFERENTIAL VARIATION OF THE LOCAL NONDIMENSIONAL PRESSURE COEFFICIENT

For each exhaust hood model test, twelve static pressures were measured on both the hub and the shroud of the models. The local nondimensional pressure coefficient, $C_P1_{,LOCAL}$ (see equation 3) , was calculated for each static pressure measured. Graphs of the local pressure coefficient versus pressure tap location were created for both the hub and the shroud. This was done to get an idea of the magnitude of the last blade excitation which occurs as a result of circumferential pressure variation in the last stage annulus. Some of these plots are located in Appendix H and are discussed below.

7.2.1 LOCAL NONDIMENSIONAL PRESSURE COEFFICIENT CURVES IN THE BEAVER VALLEY MODEL

Figures H.1 and H.2 in Appendix H show the circumferential variation of the local nondimensional pressure coefficient for two tests of the original Beaver Valley with the screen but without the condenser neck (hood alone).Figure H.1 represents a low annulus Mach number (M_{AN} = 0.330) and figure H.2 had a higher annulus Mach number (M_{AN} = 0.747). The curves for the hub are generally smooth and symmetric. The shroud curves are less symmetric. A "bump" consistently appears on the shroud curves at higher annulus Mach numbers. This "bump" occurs at 105 degrees (see figure 13) and may have been the result of an air leakage at the static pressure tap.

The figures show that the highest local static pressure for both the hub and the shroud was located at about 180 degrees, which corresponded to the top of the hood (see figure 13). The values of the local nondimensional pressure coefficient, $C_P1_{,LOCAL}$, have an average of 0.249 at the low annulus Mach number (figure H.1) and decreases to 0.217 at the higher annulus Mach number. The average shroud pressure coefficient, on the other hand, increases from -.257 at M_{AN} = 0.330 to -0.069 at M_{AN} = 0.747. Also, as the annulus Mach number increases, the difference between the local nondimensional pressure coefficient curves of the hub and the shroud decreases and the curves become flatter. The same general characteristics are seen for the original Beaver Valley for the case of the hood alone and without the screen (figures H.3 and H.4 in Appendix H), with the condenser neck and with screen (figures H.5 and H.6), and with the condenser neck and without the screen (figures H.7 and H.8).

Figures H.17 and H.18 in Appendix H show the local nondimensional pressure coefficient curves for modification F of the Beaver Valley model which had lower exhaust hood losses than the original. The same general characteristics described for the original Beaver Valley model are seen in these plots. The shroud curves are more symmetric than the original Beaver Valley hood.

7.2.2 LOCAL NONDIMENSIONAL PRESSURE COEFFICIENT CURVES IN THE HATFIELD FERRY MODEL

Figures H.9 and H.10 in Appendix H show circumferential variation of $C_P1_{,LOCAL}$ in the original Hatfield Ferry model for the case of the model tests run with

the screen. These pressure curves are much flatter than those of the corresponding Beaver Valley curves. Both the hub and shroud curves are less symmetric about the 180 degree location at higher annulus Mach numbers than at lower ones. At higher annulus Mach numbers the maximum value of the static pressure was observed to occur at approximately 300 degrees (see figure 13).

Figures H.9 and H.10 show that both the hub and shroud nondimensional pressure curves for the Hatfield Ferry model increase as the annulus Mach number increases. The average value of the local nondimensional pressure coefficient for the hub at $M_{AN} = 0.462$ is 0.164 and it increases to 0.373 at $M_{AN} = 0.768$. Similarly, the shroud nondimensional pressure coefficient values increase as the annulus Mach number increases. At $M_{AN} = 0.462$ the average shroud value is -0.374 and it increases to -0.093 at $M_{AN} = 0.768$. These trends are also seen for the case of the original Hatfield Ferry model tested with and without the screen (figures H.11 and H.12), with the condenser neck and with the screen (figures H.13 and H.14), and with the condenser neck and without the screen (figures H.15 and H.16).

7.3 TOTAL PRESSURE DISTRIBUTION ACROSS THE ANNULUS

The total pressure plots for the original Beaver Valley model tested with the screen are shown in appendix I.1 to I.7 in appendix I. The plots for the original Beaver Valley model tested without the screen are shown in figures I.8 to I.14. The effect of wakes created by the screen on the total pressure distribution is represented by the wavy shape. The lowest points, or dips, in the curves correspond to the wakes from

individual wire strands in the screen. The dips in the curves formed by the wakes are deeper at higher annulus Mach numbers. Without the screen in the annulus, as shown in figures I.8 to I.14 the total pressure distribution is uniform across the annulus and the curves appear flat until the annulus walls are reached.

Figures I.15 to I.21 show the original Hatfield Ferry model total pressure distribution across the annulus for all seven traverses. The curves appear, in general, less symmetric than those in the Beaver Valley model at intermediate annulus Mach numbers. At high annulus Mach numbers, the same type of jagged curves exist in the Hatfield Ferry model as with the Beaver Valley model. Figures I.22 to I.28 in Appendix I show the Hatfield Ferry total pressure distribution for the model without the screen. As in the Beaver Valley model, the total pressure distribution is uniform across the annulus.

Beaver Valley Modification F has lower exhaust hood losses than the original Beaver Valley model. Figures I.29 to I.31 show the total pressure distribution of this modification tested with the screen, and figures I.32 to I.34 show the corresponding curves for the tests without the screen. The same general characteristics that were seen in the original Beaver Valley model were observed in this modification, but the total pressure distribution curves are lower at similar annulus Mach numbers.

8 CONCLUSIONS

The losses of the Beaver Valley and Hatfield Ferry exhaust hoods were determined in this experimental model study. Tests were performed with and without a condenser neck on exhaust hood models which used air as the working fluid. Curves combining the results obtained with and without a screen in the models were produced. They allow the determination of the hood loss coefficient for a given average annulus Mach number.

Several observations can be made:

- The exhaust hood losses increase as the annulus Machnumber increases.
- The size of the exhaust hood affects the hood losses. A larger hood has lower losses than a smaller hood when all other geometric parameters are held constant.
- Proper design of the fixed guide vane and bearing cone can significantly lower the hood losses.
- The back plate is an important component in exhaust hoods. The exhaust hood losses were lower with the back plate in the modified Beaver Valley model than without the back plate.
- The losses with the screen in the hood models were lower than those obtained without the screen. This indicates that the flow pattern may be different between the two cases and should be investigated further.

- The addition of the condenser neck to the exhaust hood models results in increased losses.

The exhaust hood losses for the Beaver Valley model were lowered with the addition of a new fixed guide vane. The losses for the original Beaver Valley model tested without a condenser neck, based on the combination curve of tests with and without a screen, ranged between 0.026 and 0.423 at annulus Mach numbers of 0.330 and 0.842, respectively. The hood losses for the modification with the new fixed guide vane were lowered to -0.034 to 0.220 at annulus Mach numbers of 0.370 and 0.871, respectively.

No improvement in performance was found through modification of the Hatfield Ferry model. The losses for the original Hatfield Ferry model, based on the combination curve of tests with and without a screen, ranged between -0.146 to 0.15 at annulus Mach numbers of 0.462 and 0.8, respectively.

Additional studies aimed at improvement of the existing Hatfield Ferry exhaust hood, and further improvement of the existing Beaver Valley exhaust hood, should concentrate on optimizing the shape of the fixed guide vane and condenser neck design. Through experimental testing it was shown that the fixed guide vane has a significant effect on the hood losses for both the Beaver Valley and Hatfield Ferry models. As expected, the losses for both the Beaver Valley and Hatfield Ferry models were higher when the condenser neck was added. These loss curves might be lowered if a more efficient condenser neck design were produced.

REFERENCES

[1] Reneau, L.R , Johnston J. P. , Kline, S.J. , "Performance and Design of Straight,Two-Dimensional Diffusers", Journal of BasicEngineering, Trans. ASME, March 1967, pp. 141-150

[2] Howard, J.H.G. , Henseler, H.J. , Thorton-Trump, A.B. ; "Performance and Flow Regimes for Annular Diffusers", ASME paper 67-WA/FE-21, 1967

[3] Fox, R.W. , Kline, S.J., "Flow Regimes in Curved Subsonic Diffusers"' Journal of Basic Engineering, Trans. ASME, series D, vol. 84, 1962, pp. 302-316

[4] Kline, S.J., "On the Nature of Stall", Journal of Basic Engineering, Trans ASME, series D, vol. 81 Sept. 1959, pp. 305-320

[5] Sovran, G. , Klomp, E.D., "Experimentally Determined Optimum Geometries for Rectilinear Diffusers with Rectangular, Conical, or Annular Cross-Section" General Motors Research Laboratory, Warren, Michigan, Printed in Fluid Mechanics of Internal Flow, G. Sovran, editor, Elsevier Publishing Co., 1967, pp. 270-319

[6] Hoffman, J.A. , Gonzalez, G., "Effects of Small-Scale, High Intensity Inlet Turbulence on Flow in a Two-Dimensional Diffuser", Journal of Fluids Engineering, vol. 106, June 1984, pp. 121-124

[7] Owczarek, J.A., Warnock, A.S. ; IMO DeLaval, "Improvement of a Low Pressure Turbine Exhaust Flow, Final Report", Lehigh University, December 1989

[8] Owczarek, J.A., Fundamentals of Gas Dynamics, International Textbook Co., Scranton, PA, 1964

[9] Anderson, J.D., Jr., Modern Compressible Flow With Historical Perspective, Second Edition, McGRaw-Hill Publishing Co., 1990, pp. 21-22

[10] Celen, S., "Performance Improvement Study of Steam Turbine Exhaust Hoods", M.S. Thesis, Lehigh University, December 1992

[11] Turegun, B. ; "Design of an Air Test Loop and Turbine Exhaust Hood Models for Performance Improvement Study", M.S. Thesis, Lehigh University, June 1991

[12] Sagi, C.J. , Johnson, J.P., "The Design and Performance of Two-Dimensional, Curved Diffusers", Journal of Basic Engineering, Trans. ASME, Series D, Vol. 89, #4, Dec. 1967, pp. 715-731

[13] Cockrell, D.J. ; Markland, E.J., "A Review of Incompressible Diffuser Flow", Aircraft Engineering, Vol. 35, 1963, pp. 286-292

[14] Purcell, E.J. , Varberg, D., Calculus With Analytic Geometry, Fifth Edition, Prentice-Hall Inc., Englewood Cliffs, NJ, pp. 446-447

[15] Kline, S.J. , Abbott, D.E. , Fox, R.W. "Optimum Design of Straight-Walled Diffusers", Journal of Basic Engineering, Trans. ASME, Series D, Vol. 81, 1959, pp. 321-329

[16] Van Dewoestine, R.V. , Fox, R.W., "An Experimental Investigation on the Effect of Subsonic Inlet Mach Number on the Performance of Conical Diffusers". International Journal of Mechanical Sciences, Vol 8, 1966, pp. 759-769

[17] Kumar, D.S. , Kumar, K.L., "Effect of Swirl on Pressure Recovery in Annular Diffusers", Journal of Mechanical Engineering Science, Vol 22, no. 6, 1980, pp. 305-313

[18] McDonald, A.T. , Fox, R.W. , Van Dewoestine, R.V., "Effects of Swirling Inlet Flow on Pressure Recovery in Conical Diffusers", AIAA paper # 71-85, 1971

[19] Thayer, E.B., "Evaluation of Curved-Wall Annular Diffusers", ASME paper # 71- WA/FE-35, 1971

[20] Taylor, A.M.P.K., Whitela, J.H.,Yianneskis, M, "Curved Ducts With Strong Secondary Motion: Velocity Measurements on Developing Laminar and Turbulent Flow", Journal of Fluids Engineering, Trans. ASME, Vol. 104, Sept. 1982, pp. 350-359

[21] Stevens, S.J., Williams, G.J., "The Influence of Inlet Conditions on the Performance of Annular Diffusers with Conical Walls", ASME Trans, Journal of Fluids Engineering, Vol 102, September 1980, pp. 357-363

[22] Seglem, C.E., Brown, R.O., "Turbine Exhaust Losses", ASME Paper #60-PWR-7

[23] Owczarek, J.A., Warnock, A.S., "Preliminary Proposal for Research Project, Part 2: Improvement of LP Turbine Hood Performance", Energy Research Center, Lehigh University, 1988

[24] Parsons, D.J., Hill, P.G.,"Effects of Curvature on Two-Dimensional Diffuser Flow", Journal of Fluids Engineering, September 1973, pp. 349-360

[25] Bean, H.S., Fluid Meters, Their Theory and Application, 6th ed., New York, ASME, 1971

BIBLIOGRAPHY

1 Horn, S.V., Shanafelt, M.E., "Aerodynamic Development of a Low Pressure Steam Turbine Exhaust Hood", Transamerica Delaval Inc., Trenton, NJ

2 Chesmejef, S. ,"Aerodynamic Testing of a Low Stimulus, Efficient Exhaust Hood-Industrial Turbines", ASME paper #77-JPGC-Pwr-2

3 Tindell, R.H., Alston, T.M., "A Comparison of Two Methods for Utilizing Steam Turbine Exhaust Hood Flow Field Data", Journal of Turbomachinery, Trans. ASME, vol. 114, April, 1992, pp.398-401

4 Holden, P.C., Barsness, E.J.,"Condenser-Exhaust Hood Air Model Tests", ASME paper #63-WA-245

5 Carlson, J.J., Johnston, J.P., Sagi, C.J., "Effects of Wall Shape on Flow Regimes and Performance in Straight, Two-Dimensional Diffusers" Journal of Basic Engineering, Trans. ASME, March 1967 pp. 151-160

6 Fowler, J.E., "Factors Affecting the Design of Turbine-Condenser Connections", Combustion, March 1977, pp. 24-32

7 Zaryankin, A.E., Kasilov, V.F., Denisov, V.N., "Features of Steam Flow in the Exhaust Pipe of a Steam Turbine at High Subsonic Speeds", Thermal Engineering (English Translation) 1987

8 Brown, R.O, Heinze, F.J., Davids, J.,"High Performance Low Pressure Turbine Elements", Journal of Engineering for Power, Trans ASME, July 1984, pp. 386-392

9 Migai, V.K., Gudkov, E.I., Nosova, I.S., "Increasing the Efficiency of Diffusers of Steam Turbine Exhausts", Thermal Engineering (English Translation) 1976

10 Owczarek, J.A., Warnock, A.S., Malik, P., "A Low Pressure Turbine Exhaust End Flow Model Study", Consolidated Edison Company of New York

11 Lagun, V.P., Simoyu, L.L.,Boitsova, E.A., Naftulin, A.B., Semenov, Y.E.,"Method and Some Correlated Results of a Study of Exhaust Hoods on Full-Scale Steam Turbines", Thermal Engineering, vol 38 (2) 1991 pp. 71-75

10 APPENDIX

10.1 APPENDIX A

GRAPHICAL DETERMINATION OF THE HOOD LOSS COEFFICIENT

and

APPENDIX A
(Graphical determination of the hood loss coefficient [7])

The non-dimensional hood loss coefficient, HL/LL, at various Mach numbers can be obtained graphically by creating a plot of the terms

$$(\frac{P_{AN}}{P_{T,AN}})^{\frac{\gamma-1}{\gamma}} \tag{A.1}$$

and

$$(\frac{P_{FL}}{P_{T,AN}})^{\frac{\gamma-1}{\gamma}} \tag{A.2}$$

versus Mach number. The term in A.1 can be found from the expression

$$(\frac{P_{AN}}{P_{T,AN}})^{\frac{\gamma-1}{\gamma}} = \frac{1}{1+\frac{\gamma-1}{2}M_{AN}^{2}} \tag{A.3}$$

which is a function of Mach number only. The term in A.2 is obtained from model tests. An example plot of terms A.1 and A.2 is shown in figure A.1.

The dimensionless hood loss coefficient is found in figure A.1 as HL/LL = C/D, where

$$C=(\frac{P_{AN}}{P_{T,AN}})^{\frac{\gamma-1}{\gamma}}-(\frac{P_{FL}}{P_{T,AN}})^{\frac{\gamma-1}{\gamma}} \tag{A.4}$$

$$D=1-(\frac{P_{AN}}{P_{T,AN}})^{\frac{\gamma-1}{\gamma}} \qquad \textbf{(A.5)}$$

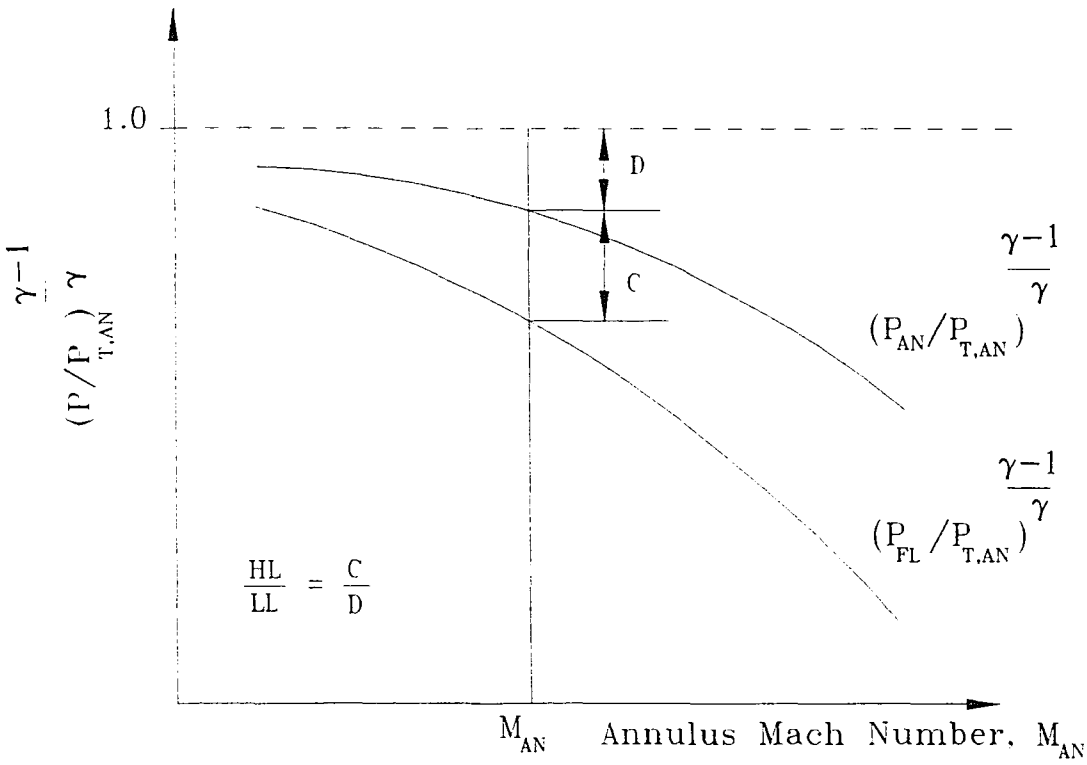

Figure A.1: Graphical determination of the hood loss coefficient

10.2 APPENDIX B

GENERIC MODEL EXHAUST HOOD LOSS CURVES

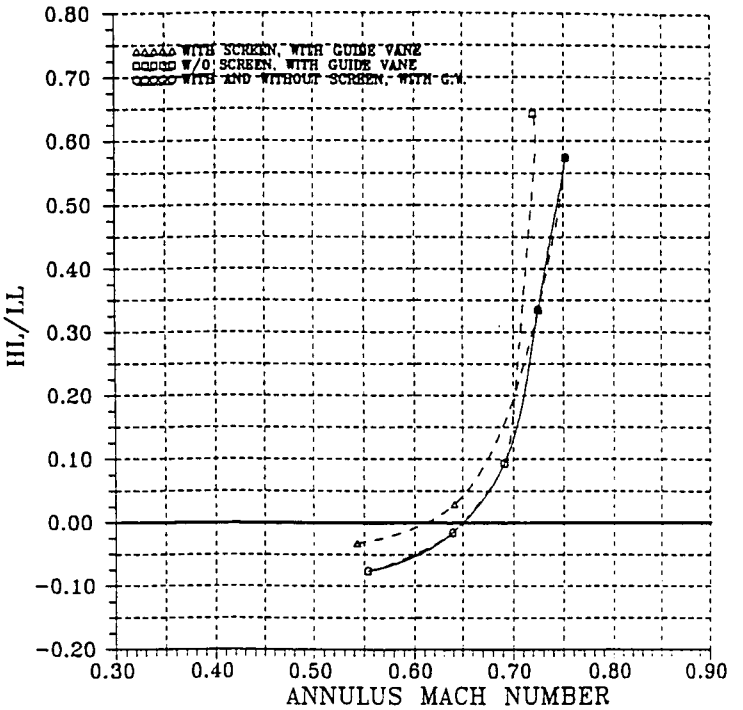

Figure B.1: Hood loss curve for configuration 1 of the generic model, with and without screen

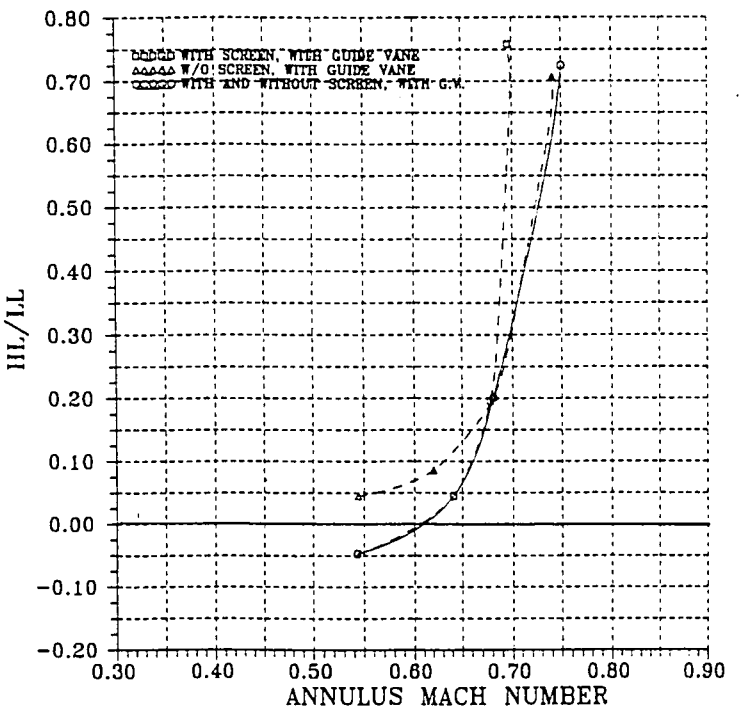

Figure B.2: Hood loss curve for configuration 2 of the generic model, with and without screen

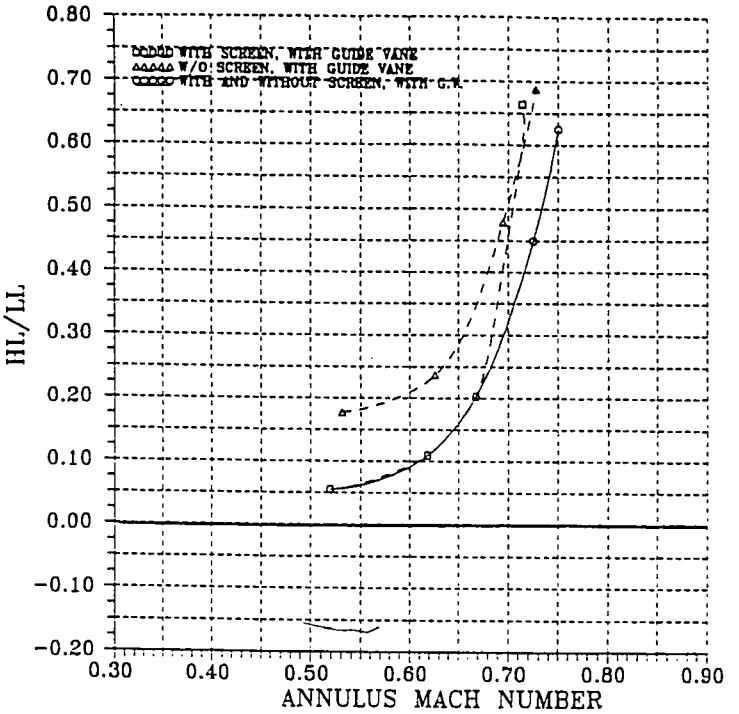

Figure B.3: Hood loss curve for configuration 3 of the generic model, with and without screen

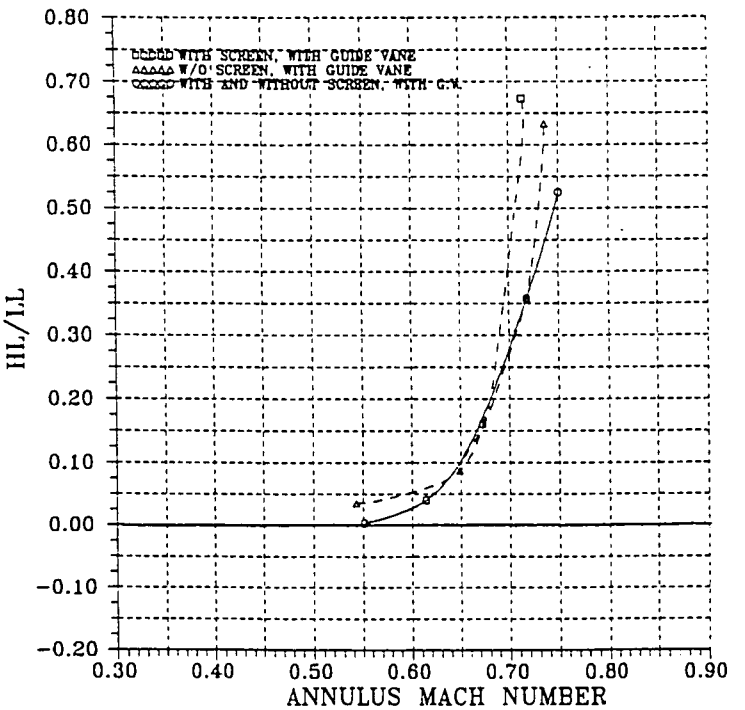

Figure B.4: Hood loss curve for configuration 4 of the generic model, with and without screen

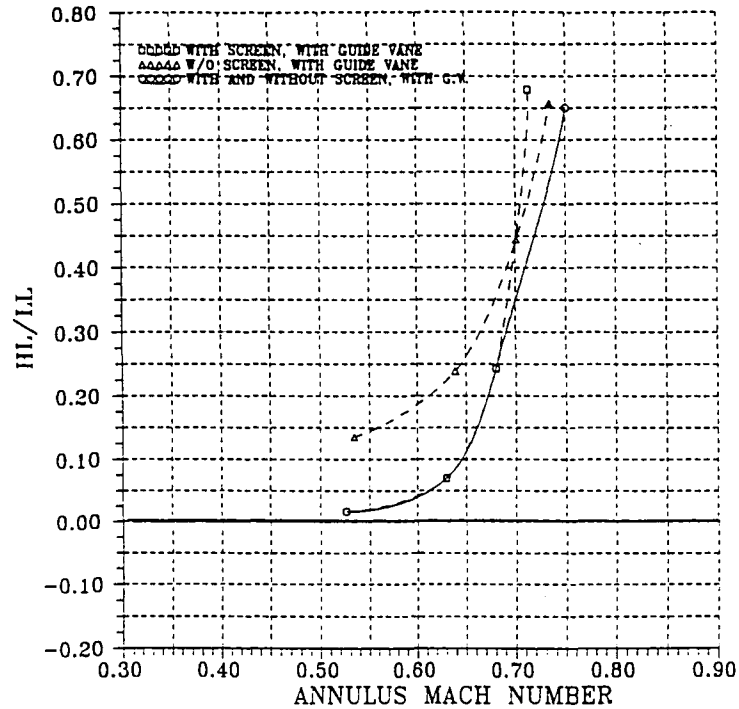

Figure B.5: Hood loss curve for configuration 5 of the generic model, with and without screen

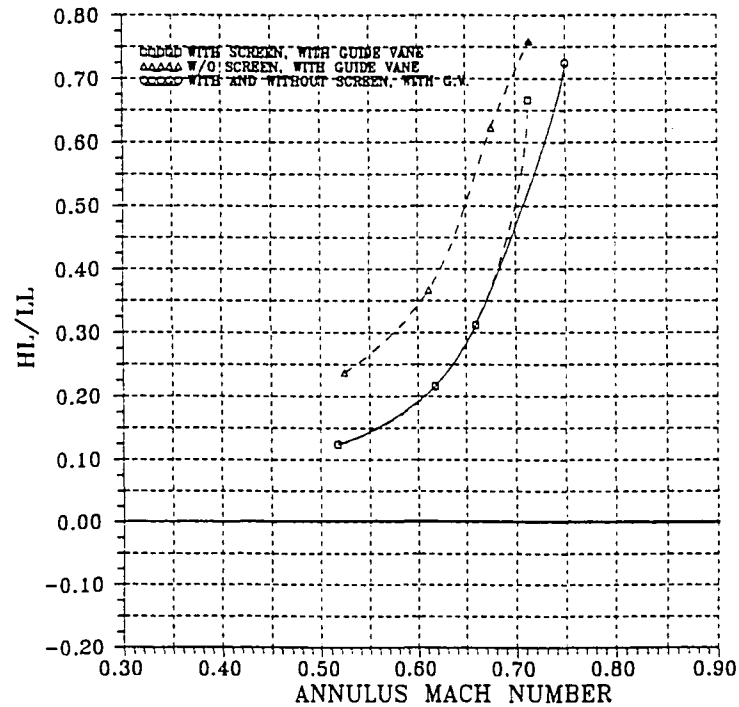

Figure B.6: Hood loss curve for configuration 6 of the generic model, with and without screen

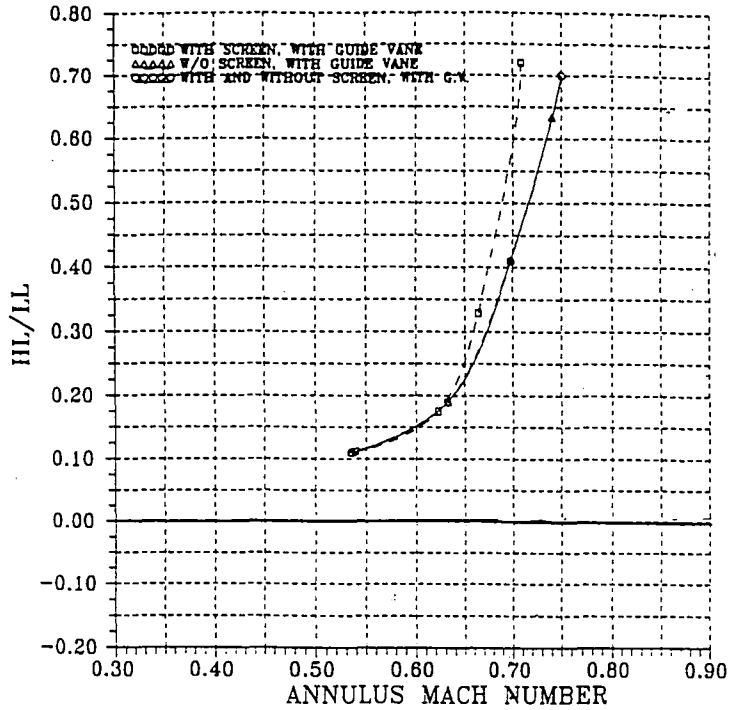

Figure B.7: Hood loss curve for configuration 7 of the generic model, with and without screen

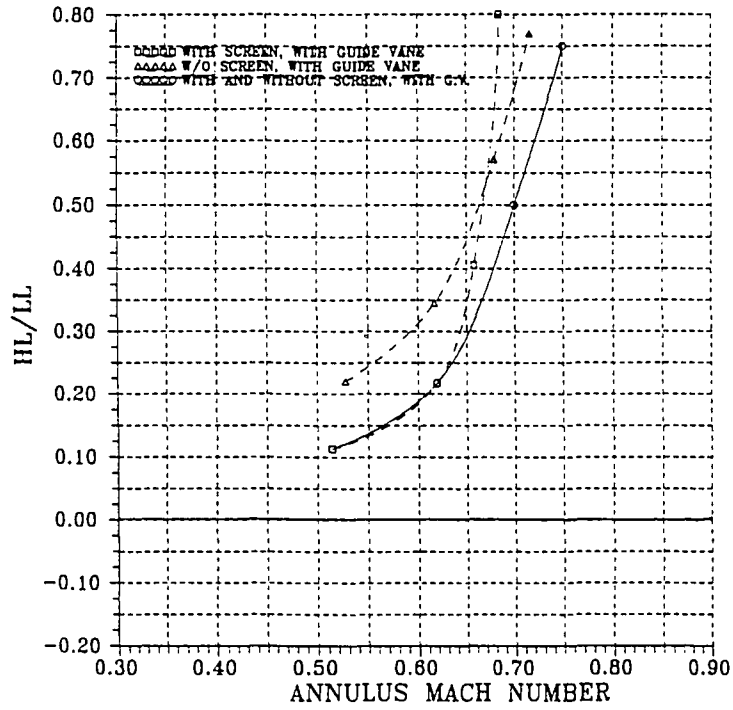

Figure B.8: Hood loss curve for configuration 8 of the generic model, with and without screen

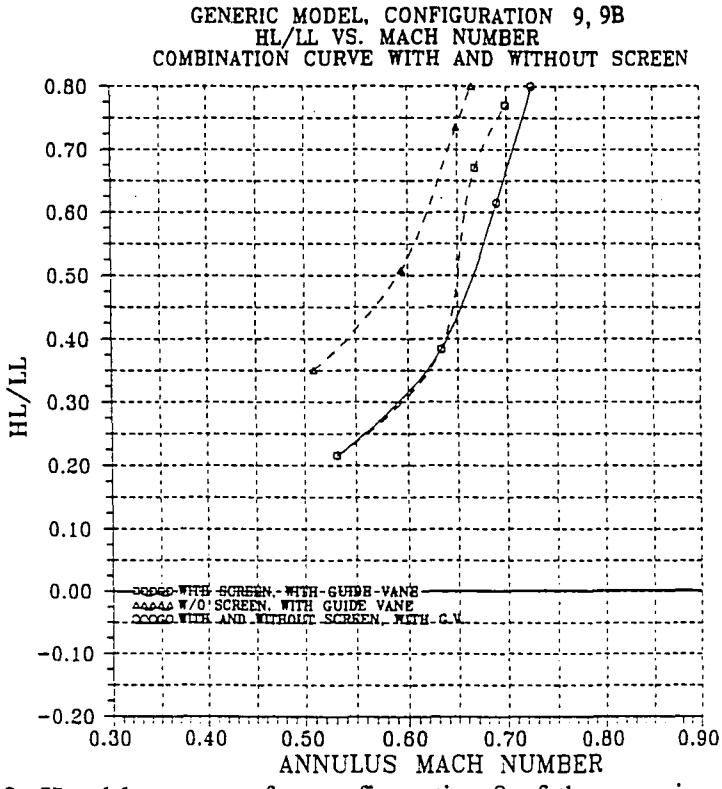

Figure B.9: Hood loss curve for configuration 9 of the generic model, with and without screen

10.3 APPENDIX C

CALIBRATION CURVES, AIR TABLES, VENTURI METER INFORMATION

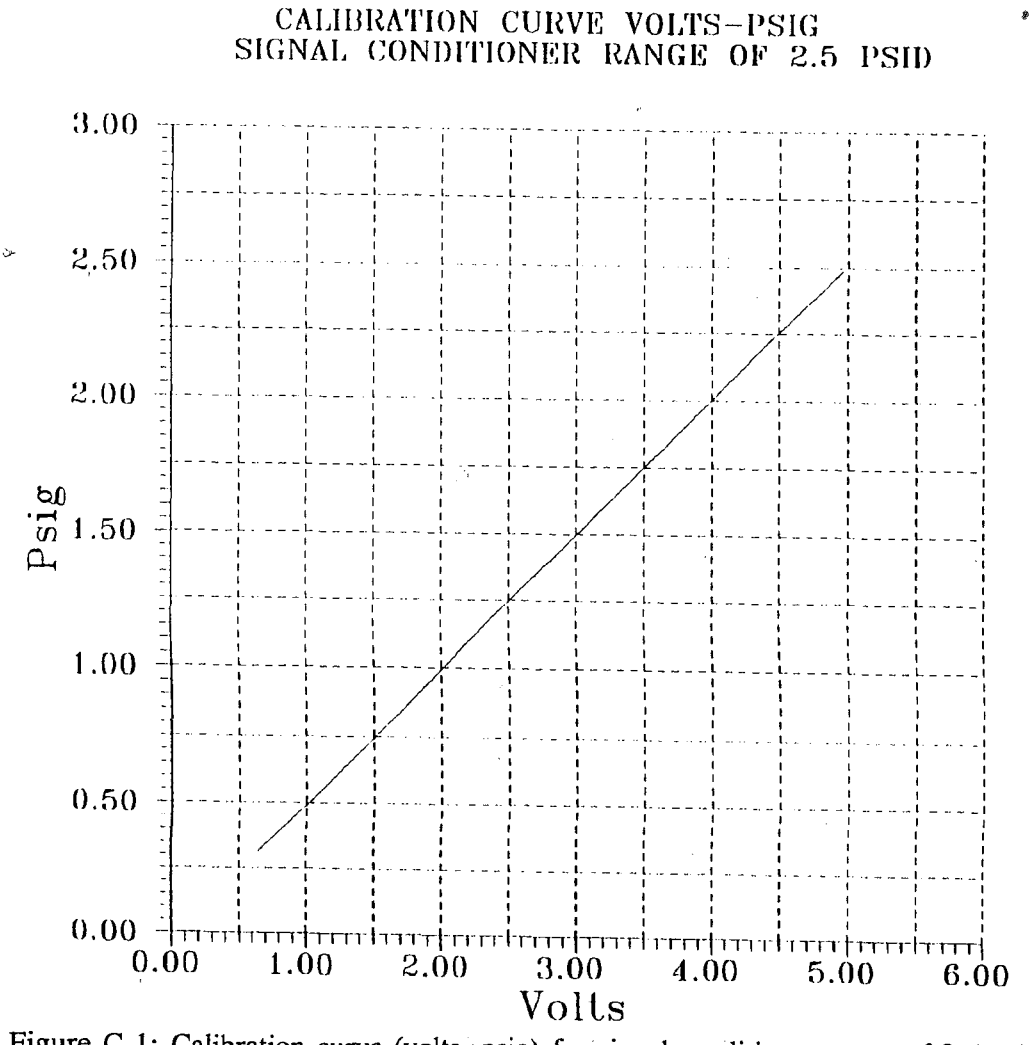

Figure C.1: Calibration curve (volts→psig) for signal conditioner range of 2.5 psid

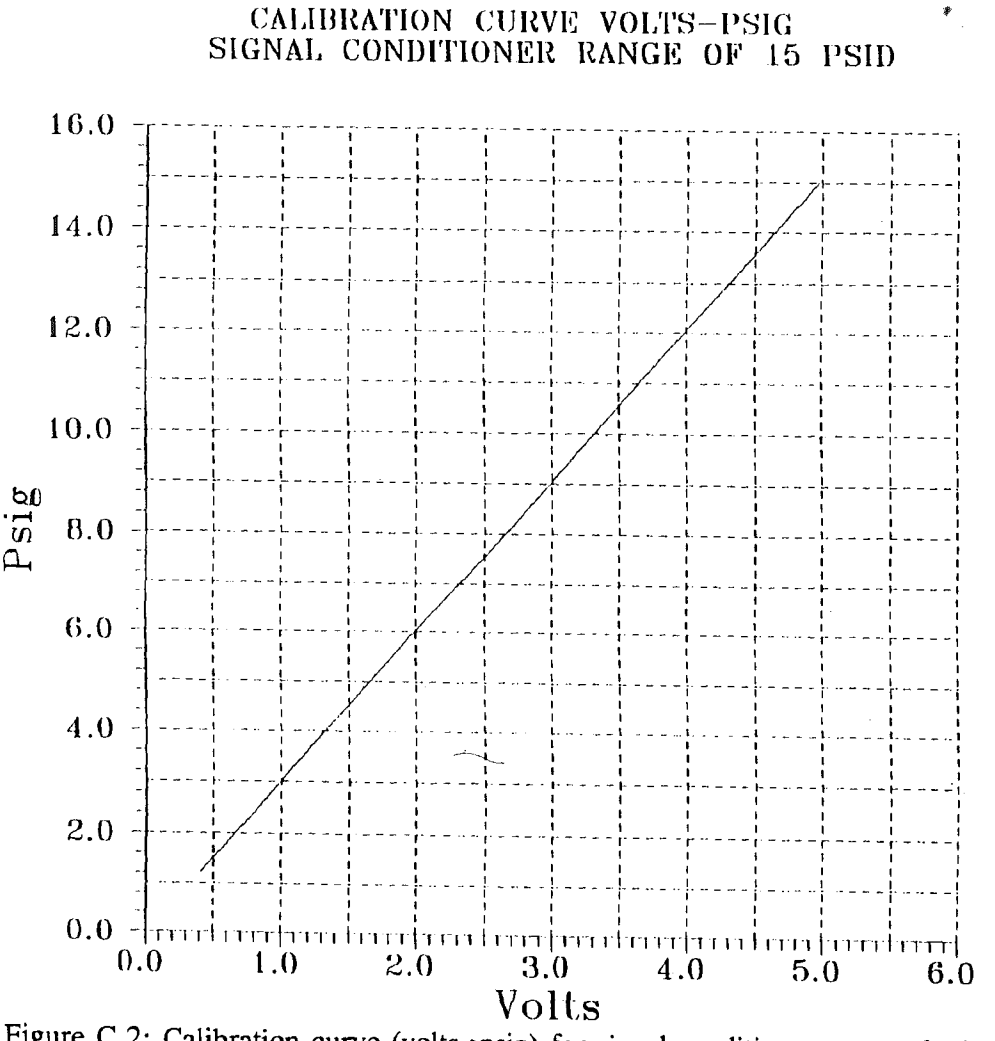

Figure C.2: Calibration curve (volts→psig) for signal conditioner range of 15 psid

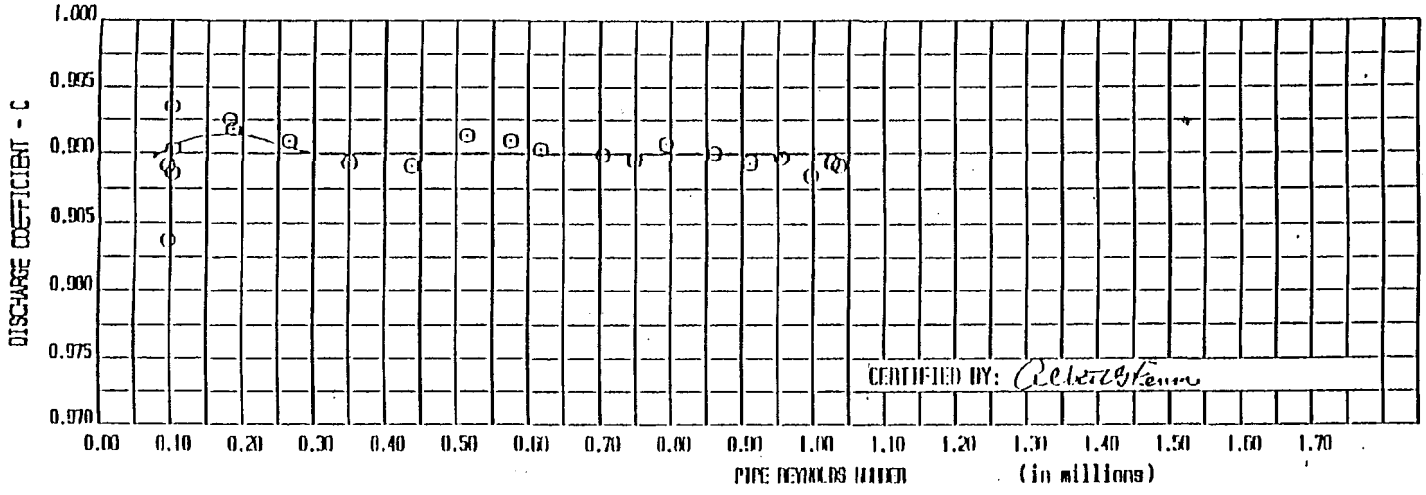

$q_a = C F_a K_N \sqrt{h}$

q_a = Actual Flow Rate (ft^3/sec)	
C = Discharge Coefficient (Dimensionless)	
h = Pressure Differential (Feet of Water at this Temperature)	
K_N = Meter Constant = $\frac{F_a \, a\sqrt{2g}}{\sqrt{1-\beta^4}}$	3.7742
F_a = Thermal Expansion Factor	
a = Throat Area (ft^2) =	0.4519
g = Local Acceleration of Gravity (ft/sec^2)	32.1600
β = Ratio of Throat to Pipe Diameter (Dimensionless) =	0.5201
Upstream Diameter (Inches) =	17.2310
Throat Diameter (Inches) =	9.1020
Dimensions By: FLUIDIC	

MEAN = 0.9890 ABOVE PIPE REYNOLDS #200000

Figure C.3: Plot showing the venturi meter discharge coefficient, C

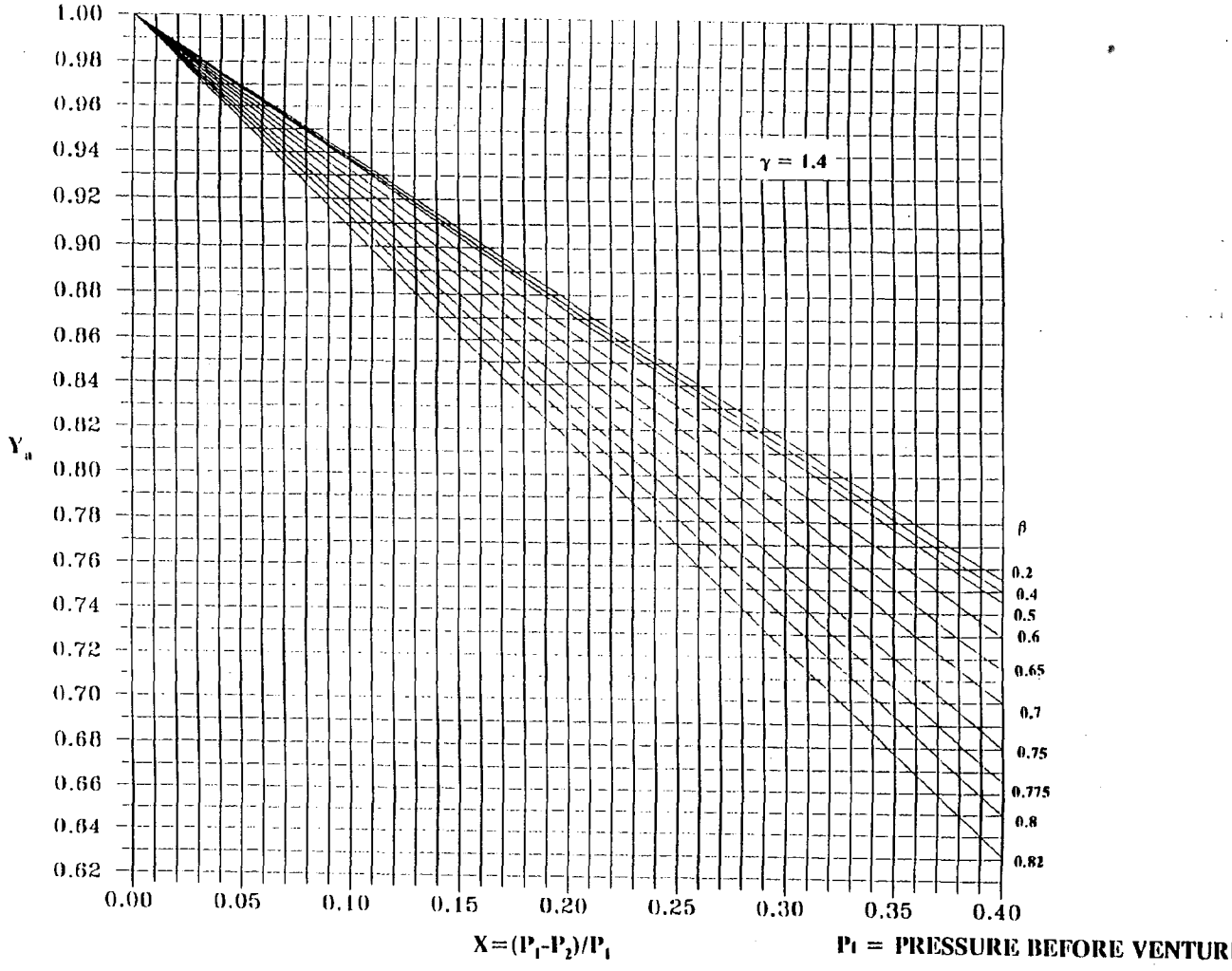

Figure C.4: Graph used to find the expansion factor Y [25]

TABLE C.1: NONDIMENSIONAL MASS FLOW RATE VS. ANNULUS MACH NUMBER	
Annulus Mach Number	$\frac{P_{T,AN}A_{AN}}{W\sqrt{RT_{T,AN}}}$
.11911	7.1093
.17013	5.0545
.20905	4.1497
.24220	3.6138
.27169	3.2505
.29863	2.9843
.32366	2.7788
.34720	2.8145
.36954	2.4796
.39090	2.3664
.41144	2.2699
.43127	2.1866
.45051	2.1138
.46922	2.0498
.48749	1.9928
.50536	1.9420
.54009	1.8550
.57372	1.7836
.60650	1.7242
.63862	1.6744
.6702	1.6323
.70144	1.5967
.73240	1.5666
.76316	1.5412
.79389	1.5200
.82461	1.5025
.85542	1.4884
.88639	1.4773
.91761	1.4691
.94914	1.4637
.98107	1.4609

TABLE C.2: SPECIFIC WEIGHT OF MERCURY AND WATER

	Specific Weight	
Temperature, °F	Mercury (lb/in^3)	Water (lb/in^3)
52	0.490164	0.036113
56	0.489966	0.036104
60	0.489769	0.036092
64	0.489572	0.036078
68	0.489375	0.036062
72	0.489178	0.036045
76	0.488981	0.036026
80	0.488784	0.036005

10.4 APPENDIX D

SAMPLE BEAVER VALLEY AND HATFIELD FERRY RAW DATA AND TEST RESULTS

DATA SHEET

TEST NO: #29
CONFIGURATION NO: (BV+CN-SCR)
MODEL: BEAVER VALLEY
COMP. SPEED(RPM):
FLOW RATE:

TEST DATE: 3/11/93
TIME(START): 9:50
TIME(END):

BAROMETRIC PRES:	29.14" Hg	10^09 AM 29.13" Hg	10^15 AM 29.14" Hg	10^26 AM 29.14" Hg	10^42 AM 29.14" Hg
BAROMETRIC TEMP:	71°F	72°F	72°F	72°F	72°F
DRY BULB:	83°F				
WET BULB:	58°F				
RELATIVE HUMIDITY:	19				

TIME:		9:54	10^02 AM	10^12 AM	10^15 AM	10^26 AM	10^41 AM
VENTURI TEMP:	(F)	97	96.	96.	96.	96.	96.
VENTURI INLET PRES:	(PSIG)	8.91	8.90	8.90	8.90	8.91	8.90
ΔP ACROSS VENTURI:	"WATER	12.80	12.80	12.80	12.80	12.80	12.80
MODEL INLET TEMP:	(F)	95.8	95.0	95.0	94.8	94.6	94.6
COMP. DISCHARGE TEMP:	(F)	186.9	187.6	188.0	187.7	187.4	186.6

DATA SHEET

TEST NO: 129
CONFIGURATION NO: (BV-HCN-SCR)
MODEL: DENVER VALVES

TEST DATE: 3/11/92

			TIME	
		9:50	10:41	
15 PSID SC. VALVE	CORRESP. PRES TAP	PSIAT (Volts)	PSIAT (Volts)	PSIAT (Volts)
16				
17	US 1	1.972	1.963	
18	US 2	1.944	1.943	
19	US 3	1.935	1.933	
20	US 4	1.945	1.942	
21				
22	II 1	.847	.853	
23	II 2	.961	.952	
24	II 3	1.187	1.186	
25	II 4	1.410	1.420	
26	II 5	1.561	1.561	
27	II 6	1.490	1.482	
28	II 7	1.322	1.358	
29	II 8	1.161	1.158	
30	II 9	0.985	.980	
31	II 10	.899	.883	
32	II 11	.852	.857	
33	II 12	.843	.846	

			TIME	
		9:53	10:46	
15 PSID SC. VALVE	CORRESP. PRES TAP	PSIAT (Volts)	PSIAT (Volts)	PSIAT (Volts)
34				
35	S 1	.181	.187	
36	S 2	.220	.232	
37	S 3	.658	.639	
38	S 4	.570	.566	
39	S 5	.595	.585	
40	S 6	.573	.568	
41	S 7	.477	.466	
42	S 8	.322	.310	
43	S 9	.247	.244	
44	S 10	.165	.159	
45	S 11	.269	.255	
46	S 12	.211	.217	
47				

TEST NO: 29
CONFIGURATION NO: (BV + CAV - SCR)
MODEL: DENVER VALVE
COMP. SPEED (RPM):

DATA SHEET

TEST DATE: 3/11/93
TIME(START): 9:50
TIME(END): 10:41

		TRAVERSE 1		TRAVERSE 2		TRAVERSE 3		TRAVERSE 4		TRAVERSE 5		TRAVERSE 6		TRAVERSE 7		
		Position (Inch)	Plot (1) (Volts)	Position (Inch)	Plot (2) (Volts)	Position (Inch)	Plot (3) (Volts)	Position (Inch)	Plot (4) (Volts)	Position (Inch)	Plot (5) (Volts)	Position (Inch)	Plot (4) (Volts)	Position (Inch)	Plot (3) (Volts)	
SHR	1	1.500	1.712	1.500	1.907	1.500	2.047	1.500	2.002	1.500	1.915	1.500	1.963	1.500	1.958	1 SHR
	2	1.450	2.288	1.450	2.972	1.450	2.584	1.450	2.569	1.450	2.521	1.450	2.598	1.450	2.586	2
	3	1.400	2.746	1.400	2.746	1.400	2.828	1.400	2.818	1.400	2.811	1.400	2.826	1.400	2.785	3
	4	1.350	2.851	1.350	2.876	1.350	2.886	1.350	2.878	1.350	2.876	1.350	2.856	1.350	2.864	4
	5	1.300	2.886	1.300	2.902	1.300	2.916	1.300	2.887	1.300	2.906	1.300	2.881	1.300	2.876	5
	6	1.250	2.912	1.250	2.912	1.250	2.909	1.250	2.902	1.250	2.914	1.250	2.892	1.250	2.887	6
	7	1.200	2.923	1.200	2.924	1.200	2.922	1.200	2.916	1.200	2.933	1.200	2.895	1.200	2.890	7
	8	1.150	2.930	1.150	2.920	1.150	2.930	1.150	2.901	1.150	2.938	1.150	2.898	1.150	2.891	8
	9	1.100	2.938	1.100	2.921	1.100	2.935	1.100	2.882	1.100	2.930	1.100	2.902	1.100	2.886	9
	10	1.050	2.939	1.050	2.934	1.050	2.934	1.050	2.878	1.050	2.932	1.050	2.904	1.050	2.892	10
	11	1.000	2.935	1.000	2.928	1.000	2.920	1.000	2.870	1.000	2.929	1.000	2.903	1.000	2.891	11
	12	0.950	2.930	0.950	2.937	0.950	2.921	0.950	2.866	0.950	2.930	0.950	2.902	0.950	2.890	12
	13	0.900	2.928	0.900	2.941	0.900	2.913	0.900	2.861	0.900	2.930	0.900	2.906	0.900	2.891	13
	14	0.850	2.914	0.850	2.941	0.850	2.911	0.850	2.869	0.850	2.937	0.850	2.901	0.850	2.890	14
	15	0.800	2.940	0.800	2.940	0.800	2.906	0.800	2.862	0.800	2.928	0.800	2.894	0.800	2.885	15
	16	0.750	2.941	0.750	2.934	0.750	2.901	0.750	2.866	0.750	2.943	0.750	2.896	0.750	2.883	16
	17	0.700	2.940	0.700	2.931	0.700	2.909	0.700	2.864	0.700	2.937	0.700	2.895	0.700	2.881	17
	18	0.650	2.940	0.650	2.937	0.650	2.888	0.650	2.863	0.650	2.939	0.650	2.896	0.650	2.881	18
	19	0.600	2.938	0.600	2.941	0.600	2.891	0.600	2.868	0.600	2.945	0.600	2.894	0.600	2.882	19
	20	0.550	2.938	0.550	2.930	0.550	2.894	0.550	2.875	0.550	2.951	0.550	2.882	0.550	2.880	20
	21	0.500	2.937	0.500	2.926	0.500	2.878	0.500	2.871	0.500	2.943	0.500	2.887	0.500	2.876	21
	22	0.450	2.940	0.450	2.940	0.450	2.874	0.450	2.868	0.450	2.942	0.450	2.891	0.450	2.874	22
	23	0.400	2.940	0.400	2.944	0.400	2.876	0.400	2.868	0.400	2.938	0.400	2.890	0.400	2.871	23
	24	0.350	2.942	0.350	2.940	0.350	2.870	0.350	2.877	0.350	2.951	0.350	2.891	0.350	2.875	24
	25	0.300	2.953	0.300	2.940	0.300	2.865	0.300	2.872	0.300	2.946	0.300	2.891	0.300	2.872	25
	26	0.250	2.946	0.250	2.938	0.250	2.876	0.250	2.872	0.250	2.950	0.250	2.891	0.250	2.874	26
	27	0.200	2.943	0.200	2.933	0.200	2.876	0.200	2.874	0.200	2.950	0.200	2.881	0.200	2.876	27
	28	0.150	2.945	0.150	2.933	0.150	2.875	0.150	2.872	0.150	2.946	0.150	2.878	0.150	2.874	28
	29	0.100	2.929	0.100	2.940	0.100	2.875	0.100	2.876	0.100	2.954	0.100	2.876	0.100	2.864	29
	30	0.050	2.616	0.050	2.928	0.050	2.627	0.050	2.803	0.050	2.899	0.050	2.830	0.050	2.501	30
HUB	31	0.000	2.315	0.000	2.262	0.000	1.701	0.000	1.745	0.000	2.015	0.000	1.896	0.000	1.685	31 HUB
			4.910		1.044											

DATA SHEET

TEST NO: 29

CONFIGURATION NO: (BV + CN - SCP)

MODEL: BEAVER VALLEY

TEST DATE: 3/11/93

		TIME	TIME	
		9:50	10:13	
2.5 PSID SC. VALVE	CORRESP. PIES TAP	PSTAT (Volts)	PSTAT (Volts)	PSTAT (Volts)
1	CN 1	+.202	+.206	
2	CN 2	-.081	-.081	
3	CN 3	-.074	-.081	
4	CN 4	+.016	+.016	
5	CN 5	-.004	-.008	
6	CN 6	+.098	+.098	
7	CN 7	-.143	-.144	
8	CN 8	+.056	+.056	
9	CN 9			
10	CN 10	+.079	+.079	
11	CN 11	+.040	+.043	
12	CN 12	+.030	+.034	
13	CN 13	-.028	-.024	
14	CN 14	-.133	-.130	
15	CN 15	-.072	-.068	

		TIME	TIME	
		9:52	10:45	
2.5 PSID SC. VALVE	CORRESP. PIES TAP	PSTAT (Volts)	PSTAT (Volts)	PSTAT (Volts)
16	CN 16	-.176	-.171	
17	CN 17	+.001	+.005	
18	CN 18	-.133	-.129	
19	CN 19	-.063	-.063	
20	CN 20	-.042	-.048	
21	CN 21	-.199	-.199	
22	CN 22	-.086	-.091	
23	CN 23	-.138	-.142	
24	CN 24	-.042	-.041	
25	CN 25	-.007	+.006	
26	CN 26	+.078	+.076	
27	CN 27	+.120	+.124	
28	CN 28			

RESULTS

MODEL: BEAVER VALLEY
CONFIGURATION: WITHOUT SCREEN / WITH CONDENSER NECK
TEST #: 29CN
TEST DATE: 3/11/93 TODAY'S DATE: 3/11/93

ATMOSPHERIC PRESSURE IN THE TEST ROOM IS	14.254	Psia
ATMOSPHERIC TEMPERATURE IN THE ROOM IS	71.80	F
TOTAL TEMPERATURE IS	554.64	R
AVERAGE TOTAL PRESSURE IN THE ANNULUS	22.9382	Psia
AVERAGE STATIC PRESSURE IN THE ANULUS	16.4223	Psia
AVERAGE PRESSURE RATIO IN THE ANNULUS	0.7159	
AVERAGE STATIC PRESSURE AT THE EXIT FLANGE	14.2417	Psia

FIRST SET OF RESULTS
(BASED ON AVERAGE TOTAL AND STATIC PRESSURES IN THE ANNULUS)

AVERAGE MACH NUMBER IN THE ANNULUS	0.7077	
HOOD LOSS COEFFICIENT	0.39816	
PRESSURE COEFFICIENT 1 [=(Pan-Pfl)/(PV ^ 2/2)an]	0.37870	
PRESSURE COEFFICIENT 2 [=(Pan-Pfl)/(Pt-Pan)]	0.33466	
CALCULATED MASS FLOW RATE	10.089	lbm/sec

SECOND SET OF RESULTS
(BASED ON MASS FLOW RATE FROM VENTURI)

AVERAGE MACH NUMBER IN THE ANNULUS	0.7109	
AVERAGE PRESSURE RATIO (BASED ON MACH #)	0.7139	
HOOD LOSS COEFFICIENT	0.38690	
PRESSURE COEFFICIENT 1 (SEE ABOVE)	0.36836	
PRESSURE COEFFICIENT 2 (SEE ABOVE)	0.32517	
MASS FLOW RATE (FROM VENTURI)	10.108	lbm/sec

Cp DISTRIBUTION

(Ploc-Pfl)/(pV ^ 2)/2

BEAVER VALLEY

TEST # 29CN

TEST DATE: 3/11/93

TODAY'S DATE: 3/11/93

TAP #	HUB	SHROUD
1	0.448	0.099
2	0.504	0.121
3	0.624	0.342
4	0.744	0.300
5	0.822	0.312
6	0.782	0.301
7	0.704	0.250
8	0.610	0.168
9	0.517	0.131
10	0.469	0.088
11	0.450	0.139
12	0.445	0.114

TOTAL PRESSURE (Psig)

BEAVER VALLEY TEST #: 29CN
CONFIGURATION: W/O SCREEN / WITH CONDENSER NECK
TEST DATE: 3/11/93 TODAY'S DATE: 3/11/93

	POINT #	DIST FROM HUB (inch)	TRAV 1 (Psig)	TRAV 2 (Psig)	TRAV 3 (Psig)	TRAV 4 (Psig)	TRAV 5 (Psig)	TRAV 6 (Psig)	TRAV 7 (Psig)
SHROUD	1	1.500	1.322	1.837	1.753	1.574	0.618	0.600	0.714
	2	1.450	6.901	7.456	7.805	7.748	7.603	7.835	7.799
	3	1.400	8.281	8.281	8.529	8.499	8.477	8.523	8.399
	4	1.350	8.598	8.673	8.704	8.679	8.679	8.613	8.637
	5	1.300	8.704	8.752	8.794	8.707	8.764	8.688	8.673
	6	1.250	8.782	8.782	8.773	8.752	8.788	8.722	8.710
	7	1.200	8.815	8.818	8.812	8.794	8.845	8.731	8.716
	8	1.150	8.836	8.806	8.836	8.749	8.860	8.740	8.719
	9	1.100	8.860	8.812	8.851	8.691	8.836	8.752	8.704
	10	1.050	8.863	8.848	8.848	8.679	8.842	8.758	8.722
	11	1.000	8.851	8.830	8.806	8.655	8.833	8.755	8.719
	12	0.950	8.836	8.842	8.809	8.643	8.836	8.752	8.716
	13	0.900	8.830	8.878	8.785	8.628	8.836	8.764	8.719
	14	0.850	8.818	8.872	8.779	8.652	8.857	8.749	8.716
	15	0.800	8.866	8.866	8.764	8.631	8.830	8.728	8.700
	16	0.750	8.869	8.848	8.752	8.643	8.875	8.734	8.694
	17	0.700	8.866	8.839	8.773	8.637	8.857	8.731	8.691
	18	0.650	8.866	8.857	8.710	8.634	8.863	8.734	8.688
	19	0.600	8.860	8.869	8.719	8.649	8.881	8.728	8.691
	20	0.550	8.860	8.836	8.728	8.670	8.899	8.691	8.685
	21	0.500	8.857	8.860	8.679	8.658	8.875	8.707	8.673
	22	0.450	8.857	8.866	8.667	8.649	8.872	8.719	8.667
	23	0.400	8.866	8.878	8.673	8.649	8.860	8.716	8.658
	24	0.350	8.866	8.866	8.655	8.661	8.899	8.719	8.670
	25	0.300	8.872	8.866	8.640	8.661	8.884	8.719	8.661
	26	0.250	8.905	8.860	8.673	8.661	8.896	8.719	8.667
	27	0.200	8.890	8.845	8.673	8.667	8.896	8.688	8.673
	28	0.150	8.875	8.845	8.670	8.661	8.884	8.679	8.667
	29	0.100	8.881	8.866	8.670	8.673	8.908	8.673	8.637
	30	0.050	8.863	8.830	7.923	8.453	8.743	8.535	7.543
HUB	31	0.000	3.234	3.925	4.603	4.265	2.828	2.558	2.565

STATIC PRESSURE VALUES FOR TRAVERSE POINTS

BEAVER VALLEY TEST #: 29CN
CONFIGURATION: W/O SCREEN / WITH CONDENSER NECK
TEST DATE: 3/11/93 TODAY'S DATE: 3/11/93

	POINT #	DIST. FROM HUB (in)	STATIC PRESSURE TRAV 1 (Psig)	TRAV 2 (Psig)	TRAV 3 (Psig)	TRAV 4 (Psig)	TRAV 5 (Psig)	TRAV 6 (Psig)	TRAV 7 (Psig)
SHROUD	1	1.500	1.322	1.837	1.753	1.574	0.618	0.600	0.714
	2	1.450	1.386	1.907	1.848	1.664	0.692	0.665	0.775
	3	1.400	1.449	1.977	1.943	1.754	0.765	0.730	0.837
	4	1.350	1.513	2.046	2.038	1.843	0.839	0.796	0.899
	5	1.300	1.577	2.116	2.133	1.933	0.913	0.861	0.961
	6	1.250	1.641	2.185	2.228	2.023	0.986	0.926	1.022
	7	1.200	1.704	2.255	2.323	2.113	1.060	0.992	1.084
	8	1.150	1.768	2.324	2.418	2.202	1.134	1.057	1.146
	9	1.100	1.832	2.394	2.513	2.292	1.207	1.122	1.207
	10	1.050	1.895	2.464	2.608	2.382	1.281	1.187	1.269
	11	1.000	1.959	2.533	2.703	2.471	1.355	1.253	1.331
	12	0.950	2.023	2.603	2.798	2.561	1.428	1.318	1.392
	13	0.900	2.087	2.672	2.893	2.651	1.502	1.383	1.454
	14	0.850	2.150	2.742	2.988	2.741	1.576	1.448	1.516
	15	0.800	2.214	2.812	3.083	2.830	1.649	1.514	1.577
	16	0.750	2.278	2.881	3.178	2.920	1.723	1.579	1.639
	17	0.700	2.342	2.951	3.273	3.010	1.796	1.644	1.701
	18	0.650	2.405	3.020	3.368	3.099	1.870	1.709	1.763
	19	0.600	2.469	3.090	3.463	3.189	1.944	1.775	1.824
	20	0.550	2.533	3.159	3.558	3.279	2.017	1.840	1.886
	21	0.500	2.596	3.229	3.653	3.368	2.091	1.905	1.948
	22	0.450	2.660	3.299	3.748	3.458	2.165	1.970	2.009
	23	0.400	2.724	3.368	3.843	3.548	2.238	2.036	2.071
	24	0.350	2.788	3.438	3.938	3.638	2.312	2.101	2.133
	25	0.300	2.851	3.507	4.033	3.727	2.386	2.166	2.194
	26	0.250	2.915	3.577	4.128	3.817	2.459	2.231	2.256
	27	0.200	2.979	3.647	4.223	3.907	2.533	2.297	2.318
	28	0.150	3.043	3.716	4.318	3.996	2.607	2.362	2.380
	29	0.100	3.106	3.786	4.413	4.086	2.680	2.427	2.441
	30	0.050	3.170	3.855	4.508	4.176	2.754	2.493	2.503
HUB	31	0.000	3.234	3.925	4.603	4.265	2.828	2.558	2.565

FLANGE PRESSURES

(MISSING #9 AND #28) TEST# 29CN

POINT #	SET 1 PRESS (volts)	SET 2 PRESS (volts)	SET 1 PRESS (Psig)	SET 2 PRESS (Psig)	AVE (Psig)
1	0.202	0.206	0.102	0.104	0.103
2	-0.081	-0.081	-0.040	-0.040	-0.040
3	-0.074	-0.081	-0.036	-0.040	-0.038
4	0.016	0.016	0.009	0.009	0.009
5	-0.004	-0.008	-0.001	-0.003	-0.002
6	0.098	0.098	0.050	0.050	0.050
7	-0.143	-0.144	-0.071	-0.071	-0.071
8	0.056	0.056	0.029	0.029	0.029
9	0.079	0.079	0.040	0.040	0.040
10	0.040	0.043	0.021	0.022	0.022
11	0.030	0.034	0.016	0.018	0.017
12	-0.028	-0.024	-0.013	-0.011	-0.012
13	-0.133	-0.130	-0.066	-0.064	-0.065
14	-0.072	-0.068	-0.035	-0.033	-0.034
15	-0.176	-0.171	-0.087	-0.085	-0.086
16	0.001	0.005	0.001	0.003	0.002
17	-0.133	-0.129	-0.066	-0.064	-0.065
18	-0.063	-0.063	-0.031	-0.031	-0.031
19	-0.042	-0.048	-0.020	-0.023	-0.022
20	-0.199	-0.199	-0.099	-0.099	-0.099
21	-0.088	-0.091	-0.043	-0.045	-0.044
22	-0.138	-0.142	-0.068	-0.070	-0.069
23	-0.042	-0.041	-0.020	-0.020	-0.020
24	0.007	0.006	0.004	0.004	0.004
25	0.078	0.078	0.040	0.040	0.040
26	0.120	0.124	0.061	0.063	0.062
FLANGE AVERAGE STATIC PRESS:				14.242	Psia

MASS FLOW CALC:
TEST # 29CN
CONFIG BEAVER VALLEY
TEST DATE: 3/11/93
TODAY'S DATE: 3/11/93

INPUTS (FROM RAW DATA SHEET):	AVG VALUE			
AVG BAROMETRIC PRESSURE:	29.138	(in Hg)		
AVG BAROMETRIC TEMPERATURE:	71.8	(F)		
DRY BULB TEMPERATURE:	83	=	83	(F)
RELATIVE HUMIDITY:	0.19	=	0.19	
VENTURI TEMPERATURE (F):	96.167	=	555.837	(R)
VENTURI INLET PRESSURE (Psig):	8.953	=	23.207	(Psia)
DELTA P ACROSS VENTURI(in WATER):	12.8	=	0.461	
MODEL INLET TEMPERATURE (F):	94.967	=	554.637	(R)

INPUT

Pg	0.5588	(FROM STEAM TABLES AT T dry bulb)		
Y	0.9890	(FROM CHART WITH (del P/Pventuri) =	0.0199	)

OUTPUT

C	0.9900
Pv	0.1062
S	0.004668
dens	0.112699
Fa	1.00038777

MASS FLOW RATE = W = 45.285*C*Y*Fa*SQRT(dens*delta P)

W= 10.108 lbm/sec

NOTE: A CORRECTION FACTOR IS INCLUDED WITH VENTURI INLET PRESSURE

DATA SHEET

TEST NO: 55 HF + CN, NO SCREEN

CONFIGURATION NO: (illegible)

MODEL: HATFIELD (illegible) (HATFIELD FERRY)

COMP. SPEED(RPM):

FLOW RATE:

TEST DATE: 4/1/92

TIME(START): 12:02

TIME(END):

BAROMETRIC PRES: 28.87" Hg

BAROMETRIC TEMP: 72°F

DRY BULB: 83°F

WET BULB: 64°F

RELATIVE HUMIDITY: 35%

TIME:		12:03	12:17 PM	12:26 PM	12:30 PM	12:35 PM	12:38 PM
		12:11 PM	12:25 PM	12:34 PM	12:37 PM	12:51 PM	
		28.89 in Hg	28.89 in Hg	28.89 in Hg		28.90 in Hg	
		73°F	72°F	72°F		72.0°F	
VENTURI TEMP:	(F)	100.	100.	100.	100.	100.	99.
VENTURI INLET PRES:	(PSIG)	3.67	3.68	3.69	3.68	3.69	3.69
ΔP ACROSS VENTURI:	"WATER	7.82	7.82	7.82	7.82	7.82	7.82
MODEL INLET TEMP:	(F)	100.1	100.0	100.1	100.0	99.9	99.8
COMP. DISCHARGE TEMP:	(F)	200.5	201.1	201.6	201.6	201.6	201.6

DATA SHEET

TEST NO: 51 HF + CN, NO SCREEN

CONFIGURATION NO: (illegible)

MODEL: (illegible)
HATFIELD FERRY

TEST DATE: 4/1/93

2.5 PSID SC. VALVE	CORRESP. PRES TAP	TIME 12:07 PSTAT (Volts)	TIME 12:50 PSTAT (Volts)	PSTAT (Volts)
1	CN 1	+.170	+.170	
2	CN 2	+.068	+.066	
3	CN 3	+.017	+.017	
4	CN 4	-.007	-.007	
5	CN 5	+.122	+.122	
6	CN 6	+.071	+.070	
7	CN 7	+.088	+.088	
8	CN 8	+.352	+.347	
9	CN 9	-.146	-.150	
10	CN 10	-.216	-.214	
11	CN 11	-.196	-.180	
12	CN 12	-.301	-.290	
13	CN 13	-.285	-.278	
14	CN 14	-.154	-.157	
15	CN 15	+.172	+.173	

2.5 PSID SC. VALVE	CORRESP. PRES TAP	TIME 12:07 PSTAT (Volts)	TIME 12:50 PSTAT (Volts)	PSTAT (Volts)
16	CN 16	+.036	+.038	
17	CN 17	-.006	-.006	
18	CN 18	+.023	+.020	
19	CN 19	-.066	-.068	
20	CN 20	-.004	-.003	
21	CN 21	+.103	+.102	
22	CN 22	-.073	-.075	
23	CN 23	-.365	-.369	
24	CN 24	-.277	-.270	
25	CN 25	-.263	-.294	
26	CN 26	-.268	-.262	
27	CN 27	-.257	-.254	
28	CN 28	-.134	-.132	

DATA SHEET

TEST NO: 15
CONFIGURATION NO: (WF-4(11) W/ SHROUD
MODEL: WF-4(11) FCMDY
COMP. SPEED (RPM):
FLOW RATE

TEST DATE: 4/1/93
TIME(START): 12:11
TIME(END): 12:50

		TRAVERSE 1		TRAVERSE 2		TRAVERSE 3		TRAVERSE 4		TRAVERSE 5		TRAVERSE 6		TRAVERSE 7			
		Position (Inch)	Plot (1) (Volts)	Position (Inch)	Plot (2) (Volts)	Position (Inch)	Plot (3) (Volts)	Position (Inch)	Plot (4) (Volts)	Position (Inch)	Plot (5) (Volts)	Position (Inch)	Plot (4) (Volts)	Position (Inch)	Plot (3) (Volts)		
SHR	1	1.500	.677	1.500	.708	1.500	.777	1.500	.6615	1.500	.671	1.500	.513	1.500	.603	1	SHR
	2	1.450	1.034	1.450	1.037	1.450	1.052	1.450	.772	1.450	.940	1.450	.764	1.450	.977	2	
	3	1.400	1.134	1.400	1.142	1.400	1.164	1.400	1.157	1.400	1.134	1.400	1.169	1.400	1.141	3	
	4	1.350	1.173	1.350	1.182	1.350	1.196	1.350	1.197	1.350	1.181	1.350	1.213	1.350	1.204	4	
	5	1.300	1.189	1.300	1.192	1.300	1.207	1.300	1.204	1.300	1.201	1.300	1.228	1.300	1.216	5	
	6	1.250	1.204	1.250	1.205	1.250	1.211	1.250	1.207	1.250	1.206	1.250	1.226	1.250	1.219	6	
	7	1.200	1.204	1.200	1.205	1.200	1.212	1.200	1.212	1.200	1.210	1.200	1.238	1.200	1.221	7	
	8	1.150	1.206	1.150	1.204	1.150	1.214	1.150	1.214	1.150	1.210	1.150	1.241	1.150	1.227	8	
	9	1.100	1.206	1.100	1.210	1.100	1.214	1.100	1.213	1.100	1.212	1.100	1.241	1.100	1.227	9	
	10	1.050	1.208	1.050	1.211	1.050	1.215	1.050	1.214	1.050	1.211	1.050	1.241	1.050	1.227	10	
	11	1.000	1.207	1.000	1.214	1.000	1.216	1.000	1.213	1.000	1.213	1.000	1.238	1.000	1.226	11	
	12	0.950	1.210	0.950	1.214	0.950	1.217	0.950	1.214	0.950	1.214	0.950	1.237	0.950	1.222	12	
	13	0.900	1.208	0.900	1.215	0.900	1.216	0.900	1.216	0.900	1.216	0.900	1.238	0.900	1.223	13	
	14	0.850	1.211	0.850	1.216	0.850	1.217	0.850	1.217	0.850	1.217	0.850	1.237	0.850	1.221	14	
	15	0.800	1.210	0.800	1.216	0.800	1.221	0.800	1.219	0.800	1.218	0.800	1.237	0.800	1.220	15	
	16	0.750	1.210	0.750	1.216	0.750	1.224	0.750	1.221	0.750	1.217	0.750	1.236	0.750	1.217	16	
	17	0.700	1.210	0.700	1.217	0.700	1.224	0.700	1.221	0.700	1.216	0.700	1.236	0.700	1.218	17	
	18	0.650	1.212	0.650	1.216	0.650	1.221	0.650	1.223	0.650	1.216	0.650	1.235	0.650	1.217	18	
	19	0.600	1.213	0.600	1.218	0.600	1.225	0.600	1.224	0.600	1.219	0.600	1.238	0.600	1.217	19	
	20	0.550	1.210	0.550	1.220	0.550	1.226	0.550	1.226	0.550	1.220	0.550	1.235	0.550	1.216	20	
	21	0.500	1.211	0.500	1.219	0.500	1.226	0.500	1.228	0.500	1.219	0.500	1.235	0.500	1.215	21	
	22	0.450	1.213	0.450	1.220	0.450	1.230	0.450	1.228	0.450	1.220	0.450	1.235	0.450	1.215	22	
	23	0.400	1.213	0.400	1.221	0.400	1.231	0.400	1.231	0.400	1.221	0.400	1.235	0.400	1.217	23	
	24	0.350	1.215	0.350	1.220	0.350	1.231	0.350	1.230	0.350	1.221	0.350	1.236	0.350	1.216	24	
	25	0.300	1.216	0.300	1.219	0.300	1.231	0.300	1.231	0.300	1.221	0.300	1.236	0.300	1.216	25	
	26	0.250	1.216	0.250	1.221	0.250	1.234	0.250	1.233	0.250	1.221	0.250	1.235	0.250	1.216	26	
	27	0.200	1.217	0.200	1.221	0.200	1.233	0.200	1.231	0.200	1.223	0.200	1.236	0.200	1.215	27	
	28	0.150	1.216	0.150	1.215	0.150	1.233	0.150	1.234	0.150	1.223	0.150	1.236	0.150	1.215	28	
	29	0.100	1.217	0.100	1.216	0.100	1.205	0.100	1.233	0.100	1.221	0.100	1.237	0.100	1.215	29	
	30	0.050	1.149	0.050	1.201	0.050	.995	0.050	1.106	0.050	1.192	0.050	1.229	0.050	1.112	30	
HUB	31	0.000	.611	0.000	.786	0.000	.427	0.000	.537	0.000	0.796	0.000	.862	0.000	.767	31	HUB

DATA SHEET

TEST NO: 55

CONFIGURATION NO: (illegible)

MODEL: (illegible)

TEST DATE: 4/1/7[illegible]

		TIME		
		12:05	12:45	
15 PSID SC. VALVE	CORRESP. PRES TAP	PSTAT (Volts)	PSTAT (Volts)	PSTAT (Volts)
16				
17	US 1	.6[illegible]	.635	
18	US 2	.622	.[illegible]31	
19	US 3	.620	.622	
20	US 4	.629	.632	
21				
22	H 1	.317	.316	
23	H 2	.241	.242	
24	H 3	.300	.30[illegible]	
25	H 4	.330	.331	
26	H 5	.337	.33[illegible]	
27	H 6	.362	.36[illegible]	
28	H 7	.343	.34[illegible]	
29	H 8	.319	.31[illegible]	
30	H 9	.310	.312	
31	H 10	.331	.33[illegible]	
32	H 11	.333	.33[illegible]	
33	H 12	.334	.33[illegible]	

		TIME		
		12:00	12:30	
15 PSID SC. VALVE	CORRESP. PRES TAP	PSTAT (Volts)	PSTAT (Volts)	PSTAT (Volts)
34				
35	S 1	-.238	-.254	
36	S 2	-.278	-.298	
37	S 3	-.280	-.279	
38	S 4	-.236	-.238	
39	S 5	-.164	-.165	
40	S 6	-.151	-.140	
41	S 7	-.208	-.206	
42	S 8	-.264	-.265	
43	S 9	-.224	-.223	
44	S 10	-.248	-.247	
45	S 11	-.198	-.198	
46	S 12	-.220	-.219	
47				

RESULTS

MODEL: HATFIELD FERRY
CONFIGURATIO NO SCREEN/WITH CONDENSER NECK
TEST #: 55HF
TEST DATE: 4/1/93 TODAY'S DATE: 5/10/93

ATMOSPHERIC PRESSURE IN THE TEST ROOM IS	14.134	Psia
ATMOSPHERIC TEMPERATURE IN THE ROOM IS	72.00	F
TOTAL TEMPERATURE IS	559.65	R
AVERAGE TOTAL PRESSURE IN THE ANNULUS	17.7549	Psia
AVERAGE STATIC PRESSURE IN THE ANNULUS	14.172	Psia
AVERAGE PRESSURE RATIO IN THE ANNULUS	0.7981	
AVERAGE STATIC PRESSURE AT THE EXIT FLANGE	14.1067	Psia

FIRST SET OF RESULTS
(BASED ON AVERAGE TOTAL AND STATIC PRESSURES IN THE ANNULUS)

AVERAGE MACH NUMBER IN THE ANNULUS	0.5768	
HOOD LOSS COEFFICIENT	0.01951	
PRESSURE COEFFICIENT 1 [=(Pan-Pfl)/(PV^2/2)an]	0.01967	
PRESSURE COEFFICIENT 2 [=(Pan-Pfl)/(Pt-Pan)]	0.01811	
CALCULATED MASS FLOW RATE	6.955	lbm/sec

SECOND SET OF RESULTS
(BASED ON MASS FLOW RATE FROM VENTURI)

AVERAGE MACH NUMBER IN THE ANNULUS	0.5723	
AVERAGE PRESSURE RATIO (BASED ON MACH #)	0.8009	
HOOD LOSS COEFFICIENT	0.03458	
PRESSURE COEFFICIENT 1 (SEE ABOVE)	0.03448	
PRESSURE COEFFICIENT 2 (SEE ABOVE)	0.03179	
MASS FLOW RATE (FROM VENTURI)	6.921	lbm/sec

BASED ON AVG Pt AND Ps

Cp DISTRIBUTION (SET		
(Ploc-Pfl)/(pV^2)/2		
HATFIELD FERRY		
TEST # 55HF		
TEST DATE:		4/1/93
TODAY'S DATE:		5/10/93
TAP #	HUB	SHROUD
1	0.297	-0.226
2	0.275	-0.264
3	0.283	-0.247
4	0.310	-0.209
5	0.335	-0.142
6	0.340	-0.125
7	0.322	-0.182
8	0.300	-0.233
9	0.292	-0.196
10	0.302	-0.218
11	0.313	-0.173
12	0.314	-0.192
AVG	0.307	-0.201
AVG OF HUB & S		**0.053**

TOTAL PRESSURE (Psig)

HATFIELD FERRY TEST #: 55HF
CONFIGURATION: NO SCREEN/WITH CONDENSER NECK
TEST DATE: 4/1/93 TODAY'S DATE: 5/10/93

	POINT #	DIST FROM HUB (inch)	TRAV 1 (Psig)	TRAV 2 (Psig)	TRAV 3 (Psig)	TRAV 4 (Psig)	TRAV 5 (Psig)	TRAV 6 (Psig)	TRAV 7 (Psig)
SHROUD	1	1.500	-0.871	-0.780	-0.467	-0.533	-0.709	-0.717	-0.629
	2	1.450	3.028	3.127	3.172	2.991	2.835	2.907	2.985
	3	1.400	3.420	3.462	3.510	3.489	3.420	3.525	3.441
	4	1.350	3.567	3.564	3.607	3.594	3.573	3.658	3.631
	5	1.300	3.585	3.594	3.640	3.631	3.622	3.703	3.667
	6	1.250	3.631	3.628	3.652	3.646	3.637	3.727	3.676
	7	1.200	3.631	3.640	3.655	3.655	3.649	3.733	3.682
	8	1.150	3.637	3.646	3.661	3.661	3.649	3.742	3.685
	9	1.100	3.643	3.649	3.661	3.658	3.655	3.742	3.685
	10	1.050	3.643	3.652	3.664	3.661	3.652	3.742	3.685
	11	1.000	3.643	3.661	3.667	3.658	3.658	3.733	3.685
	12	0.950	3.649	3.661	3.670	3.661	3.661	3.730	3.685
	13	0.900	3.643	3.664	3.673	3.667	3.667	3.733	3.688
	14	0.850	3.652	3.667	3.676	3.670	3.670	3.730	3.682
	15	0.800	3.649	3.667	3.682	3.676	3.673	3.730	3.679
	16	0.750	3.649	3.667	3.691	3.682	3.670	3.727	3.670
	17	0.700	3.649	3.670	3.691	3.685	3.673	3.727	3.673
	18	0.650	3.655	3.673	3.694	3.688	3.673	3.724	3.670
	19	0.600	3.658	3.673	3.694	3.691	3.676	3.727	3.670
	20	0.550	3.649	3.679	3.697	3.697	3.679	3.724	3.667
	21	0.500	3.652	3.676	3.697	3.703	3.676	3.724	3.664
	22	0.450	3.652	3.679	3.709	3.703	3.679	3.724	3.664
	23	0.400	3.658	3.682	3.715	3.712	3.682	3.724	3.670
	24	0.350	3.658	3.679	3.712	3.709	3.682	3.727	3.667
	25	0.300	3.664	3.676	3.715	3.712	3.682	3.727	3.667
	26	0.250	3.667	3.682	3.721	3.718	3.688	3.724	3.667
	27	0.200	3.667	3.685	3.724	3.715	3.688	3.727	3.664
	28	0.150	3.670	3.694	3.718	3.721	3.685	3.727	3.664
	29	0.100	3.667	3.697	3.634	3.718	3.682	3.730	3.664
	30	0.050	3.658	3.625	2.844	3.335	3.613	3.703	3.353
HUB	31	0.000	0.893	0.952	1.087	1.065	0.954	0.982	1.008

STATIC PRESSURE VALUES FOR TRAVERSE POINTS

HATFIELD FERRY TEST #: 55HF
CONFIGURATION: NO SCREEN/WITH CONDENSER NECK
TEST DATE: 4/1/93 TODAY'S DATE: 5/10/93

	POINT #	DIST. FROM HUB (in)	STATIC PRESSURE TRAV 1 (Psig)	TRAV 2 (Psig)	TRAV 3 (Psig)	TRAV 4 (Psig)	TRAV 5 (Psig)	TRAV 6 (Psig)	TRAV 7 (Psig)
SHROU	1	1.500	-0.871	-0.780	-0.467	-0.533	-0.709	-0.717	-0.629
	2	1.450	-0.812	-0.723	-0.416	-0.480	-0.654	-0.660	-0.575
	3	1.400	-0.753	-0.665	-0.364	-0.426	-0.599	-0.604	-0.520
	4	1.350	-0.694	-0.607	-0.312	-0.373	-0.543	-0.547	-0.466
	5	1.300	-0.636	-0.549	-0.260	-0.320	-0.488	-0.490	-0.411
	6	1.250	-0.577	-0.492	-0.208	-0.267	-0.432	-0.434	-0.357
	7	1.200	-0.518	-0.434	-0.157	-0.213	-0.377	-0.377	-0.302
	8	1.150	-0.459	-0.376	-0.105	-0.160	-0.321	-0.321	-0.247
	9	1.100	-0.400	-0.318	-0.053	-0.107	-0.266	-0.264	-0.193
	10	1.050	-0.342	-0.261	-0.001	-0.054	-0.210	-0.207	-0.138
	11	1.000	-0.283	-0.203	0.051	-0.000	-0.155	-0.151	-0.084
	12	0.950	-0.224	-0.145	0.103	0.053	-0.100	-0.094	-0.029
	13	0.900	-0.165	-0.087	0.154	0.106	-0.044	-0.038	0.025
	14	0.850	-0.106	-0.030	0.206	0.160	0.011	0.019	0.080
	15	0.800	-0.047	0.028	0.258	0.213	0.067	0.076	0.135
	16	0.750	0.011	0.086	0.310	0.266	0.122	0.132	0.189
	17	0.700	0.070	0.144	0.362	0.319	0.178	0.189	0.244
	18	0.650	0.129	0.201	0.413	0.373	0.233	0.246	0.298
	19	0.600	0.188	0.259	0.465	0.426	0.288	0.302	0.353
	20	0.550	0.247	0.317	0.517	0.479	0.344	0.359	0.408
	21	0.500	0.305	0.375	0.569	0.532	0.399	0.415	0.462
	22	0.450	0.364	0.432	0.621	0.586	0.455	0.472	0.517
	23	0.400	0.423	0.490	0.673	0.639	0.510	0.529	0.571
	24	0.350	0.482	0.548	0.724	0.692	0.566	0.585	0.626
	25	0.300	0.541	0.606	0.776	0.746	0.621	0.642	0.680
	26	0.250	0.599	0.663	0.828	0.799	0.676	0.698	0.735
	27	0.200	0.658	0.721	0.880	0.852	0.732	0.755	0.790
	28	0.150	0.717	0.779	0.932	0.905	0.787	0.812	0.844
	29	0.100	0.776	0.837	0.983	0.959	0.843	0.868	0.899
	30	0.050	0.835	0.894	1.035	1.012	0.898	0.925	0.953
HUB	31	0.000	0.893	0.952	1.087	1.065	0.954	0.982	1.008

FLANGE PRESSURES

(MISSING #9 AND #28) TEST# 55HF

POINT #	SET 1 PRESS (volts)	SET 2 PRESS (volts)	SET 1 PRESS (Psig)	SET 2 PRESS (Psig)	AVE (Psig)
1	0.170	0.170	0.085	0.085	0.085
2	0.068	0.066	0.034	0.033	0.034
3	0.017	0.017	0.009	0.009	0.009
4	-0.007	-0.007	-0.004	-0.004	-0.004
5	0.122	0.122	0.061	0.061	0.061
6	0.071	0.070	0.036	0.035	0.035
7	0.088	0.088	0.044	0.044	0.044
8	0.352	0.347	0.176	0.174	0.175
9	-0.146	-0.150	-0.073	-0.075	-0.074
10	-0.216	-0.204	-0.108	-0.102	-0.105
11	-0.196	-0.180	-0.098	-0.090	-0.094
12	-0.305	-0.290	-0.153	-0.145	-0.149
13	-0.285	-0.283	-0.143	-0.142	-0.142
14	-0.154	-0.157	-0.077	-0.079	-0.078
15	0.172	0.173	0.086	0.087	0.086
16	0.036	0.038	0.018	0.019	0.019
17	0.006	0.006	0.003	0.003	0.003
18	0.023	0.020	0.012	0.010	0.011
19	0.066	0.068	0.033	0.034	0.034
20	-0.004	-0.003	-0.002	-0.002	-0.002
21	0.103	0.102	0.052	0.051	0.051
22	0.073	0.075	0.037	0.038	0.037
23	-0.365	-0.369	-0.183	-0.185	-0.184
24	-0.277	-0.270	-0.139	-0.135	-0.137
25	-0.263	-0.294	-0.132	-0.147	-0.139
26	-0.268	-0.262	-0.134	-0.131	-0.133
27	-0.257	-0.254	-0.129	-0.127	-0.128
28	-0.154	-0.152	-0.077	-0.076	-0.077
FLANGE AVERAGE STATIC PRESS:				14.107	Psia

MASS FLOW CALC:
TEST # 55HF
CONFIG HATFIELD FERRY
TEST DATE: 4/1/93
TODAY'S DATE: 5/10/93

INPUTS (FROM RAW DATA SHEET):	**AVG VALUE**			
AVG BAROMETRIC PRESSURE:	28.893	(in Hg)		
AVG BAROMETRIC TEMPERATURE:	72	(F)		
DRY BULB TEMPERATURE:	83	=	83	(F)
RELATIVE HUMIDITY:	0.35	=	0.35	
VENTURI TEMPERATURE (F):	99.833	=	559.503	(R)
VENTURI INLET PRESSURE (Psig):	3.733	=	17.867	(Psia)
DELTA P ACROSS VENTURI(in WATE	7.82	=	0.282	
MODEL INLET TEMPERATURE (F):	99.983	=	559.653	(R)

INPUT

Pg	0.5588	(FROM STEAM TABLES AT T dry bulb)
Y	0.9910	(FROM CHART WITH (del P/Pventuri)= 0.0158)

OUTPUT

C	0.9900
Pv	0.1956
S	0.00873
dens	0.08599
Fa	1.00044

MASS FLOW RATE = W = 45.285*C*Y*Fa*SQRT(dens*delta P)

W= 6.921 lbm/sec

NOTE: A CORRECTION FACTOR IS INCLUDED WITH VENTURI INLET PRESSURE

10.5 APPENDIX E

BEAVER VALLEY AND HATFIELD FERRY EXHAUST HOOD TABULATED RESULTS

CALCULATION METHOD 1: BASED ON THE AVERAGE TOTAL AND STATIC PRESSURE IN THE MODEL ANNULUS

TABLE E.1
ORIGINAL BEAVER VALLEY EXHAUST HOOD SUMMARY CALULATION METHOD 1: BASED ON AVERAGE TOTAL AND STATIC PRESSURE IN THE MODEL ANNULUS

TEST #	MACH #	HL/LL	Cp1*	Cp2**	MASS FL. (lbm/sec)	MODEL SETUP
14	0.4647	-0.00114	-0.00140	-0.00108	5.603	
15	0.5625	0.03374	0.03365	0.03111	6.825	
16	0.6530	0.05180	0.05151	0.04636	8.087	
17	0.7528	0.06869	0.06802	0.05916	9.562	HOOD ALONE/
18	0.9956	-0.04225	-0.04269	-0.03354	12.729	WITH SCREEN
19	0.3413	-0.03917	-0.03921	-0.03809	4.148	
20	1.0086	-0.03306	-0.03333	-0.02602	12.884	
21	0.8764	0.06747	0.06660	0.05517	11.652	
22	0.7713	0.08388	0.08284	0.07156	10.096	
13	0.7507	0.18211	0.17748	0.15448	10.025	
23	0.6367	0.18492	0.18148	0.16417	8.182	
24	0.5515	0.12891	0.12765	0.11837	6.862	CONDENSER NECK/
25	0.4310	0.08271	0.08239	0.07867	5.243	WITH SCREEN
26	0.7296	0.18179	0.17744	0.15561	9.596	
27	0.8335	0.25774	0.24641	0.20777	11.917	
28	0.8013	0.52842	0.48510	0.41426	12.759	
29	0.7077	0.39816	0.37870	0.33466	10.089	CONDENSER NECK/
30	0.5999	0.25487	0.24908	0.22783	7.784	NO SCREEN
31	0.6526	0.31745	0.30687	0.27620	8.797	
32	0.5168	0.18252	0.18030	0.16874	6.507	
33	0.8439	0.41614	0.38621	0.32430	13.350	
34	0.7341	0.25234	0.24388	0.21354	10.217	HOOD ALONE/
35	0.6559	0.19198	0.18805	0.16908	8.715	NO SCREEN
36	0.4851	0.07370	0.07328	0.06911	6.014	
37	0.6024	0.13549	0.13365	0.12214	7.788	

* $C_{P1} = (P_{an}-P_{fl})/(\rho V^2/2)$

** $C_{P2} = (P_{an}-P_{fl})/(P_{t,an}-P_{an})$

TABLE E.2
MODIFIED BEAVER VALLEY EXHAUST HOOD SUMMARY CALULATION METHOD 1: BASED ON AVERAGE TOTAL AND STATIC PRESSURE IN THE MODEL ANNULUS

TEST #	MACH #	HL/LL	Cp1*	Cp2**	MASS FL. (lbm/sec)	MODEL SETUP
57	0.7843	0.41863	0.39014	0.33471	11.860	**MOD A**
58	0.6398	0.11650	0.11407	0.10299	8.209	ALL TESTS VANE POS. B
59	0.5492	0.05311	0.05221	0.04842	6.833	(ALONG BEARING CONE)
60	0.4352	0.05820	0.05766	0.05498	5.333	HOOD ALONE/WITH SCREEN
61	0.3285	0.06875	0.06847	0.06665	3.998	
62	0.7250	0.31177	0.29697	0.26035	10.216	**MOD A**
63	0.6310	0.15042	0.14712	0.13319	8.171	ALL TESTS VANE POS. A
64	0.5576	0.08458	0.08329	0.07706	6.971	(FURTHEST AWAY FROM
65	0.4628	0.06784	0.06727	0.06376	5.668	BEARING CONE)
						HOOD ALONE/WITH SCREEN
						MOD A1
						(ENLARGED WOODEN BLOC
66	0.7391	0.29292	0.27943	0.24381	10.267	TESTS 66 & 67 VANE POS. A
67	0.5803	0.07389	0.07274	0.06687	7.213	TEST 68 BEGUN AT VANE
68	-	-	-	-	-	POS. B
						HOOD ALONE/WITH SCREEN
69	0.7509	0.28394	0.27201	0.23658	10.325	**MOD B**
70	0.6459	0.12092	0.11878	0.10708	8.112	TESTS 69-71 & 73 G.V. POS A
71	0.5594	0.05611	0.05551	0.05134	6.820	TEST 72 G.V. POS. B
72	0.5657	0.05187	0.05134	0.04741	6.889	6 PARTITIONS IN ANNULUS
73	0.3884	0.04571	0.04547	0.04378	4.656	HOOD ALONE/WITH SCREEN
74	0.8525	0.12943	0.12350	0.10309	11.593	**MOD B**
75	0.7814	0.04832	0.04518	0.03879	10.043	ALL TESTS G.V. POS. B
76	0.6493	-0.03398	-0.03570	-0.03212	7.964	6 PARTITIONS IN ANNULUS
77	0.5517	-0.03814	-0.03891	-0.03606	6.670	HOOD ALONE/WITH SCREEN
78	0.4130	-0.05815	-0.05858	-0.05613	4.963	
79	0.7553	0.24253	0.23251	0.20172	10.250	**MOD C**
80	0.7600	0.21011	0.20204	0.17498	10.205	TESTS 79 & 82 G.V. POS A
81	0.7597	0.19787	0.19043	0.16494	10.128	TESTS 81 & 84 G.V. POS B
82	0.5771	0.07116	0.06944	0.06386	7.086	TESTS 80 & 83 G.V. POS. C
83	-	-	-	-	-	6 PARTITIONS IN ANNULUS
84	-	-	-	-	-	HOOD ALONE/WITH SCREEN
85	0.7769	0.29903	0.28559	0.24612	10.934	**MOD C**
86	0.7850	0.26046	0.25002	0.21482	10.876	TESTS 86 & 87 G.V. POS. C
87	0.6031	0.03712	0.03674	0.03357	7.410	TEST 85 G.V. POS. A
						6 PARTITIONS IN ANNULUS
						HOOD ALONE/NO SCREEN

* $Cp1 = (P_{an}-P_{fl})/(\rho V^2/2)$

** $Cp2 = (P_{an}-P_{fl})/(P_{t,an}-P_{an})$

TABLE E.3
MODIFIED BEAVER VALLEY EXHAUST HOOD SUMMARY CALULATION METHOD 1: BASED ON AVERAGE TOTAL AND STATIC PRESSURE IN THE MODEL ANNULUS

TEST #	MACH #	HL/LL	Cp1*	Cp2**	MASS FL (lbm/sec)	MODEL SETUP
						BEAVER VALLEY
88	0.7668	0.33758	0.31861	0.27507	10.948	**MOD C**
89	0.6616	0.27708	0.26717	0.23943	8.852	HOOD ALONE/
90	-	-	-	-	-	WITH SCREEN
91	0.3970	0.26658	0.26358	0.25339	4.888	LOWER HALF OF
92	0.5250	0.27410	0.26833	0.25044	6.686	G.V. REMOVED
						BEAVER VALLEY
93	0.8003	0.43050	0.40150	0.34296	12.176	**MOD C**
94	0.7673	0.31919	0.30455	0.26347	10.942	HOOD ALONE/
95	0.6777	0.26726	0.25923	0.23143	9.097	NO SCREEN
96	0.6036	0.26858	0.26177	0.23912	7.913	LOWER HALF OF G.V. REMOVED
						BEAVER VALLEY
97	0.7536	0.56279	0.51893	0.45105	11.869	**MOD C**
98	0.7264	0.42941	0.40510	0.35551	10.653	HOOD ALONE/
99	0.6795	0.29314	0.28280	0.25220	9.264	NO SCREEN
100	0.6244	0.19073	0.18656	0.16929	8.088	UPPER HALF OF G.V. REMOVED
						BEAVER VALLEY
101	0.8200	0.40081	0.37399	0.31691	12.431	**MOD C**
102	0.7526	0.61186	0.55909	0.48561	11.996	HOOD ALONE/
103	0.7079	0.40224	0.38210	0.33757	10.120	NO SCREEN
104	0.6433	0.27722	0.26905	0.24281	8.559	NO BACKPLATE OR
105	-	-	-	-	-	FLOW DIVIDER G.V. REMOVED

* $Cp1 = (P_{an}-P_{fl})/(\rho V^2/2)$

** $Cp2 = (P_{an}-P_{fl})/(P_{t,an}-P_{an})$

TABLE E.4
MODIFIED BEAVER VALLEY EXHAUST HOOD SUMMARY CALULATION METHOD 1: BASED ON AVERAGE TOTAL AND STATIC PRESSURE IN THE MODEL ANNULUS

TEST #	MACH #	HL/LL	Cp1*	Cp2**	MASS FL. (lbm/sec)	MODEL SETUP	GUIDE VANE POSITION
109	0.8232	0.16784	0.16232	0.13734	11.207	HOOD ALONE	4
111	0.8078	0.18639	0.18030	0.15352	11.043	NO SCREEN	2
112	0.8008	0.20384	0.19687	0.16810	11.012	MOD "D"	0
113	0.5154	0.00266	0.00254	0.00238	6.285	WITH ENLARGE	0
114	0.5151	-0.01908	-0.01907	-0.01785	6.255	HEIGHT	4
115	0.7549	0.35170	0.33413	0.29030	10.913		4
116	0.8085	0.18166	0.17592	0.14876	11.076		0
117	0.5126	0.03408	0.03410	0.03195	6.294		0
118	0.5049	0.12878	0.12798	0.12016	6.300	HOOD ALONE	4
119	0.8039	0.44054	0.41012	0.34989	12.457	NO SCREEN	4
121	0.8625	0.25725	0.24462	0.20374	12.568	MOD "D"	2
122	0.8593	0.26672	0.25340	0.21136	12.555	WITH ORIGINAL	0
123	0.7190	0.08227	0.08152	0.07117	9.266	HEIGHT	0
124	0.7196	0.07712	0.07640	0.06724	9.272		2
126	0.6862	0.21196	0.20696	0.18427	9.179		4
127	0.5375	0.05955	0.05937	0.05527	6.619	HOOD ALONE	0
128	0.5408	0.03412	0.03408	0.03169	6.616	NO SCREEN	2
129	0.7181	0.11149	0.11000	0.09687	9.278	MOD "D"	0
130	0.7225	0.09313	0.09216	0.08104	9.279	WITH ORIGINAL	2
131	0.8442	0.28131	0.26726	0.22434	12.260	HEIGHT	0
132	0.8508	0.26148	0.24903	0.20846	12.277		2
133	0.8280	0.33892	0.31936	0.26981	12.351	HOOD ALONE	FIXED
134	0.7921	0.25175	0.24191	0.20732	11.149	NO SCREEN	FIXED
135	0.7223	0.12646	0.12442	0.10940	9.455	MOD "E"	FIXED
136	0.5393	0.00249	0.00276	0.00257	6.599	NO BACK PLATE	FIXED

* $C_{P1} = (P_{an}-P_{fl})/(\rho V^2/2)$

** $C_{P2} = (P_{an}-P_{fl})/(P_{t,an}-P_{an})$

TABLE E.5
MODIFIED BEAVER VALLEY EXHAUST HOOD SUMMARY CALULATION METHOD 1: BASED ON AVERAGE TOTAL AND STATIC PRESSURE IN THE MODEL ANNULUS

TEST #	MACH #	HL/LL	Cp1*	Cp2**	MASS FL (lbm/sec)	MODEL SETUP	GUIDE VANE POSITION
137	0.8723	0.21619	0.20714	0.17186	12.479	HOOD ALONE	FIXED
138	0.8369	0.12026	0.11741	0.09883	11.242	NO SCREEN	FIXED
139	0.7604	0.02346	0.02322	0.02013	9.590	MOD "F"	FIXED
140	0.5605	-0.07424	-0.07460	-0.06902	6.748	ORIG. BRG. CONE	FIXED
141	0.5402	0.00068	0.00086	0.00080	6.584		0
142	0.5410	-0.02605	-0.02594	-0.02412	6.565	HOOD ALONE	2
143	0.5319	0.05111	0.05103	0.04757	6.561	NO SCREEN	4
144	0.7533	0.04929	0.04886	0.04249	9.588	MOD "D"	0
145	0.7637	0.02608	0.02595	0.02247	9.648	WITH BACK PLATE	2
146	0.8686	0.21346	0.20464	0.17005	12.357		0
147	0.8776	0.18311	0.17647	0.14610	12.312		2
148	0.5354	-0.09134	-0.09294	-0.08648	6.400	HOOD ALONE	0
149	0.5400	-0.12785	-0.13012	-0.12092	6.399	WITH SCREEN	2
150	0.6750	-0.08337	-0.08662	-0.07723	8.142	WITH BACK PLATE	0
151	0.6790	-0.10123	-0.10474	-0.09327	8.134	MOD "D"	2
152	0.7998	0.00254	0.00002	0.00002	10.050	HOOD ALONE	FIXED
153	0.6650	-0.10247	-0.10503	-0.09404	7.961	WITH SCREEN	FIXED
154	0.3804	-0.08436	-0.08467	-0.08167	4.526	WITH BACK PLATE	FIXED
155	0.5842	-0.10402	-0.10568	-0.09704	6.948	ORIG. BRG. CONE	
156	0.5107	-0.11718	-0.11862	-0.11113	6.054	MOD "F"	

* $C_{P1} = (P_{an}-P_{fl})/(\rho V^2/2)$

** $C_{P2} = (P_{an}-P_{fl})/(P_{t,an}-P_{an})$

TABLE E.6
ORIGINAL HATFIELD FERRY EXHAUST HOOD SUMMARY CALULATION METHOD 1: BASED ON AVERAGE TOTAL AND STATIC PRESSURE IN THE MODEL ANNULUS

TEST #	MACH #	HL/LL	Cp1*	Cp2**	MASS FL. (lbm/sec)	MODEL SETUP
38	0.7584	0.53966	0.49558	0.42882	11.926	
39	0.7271	0.16378	0.16026	0.14067	9.723	CONDENSER NECK/
40	0.5827	0.01082	0.01081	0.00994	7.293	WITH SCREEN
41	0.3758	-0.05034	-0.05043	-0.04868	4.587	
42	1.1152	-0.20236	-0.21541	-0.15948	12.803	
43	0.7426	0.1109	0.10921	0.09533	9.969	
44	0.6875	-0.03656	-0.03671	-0.03267	8.625	HOOD ALONE/
45	0.5810	-0.10428	-0.1052	-0.09676	7.090	WITH SCREEN
46	0.4598	-0.13905	-0.14007	-0.13290	5.583	
47	0.7934	0.51299	0.47291	0.40509	12.765	
48	0.7779	0.26059	0.25048	0.21583	11.046	HOOD ALONE/
49	0.7272	0.02175	0.02169	0.01903	9.255	NO SCREEN
50	0.5793	-0.08864	-0.08913	-0.08203	7.016	
51	0.4066	-0.13046	-0.13116	-0.12587	4.887	
52	0.7822	0.57245	0.52361	0.45026	12.381	
53	0.7718	0.37466	0.35436	0.30606	11.145	CONDENSER NECK/
54	0.7239	0.14971	0.14702	0.12923	9.414	NO SCREEN
55	0.5768	0.01951	0.01967	0.01811	6.955	
56	0.3935	-0.03446	-0.03455	-0.03324	4.674	

* $C_{P1} = (P_{an}-P_{fl})/(\rho V^2/2)$

** $C_{P2} = (P_{an}-P_{fl})/(P_{t,an}-P_{an})$

TABLE E.7
MODIFIED HATFIELD FERRY EXHAUST HOOD SUMMARY CALULATION METHOD 1: BASED ON AVERAGE TOTAL AND STATIC PRESSURE IN THE MODEL ANNULUS

TEST #	MACH #	HL/LL	Cp1*	Cp2**	MASS FL. (lbm/sec)	MODEL SETUP
106	0.7812	0.43751	0.40891	0.35184	11.878	NO SCREEN/
107	0.6991	0.19706	0.19198	0.17010	9.327	HOOD ALONE
108	0.6094	0.11091	0.10962	0.09997	7.687	LOWER HALF OF G.V. REMOVED
						MOD A
157	0.7497	0.13254	0.12696	0.11024	9.852	HOOD ALONE/
158	0.6957	-0.00464	-0.00783	-0.00693	8.563	WITH SCREEN
						MOD C
160	0.7052	-0.01665	-0.01939	-0.01711	8.806	HOOD ALONE/ WITH SCREEN
						MOD D
161	0.6697	0.07645	0.07337	0.06553	8.591	HOOD ALONE/ WITH SCREEN
						MOD E
162	0.6991	-0.04087	-0.04356	-0.03852	8.636	HOOD ALONE/ WITH SCREEN

* $C_{p1} = (P_{an}-P_{fl})/(\rho V^2/2)$

** $C_{p2} = (P_{an}-P_{fl})/(P_{t,an}-P_{an})$

10.6 APPENDIX F

BEAVER VALLEY AND HATFIELD FERRY EXHAUST HOOD TABULATED RESULTS

CALCULATION METHOD 2: BASED ON THE MASS FLOW RATE THROUGH THE VENTURI METER

TABLE F.1
ORIGINAL BEAVER VALLEY EXHAUST HOOD SUMMARY
CALULATION METHOD 2: BASED ON THE MASS FLOW RATE THROUGH THE VENTURI METER

TEST #	MACH #	HL/LL	Cp1*	Cp2**	MASS FL. (lbm/sec)	MODEL SETUP
14	0.4543	0.04318	0.04309	0.04093	5.507	
15	0.5553	0.05901	0.05874	0.05442	6.764	
16	0.6486	0.06500	0.06455	0.05818	8.056	
17	0.7467	0.08452	0.08353	0.07281	9.529	HOOD ALONE/
18	0.7571	0.54062	0.50003	0.43419	12.025	WITH SCREEN
19	0.3300	0.02604	0.02602	0.02532	4.026	
20	0.7561	0.59316	0.54456	0.47303	12.166	
21	0.7675	0.34860	0.33107	0.28638	11.217	
22	0.7650	0.09987	0.09842	0.08521	10.067	
13	0.7460	0.19558	0.19032	0.16593	9.998	
23	0.6357	0.18831	0.18475	0.16717	8.174	
24	0.5408	0.17161	0.16946	0.15760	6.774	CONDENSER NECK/
25	0.4202	0.13699	0.13616	0.13031	5.137	WITH SCREEN
26	0.7136	0.23034	0.22367	0.19726	9.502	
27	0.7808	0.41164	0.38646	0.33262	11.678	
28	0.8044	0.51804	0.47607	0.40606	12.773	
29	0.7109	0.38690	0.36836	0.32517	10.108	CONDENSER NECK/
30	0.6013	0.24965	0.24407	0.22317	7.793	NO SCREEN
31	0.6521	0.31946	0.30875	0.27794	8.790	
32	0.5082	0.22054	0.21742	0.20391	6.431	
33	0.8417	0.42268	0.39198	0.32943	13.340	
34	0.7376	0.24162	0.23378	0.20444	10.237	HOOD ALONE/
35	0.6623	0.17092	0.16774	0.15051	8.757	NO SCREEN
36	0.4800	0.09530	0.09477	0.08950	5.967	
37	0.6016	0.13812	0.13640	0.12471	7.781	

* $C_{P1} = (P_{an}-P_{fl})/(\rho V^2/2)$

** $C_{P2} = (P_{an}-P_{fl})/(P_{t,an}-P_{an})$

TABLE F.2
MODIFIED BEAVER VALLEY EXHAUST HOOD SUMMARY
CALULATION METHOD 2: BASED ON THE MASS FLOW RATE THROUGI THE VENTURI METER

TEST #	MACH #	HL/LL	Cp1*	Cp2**	MASS FL. (lbm/sec)	MODEL SETUP
57	0.7742	0.45196	0.42218	0.36427	11.804	**MOD A**
58	0.6233	0.17172	0.16887	0.15339	8.088	ALL TESTS VANE POS. B
59	0.5336	0.11211	0.11122	0.10363	6.700	(ALONG BEARING CONE)
60	0.4197	0.13480	0.13400	0.12825	5.181	HOOD ALONE/WITH SCREEN
61	0.3196	0.12792	0.12750	0.12429	3.900	
62	0.7124	0.35384	0.33824	0.29842	10.137	**MOD A**
63	0.6187	0.19316	0.18962	0.17247	8.078	ALL TESTS VANE POS. A
64	0.5386	0.15785	0.15605	0.14521	6.813	(FURTHEST AWAY FROM
65	0.4484	0.13424	0.13334	0.12684	5.534	BEARING CONE)
						HOOD ALONE/WITH SCREEN
						MOD A1
						(ENLARGED WOODEN BLOC
66	0.7223	0.34772	0.33223	0.29211	10.167	TESTS 66 & 67 VANE POS. A
67	0.5526	0.16295	0.16090	0.14902	7.016	TEST 68 BEGUN AT VANE
68	-	-	-	-	-	POS. B
						HOOD ALONE/WITH SCREEN
69	0.7056	0.43691	0.41366	0.36584	10.055	**MOD B**
70	0.6082	0.25320	0.24732	0.22568	7.842	TESTS 69-71 & 73 G.V. POS A
71	0.5272	0.18136	0.17908	0.16714	6.551	TEST 72 G.V. POS. B
72	0.5295	0.19149	0.18893	0.17623	6.590	6 PARTITIONS IN ANNULUS
73	0.3749	0.12015	0.11965	0.11553	4.519	HOOD ALONE/WITH SCREEN
74	0.781	0.31818	0.30304	0.26018	11.297	**MOD B**
75	0.7318	0.17933	0.17506	0.15341	9.795	ALL TESTS G.V. POS. B
76	0.6366	0.00189	0.00189	0.00171	7.797	6 PARTITIONS IN ANNULUS
77	0.5263	0.0514	0.05122	0.04781	6.458	HOOD ALONE/WITH SCREEN
78	0.3919	0.04263	0.04256	0.04096	4.756	
79	0.7278	0.32838	0.31435	0.27586	10.097	**MOD C**
80	0.7351	0.28491	0.27411	0.23993	10.071	TESTS 79 & 82 G.V. POS A
81	0.7354	0.27006	0.26034	0.22785	9.998	TESTS 81 & 84 G.V. POS B
82	0.5627	0.12311	0.12192	0.11271	6.97	TESTS 80 & 83 G.V. POS. C
83	-	-	-	-	-	6 PARTITIONS IN ANNULUS
84	-	-	-	-	-	HOOD ALONE/WITH SCREEN
						MOD C
85	0.7555	0.36568	0.347	0.30148	10.821	TESTS 86 & 87 G.V. POS. C
86	0.7549	0.3517	0.33442	0.29062	10.721	TEST 85 G.V. POS. A
87	0.5793	0.11793	0.11677	0.10745	7.23	6 PARTITIONS IN ANNULUS
						HOOD ALONE/NO SCREEN

* $Cp1 = (P_{an}-P_{fl})/(\rho V^2/2)$

** $Cp2 = (P_{an}-P_{fl})/(P_{t,an}-P_{an})$

TABLE F.3
MODIFIED BEAVER VALLEY EXHAUST HOOD SUMMARY CALULATION METHOD 2: BASED ON THE MASS FLOW RATE THROUGH THE VENTURI METER

TEST #	MACH #	HL/LL	Cp1*	Cp2**	MASS FL (lbm/sec)	MODEL SETUP
						BEAVER VALLEY
88	0.7304	0.45953	0.43205	0.37879	10.741	**MOD C**
89	0.6413	0.35243	0.33984	0.30697	8.707	HOOD ALONE/
90	-	-	-	-	-	WITH SCREEN
91	0.3861	0.33674	0.33253	0.32041	4.776	LOWER HALF OF
92	0.5152	0.32022	0.31347	0.29348	6.595	G.V. REMOVED
						BEAVER VALLEY
93	0.7648	0.55121	0.50821	0.44005	11.988	**MOD C**
94	0.7347	0.42630	0.40234	0.35221	10.759	HOOD ALONE/
95	0.6554	0.34752	0.33474	0.30101	8.940	NO SCREEN
96	0.5871	0.33591	0.32630	0.29958	7.778	LOWER HALF OF
						G.V. REMOVED
						BEAVER VALLEY
97	0.7152	0.71754	0.65409	0.57654	11.611	**MOD C**
98	0.6879	0.57799	0.53954	0.48002	10.390	HOOD ALONE/
99	0.6409	0.43970	0.42020	0.37960	8.988	NO SCREEN
100	0.5918	0.31604	0.30739	0.28185	7.833	UPPER HALF OF
						G.V. REMOVED
						BEAVER VALLEY
101	0.7572	0.61398	0.56183	0.48783	12.102	**MOD C**
102	0.7525	0.61218	0.56095	0.48792	11.994	HOOD ALONE/
103	0.7156	0.37489	0.35724	0.31484	10.168	NO SCREEN
104	0.6463	0.26604	0.25873	0.23333	8.579	NO BACKPLATE OR
105	-	-	-	-	-	FLOW DIVIDER
						G.V. REMOVED

* $C_{P1} = (P_{an}-P_{fl})/(\rho V^2/2)$

** $C_{P2} = (P_{an}-P_{fl})/(P_{t,an}-P_{an})$

TABLE F.4
MODIFIED BEAVER VALLEY EXHAUST HOOD SUMMARY CALULATION METHOD 2: BASED ON THE MASS FLOW RATE THROUGH THE VENTURI METER

TEST #	MACH #	HL/LL	Cp1*	Cp2**	MASS FL (lbm/sec)	MODEL SETUP	GUIDE VANE POSITION
109	0.8203	0.17516	0.17006	0.14415	11.195	HOOD ALONE	4
111	0.8009	0.20453	0.19790	0.16903	11.013	NO SCREEN	2
112	0.7865	0.24307	0.23407	0.20104	10.946	MOD "D"	0
113	0.4914	0.09767	0.09710	0.09144	6.076	WITH ENLARGE	0
114	0.4960	0.05401	0.05384	0.05064	6.089	HEIGHT	4
115	0.7526	0.35909	0.34121	0.29677	10.899		4
116	0.8155	0.16370	0.15930	0.13528	11.104		0
117	0.4945	0.10738	0.10667	0.10038	6.135		0
118	0.4876	0.20657	0.20404	0.19234	6.144	HOOD ALONE	4
119	0.7874	0.49437	0.45764	0.39290	12.373	NO SCREEN	4
121	0.8516	0.28535	0.27089	0.22675	12.531	MOD "D"	2
122	0.8496	0.2921	0.27703	0.23208	12.521	WITH ORIGINAL	0
123	0.6996	0.13762	0.13531	0.11992	9.152	HEIGHT	0
124	0.7043	0.12018	0.1184	0.10476	9.183		2
126	0.6675	0.27487	0.26655	0.23876	9.054		4
127	0.5191	0.13212	0.13094	0.12247	6.457	HOOD ALONE	0
128	0.5223	0.10429	0.10355	0.09677	6.457	NO SCREEN	2
129	0.6995	0.16593	0.16259	0.14409	9.169	MOD "D"	0
130	0.7068	0.13755	0.13520	0.11952	9.188	WITH ORIGINAL	2
131	0.8378	0.29858	0.28326	0.23844	12.235	HEIGHT	0
132	0.8464	0.27315	0.26005	0.21814	12.260		2
133	0.8389	0.30860	0.29221	0.24586	12.393	HOOD ALONE	FIXED
134	0.7908	0.25539	0.24536	0.21038	11.143	NO SCREEN	FIXED
135	0.7108	0.15988	0.15668	0.13831	9.387	MOD "E"	FIXED
136	0.5225	0.06445	0.06416	0.05996	6.453	NO BACK PLATE	FIXED

* $C_{p1} = (P_{an}-P_{fl})/(\rho V^2/2)$

** $C_{p2} = (P_{an}-P_{fl})/(P_{t,an}-P_{an})$

TABLE F.5
MODIFIED BEAVER VALLEY EXHAUST HOOD SUMMARY
CALULATION METHOD 2: BASED ON THE MASS FLOW RATE THROUGH THE VENTURI METER

TEST #	MACH #	HL/LL	Cp1*	Cp2**	MASS FL. (lbm/sec)	MODEL SETUP	GUIDE VANE POSITION
137	0.8705	0.22041	0.21136	0.17554	12.472	HOOD ALONE	FIXED
138	0.8279	0.14188	0.13846	0.11701	11.209	NO SCREEN	FIXED
139	0.7449	0.06208	0.06155	0.05369	9.512	MOD "F"	FIXED
140	0.5426	-0.01568	-0.01570	-0.01459	6.606	ORIG. BRG. CONE	FIXED
141	0.5227	0.06526	0.06497	0.06071	6.432		0
142	0.5260	0.02721	0.02716	0.02536	6.436	HOOD ALONE	2
143	0.5125	0.12793	0.12686	0.11885	6.392	NO SCREEN	4
144	0.7410	0.08076	0.07987	0.06976	9.525	MOD "D"	0
145	0.7483	0.06422	0.06364	0.05544	9.571	WITH BACK PLATE	2
146	0.8652	0.22165	0.21260	0.17696	12.346		0
147	0.8700	0.20094	0.19342	0.16067	12.288		2
148	0.5158	-0.02501	-0.02505	-0.02345	6.235	HOOD ALONE	0
149	0.5197	-0.06203	-0.06229	-0.05825	6.229	WITH SCREEN	2
150	0.6501	-0.01775	-0.01778	-0.01601	7.984	WITH BACK PLATE	0
151	0.6499	-0.02604	-0.02611	-0.02352	7.951	MOD "D"	2
152	0.7425	0.14514	0.14226	0.12419	9.781	HOOD ALONE	FIXED
153	0.6410	-0.03939	-0.03955	-0.03573	7.807	WITH SCREEN	FIXED
154	0.3701	-0.03430	-0.03434	-0.03319	4.424	WITH BACK PLATE	FIXED
155	0.5632	-0.04043	-0.04056	-0.03749	6.787	ORIG. BRG. CONE	FIXED
156	0.4882	-0.03801	-0.0381	-0.03591	5.863	MOD F	FIXED

* $Cp1 = (P_{an}-P_{fl})/(\rho V^2/2)$

** $Cp2 = (P_{an}-P_{fl})/(P_{t,an}-P_{an})$

TABLE F.6
ORIGINAL HATFIELD FERRY EXHAUST HOOD SUMMARY CALULATION METHOD 2: BASED ON THE MASS FLOW RATE THROUGH THE VENTURI METER

TEST #	MACH #	HL/LL	Cp1*	Cp2**	MASS FL. (lbm/sec)	MODEL SETUP
38	0.7558	0.54933	0.50758	0.44096	11.909	
39	0.7382	0.13244	0.13007	0.11372	9.784	CONDENSER NECK/
40	0.5841	0.00639	0.00639	0.00587	7.301	WITH SCREEN
41	0.3775	-0.05827	-0.05839	-0.05636	4.601	
42	0.7807	0.46219	0.43055	0.37059	12.358	
43	0.7678	0.04630	0.04598	0.03977	10.098	
44	0.6906	-0.04444	-0.04467	-0.03971	8.641	HOOD ALONE/
45	0.5805	-0.10283	-0.10372	-0.09541	7.084	WITH SCREEN
46	0.4617	-0.14600	-0.14714	-0.13954	5.600	
47	0.8074	0.46666	0.43224	0.36825	12.835	
48	0.7813	0.25078	0.24133	0.20768	11.061	HOOD ALONE/
49	0.7250	0.02740	0.02730	0.02398	9.242	NO SCREEN
50	0.5710	-0.06362	-0.06395	-0.05898	6.952	
51	0.3966	-0.08731	-0.08761	-0.08424	4.787	
52	0.8041	0.49726	0.45857	0.39119	11.492	
53	0.7804	0.34785	0.32981	0.28391	11.187	CONDENSER NECK/
54	0.7246	0.14765	0.14481	0.12723	9.416	NO SCREEN
55	0.5723	0.03458	0.03448	0.03179	6.921	
56	0.3920	-0.02704	-0.02707	-0.02605	4.659	

* $Cp1 = (P_{an}-P_{fl})/(\rho V^2/2)$

** $Cp2 = (P_{an}-P_{fl})/(P_{t,an}-P_{an})$

TABLE F.7
MODIFIED HATFIELD FERRY EXHAUST HOOD SUMMARY
CALULATION METHOD 2: BASED ON THE MASS FLOW RATE THROUGH THE VENTURI METER

TEST #	MACH #	HL/LL	Cp1*	Cp2**	MASS FL. (lbm/sec)	MODEL SETUP
106	0.7966	0.38859	0.36522	0.31246	11.957	NO SCREEN/
107	0.7022	0.18765	0.18335	0.16234	9.347	HOOD ALONE
108	0.6102	0.10832	0.10723	0.09779	7.692	LOWER HALF OF G.V. REMOVED
						MOD A
157	0.7687	0.08302	0.08201	0.07091	9.946	HOOD ALONE/
158	0.7067	-0.03268	-0.03281	-0.02901	8.625	WITH SCREEN
						MOD C
160	0.6943	0.01163	0.01162	0.01031	8.741	HOOD ALONE/ WITH SCREEN
						MOD D
161	0.6761	0.05776	0.05738	0.05126	8.631	HOOD ALONE/ WITH SCREEN
						MOD E
162	0.6924	-0.02380	-0.02387	-0.02120	8.596	HOOD ALONE/ WITH SCREEN

* $Cp1 = (P_{an}-P_{fl})/(\rho V^2/2)$

** $Cp2 = (P_{an}-P_{fl})/(P_{t,an}-P_{an})$

10.7 APPENDIX G

MODIFIED BEAVER VALLEY EXHAUST HOOD RESULTS

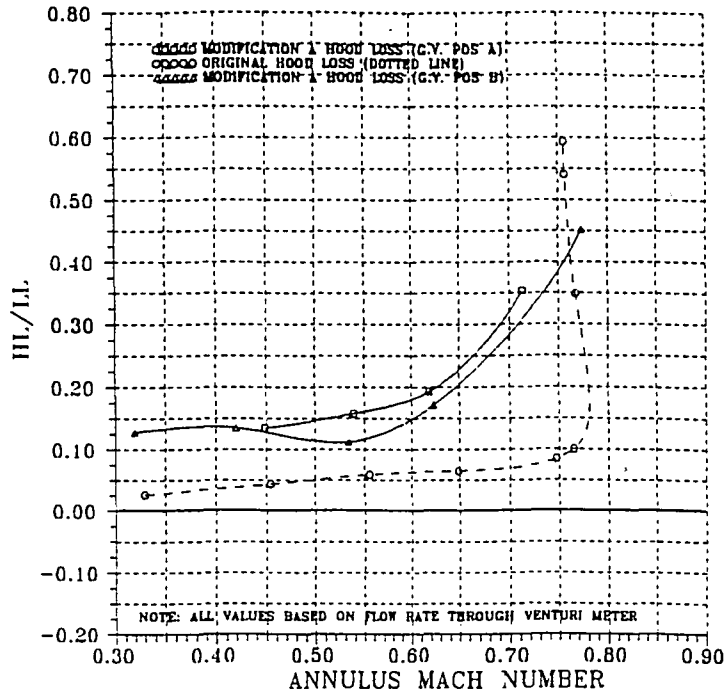

Figure G.1: Comparison of the hood loss curves of BV Modification A with that of the original Beaver Valley hood

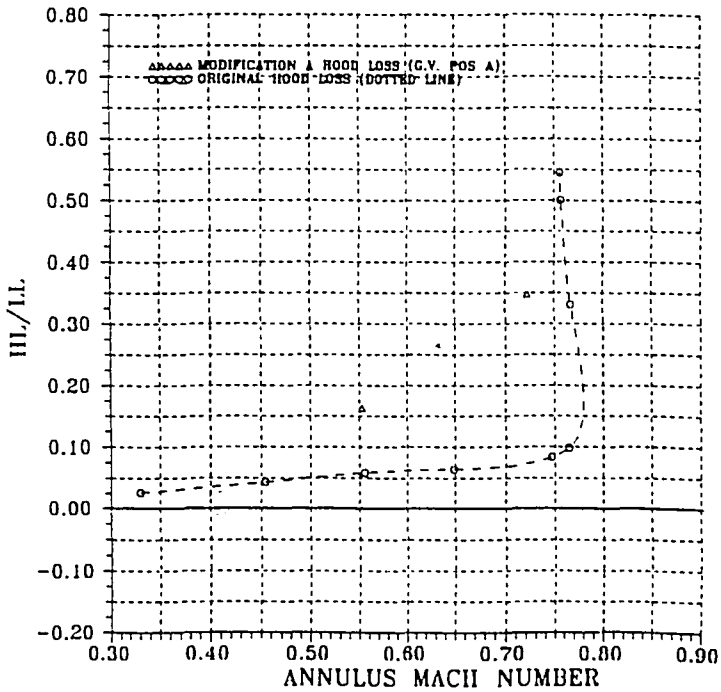

Figure G.2: Comparison of the hood loss curves of BV Modification A1 with that of the original Beaver Valley hood

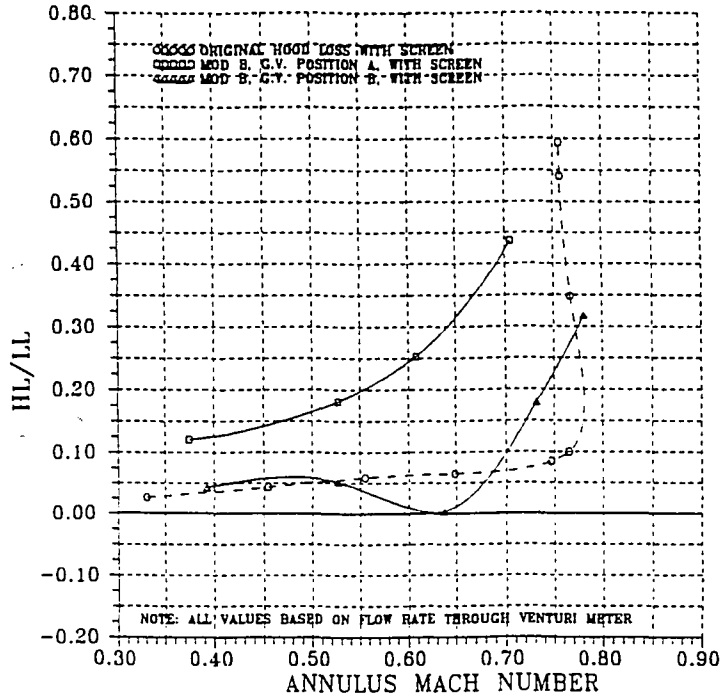

Figure G.3: Comparison of the hood loss curves of BV Modification B with that of the original Beaver Valley hood

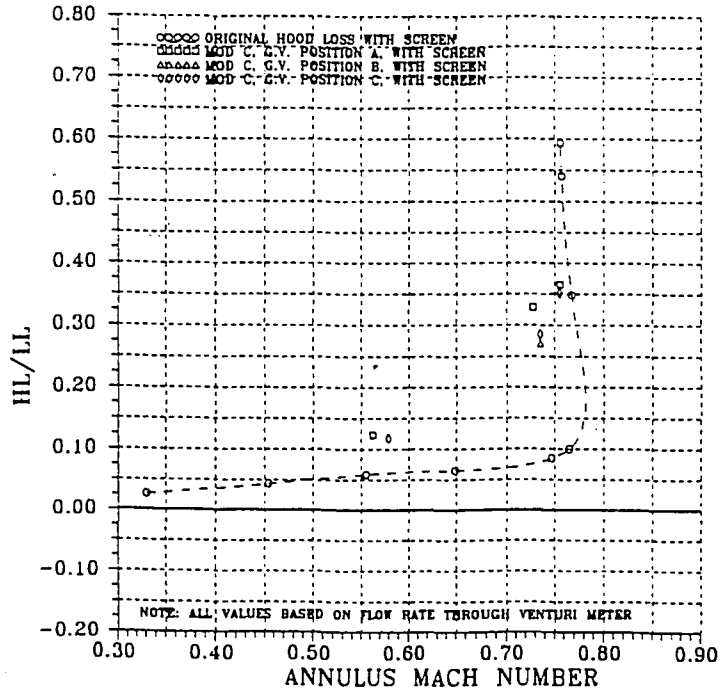

Figure G.4: Comparison of the hood loss curves of BV Modification C with that of the original Beaver Valley hood

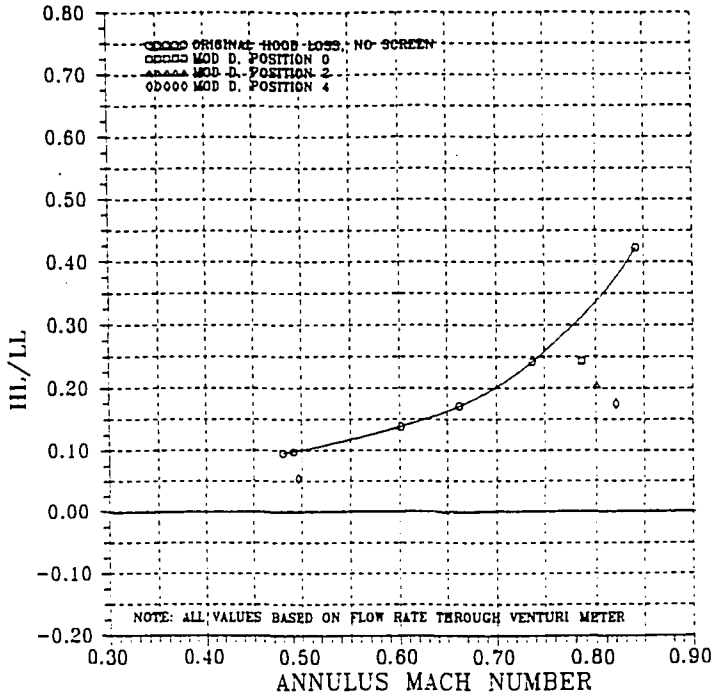

Figure G.5: Comparison of the hood loss curves of BV Modification D (with increased height) with that of the original Beaver Valley hood

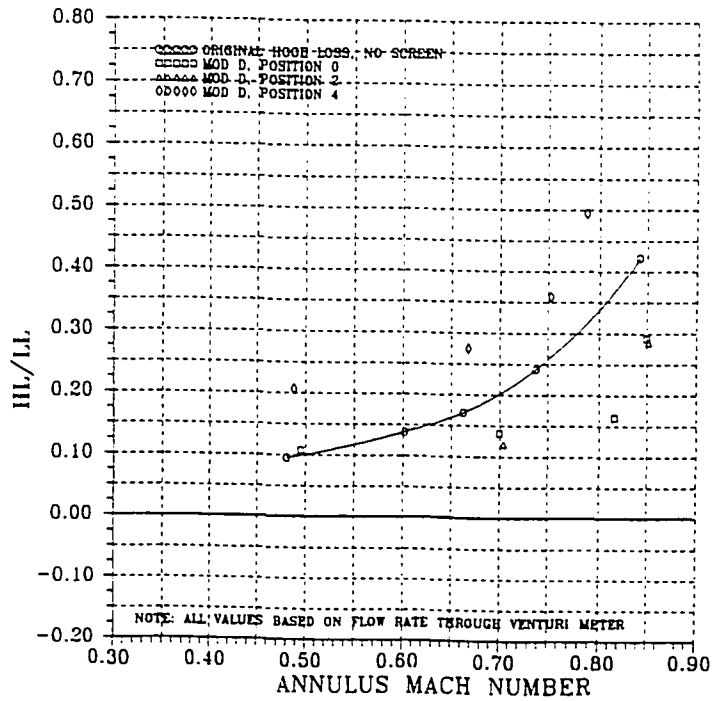

Figure G.6: Comparison of the hood loss curves of BV Modification D (with original height) with that of the original Beaver Valley hood

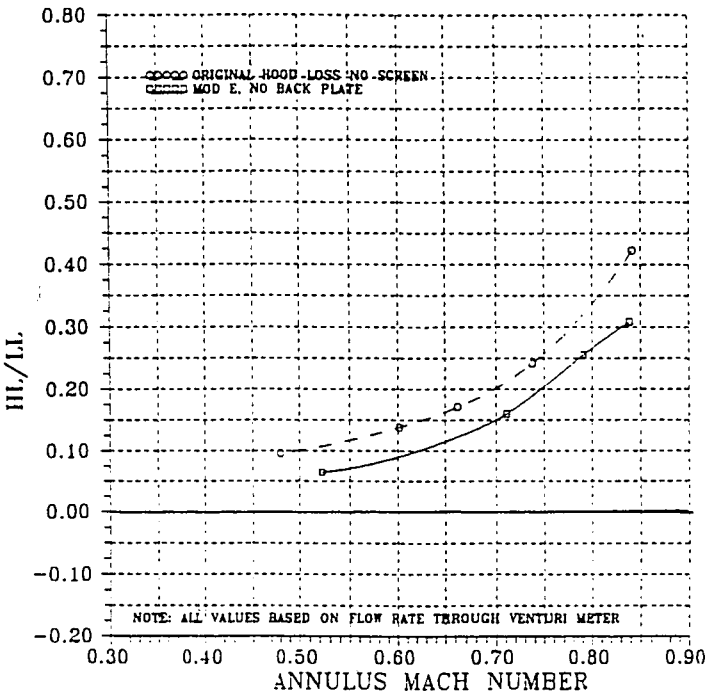

Figure G.7: Comparison of the hood loss curves of BV Modification E with that of the original Beaver Valley hood

10.8 APPENDIX H

CIRCUMFERENTIAL VARIATION OF THE LOCAL NONDIMENSIONAL PRESSURE COEFFICIENT FOR BEAVER VALLEY AND HATFIELD FERRY EXHAUST HOOD MODEL TESTS

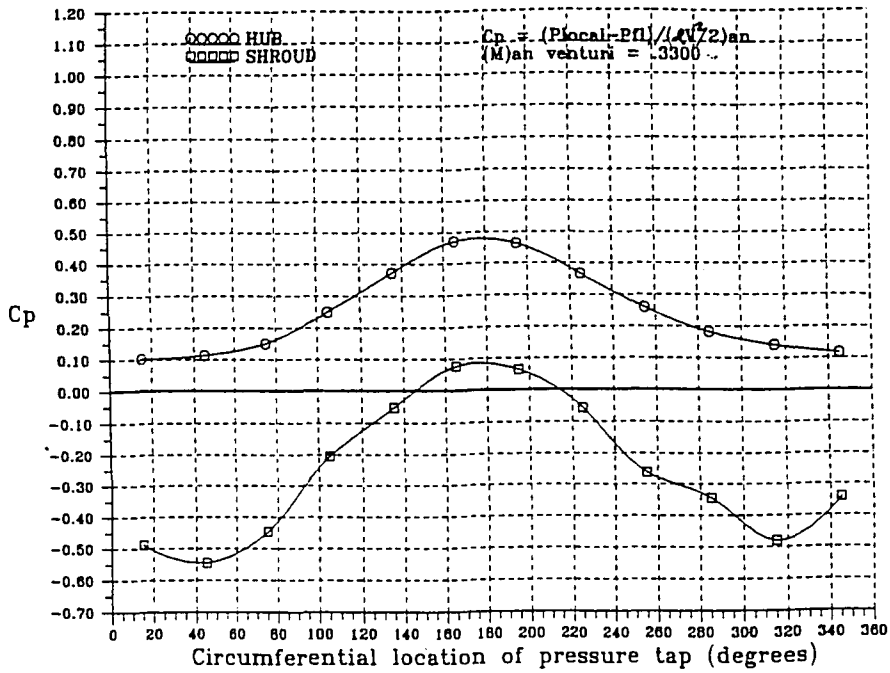

Figure H.1: Circumferential variation of the local dimensionless pressure coefficient for one test of the original Beaver Valley hood with screen, hood alone (M_{AN} = 0.330)

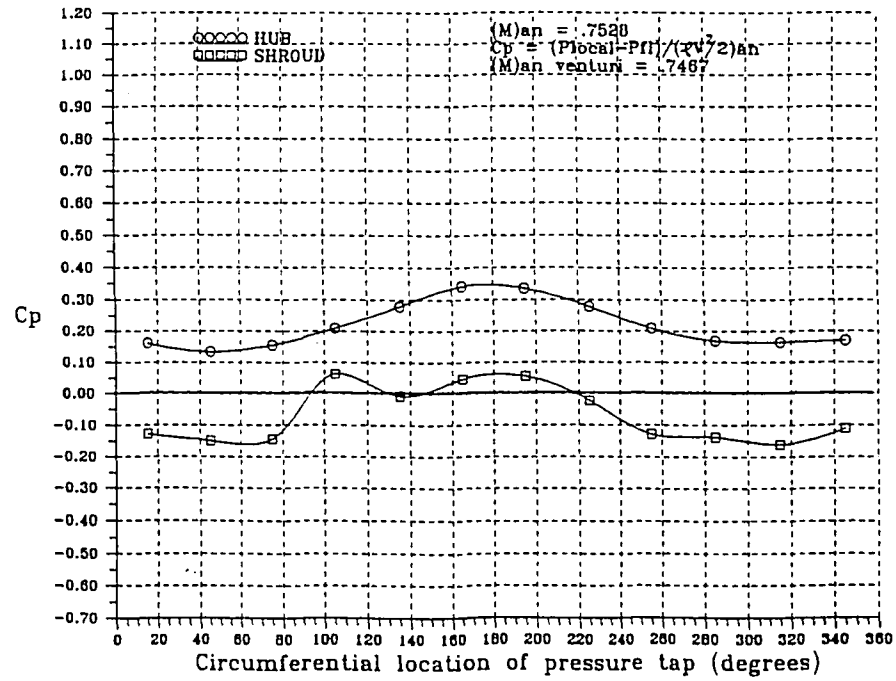

Figure H.2: Circumferential variation of the local dimensionless pressure coefficient for one test of the original Beaver Valley hood with screen, hood alone (M_{AN} = 0.747)

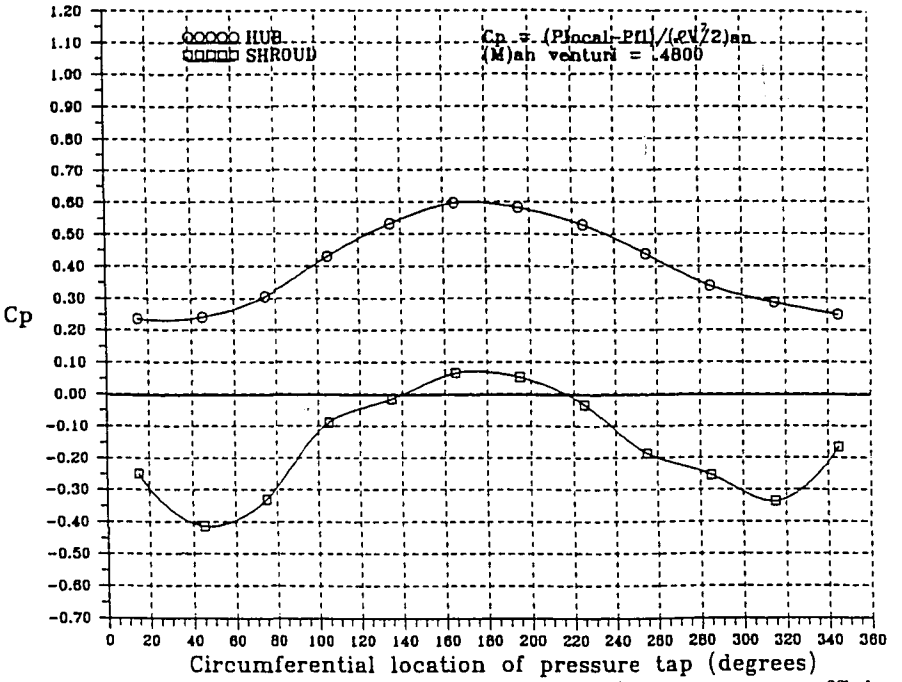

Figure H.3: Circumferential variation of the local dimensionless pressure coefficient for one test of the original Beaver Valley hood without screen, hood alone (M_{AN} = 0.480)

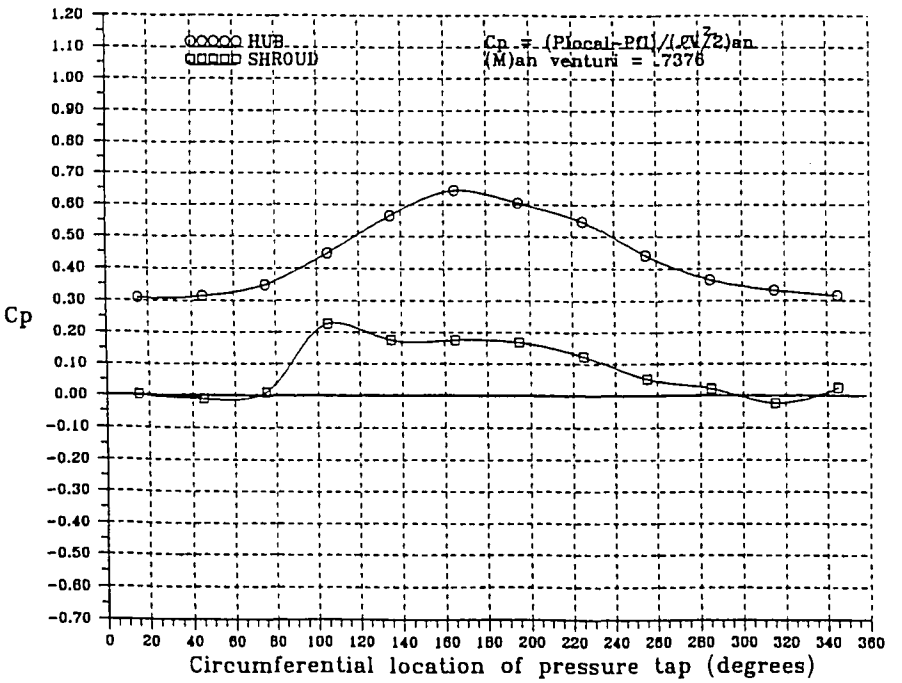

Figure H.4: Circumferential variation of the local dimensionless pressure coefficient for one test of the original Beaver Valley hood without screen, hood alone (M_{AN} = 0.738)

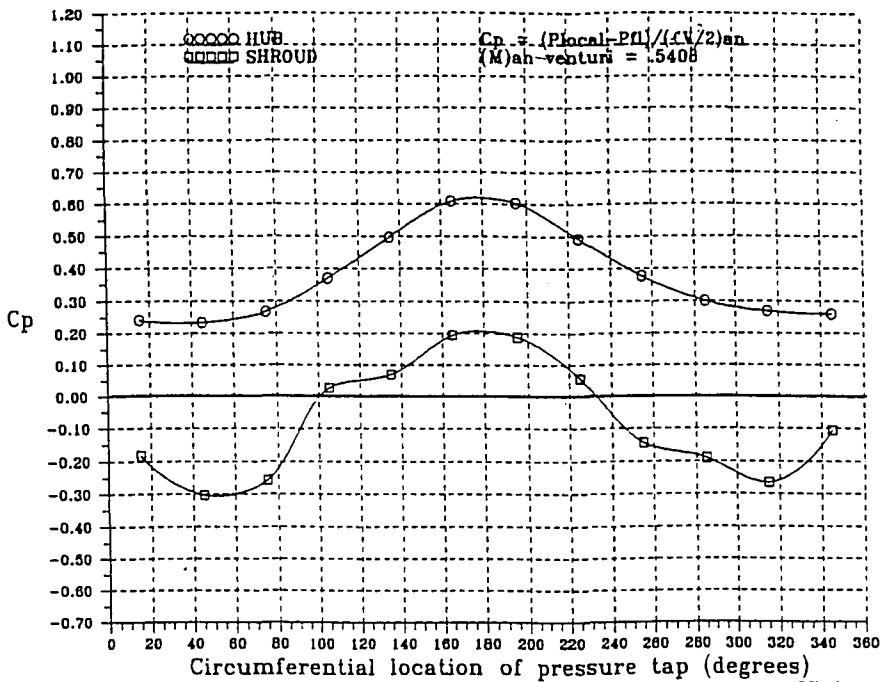

Figure H.5: Circumferential variation of the local dimensionless pressure coefficient for a test of the original Beaver Valley hood with screen, with condenser neck (M_{AN} = 0.541)

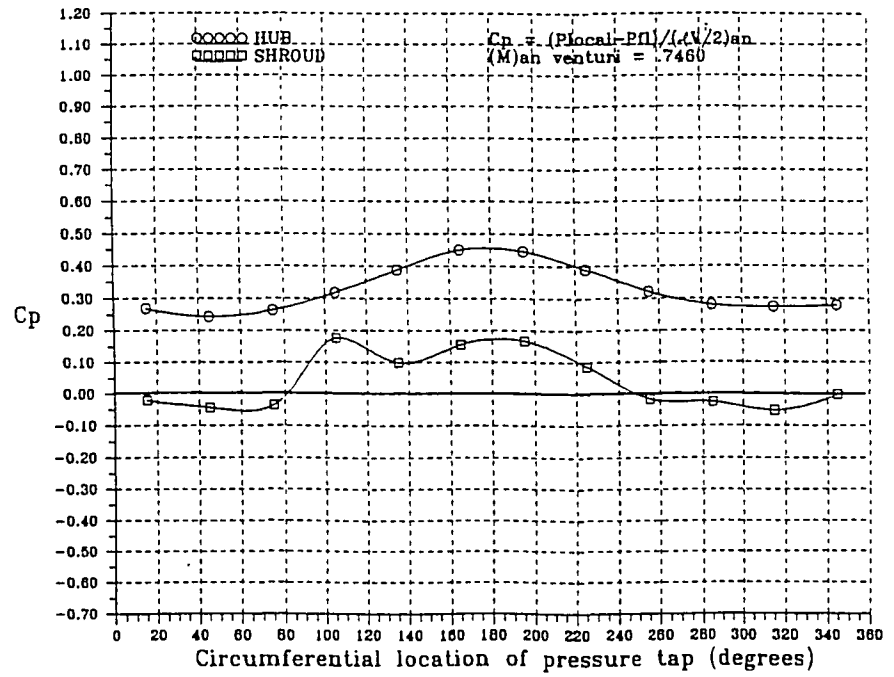

Figure H.6: Circumferential variation of the local dimensionless pressure coefficient for a test of the original Beaver Valley hood with screen, with condenser neck (M_{AN} = 0.746)

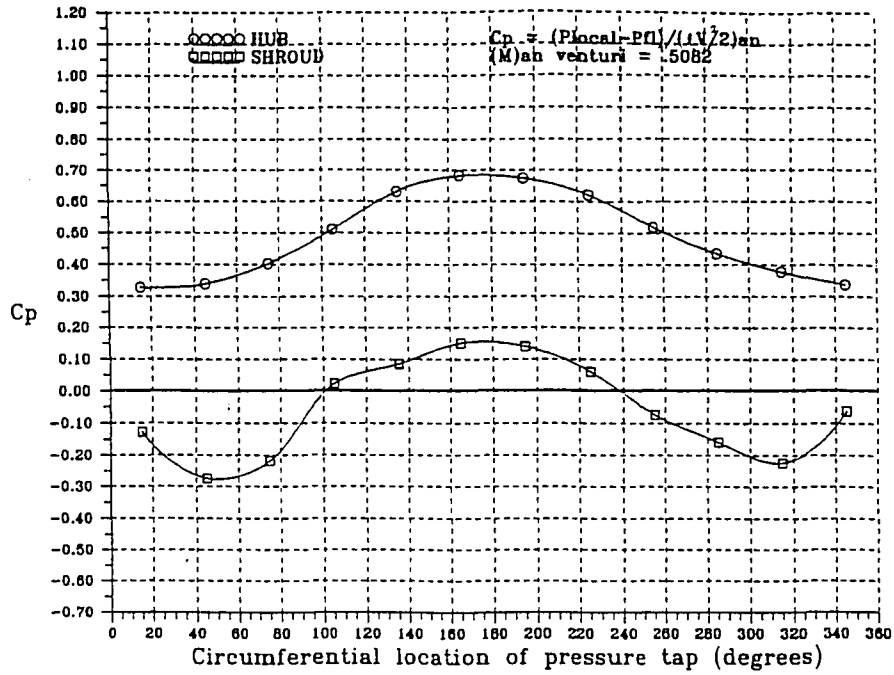

Figure H.7: Circumferential variation of the local dimensionless pressure coefficient for a test of the original Beaver Valley hood without screen, with condenser neck (M_{AN} =0.508)

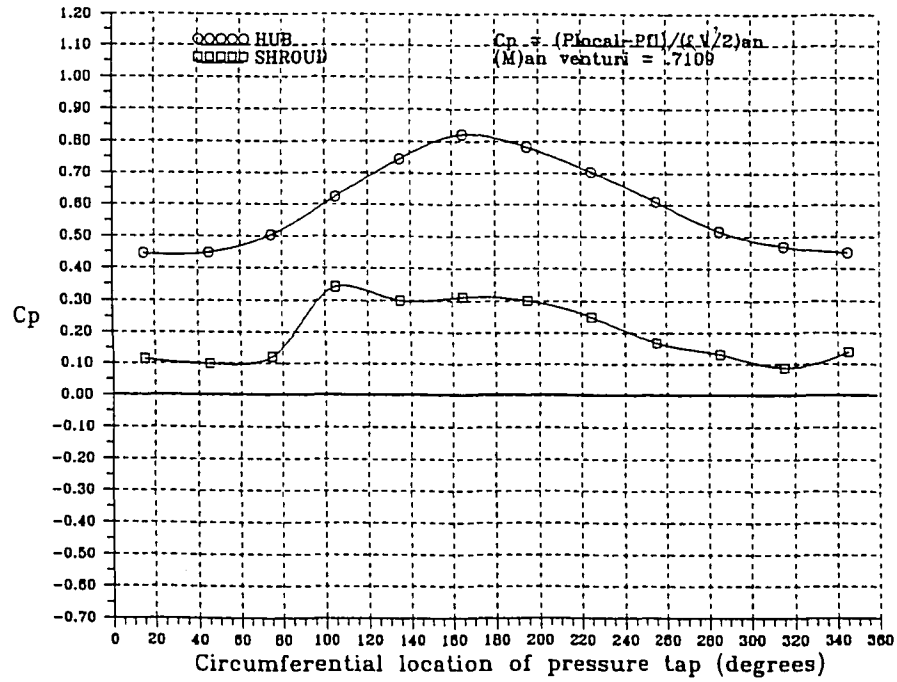

Figure H.8: Circumferential variation of the local dimensionless pressure coefficient for a test of the original Beaver Valley hood without screen, with condenser neck (M_{AN} =0.711)

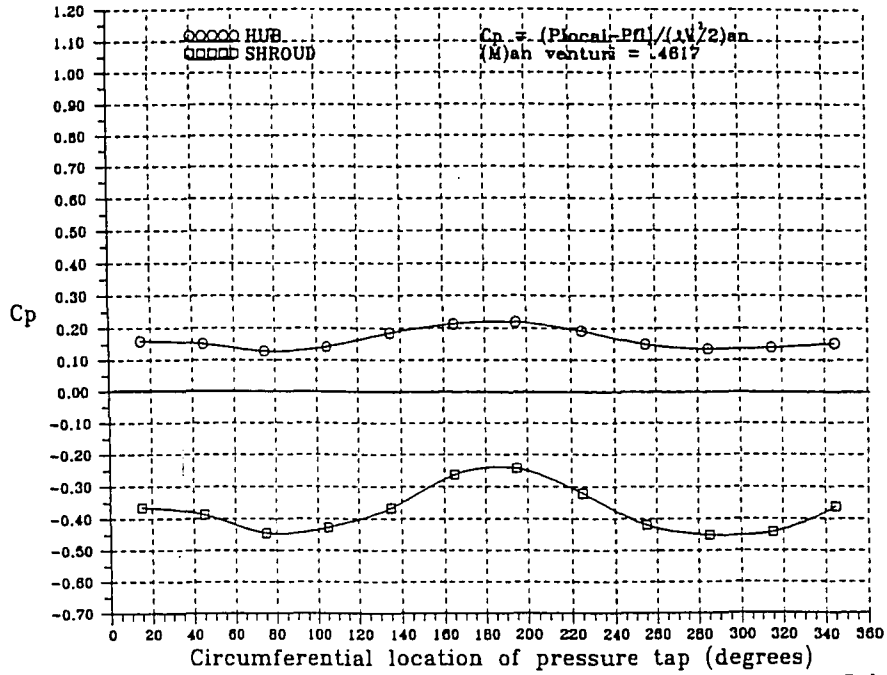

Figure H.9: Circumferential variation of the local dimensionless pressure coefficient for a test of the original Hatfield Ferry hood with screen, hood alone (M_{AN} = 0.462)

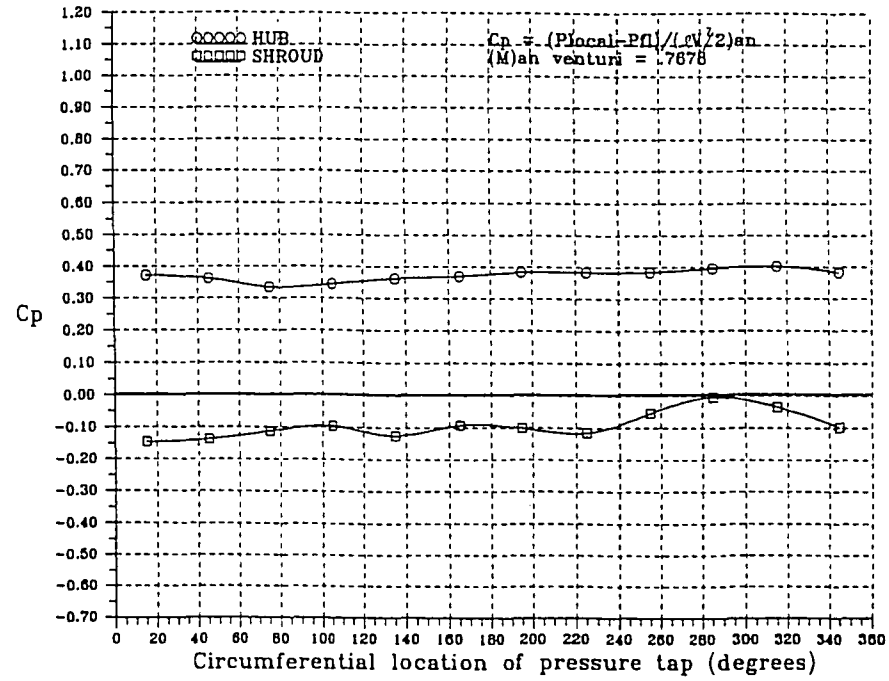

Figure H.10: Circumferential variation of the local dimensionless pressure coefficient for a test of the original Hatfield Ferry hood with screen, hood alone (M_{AN} = 0.768)

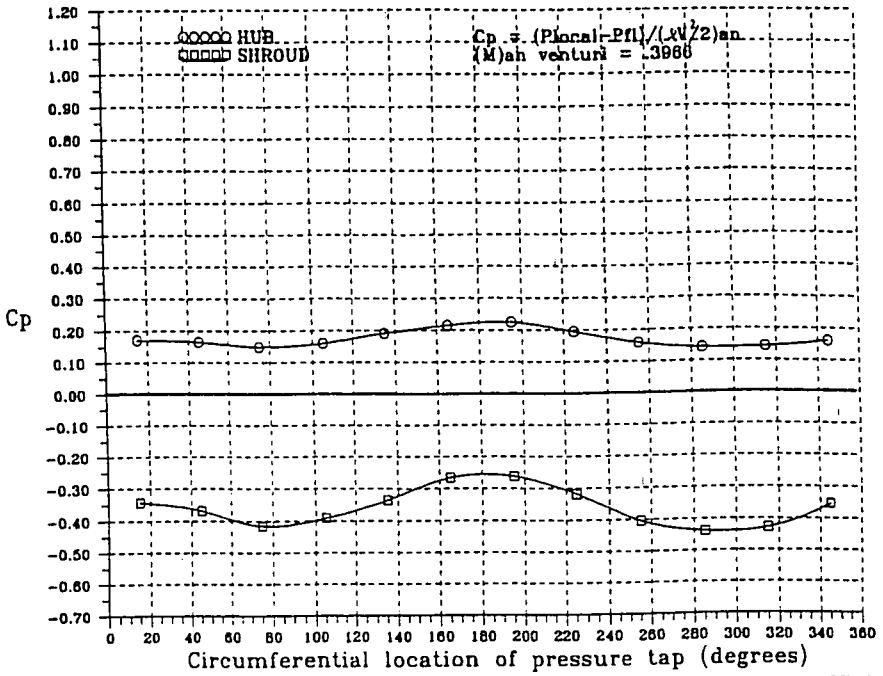

Figure H.11: Circumferential variation of the local dimensionless pressure coefficient for a test of the original Hatfield Ferry hood without screen, hood alone (M_{AN} = 0.397)

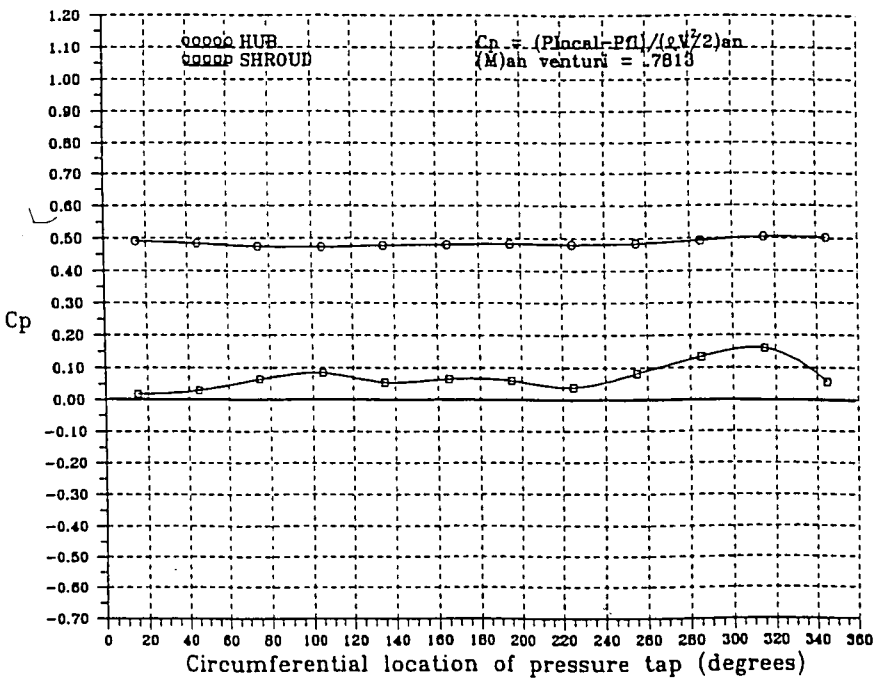

Figure H.12: Circumferential variation of the local dimensionless pressure coefficient for a test of the original Hatfield Ferry hood without screen, hood alone (M_{AN} = 0.781)

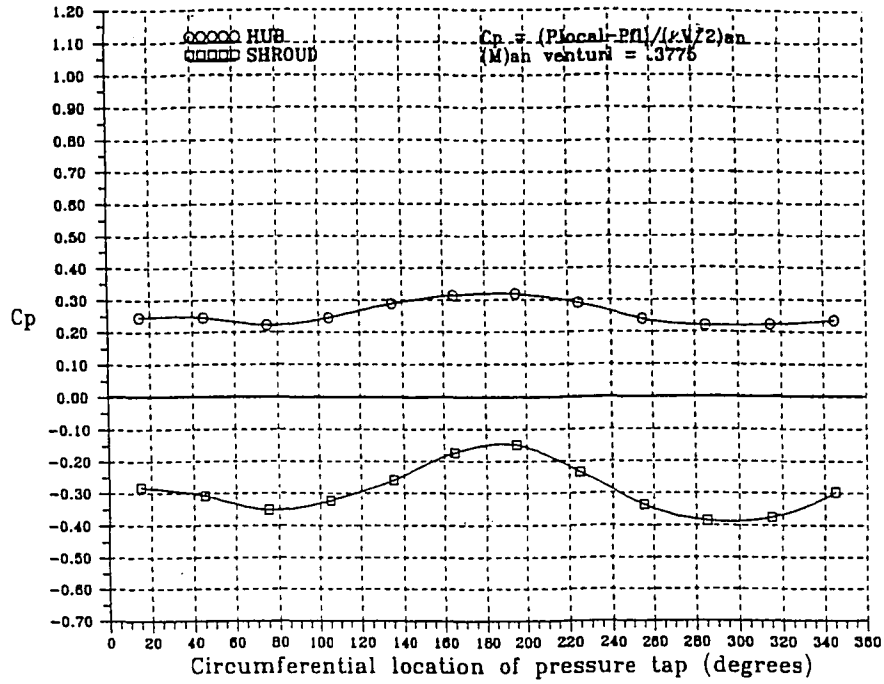

Figure H.13: Circumferential variation of the local dimensionless pressure coefficient for a test of the original Hatfield Ferry hood with screen, with condenser neck (M_{AN} = 0.378)

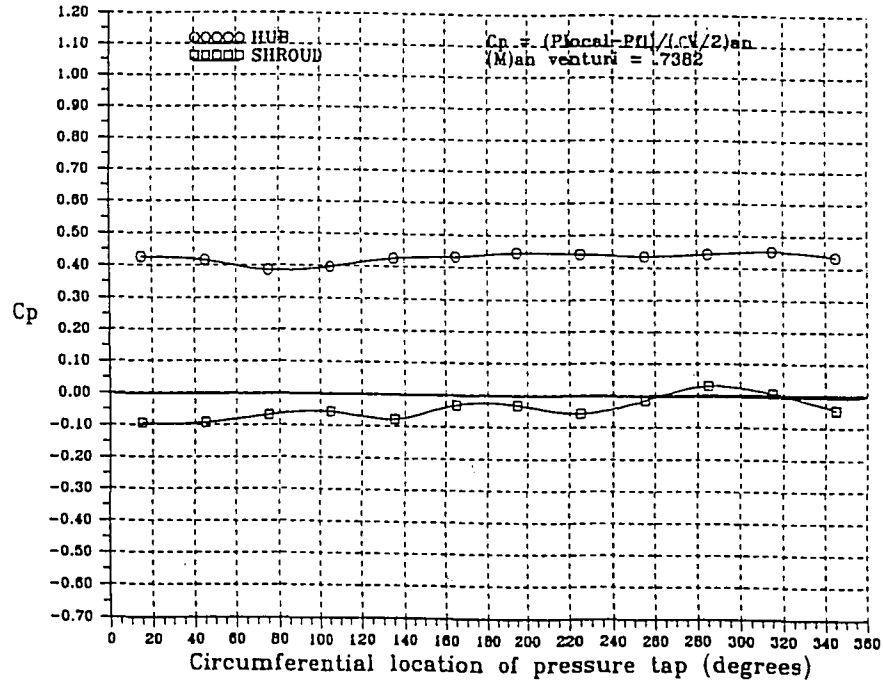

Figure H.14: Circumferential variation of the local dimensionless pressure coefficient a one test of the original Hatfield Ferry hood with screen, with condenser neck (M_{AN} = 0.738)

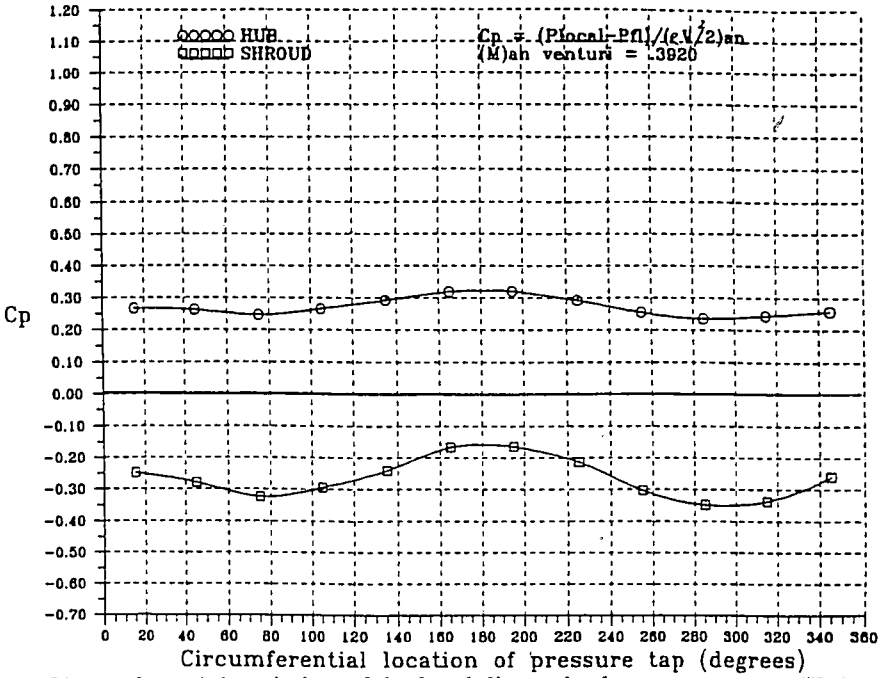

Figure H.15: Circumferential variation of the local dimensionless pressure coefficient a one test of the original Hatfield Ferry hood without screen, with condenser neck (M_{AN}=0.392)

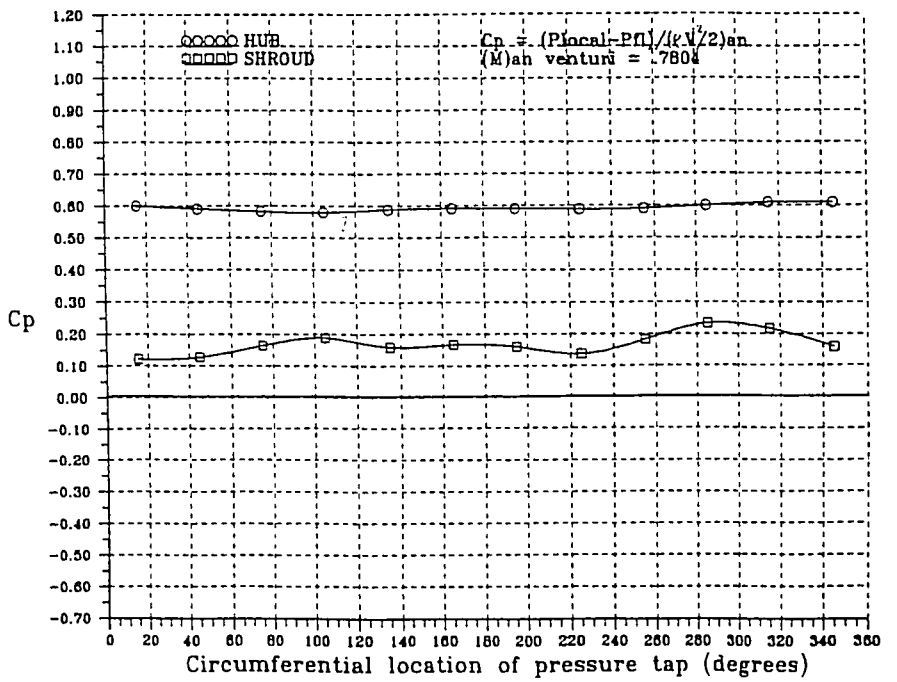

Figure H.16: Circumferential variation of the local dimensionless pressure coefficient for a test of the original Hatfield Ferry hood without screen, with condenser neck (M_{AN}=0.780)

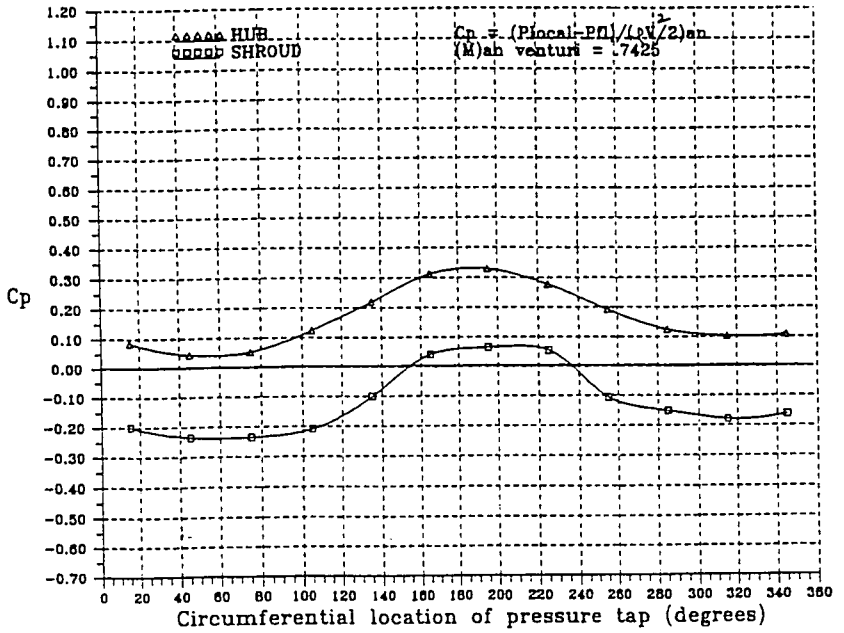

Figure H.17: Circumferential variation of the local dimensionless pressure coefficient for a test of BV Modification F, hood alone, with screen, (M_{AN} = 0.370)

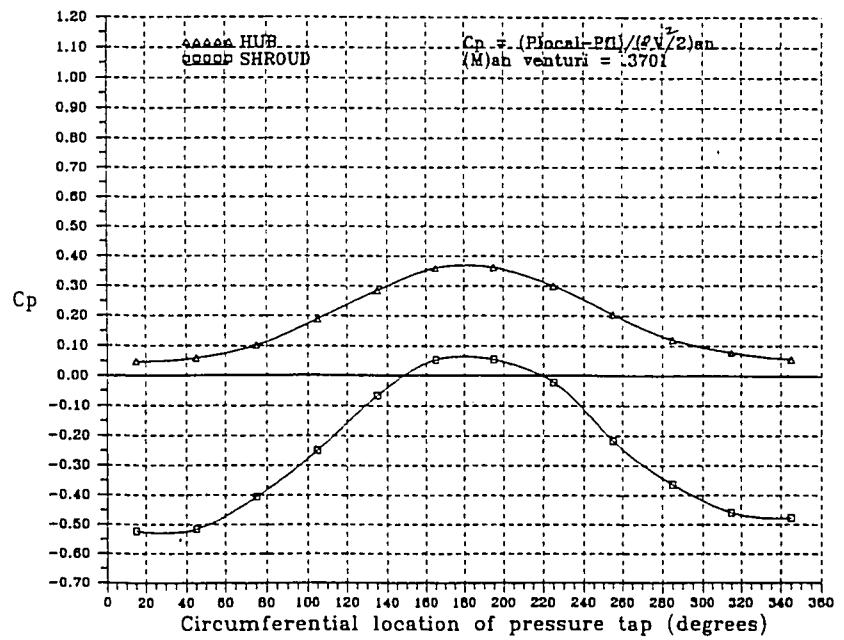

Figure H.18: Circumferential variation of the local dimensionless pressure coefficient for a test of BV Modification F, hood alone, with screen, (M_{AN} = 0.7425)

10.9 APPENDIX I

TOTAL PRESSURE DISTRIBUTION ACROSS THE ANNULUS OF THE BEAVER VALLEY AND HATFIELD FERRY MODELS

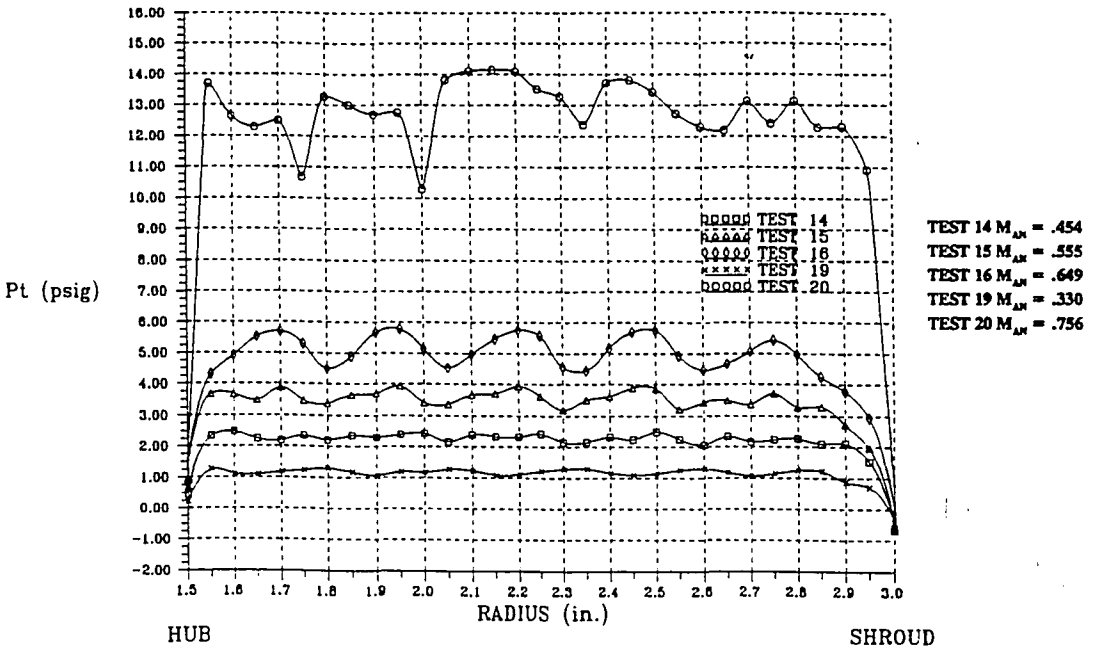

Figure I.1: Total pressure distribution for the original Beaver Valley model, hood alone, with screen - traverse 1

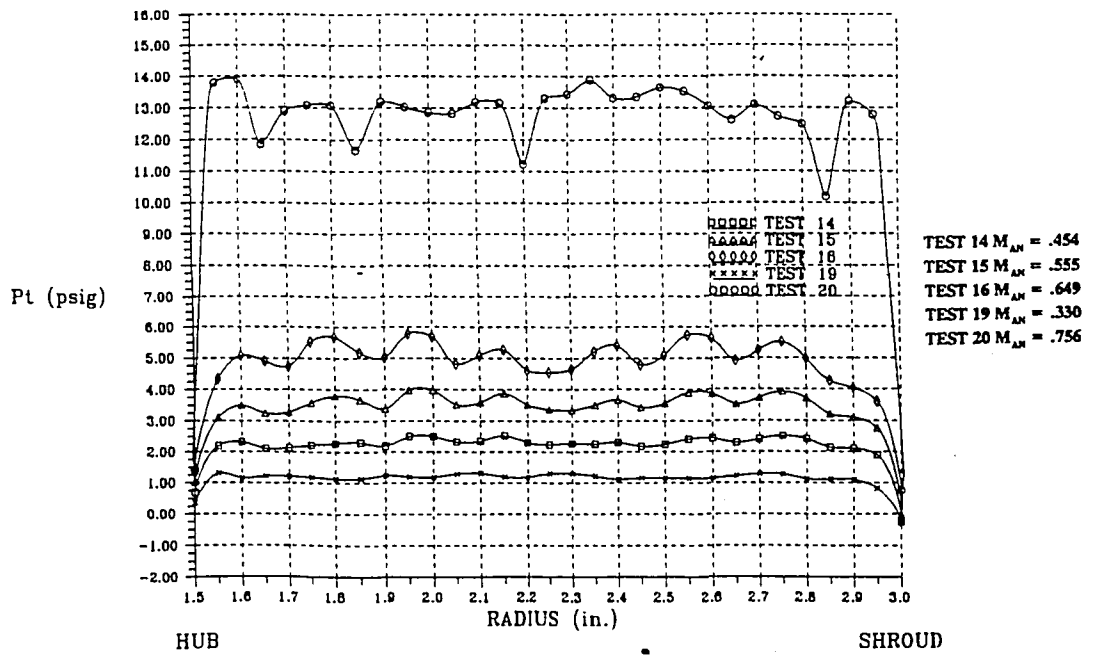

Figure I.2: Total pressure distribution for the original Beaver Valley model, hood alone, with screen - traverse 2

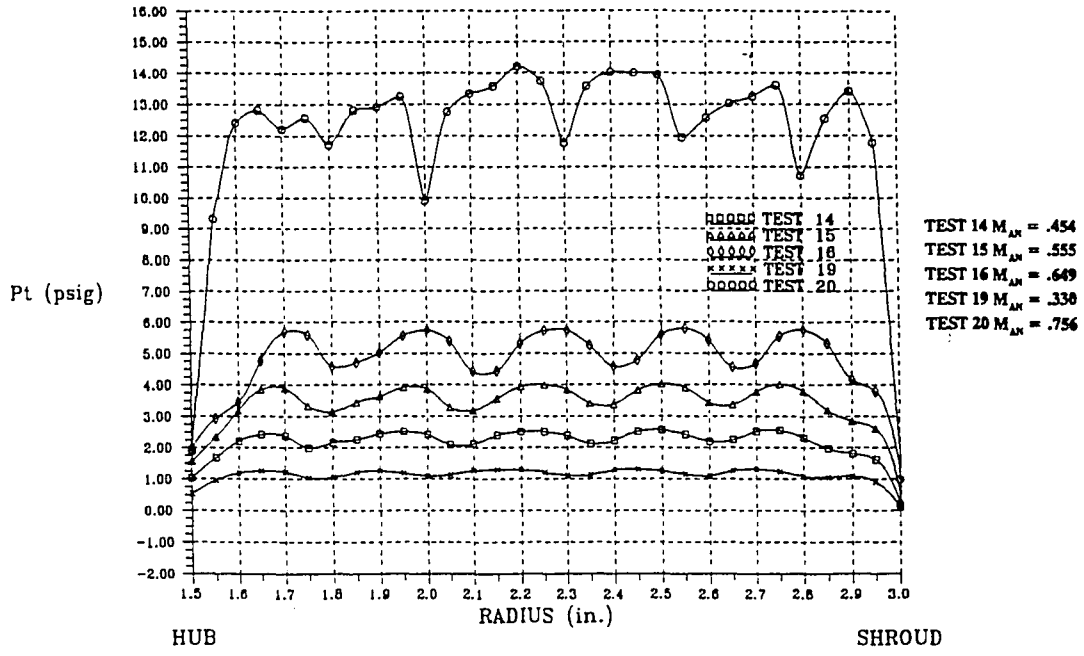

Figure I.3: Total pressure distribution for the original Beaver Valley model, hood alone, with screen - traverse 3

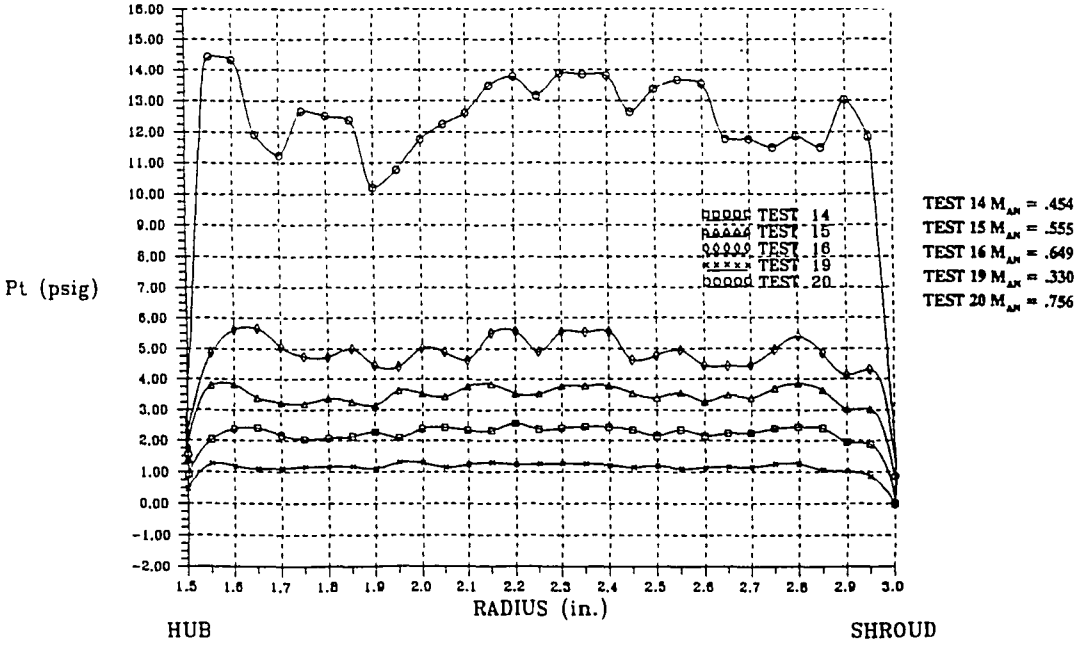

Figure I.4: Total pressure distribution for the original Beaver Valley model, hood alone, with screen - traverse 4

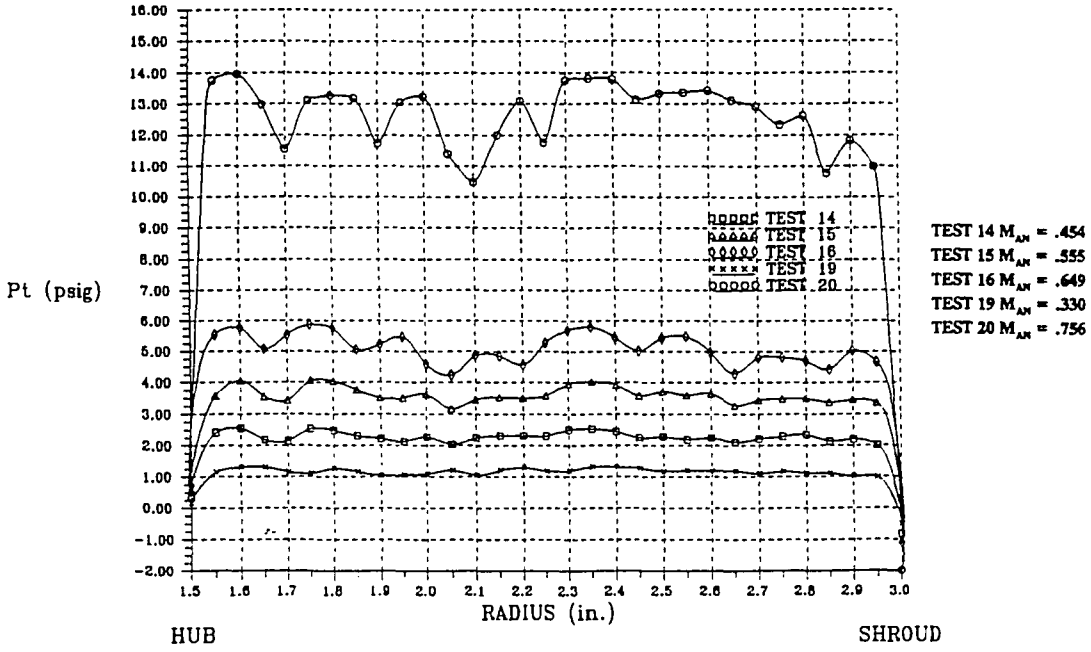

Figure I.5: Total pressure distribution for the original Beaver Valley model, hood alone, with screen - traverse 5

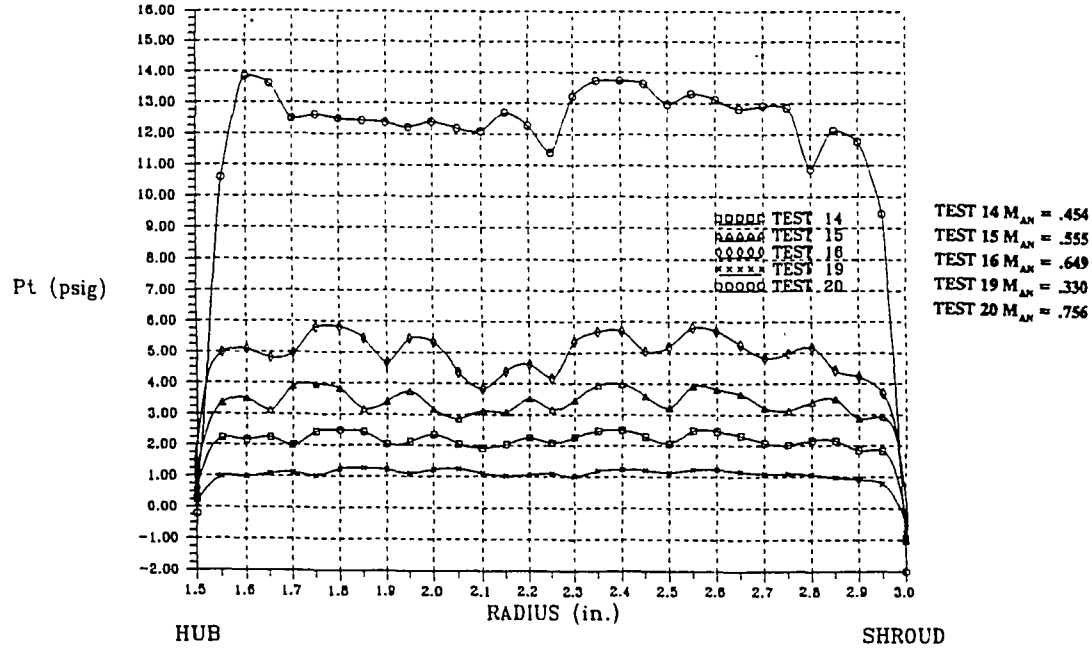

Figure I.6: Total pressure distribution for the original Beaver Valley model, hood alone, with screen - traverse 6

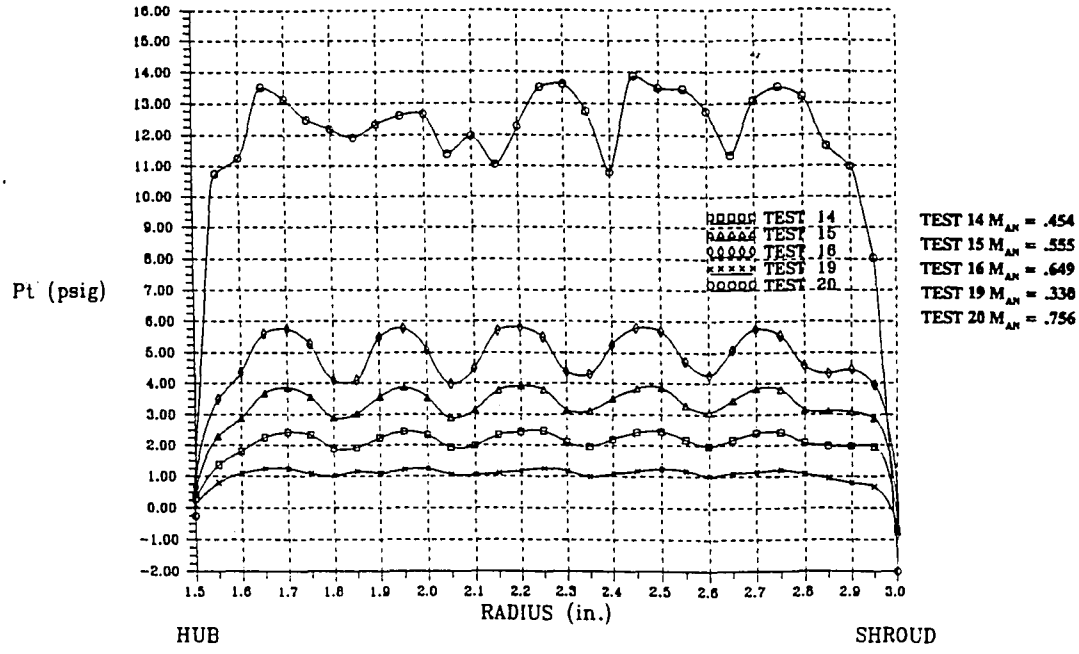

Figure I.7: Total pressure distribution for the original Beaver Valley model, hood alone, with screen - traverse 7

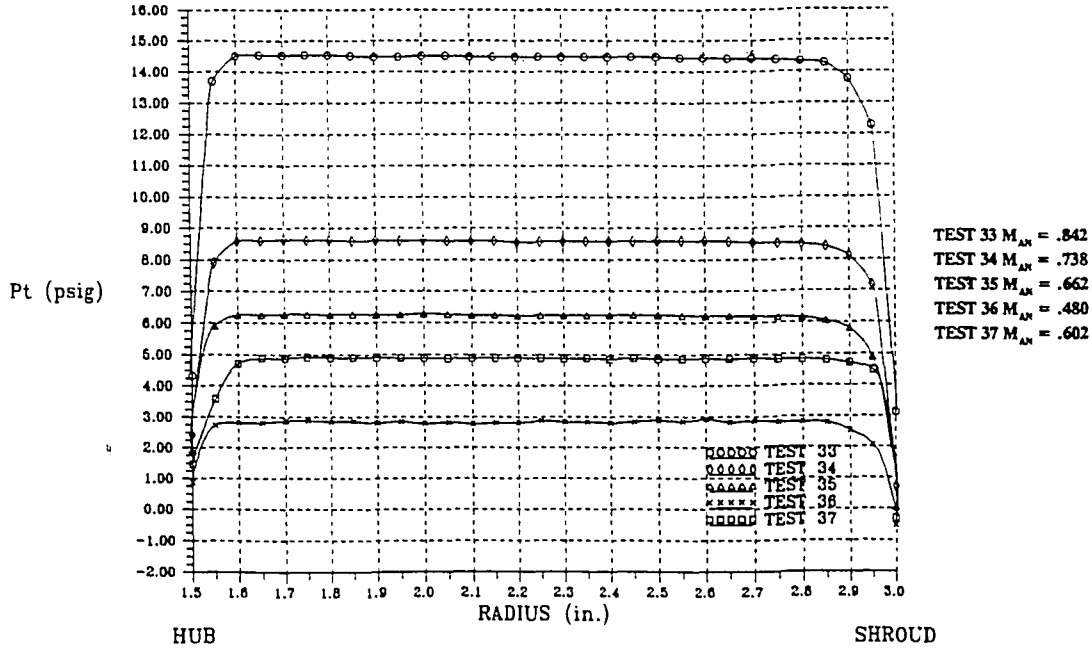

Figure I.8: Total pressure distribution for the original Beaver Valley model, hood alone, without screen - traverse 1

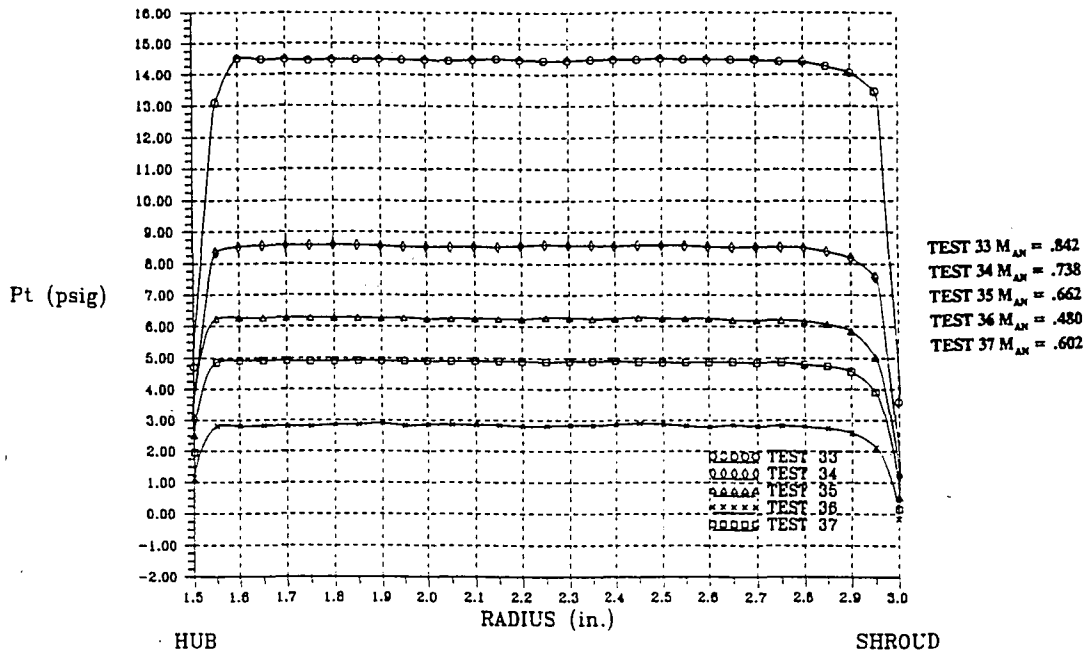

Figure I.9: Total pressure distribution for the original Beaver Valley model, hood alone, without screen - traverse 2

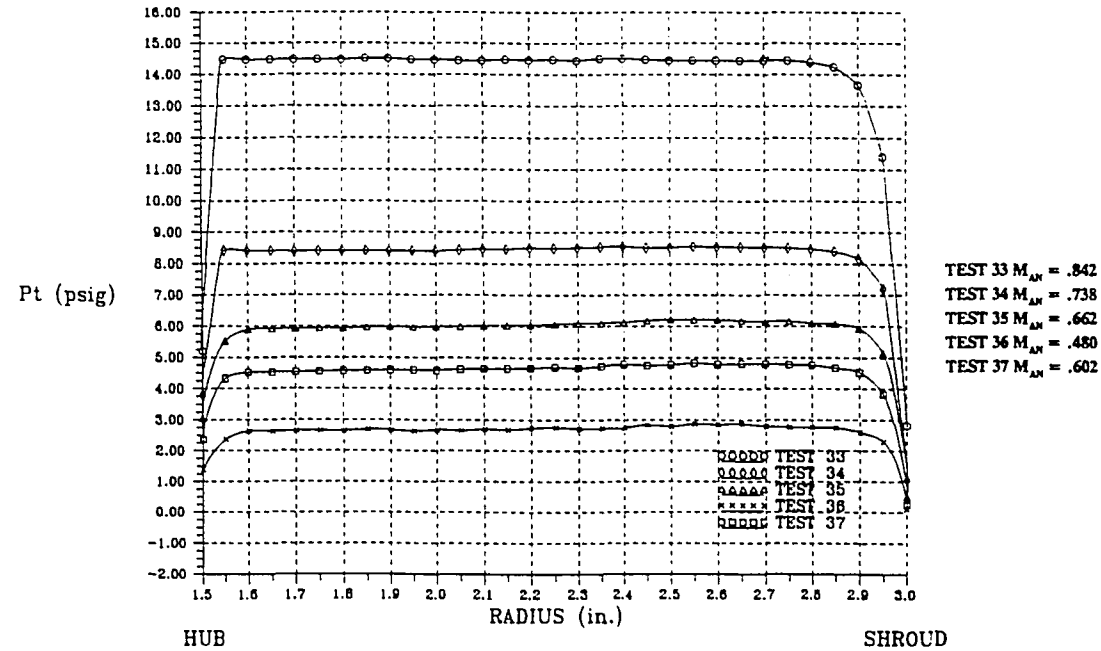

Figure I.10: Total pressure distribution for the original Beaver Valley model, hood alone, without screen - traverse 3

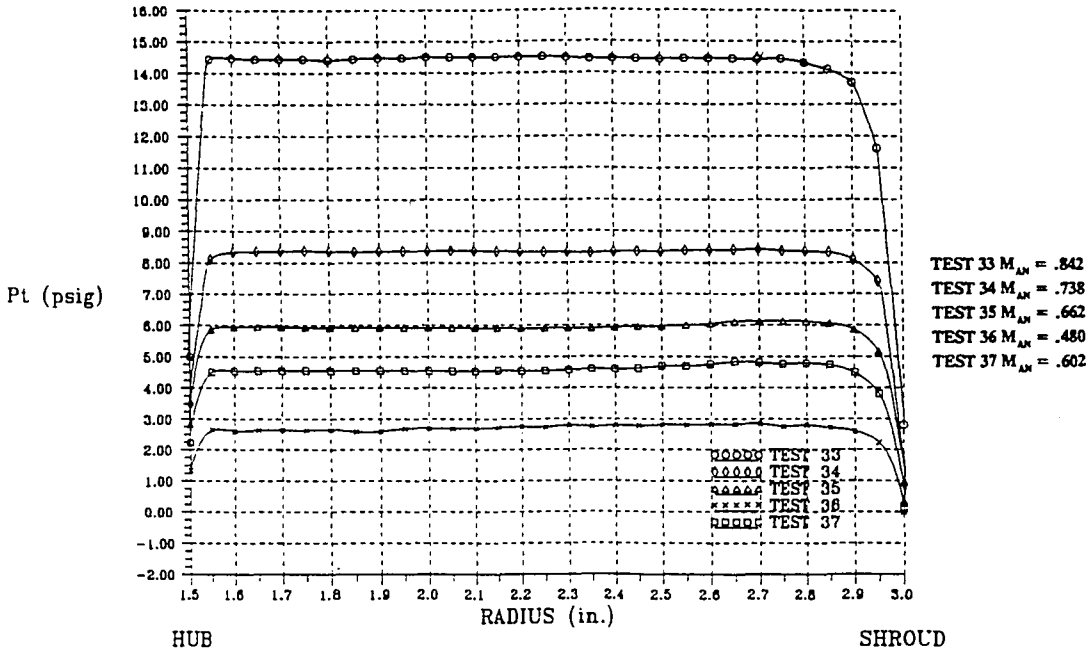

Figure I.11: Total pressure distribution for the original Beaver Valley model, hood alone, without screen - traverse 4

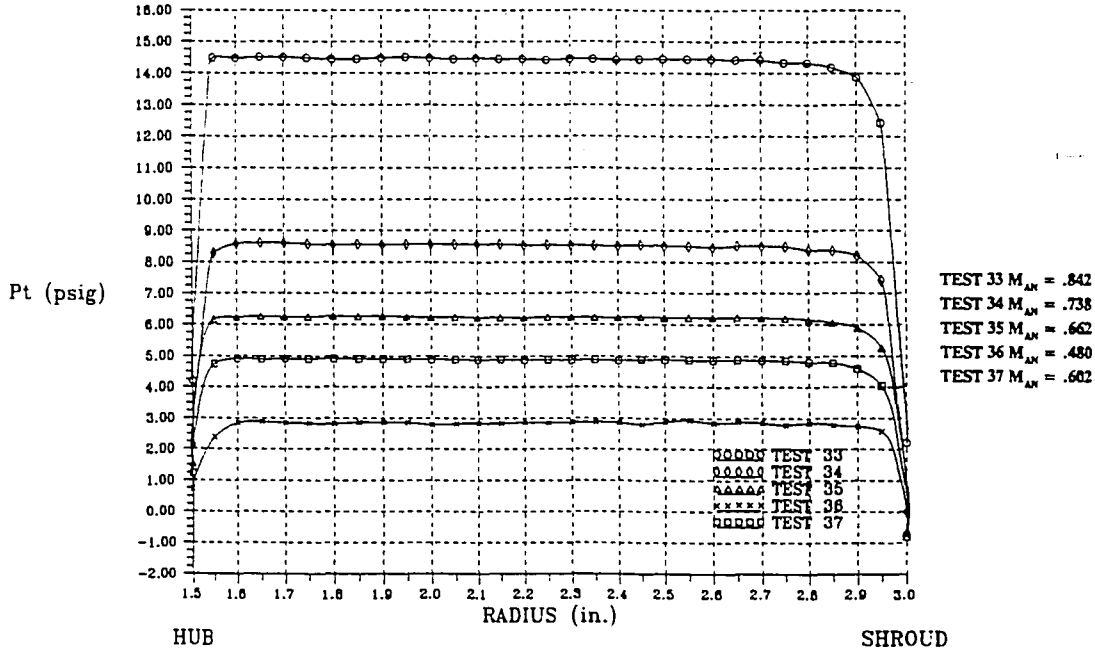

Figure I.12: Total pressure distribution for the original Beaver Valley model, hood alone, without screen - traverse 5

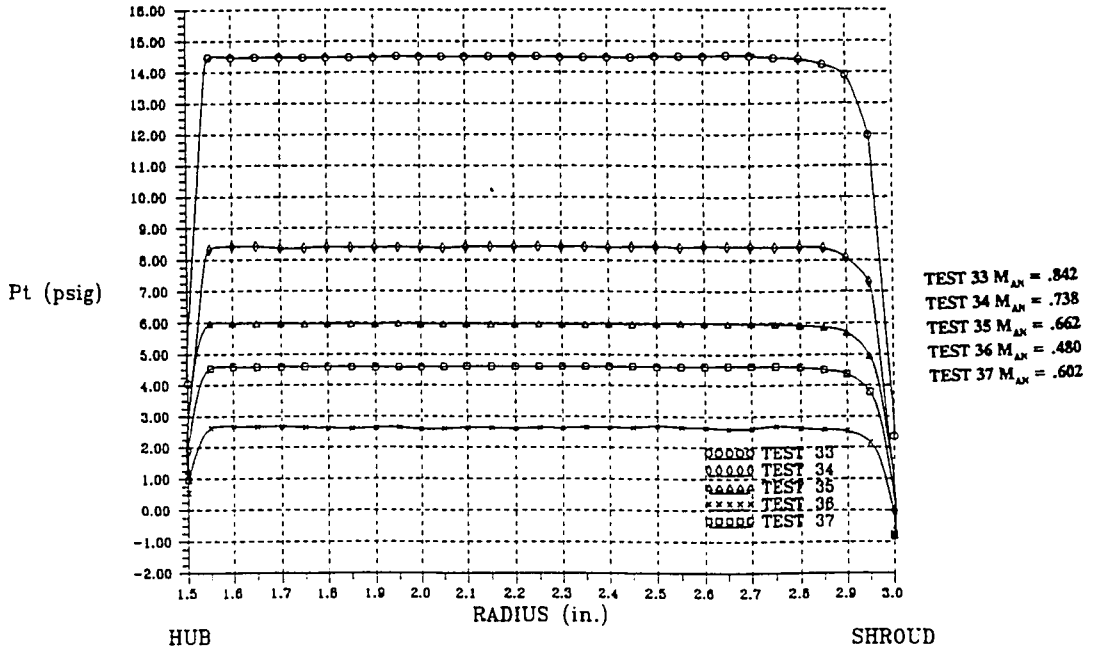

Figure I.13: Total pressure distribution for the original Beaver Valley model, hood alone, without screen - traverse 6

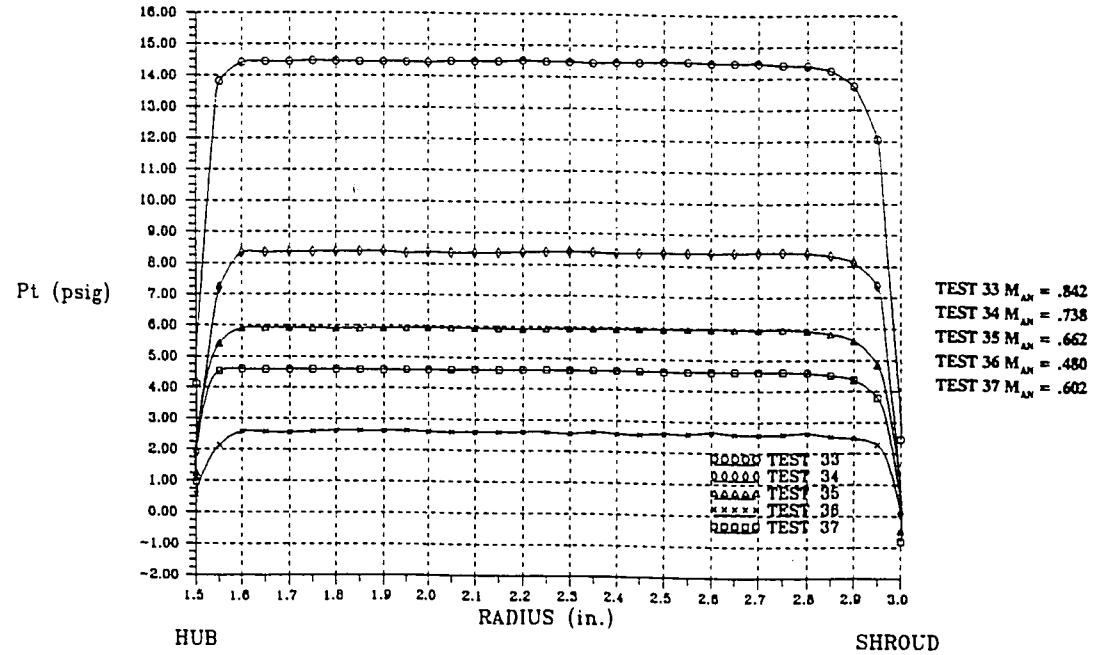

Figure I.14: Total pressure distribution for the original Beaver Valley model, hood alone, without screen - traverse 7

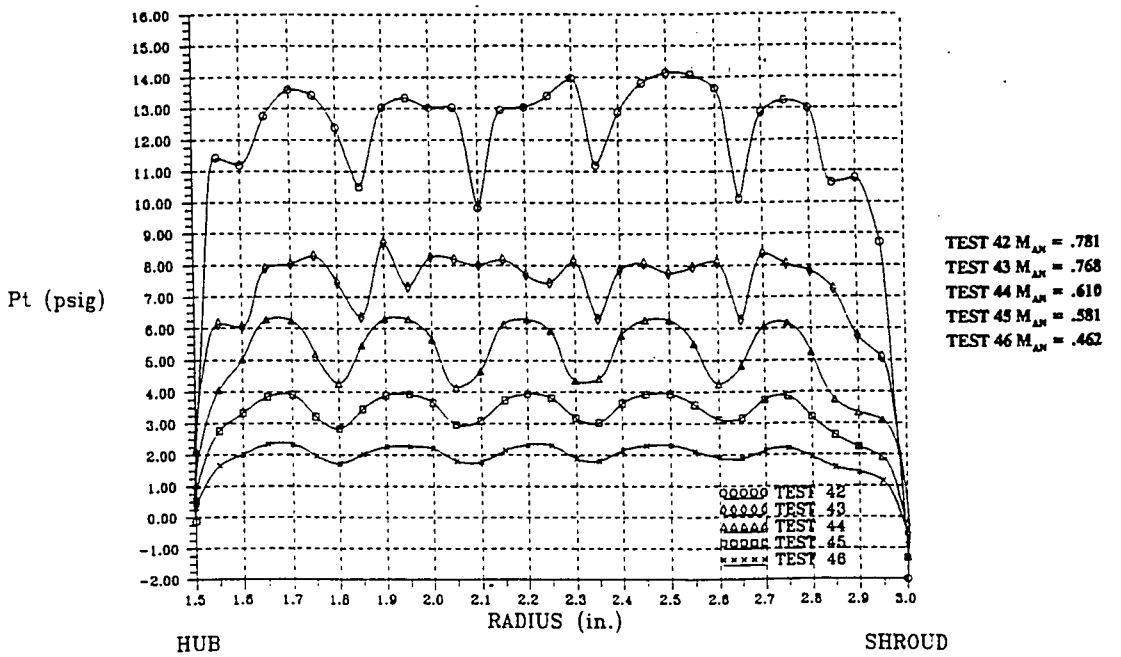

Figure I.15: Total pressure distribution for the original Hatfield Ferry model, hood alone, with screen - traverse 1

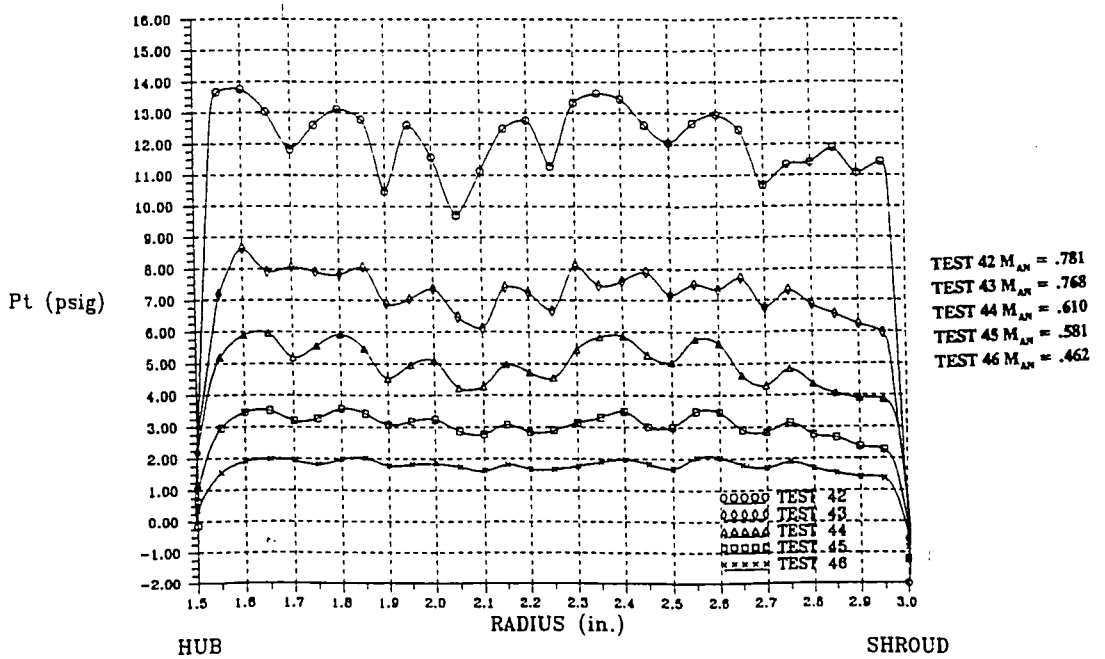

Figure I.16: Total pressure distribution for the original Hatfield Ferry model, hood alone, with screen - traverse 2

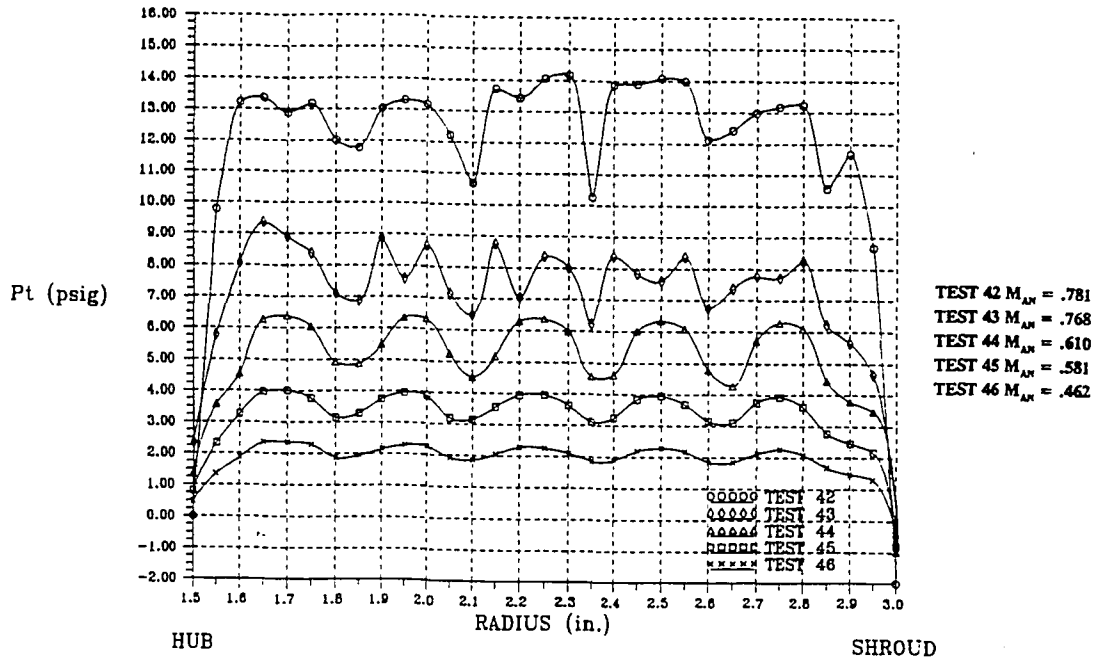

Figure I.17: Total pressure distribution for the original Hatfield Ferry model, hood alone, with screen - traverse 3

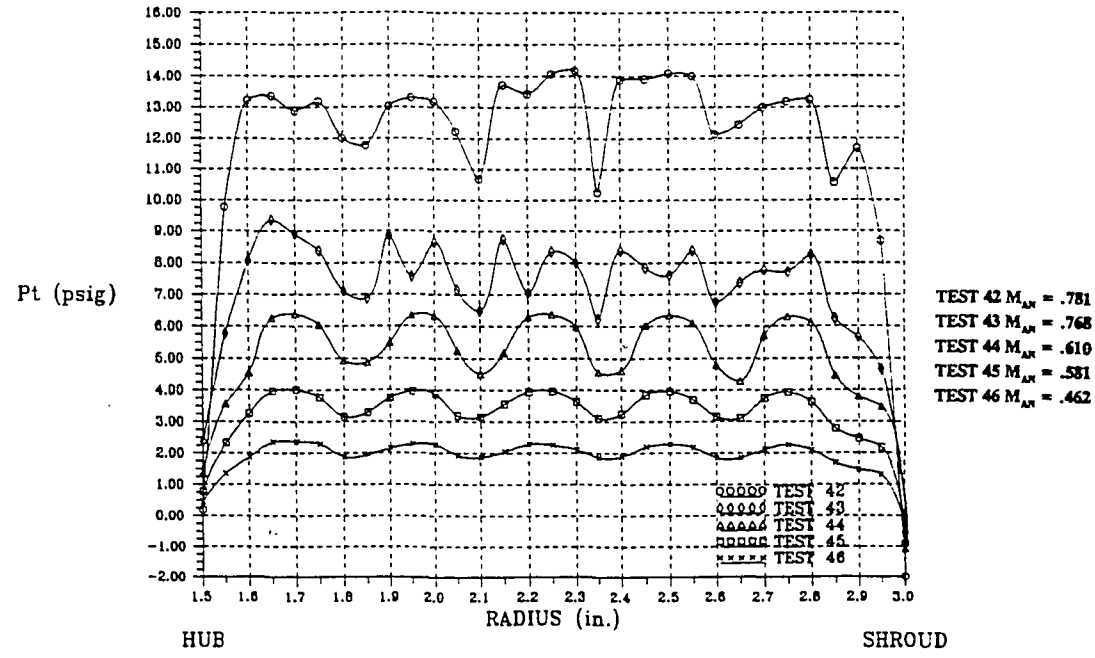

Figure I.18: Total pressure distribution for the original Hatfield Ferry model, hood alone, with screen - traverse 4

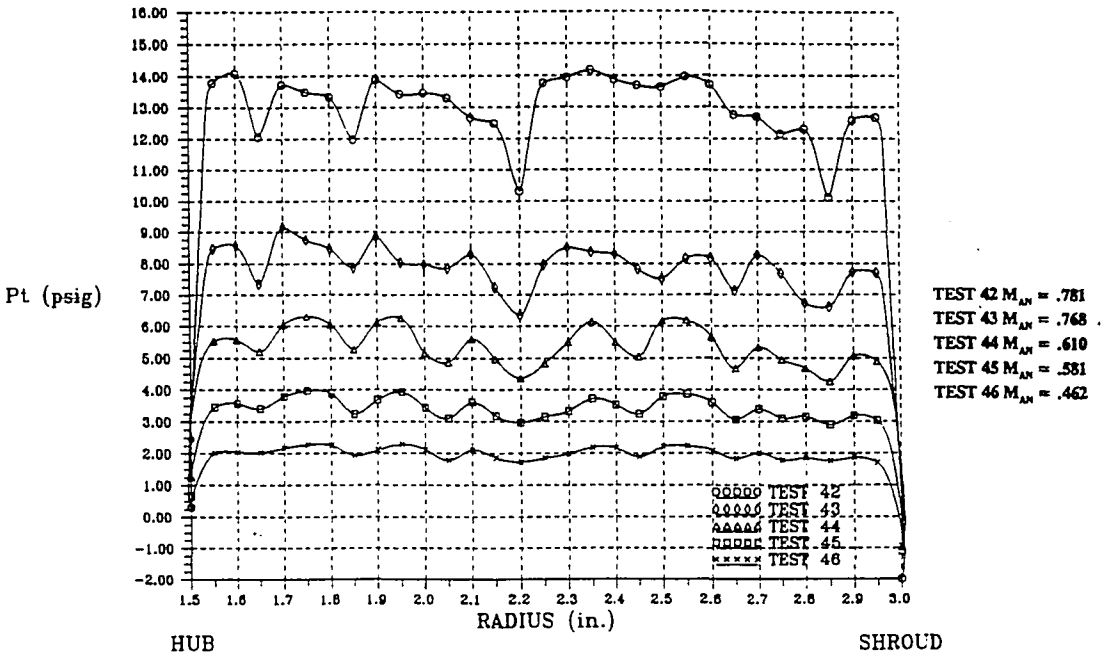

Figure I.19: Total pressure distribution for the original Hatfield Ferry model, hood alone, with screen - traverse 5

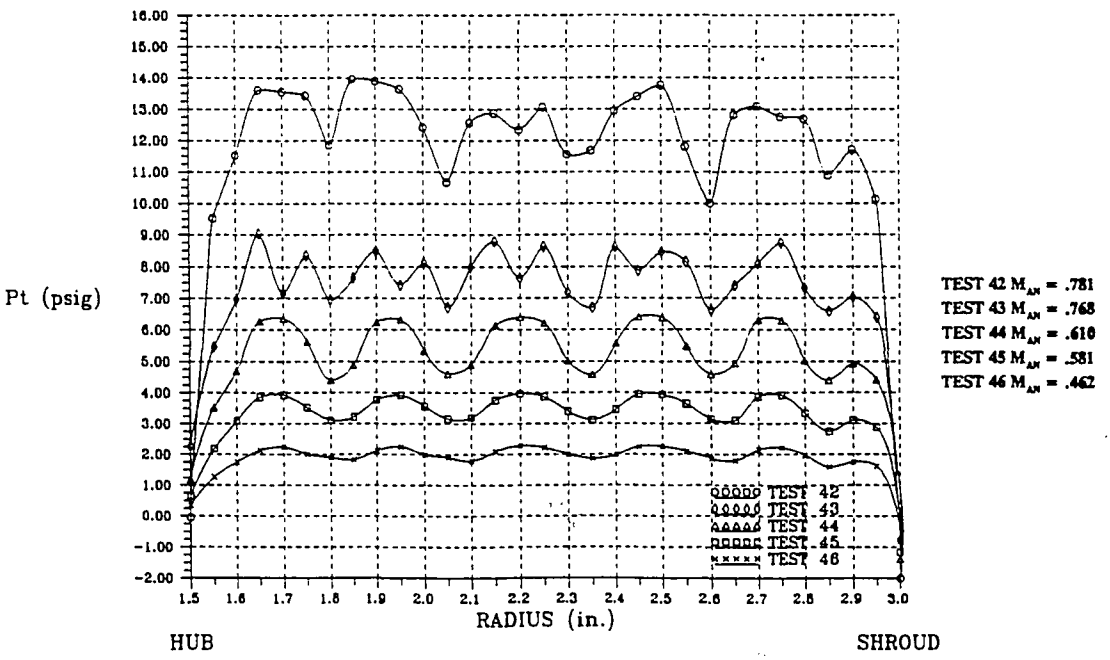

Figure I.20: Total pressure distribution for the original Hatfield Ferry model, hood alone, with screen - traverse 6

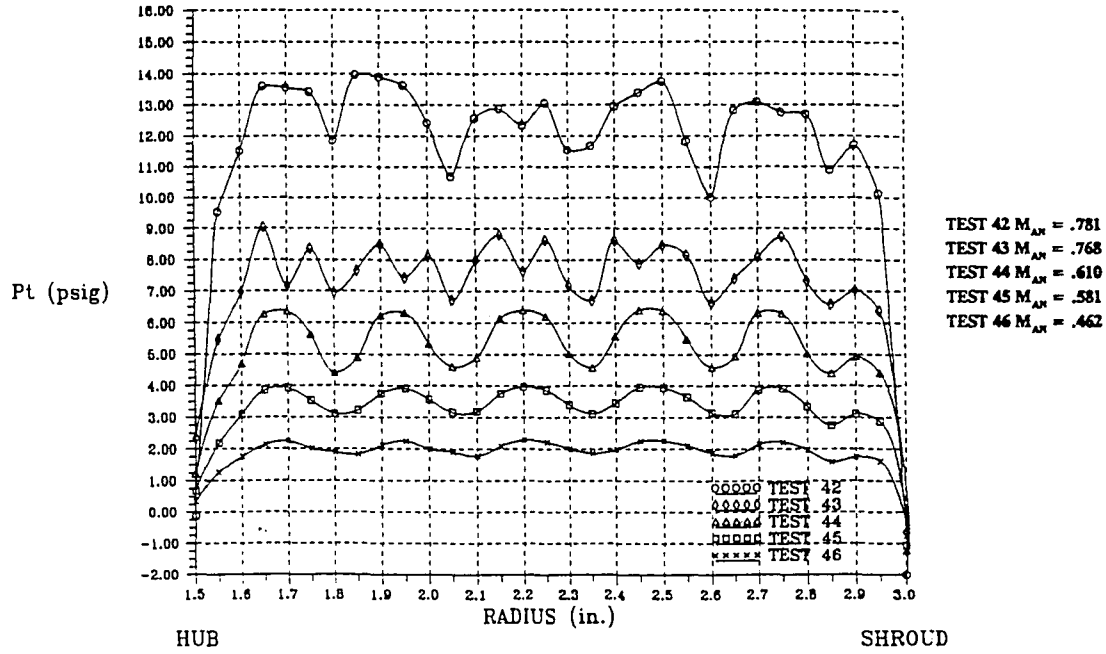

Figure I.21: Total pressure distribution for the original Hatfield Ferry model, hood alone, with screen - traverse 7

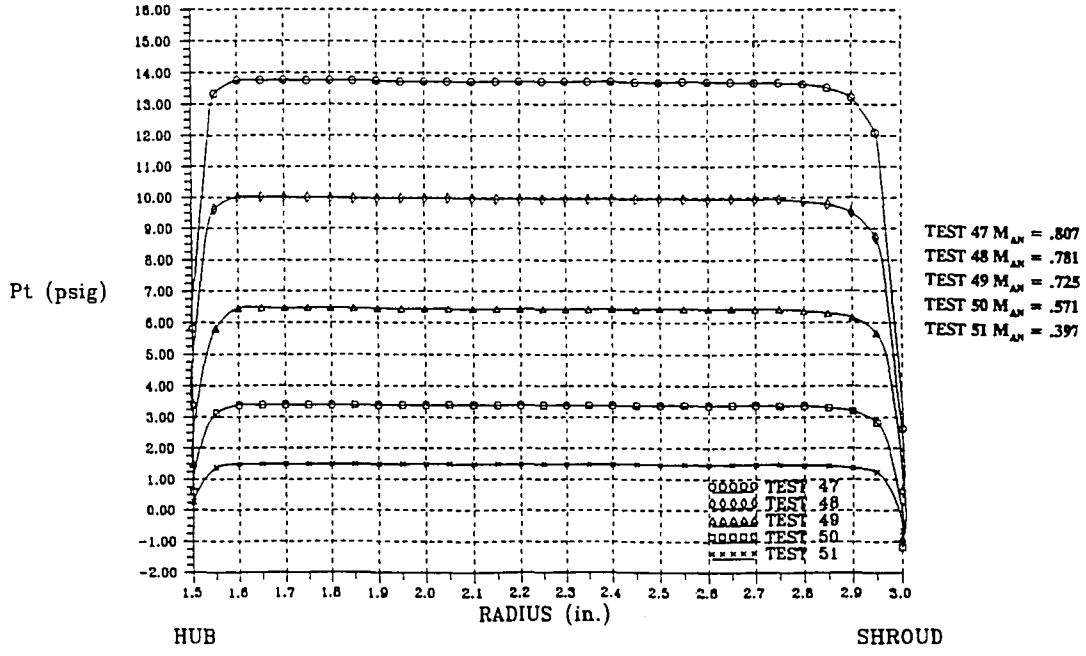

Figure I.22: Total pressure distribution for the original Hatfield Ferry model, hood alone, without screen - traverse 1

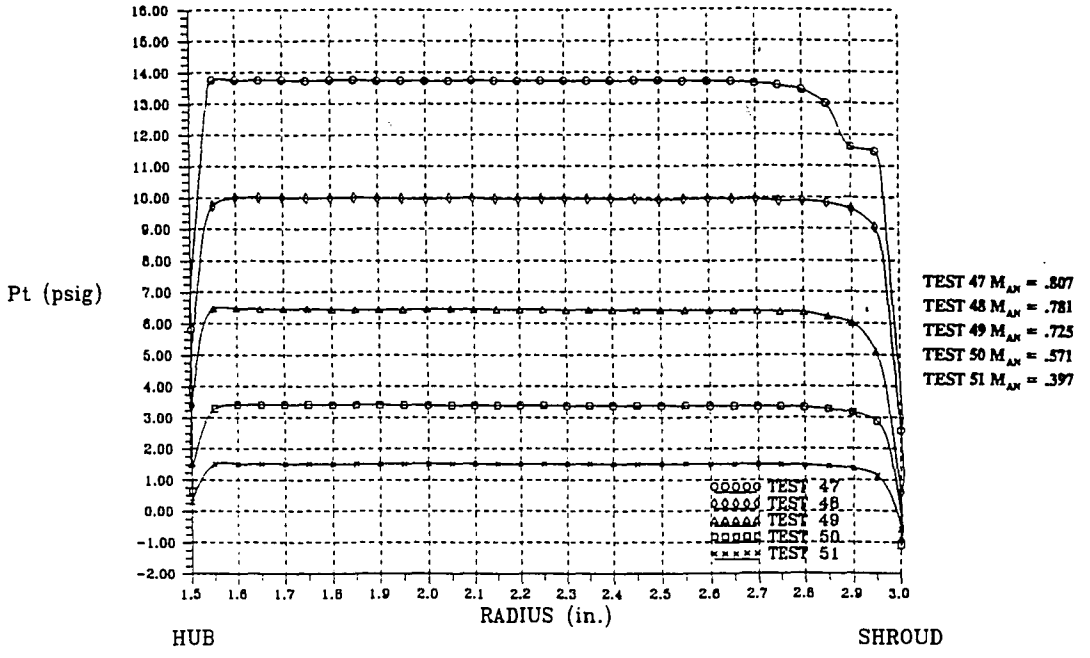

Figure I.23: Total pressure distribution for the original Hatfield Ferry model, hood alone, without screen - traverse 2

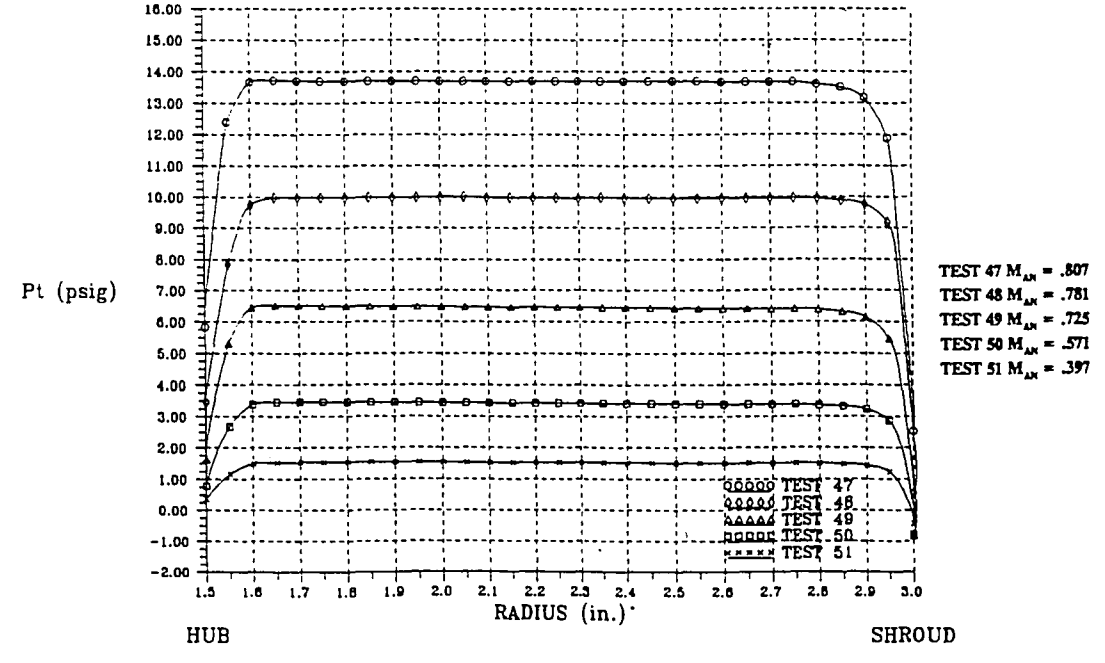

Figure I.24: Total pressure distribution for the original Hatfield Ferry model, hood alone, without screen - traverse 3

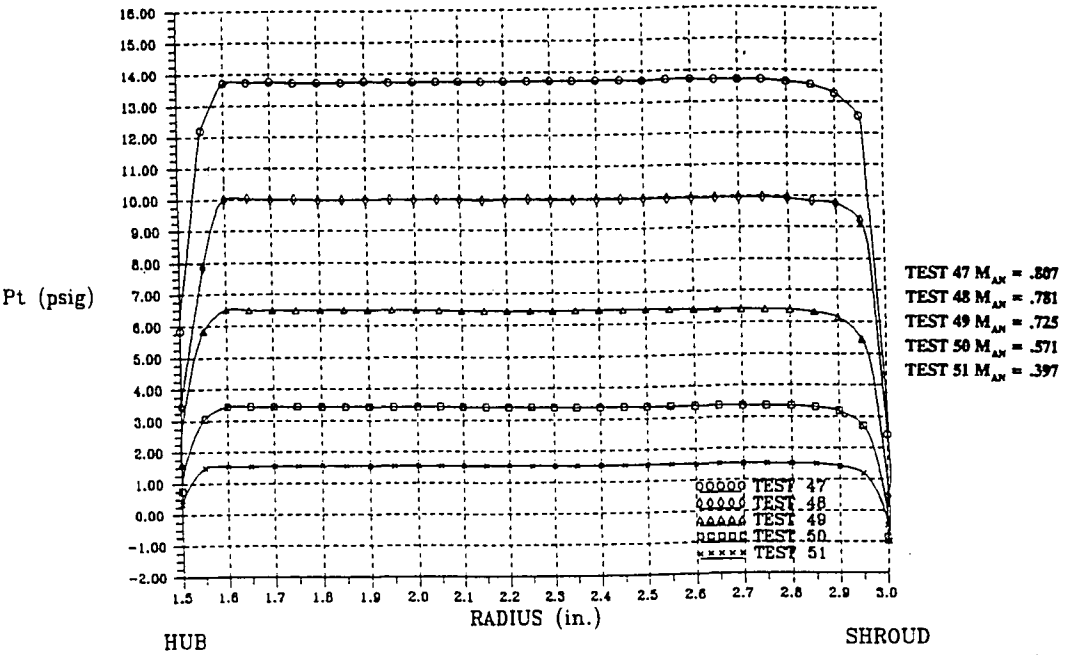

Figure I.25: Total pressure distribution for the original Hatfield Ferry model, hood alone, without screen - traverse 4

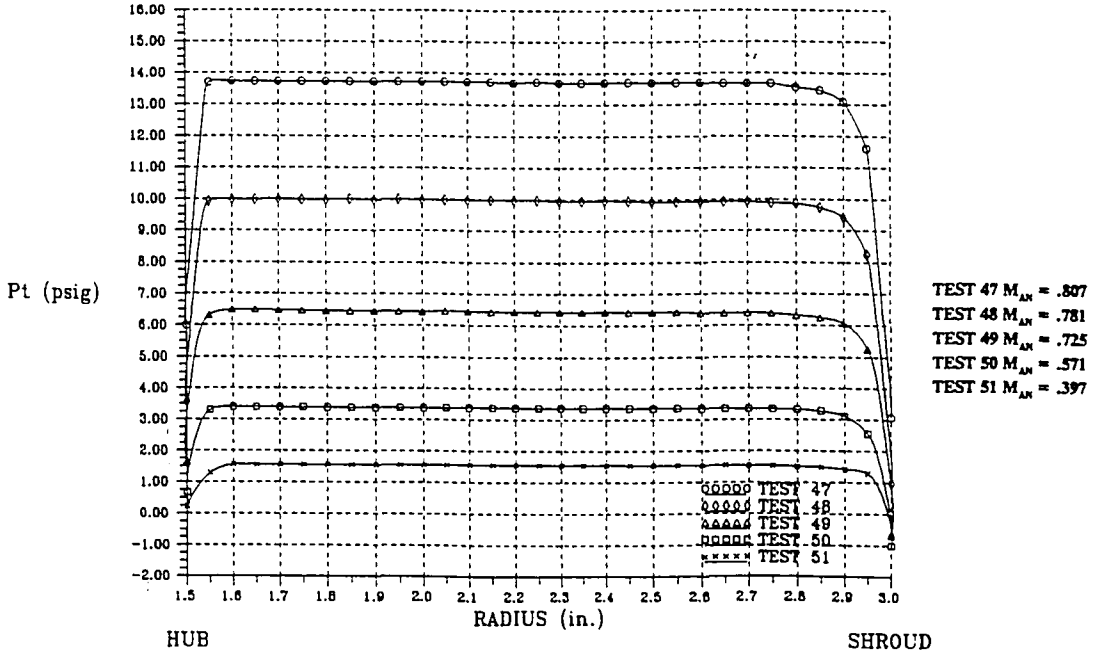

Figure I.26: Total pressure distribution for the original Hatfield Ferry model, hood alone, without screen - traverse 5

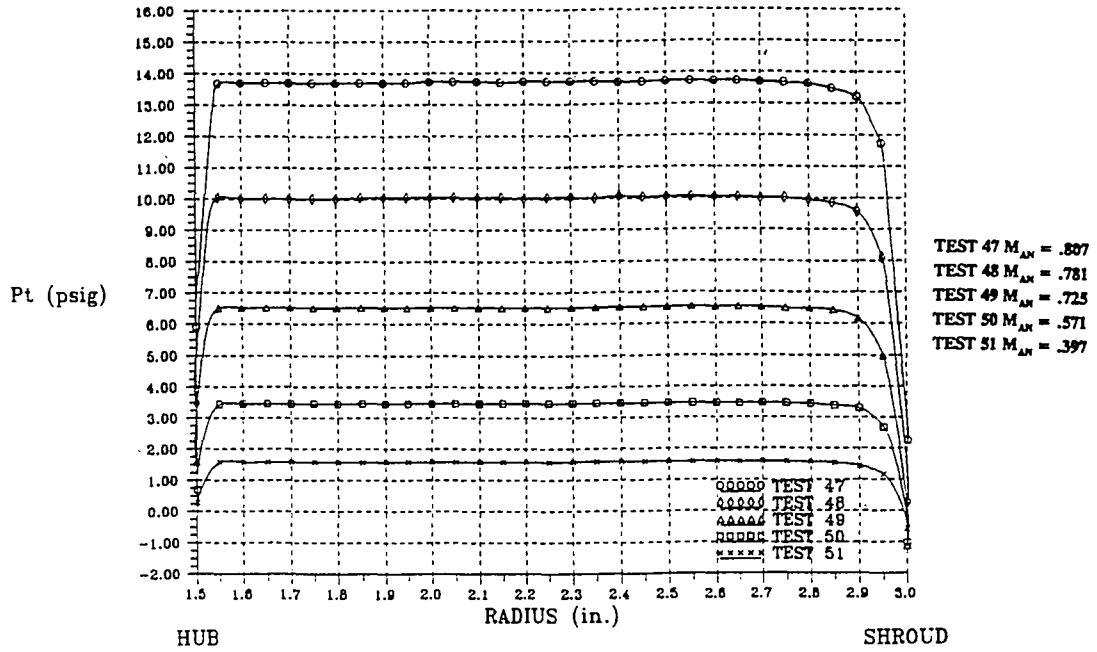

Figure I.27: Total pressure distribution for the original Hatfield Ferry model, hood alone, without screen - traverse 6

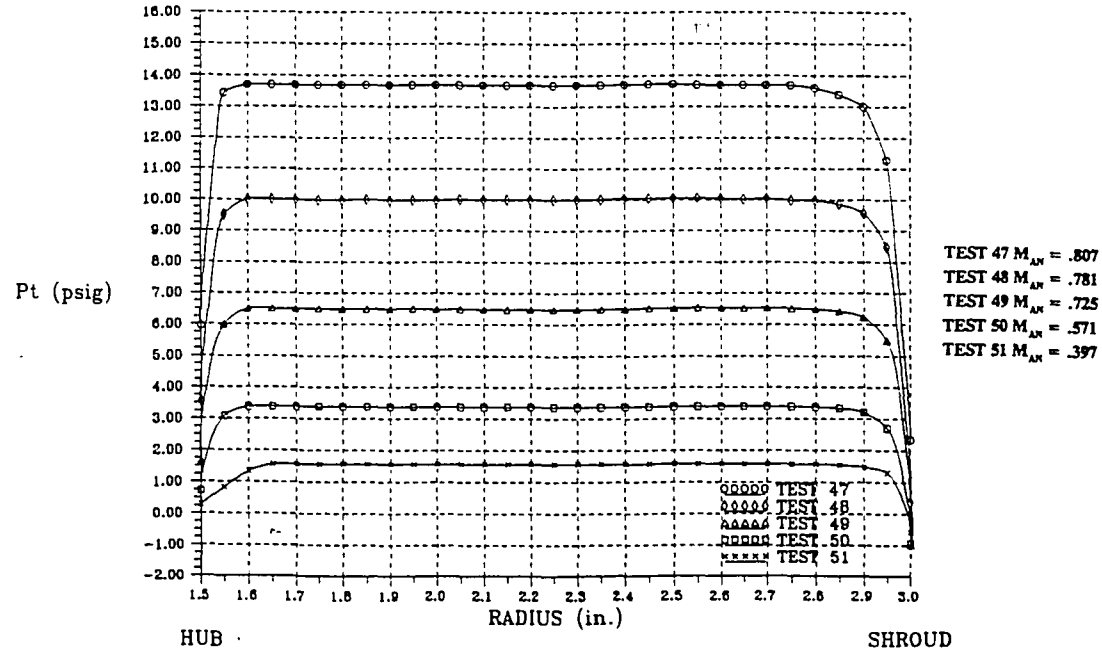

Figure I.28: Total pressure distribution for the original Hatfield Ferry model, hood alone, without screen - traverse 7

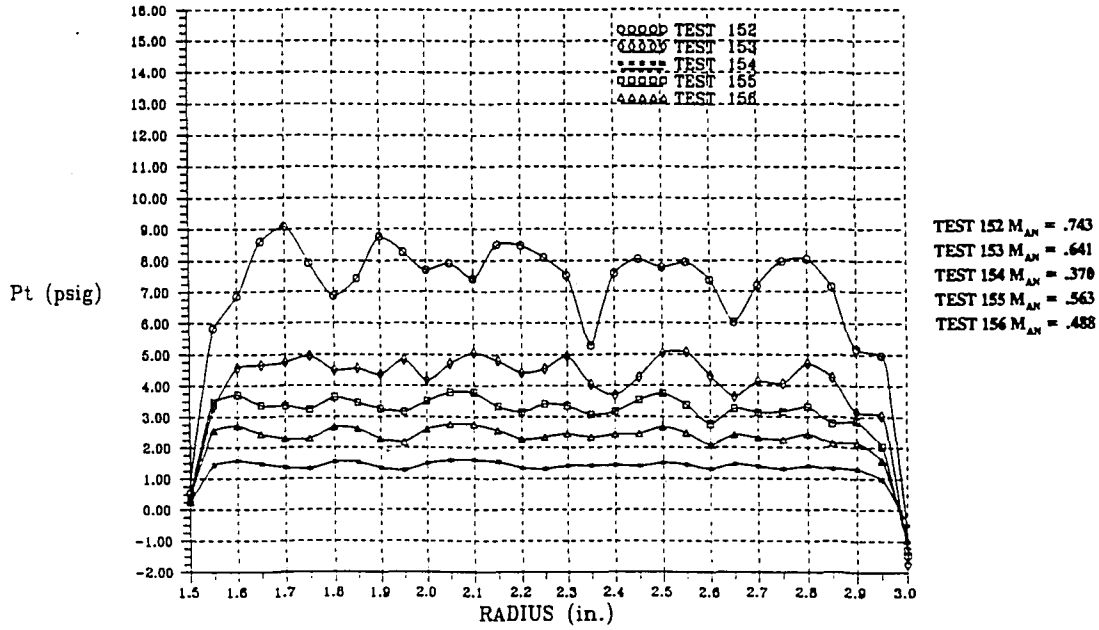

Figure I.29: Total pressure distribution for BV Modification F, hood alone, with screen - traverse 1

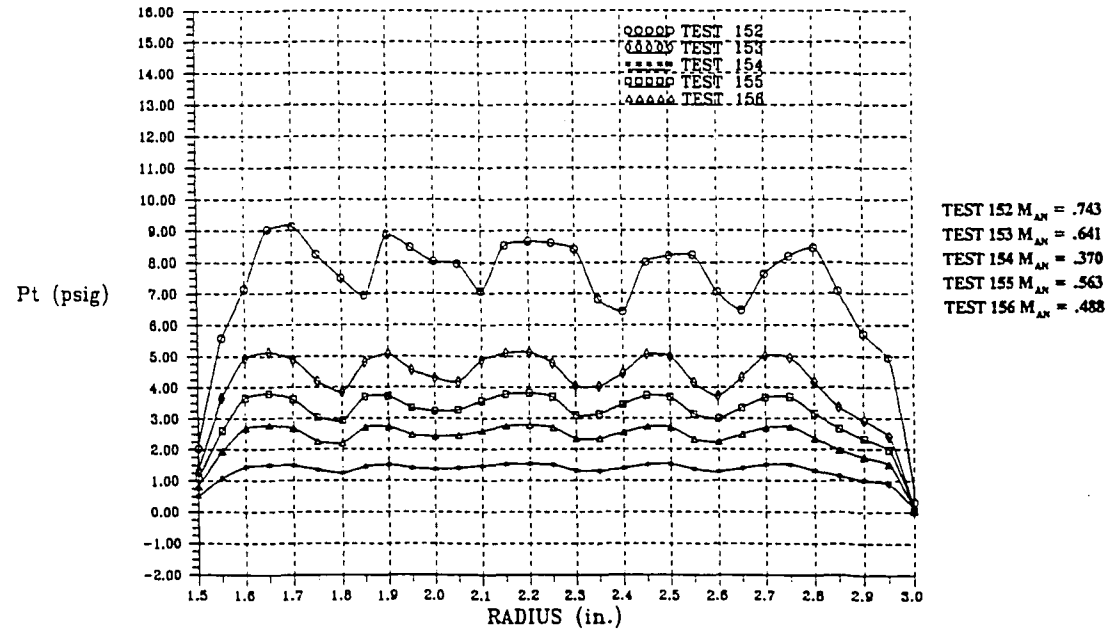

Figure I.30: Total pressure distribution for BV Modification F, hood alone, with screen - traverse 3

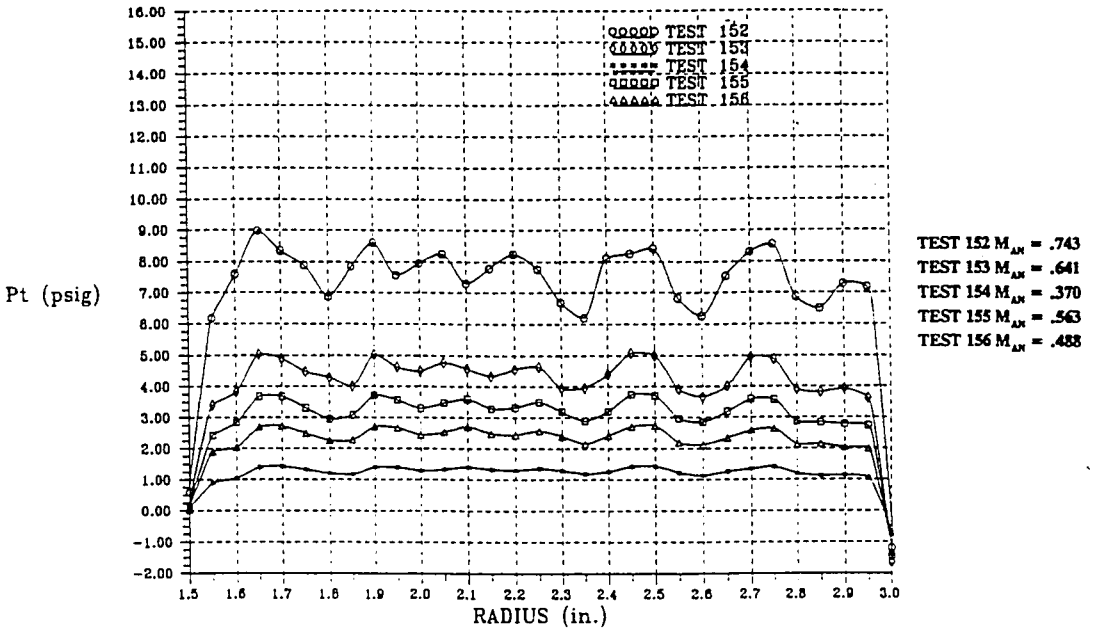

Figure I.31: Total pressure distribution for BV Modification F, hood alone, with screen - traverse 7

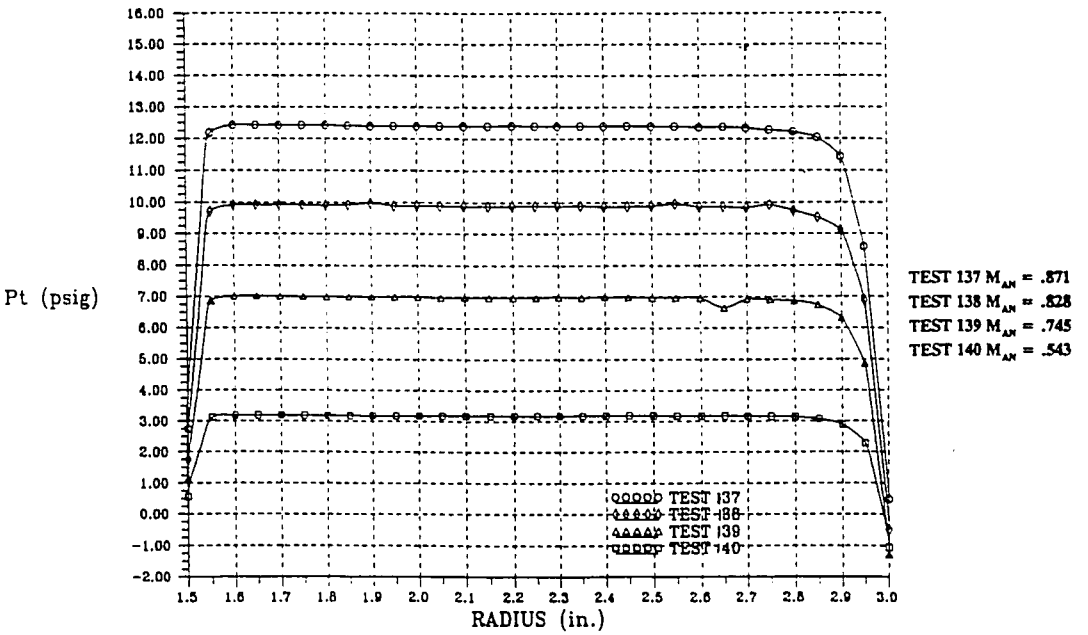

Figure I.32: Total pressure distribution for BV Modification F, hood alone, without screen - traverse 1

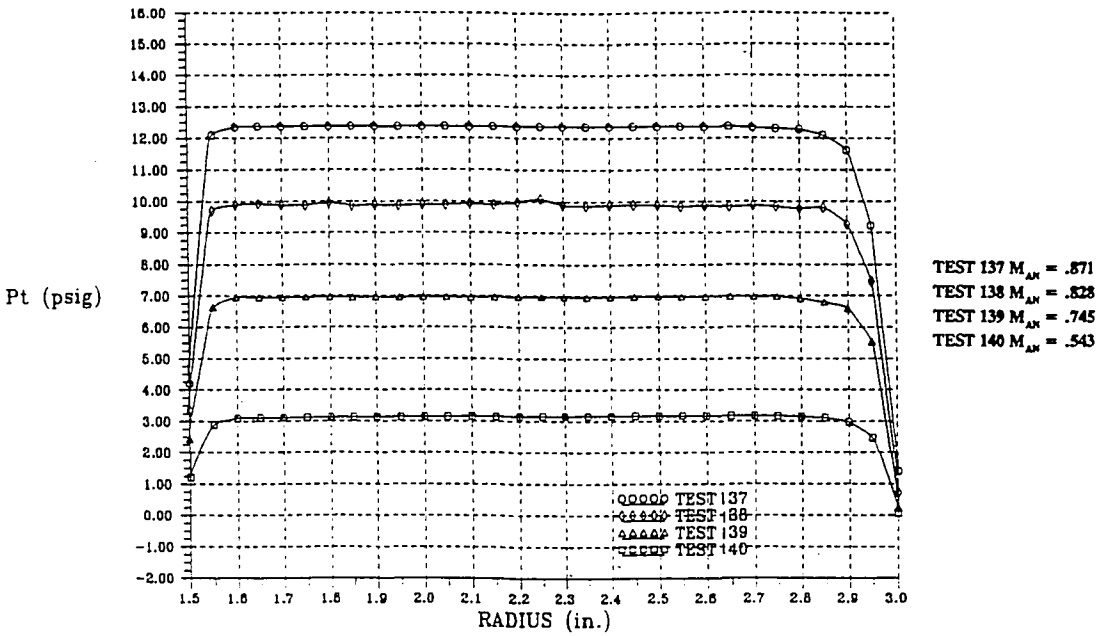

Figure I.33: Total pressure distribution for BV Modification F, hood alone, without screen - traverse 3

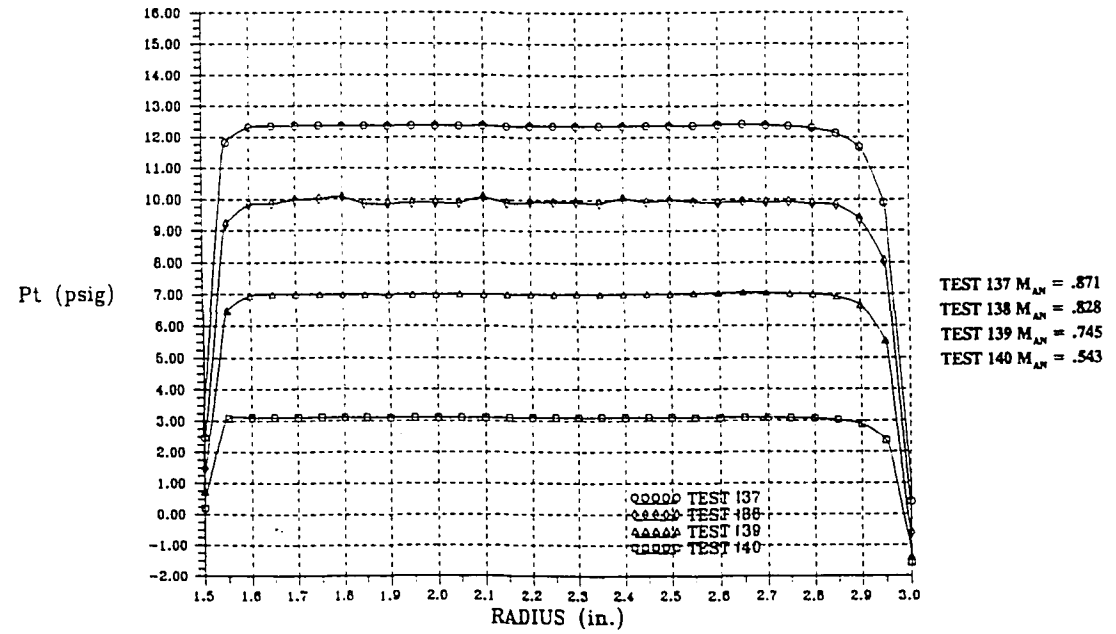

Figure I.34: Total pressure distribution for BV Modification F, hood alone, without screen - traverse 7

VITA

Mark Joseph Pechulis, the son of Anthony and Catherine Pechulis, was born in Enfield, Connecticut, on July 10, 1969. He graduated from Enrico Fermi High School located in Enfield, CT. He was awarded his B.S. degree in Mechanical Engineering from Western New England College in the Spring of 1992 where he also became a member of the Tau Beta Pi engineering honors fraternity. In the Fall of 1992 he entered Lehigh University and worked as a Research Assistant for the Energy Research Center under the direction of Dr. J.A. Owczarek and Dr. E.K. Levy. During his graduate studies at Lehigh University, he also worked as a Teaching Assistant for the Mechanical Engineering Department.

END

OF

TITLE